ANL-79-45

Dr. 1975

ANL-79-45

353
11/12/80
T.S.

MASTER

CHEMICAL ENGINEERING DIVISION

FUEL CYCLE PROGRAMS QUARTERLY PROGRESS REPORT

January—March 1979

by

M. J. Steindler, Milton Ader, R. E. Barletta, J. K. Bates,
C. H. Bean, R. A. Couture, E. D. Creamer, K. F. Flynn,
T. J. Gerding, L. J. Jardine, D. K. Kroeck, Michael Krumpelt,
W. J. Mecham, J. H. Meisenhelder, K. M. Myles, R. H. Pelto,
M. G. Seitz, Seymour Vogler, and Jacqueline Williams

ARGONNE NATIONAL LABORATORY

ARGONNE NATIONAL LABORATORY, ARGONNE, ILLINOIS

Prepared for the U. S. DEPARTMENT OF ENERGY
under Contract W-31-109-Eng-38

DISTRIBUTION OF THIS DOCUMENT IS UNLIMITED

DISCLAIMER

This report was prepared as an account of work sponsored by an agency of the United States Government. Neither the United States Government nor any agency Thereof, nor any of their employees, makes any warranty, express or implied, or assumes any legal liability or responsibility for the accuracy, completeness, or usefulness of any information, apparatus, product, or process disclosed, or represents that its use would not infringe privately owned rights. Reference herein to any specific commercial product, process, or service by trade name, trademark, manufacturer, or otherwise does not necessarily constitute or imply its endorsement, recommendation, or favoring by the United States Government or any agency thereof. The views and opinions of authors expressed herein do not necessarily state or reflect those of the United States Government or any agency thereof.

DISCLAIMER

Portions of this document may be illegible in electronic image products. Images are produced from the best available original document.

The facilities of Argonne National Laboratory are owned by the United States Government. Under the terms of a contract (W-31-109-Eng-38) among the U. S. Department of Energy, Argonne Universities Association and The University of Chicago, the University employs the staff and operates the Laboratory in accordance with policies and programs formulated, approved and reviewed by the Association.

MEMBERS OF ARGONNE UNIVERSITIES ASSOCIATION

The University of Arizona
Carnegie-Mellon University
Case Western Reserve University
The University of Chicago
University of Cincinnati
Illinois Institute of Technology
University of Illinois
Indiana University
The University of Iowa
Iowa State University
The University of Kansas
Kansas State University
Loyola University of Chicago
Marquette University
The University of Michigan
Michigan State University
University of Minnesota
University of Missouri
Northwestern University
University of Notre Dame
The Ohio State University
Ohio University
The Pennsylvania State University
Purdue University
Saint Louis University
Southern Illinois University
The University of Texas at Austin
Washington University
Wayne State University
The University of Wisconsin-Madison

NOTICE

This report was prepared as an account of work sponsored by an agency of the United States Government. Neither the United States Government or any agency thereof, nor any of their employees, make any warranty, express or implied, or assume any legal liability or responsibility for the accuracy, completeness, or usefulness of any information, apparatus, product, or process disclosed, or represent that its use would not infringe privately owned rights. Reference herein to any specific commercial product, process, or service by trade name, mark, manufacturer, or otherwise, does not necessarily constitute or imply its endorsement, recommendation, or favoring by the United States Government or any agency thereof. The views and opinions of authors expressed herein do not necessarily state or reflect those of the United States Government or any agency thereof.

Printed in the United States of America
Available from
National Technical Information Service
U. S. Department of Commerce
5285 Port Royal Road
Springfield, VA 22161

NTIS price codes
Printed copy: A10
Microfiche copy: A01

Distribution Category:
Nuclear Waste Management (UC-70)
Chemical Separations Processes for
Plutonium and Uranium (UC-10)

ANL-79-45

ARGONNE NATIONAL LABORATORY
9700 South Cass Avenue
Argonne, Illinois 60439

CHEMICAL ENGINEERING DIVISION

FUEL CYCLE PROGRAMS QUARTERLY PROGRESS REPORT

January-March 1979

by

M. J. Steindler, Milton Ader, R. E. Barletta, J. K. Bates,
C. H. Bean, R. A. Couture, E. D. Creamer, K. F. Flynn,
T. J. Gerding, L. J. Jardine, D. K. Kroeck, Michael Krumpelt,
W. J. Mecham, J. H. Meisenhelder, K. M. Myles, R. H. Pelto,
M. G. Seitz, Seymour Vogler, and Jacqueline Williams

DISCLAIMER

This book was prepared as an account of work sponsored by an agency of the United States Government. Neither the United States Government nor any agency thereof, nor any of their employees, makes any warranty, express or implied, or assumes any legal liability or responsibility for the accuracy, completeness, or usefulness of any information, apparatus, product, or process disclosed, or represents that its use would not infringe privately owned rights. Reference herein to any specific commercial product, process, or service by trade name, trademark, manufacturer, or otherwise, does not necessarily constitute or imply its endorsement, recommendation, or favoring by the United States Government or any agency thereof. The views and opinions of authors expressed herein do not necessarily state or reflect those of the United States Government or any agency thereof.

January 1980

Previous reports in this series

ANL-78-68 January-March 1978
ANL-78-76 April-June 1978
ANL-79-6 July-September 1978
ANL-79-29 October-December 1978

DISTRIBUTION OF THIS DOCUMENT IS UNLIMITED

THIS PAGE

WAS INTENTIONALLY

LEFT BLANK

TABLE OF CONTENTS

	Page
ABSTRACT	1
SUMMARY	2
I. PYROCHEMICAL AND DRY PROCESSING METHODS PROGRAM	7
A. Introduction	7
B. Management	7
C. Engineering Analysis and Separations Processes	9
1. Materials Development for PDPM	9
2. Carbide Fuel Reprocessing	19
3. Thorium-Uranium Salt-Transport Processing	20
4. Uranium-Plutonium Salt Transport Processing	36
5. Fabrication of Process-Size Refractory Metal Vessels	83
6. Chloride Volatility Processing of Thorium-Based Fuel	86
7. Material Characterization and Process Analysis	97
8. Molten Nitrate Salt Oxidation Processes	112
9. Molten Salt Processes Applied to Nuclear Fuels	115
10. Molten Tin Process for Reactor Fuels	121
11. Engineering Support for the PDPM Program	124
II. ENCAPSULATION OF RADIOACTIVE WASTE IN METAL	130
A. Leach Rates of Simulated Radioactive Waste Materials	130
1. Introduction	130
2. Experimental Materials, Procedures, and Results	130
3. Conclusions	141
B. Evaluation of Impact Resistance of Waste Forms	141
1. Engineering Studies of Brittle Fracture: A Chronological Review	142
2. Mechanics of Ceramics: A Current Summary	147
III. TRANSPORT PROPERTIES OF NUCLEAR WASTE IN GEOLOGIC MEDIA	150
A. Introduction	150
B. Concentration Dependence of Trace-Element Migration--A Theoretical Treatment	140
1. Exchange of Species With Like Charges	151
2. Saturation of Exchange Sites	152
C. Concentration Dependence of Cesium Adsorption on Limestone	155

TABLE OF CONTENTS (contd)

Page

D. Cesium Concentrations as a Controlled Variable in Infiltration Experiments 160

E. Discussion of Concentration Dependence on Cesium Adsorption by Limestone 161

F. Effect of pH Groundwater Solution on Cesium Migration in Limestone 164

1. pH of Solutions 164
2. Infiltration Experiments with Cesium in Limestone 165
3. Discussion of Results Using Solutions of Different pH 166
4. Estimate of Cesium Loading on Limestone 167

G. Conclusions 169

IV. TRACE-ELEMENT TRANSPORT IN LITHIC MATERIAL BY FLUID FLOW AT HIGH TEMPERATURE 170

A. Introduction 170

B. Adsorption of Iodate by Hematite 170

1. Experimental Methods 170
2. Results 172

C. Discussion 174

APPENDIX A 175

APPENDIX B 185

REFERENCES 187

LIST OF FIGURES

No.	Title	Page
1.	Micrograph of a Recrystallized Mo-30% W Alloy after about 120 h Exposure to Zinc and Molten $CaCl_2$-KCl Salt System at about 800°C	14
2.	Micrograph of an As-rolled Mo-30% W Alloy after about 120 h Exposure to Zinc and Molten $CaCl_2$-KCl Salt System at about 800°C	14
3.	Scans of Titanium Diboride After Exposure to a Mixture of Zinc and KCl-$CaCl_2$ Eutectic for 120 h at 800°C	16
4.	Micrographs of Plasma-sprayed Tungsten	18
5.	Tungsten-coated Alumina-Yttria Crucible	19
6.	Conceptual Flowsheet for Thorium-Based Fuels	21
7.	Solubility of Thorium in Cadmium	22
8.	Current vs. Potential Plots for Electrolysis of CaO in 15 wt % CaF_2/$CaCl_2$ at 690°C using a Carbon Anode and a Molten Cadmium Cathode	26
9.	Current vs. Potential Plots of CaO 15 wt % CaF_2-$CaCl_2$ in 15 wt % CaF_2-$CaCl_2$ at 695°C using a Carbon Anode and a Molten Cathode of 35 wt % Mg-Cu	28
10.	Cyclic Voltammograms of CaO in 15 wt % CaF_2-$CaCl_2$ at 697°C after 543 Min of Electrolysis	29
11.	Current-Potential Curves for the CaO-CaF_2-$CaCl_2$ System at 675°C	31
12.	Current vs. Potential Curves for Fused 15 wt % CaF_2-$CaCl_2$ Containing 5 wt % CaO at 695°C	34
13.	Graphite Anodes Used in Molten Salt Electrolysis of CaO	35
14.	Connection of Process Vessels	42
15.	Salt Transport Process Flow Diagram	44
16.	Salt Transport Turntable Design	45
17.	Turntable Process Timing Diagram	50
18.	Floor Layout for Salt Transport Turntable Concept	51

LIST OF FIGURES (contd)

No.	Title	Page
19.	Flow Diagram, Mixer-Settler Continuous Salt Transport	53
20.	Typical Mixer-Settler Stage For Salt Transport	54
21.	Preliminary Phase of the Experimental Work Plan	63
22.	Major Phase of the Experimental Work Plan	64
23.	Chloride Volatility Coprocessing of Thoria-Urania Spent Fuel	87
24.	U-Zn Phase Diagrams	92
25.	U-Pu Phase Diagram	93
26.	Pu-Zn Phase Diagram	94
27.	Tantalum Crucible	96
28.	Pulverization when Oxygen was Added after Fuel Reached Oxidation Temperature	108
29.	Degree of Pulverization after the Second Cycle at Various Oxygen Pressures	109
30.	Fuel Not Completely Pulverized during Oxidation but Readily Pulverized by Pressure Sieving	111
31.	Rapid Oxidation during Second Cycle Reduces Pulverization of Finely Divided Product	112
32.	Dissolution of UO_2 Microspheres in $LiCl/AlCl_3$	119
33.	Pulsed Liquid Mass Transfer Dimensionless Correlation	128
34.	Effect of Temperature on Leach Rate of 76-68 PNL Glass in Distilled Water for Initial 7-day Leaching Period	138
35.	Frequency Curves of New Surface Produced per Unit of Energy Input and Average Energy Concentration at Fracture for Single Particles	144
36.	The Partition Coefficient for Cesium on Limestone is Dependent on Cesium Concentrations as low as about 10^{-9} M	159
37.	Cumulative Activity of Cesium Eluted Through Limestone in Groundwater Solutions Containing Various Amounts of Cesium	162

LIST OF FIGURES (contd)

No.	Title	Page
38.	Cesium Activity in the Eluate Versus Eluate Volume. The solution fed to the column had a pH of 3.5 and an activity of 0.98 c/s.mL	165
39.	Cesium Activity in the Eluate Versus Eluate Volume. The infiltrating solution had a pH of 7.79 and an initial cesium-134 activity of 0.96 c/s.mL	166
40.	Adsorption of Iodate by Hematite as a Function of pH in 0.1M $NaClO_4$ Solution	172
41.	Adsorption of Iodate by Hematite	173

LIST OF TABLES

No.	Title	Page
1.	PDPM Work Packages	8
2.	Corrosion of Mo-30W by Molten Zinc and Molten $LiCl-MgCl_2-ZnCl_2$	11
3.	Solubility of Thorium in Cadmium at 325°C to 600°C	23
4.	Mass-Spectrometric Analyses of Gas Effluent from CaO Electrolysis	25
5.	Chemical Analyses of Materials from CaO Electrolysis	27
6.	Decomposition Potentials, E_d, for the $CaO-CaF_2-CaCl_2$ System. Temp: 675-800°C	30
7.	Decomposition Potentials for the $CaO-CaF_2-CaCl_2$ System. Temp: 700°C	33
8.	Chemical Analyses of Solutions from CaO Electrolysis	34
9.	Initial Calcium Recycle Experiments	38
10.	Steps in Sequence of Events in Salt Transport Processing	46
11.	Process Design Abbreviations and Descriptions	52
12.	Compositions of Metals used in the Proof-of-Principle Experiments	58
13.	Impurity Content for Depleted Uranium	59
14.	Impurity Content for Zirconium Metal	60
15.	Compositions of Major Salt Mixtures	62
16.	Single Process Proliferation Study Approach	65
17.	Preliminary Time Schedule for the Proliferation Study	67
18.	Heel Volumes in Salt Transport Process - Turntable Concept	69
19.	Salt Transport Operating Parameters	71
20.	Salt Transport Distribution Coefficients and Solubilities	72
21.	Calculated Salt Transport Results for Core/Axial Blanket	73

LIST OF TABLES (contd)

No.	Title	Page
22.	Core/Axial Blanket Reference Fuel - U-Pu Transport Steps	75
23.	Radiation Data for AI Reference LMFBR Oxide Core + Axial Blanket Fuel Subassembly	76
24.	The FP-3 Fission Product Concentration in FP-3 and U-Pu Transport Alloys upon Recycle of Salt and Alloy	76
25.	Material Balance for Materials in Solution in Salt Transport Process for a Core/Axial Blanket Assembly	77
26.	Product and Side Stream Enrichment and Radioactivity	81
27.	Physical and Chemical States of Elements Used to Provide Proliferation Resistance for the Chloride Volatility Coprocess	88
28.	Free Energies of Reaction for Chlorination of Radioactive Species	89
29.	Gamma Radioactivity Provided by Selected Elements for Proliferation Resistance	90
30.	Distribution of Products from Chlorination of UO_2 and Fission Products	95
31.	Elemental Mass Balance For Chlorination Experiments	95
32.	Properties of UO_2 Prepared from Uranium Metal	99
33.	Sintering Characteristics of UO_2 Powders Produced from Uranium Metal	100
34.	Typcial Fuel Powder Specifications and Characteristics	101
35.	Oxidation Rates of Uranium and Binary Uranium Alloys in Air at 500°C	103
36.	Pulverization Test Conditions	107
37.	Particle Size Distribution of Product	107
38.	Effect of Hydrogen Concentration during Reduction	109
39.	Effect of Continued Sieving on Particle Size Distribution of Oxidized UO_2 Powder	110
40.	Weights and Volumes of Solvents for Reductive Extractions at 640 and 688°C per 100 kg of Uranium	118

LIST OF TABLES (contd)

No.	Title	Page
41.	Initial Rates of Dissolution of UO_2 Microspheres in $LiCl/AlCl_3$ at 120°C	119
42.	Initial Rate of Dissolution of UO_2 Microspheres in $LiCl/AlCl_3$ at 220°C	120
43.	Pulsed Liquid Mass Transfer	126
44.	Sequential Leach Tests for 76-68 PNL-Glass in 25°C Quiescent Distilled Water	131
45.	Sequential Leach Tests for 76-68 PNL-Glass in Tap Water	132
46.	Sequential Leach Tests for 76-68 PNL-Glass in Carbonate Water	133
47.	Sequential Leach Tests for 76-68 PNL-Glass in WIPP Brine (25°C)	134
48.	Sequential Leach Tests for 76-68 PNL-Glass in WIPP Brine (109°C)	135
49.	Initial Incremental Leach Rates for 76-68 PNL-Glass Using a Variety of Leaching Media	136
50.	Initial Leach Rates for 76-68 PNL-Glass in Distilled Water	137
51.	Activation Products in Potential Materials for Application to Nuclear Waste Disposal	139
52.	Initial Incremental Leach Rates for Various Materials Assoicated with Nuclear High-Level-Waste	140
53.	Fracture Surface Energy of Slow-Compression Crushing of Small Pyrex Glass Cylinders and Spheres	146
54.	Cesium Concentrations and Activities of Solutions Used in the Batch-Adsorption Experiments	156
55.	Activities of Solutions and Partition Coefficients in Batch Experiments for Cesium Adsorption on Oolitic Limestone	157
56.	Conditions and Results of Experiments Used to Measure the Behavior of Cesium in a Limestone Column at Several Concentrations of Dissolved Cesium	161

LIST OF TABLES (contd)

No.	Title	Page
57.	pHs of Solution Used in Leach-Migration and Conventional Infiltration Experiments with Cesium	164
58.	Calculated Mass Loadings of Cesium on Limestone, Using the Two Assumptions Described in the Text	168
59.	Compositions of Buffer Solutions	171

CHEMICAL ENGINEERING DIVISION

FUEL CYCLE PROGRAMS
QUARTERLY PROGRESS REPORT

January-March 1979

by

M. J. Steindler, Milton Ader, R. E. Barletta, J. K. Bates,
C. H. Bean, R. A. Couture, E. D. Creamer, K. F. Flynn,
T. J. Gerding, L. J. Jardine, D. K. Kroeck, Michael Krumpelt,
W. J. Mecham, J. H. Meisenhelder, K. M. Myles, R. H. Pelto,
M. G. Seitz, Seymour Vogler, and Jacqueline Williams

ABSTRACT

In the program on pyrochemical and dry processing methods (PDPM) for nuclear fuel, corrosion testing of refractory metals and alloys, graphite, and SiC in PDPM environments was done and a tungsten-metallized Al_2O_3-3% Y_2O_3 crucible was successfully fabricated. Also, the tungsten microstructure of a plasma-sprayed tungsten crucible was stabilized by nickel infiltration and heat treatment. Solubility measurements of thorium in cadmium and cadmium-magnesium alloys have been continued, as have experiments to study the reduction of high-fired ThO_2. Work on the fused salt electrolysis of CaO also has continued. The method of coprocessing of uranium and plutonium by a salt transport process has been modified. Tungsten-coated molybdenum crucibles have been fabricated. The proliferation resistance of chloride volatility processing of thorium-based fuels is being evaluated by studying the behavior of fission product elements during chlorination of uranium and thorium. Thermodynamic analysis of the phase relationships in the U-Pu-Zn system was initiated. The Pyro-Civex reprocessing method is being reviewed. The reactivity of uranium dioxide and plutonium dioxide with molten equimolar sodium nitrate-potassium nitrate is being studied along with the behavior of selected fission product elements. Work was continued on the reprocessing of actinide oxides by extracting the actinides from a bismuth solution. The rate of dissolution of UO_2 microspheres in $LiCl/AlCl_3$ was measured. Nitriding rates of thorium and uranium dissolved in molten tin have been measured. In work to provide engineering support for the PDPM program, the use of a pulsed liquid packed-bed system for mass transfer operations was studied.

In work on the encapsulation of radioactive waste in metal, leach rates of a simulated waste glass have been studied. Rates of dissolution of metals (potential barrier materials) in aqueous media are being studied.

In work on the transport properties of nuclear waste in geologic media, the adsorption of iodate by hematite as a function of pH and iodate concentration was measured. The migration behavior of cesium in limestone was studied in relation to the cesium concentration and pH of simulated groundwater solutions.

SUMMARY

Pyrochemical and Dry Processing Methods Program

Materials Development for PDPM. Refractory metals and alloys were exposed to molten zinc and $CaCl_2$-KCl salt mixture at 800°C for 110-120 h in an argon atmosphere. Tungsten and W-25% Re alloys were unaffected. An adherent and nonuniform black surface coating formed on tantalum and Ta-10% W alloys, which were embrittled, but not visibly attacked. For Mo-30% W alloy, a recrystallized specimen suffered intergranular penetration with an average corrosion rate of 19.2 mils per year. An as-rolled specimen had a corrosion rate of 7.7 mils per year.

In similar tests, graphite and SiC appeared to be promising materials of construction.

Nickel infiltration and subsequent heat treatment of a plasma-sprayed tungsten crucible were very successful in consolidating the tungsten microstructure.

A tungsten-metallized Al_2O_3-3% Y_2O_3 crucible has been fabricated and is being service-tested to prove out the concept.

Thorium-Uranium Salt Transport Processing. A paper describing the reprocessing of thorium-based fuels was presented at the ACS/CSJ meeting in Hawaii, April 1-6, 1979. In addition, solubility studies of thorium in cadmium and cadmium-magnesium alloys are almost complete.

The solubility of thorium ($ThCd_{11}$) in cadmium, was measured between 329 and 569°C. In this range, the solubility is linear with respect to 1/T. At 569°C, $ThCd_{11}$ peritectically decomposes to a lower order compound.

In the cadmium-magnesium-thorium system, the solid phases in equilibrium with the solution have been studied with an electron microprobe and appear to consist of two "pseudo-binary" compounds whose compositions change with the composition of the original cadmium-magnesium alloy.

Studies of the reduction of high-fired thoria to metal indicate a low reduction rate and the need for further studies.

Preliminary experiments on the electrochemical reduction of CaO in molten 15 wt % CaF_2-$CaCl_2$ with the regenerated calcium collected in a molten alloy cathode were inconclusive, indicating the necessity of determining the decomposition potentials of the species present in the system. Study of the decomposition potentials indicated that the electrochemical reaction involving the liberation of CO/CO_2 on graphite has an overpotential of 0.6 V compared to the calculated decomposition potential. This value is similar to the overpotential observed during molten salt electrolysis of alumina, using graphite

anodes. A molten salt electrolysis of CaO has been performed at a constant potential of 3 V. Comparison of current-potential curves before and after electrolysis suggests that nearly all of the CaO had been electrolyzed.

Uranium-Plutonium Salt Transport Processing. During this period, a Waste Awareness Meeting was presented to Rocky Flats personnel. Work on the Waste Management Outline is continuing. The literature search on zinc/cladding separation is continuing. The base computer model is complete and is being used in process design, waste management, and proliferation analyses. Modifications to the Salt Transport Process Turntable conceptual design have been made and are presented. A preliminary mixer-settler conceptual design alternative is presented. Other alternative concepts to be reviewed are presented.

Laboratory studies have begun in both the Salt Purification Laboratory and the Proof-of-Principle Laboratory.

Fabrication of Process-Size Refractory Metal Vessels. The molybdenum crucibles coated with tungsten by chemical vapor deposition look very promising. No coating separation occurred during cutting of the lip nor when one crucible was thermal cycled to 850°C. The impregnation and sintering of the plasma-sprayed tungsten crucibles (plasma-sprayed with tungsten) belonging to Argonne National Laboratory is nearly complete. Metalwerk Plansee states that they can make a double layer, riveted, tungsten crucible having Palnisil 10 braze inserted between the layers for added strength. Fixturing for brazing a tungsten crucible became a major problem because of the requirements of Palnisil 10 braze.

Spinning of molybdenum crucibles was accomplished with ease in comparison to tungsten spinning. The production of additional spun tungsten crucibles was postponed.

Chloride Volatility Processing of Thorium-Based Fuels. Evaluation of the proliferation resistance of the chloride volatility coprocess was initiated. The behavior of fission product elements during the laboratory-scale chlorination of uranium and thorium was determined. The bulk of the strontium, barium and cesium remained as a residue in the boat. The antimony and ruthenium distributed between the boat and the traps. Most of the zirconium was collected in the cold trap or scrubber.

Thermodynamic analysis of the phase relationships in the U-Pu-Zn system was initiated with emphasis on the low-plutonium region at 1000°C. In addition to the analytically derived phase diagram, measurements will be made on the U-Pu-Zn system to confirm the calculations.

Material Characterization and Process Analysis. The Pyro-Civex reprocessing method is being reviewed, and an engineering analysis has been initiated as a basis for the economic analysis. Information is being obtained on fuel cycle costs associated with transportation, waste treatment, waste storage, fuel element fabrication, and plant decommissioning. A literature search of Nuclear Science Abstracts and Energy Data Base on the oxidation of uranium and plutonium alloys has been completed, and this material is being evaluated.

In addition to these tasks, AIROX closeout work has been completed. Characterization of the products from AIROX reprocessing tests has been completed, and the AIROX topical report discussing these results is undergoing internal review. The literature review of AIROX, RAHYD, and CARBOX dry processing methods has been reviewed internally, and revisions are being made.

Molten Nitrate Salt Oxidation Processes. Additional studies of the behavior of plutonium dioxide in molten equimolar sodium nitrate-potassium nitrate have confirmed preliminary tests reported in FY 1978. Plutonium dioxide does not react with the nitrate melt or form a soluble species upon the addition of 100% HNO_3 to the melt.

Initial studies have also been conducted on two compositions of mixed plutonium dioxide-uranium dioxide. One material contains 5.44% plutonium dioxide; the other material contains 27.56% plutonium dioxide. The uranium dioxide contained in the material with the lower plutonium content is oxidized without difficulty under the conditions utilized for uranium dioxide alone. For the higher plutonium content material, a higher temperature was required to initiate uranium oxidation and the rate of reaction was much less. After completion of the oxidative reaction, the uranium in both materials dissolved readily upon the addition of 100% HNO_3 to the melt. Plutonium dioxide did not react but remained insoluble throughout the experiment.

Experiments were carried out to simulate the effect of the molten nitrate melt on selected fission products. Using cesium, europium, and antimony tracers, it was found that cesium remained in the melt during the nitrate reaction step, the addition of nitric acid vapor, and the thermal decomposition step. During these steps, europium and antimony were partitioned, with most of the europium and about one-fourth of the antimony remaining in the melt.

Molten Salt Processes Applied to Nuclear Fuels. The possibility of recovery of the actinides from bismuth without the use of salt has been examined but appears to be less promising than the planned ammonium chloroaluminate extraction. Reference temperatures have been established for the lithium chloride-bismuth extractions of the uranium and coprocessed streams, and a heuristic set of solvent weights and volumes has been calculated for the extractions.

The initial rates of dissolution of UO_2 microspheres into 40/60 mol % $LiCl/AlCl_3$ mixtures have been measured at 120°C and 220°C. With sufficient stirring, the time dependence of the dissolution is the same as that previously reported for ThO_2. For low rates of stirring and small microspheres however, clumping of the microspheres greatly reduces the dissolution rate.

Molten Tin Process for Reactor Fuels. Complete data are not yet available on separation factors between uranium and thorium, but it has been observed that at 1900K, nitriding of thorium occurs at approximately one-fourth the rate of uranium. It is planned to use this kinetic effect to achieve separation.

A nitriding experiment has been completed on a $^{238}U/^{239}Pu$ mixture in molten tin, but results are not yet available.

Engineering Support for the PDPM Program. A dimensionless correlation for a pulsed liquid, packed bed system as an alternative to impeller mixing for mass transfer operations was confirmed experimentally. The dissolution of brass in an aqueous iodine-sucrose solution was utilized as an investigative technique. The degree of agitation produced in a pulsed, packed bed as expressed by the Sherwood number, Sh, was related to the pulsating action represented by the Reynolds number, Re, and the physical properties of the solution as characterized by the Schmidt number, Sc, by:

$$Sh = 1.6Re^{1/2} \quad Sc^{1/3}$$

This dimensionless correlation can be extended to pulsed-bed oxide reduction studies to determine if any of the reactions are mass transfer limited.

Encapsulation of Radioactive Waste in Metal

The effect on the leach rates of radioisotopes of changing various parameters associated with the leaching medium has been studied using neutron activation analysis techniques. For the particular waste form studied (a simulated high-level waste glass), the effects of pH and salinity were small. However, the effect of increasing the temperature was dramatic--particularly at the high temperatures that may be associated with future short-cooled reprocessing wastes. Large differences as a function of temperature were observed in the leaching behavior of chemically dissimilar elements such as cesium and europium. Possible explanations of this behavior and a proposed experimental program to establish the significance of this behavior are presented.

Studies of the rate of dissolution of metals by interaction with aqueous media have been initiated. Preliminary experiments have established that the neutron activation technique which has been suitable for nuclear wastes is also suitable for determinations for metals. Metals are being evaluated which have been suggested as potential canister or matrix (barrier) materials in the disposal of high-level waste.

In this quarterly report, relevant topics on (1) engineering studies of brittle fracture and (2) materials science studies of fracture mechanics of ceramics are summarized. The descriptive and calculational models of impact deformation of solid waste forms in a paper to be presented at a technical meeting are summarized.

Trace-Element Transport in Lithic Material by Fluid Flow at High Temperature

The isotherm for adsorption of iodate by hematite is reported as a function of pH and iodate concentration. Hematite can adsorb over 10 μmol IO_3^-/g Fe_2O_3 in slightly acidic solutions but appears to have near-zero capacity at a pH about 9 or 9.5. It is suggested that iodate may have an affinity for the iron oxides that occur in rocks, sediments, and soils.

Transport Properties of Nuclear Waste in Geologic Media

Previous work in this program demonstrated that the migration behavior observed for cesium in limestone depends upon how the groundwater solution containing cesium is formulated. Cesium leached from a glass was seen to be more mobile than cesium (added as CsCl solution) diluted in a large quantity of groundwater, and the latter, in turn, was more mobile than cesium in a concentrated CsCl solution added directly to rock.

This quarter's efforts focused on understanding these differences. We found that the amount of cesium adsorbed by limestone varies nonlinearly with cesium concentration at concentrations from about 10^{-3}M to as low as 10^{-9}M cesium. This effect is probably due to the very low exchange capacity of limestone and can explain the differences in cesium behavior seen in this program. The effect may also be responsible for large discrepancies in partition coefficients measured in different laboratories and invalidates the use of a single partition coefficient to describe cesium migration in limestone for solutions containing more than 10^{-9}M cesium.

To examine the effect of solution pH on cesium migration, infiltration experiments with columns of limestone were done with groundwater solutions of differing pH. Results showed that cesium migration is not dependent of pH, probably because of buffer capacity of the limestone.

During this quarter, we concluded that nonlinear adsorption of radionuclides by rock caused by a limited exchange capacity of the rock strongly affects nuclide migration by flowing groundwater in geologic formations. Nonlinear adsorption ranks with slow reaction kinetics (previously documented) in generating migration behavior different from that currently assumed in migration models.

I. PYROCHEMICAL AND DRY PROCESSING METHODS PROGRAM
(C. H. Bean, K. M. Myles, and M. J. Steindler)

A. Introduction

A Pyrochemical and Dry Processing Methods (PDPM) Program (Table 1) was established at the beginning of FY 1978 within the Chemical Engineering (CEN) Division Fuel Cycle Section at Argonne National Laboratory (ANL). Upon redirection of the Fuel Cycle Development Program by DOE for FY 1979, the PDPM Program was included in the Consolidated Fuel Reprocessing Program under the direction of Oak Ridge Operations/Oak Ridge National Laboratory (ORO/ORNL). Under this arrangement, ANL continues to provide PDPM work plans, management plans, and cost plans to the Chicago Operations Office (CH) for approval as required by DOE. Additional work authorization and agreement forms for each of the PDPM Program subtasks are submitted to the Chicago Operations Office for approval by ORNL. The CEN Fuel Cycle Section continues to provide the technical direction of the PDPM Program.

The PDPM Program provides for the reprocessing of spent fuel by processes that reduce the risk of proliferation of nuclear weapons. The work on this program is being performed at ANL, by other DOE multipurpose laboratories, and by industrial contractors.

B. Management
(C. H. Bean, K. M. Myles, and Seymour Vogler)

The PDPM Program was reviewed by ORO/ORNL at a meeting with ORNL Consolidated Fuel Reprocessing Program management on January 11, 1979. Reviewed were the program budget for FY 1979, the technical program plan, program management, and reporting requirements. To comply with the Consolidated Fuel Reprocessing Program reporting requirements, ORNL requested monthly and quarterly technical progress reports and monthly cost reports from the PDPM Program. These requirements are not inconsistent with ongoing PDPM reporting requirements except that the deadline for reporting requires an earlier cut-off for reported effort each month. This results in some inconsistency in the information contained in ORNL reports vis-a-vis ANL reports.

The PDPM Program Management agreed to provide ORO/ORNL with Work Authorization and Agreement (WAA) statements for each of the three subtasks identified in the PDPM Work Breakdown Structure. These subtasks, PDPM Program Management, Studies and Analysis, and Fuel Reprocessing, constitute the basis for the levels of program reporting. Completed WAA statements were submitted to CH for transmittal to ORO/ORNL on January 12, 1979. The WAA statements were approved by ORNL on March 9, 1979.

After final program approval and authorization of PDPM Program operating and equipment funds by ORO/ORNL for FY 1979, requisitions and contract revisions were completed to cover the distribution of operating funds to PDPM contractors. Equipment requirements were evaluated and individual items were identified to establish the most effective use of available funds. All equipment has been ordered for delivery in FY 1979.

Table 1. PDPM Work Packages

Work Package No.	ANL Activity	Work Package Title	Location
00	OO	Management Planning, Reporting, Costing, and QA	ANL
01	AO	Materials Development for PDPM	ANL
02	BO	Carbide Fuel Processing	ANL
03	CO	Thorium-Uranium Salt-Transport Processing	ANL
04	DO	Uranium-Plutonium Salt-Transport Processing	RI-RF[a]
05	EO	Fabrication of Process-Size Refractory Metal Vessels	RI-RF
06	FO	Aluminum-Alloy Processing of Thorium- and Uranium-Based Fuels	IRT[b]
07	GO	Chloride Volatility Processing of Thorium-Based Fuels	B&W[c]
08	HO	Material Characterization and Process Analysis	RI-AI[d]
09	JO	Molten Nitrate Salt Oxidation Processes	PNL[e]
10	KO	Molten Salt Processes Applied to Ceramic Fuels	ORNL[f]
11	LO	Reprocessing of Thoria-Urania Fuel in Molten Salt Containing $ThCl_4$	AMES[g]
12	MO	Molten-Tin Process for Reactor Fuels	LLL[h]
13	NO	Engineering Support for PDPM Processes	ANL

[a]Rockwell International - Rocky Flats

[b]IRT Corporation.

[c]Babcock & Wilcox

[d]Rockwell International-Atomics International.

[e]Pacific Northwest Laboratory.

[f]Oak Ridge National Laboratory.

[g]Ames Laboratory.

[h]Lawrence Livermore Laboratory.

The draft report, "A Proliferation Evaluation of an Exportable Pyrochemical Process," being compiled by ORNL was reviewed by ANL, and comments were forwarded to ORNL. Comments included details of process chemistry, additional analysis of the reference Zinc Distillation Process, and a comparison of proliferation resistance and exportability of PDPM reprocessing with aqueous reprocessing. It is expected that the ORNL study will show an assessment of technology requirements, key areas of concern, and identification of problem areas for pyro processes. The report will highlight the positive features of pyro processes, particularly the nonproliferation advantages.

Meetings were held with several of the PDPM contractors to review the status and direction of FY 1979 work packages. Since the Chloride Volatility process is being phased out at B&W, the process is being analyzed for its proliferation resistance, using criteria identified in the ORNL draft report discussed above. Effort at B&W has been redirected to include the development of a U-Pu-Zn ternary phase diagram to support the Zinc Distillation Process. Engineering for the process scale-up of the U-Pu salt transport process was reviewed with principal investigators at Rocky Flats. This scale-up study is an extension of studies conducted as input to the ORNL draft report and will be useful for an economic analysis of the process. The scope of redirected effort for Work Package 08 was reviewed with Atomics International Division, Rockwell International, in January. The revised FY 1979 ANL Statement of Work (0030-0096, Revision II) provided AI with additional guidance for the analysis of the reference Zinc Distillation Process for reprocessing of (U, Pu)O_2 fuel. Atomics International will also investigate the retention of ruthenium in the actinide product during conversion from metal to sinterable-grade oxide fuel.

A performance appraisal of the PDPM Program was conducted by a DOE appraisal team from NPD-HQ, RPD-CH, and OPE-CH during the week of January 29. There were no reported findings for corrective action, change in program direction, or change in program management.

C. Engineering Analysis and Separations Processes

In the engineering analysis, prior work will be be examined and evaluated. From these evaluations, a flowsheet will be devised for each of the prospective reprocessing techniques. Gaps in the data which must be filled to obtain an operable flowsheet will be filled by experimental work carried out under the separations process subtasks.

1. Materials Development for PDPM

(R. M. Arons* and J. Y. N. Wang*)

The project objectives are to anticipate, identify, and scope potential materials or materials fabrication problems that may limit the practical realization of candidate processes in the PDPM program; to devise,

*Materials Science Division, Argonne National Laboratory.

through analytical and experimental methods, means to resolve these problems; to assess the refabricability of the fuel after reprocessing; and to provide program support to the PDPM Program Office by coordinating materials activities and by lending technical assistance within the program.

a. Engineering Analysis
(J. Y. N. Wang*)

Certain systems consisting of liquid metals and halide salts are potential candidate solvent media in the PDPM [LAWROSKI-1964]. For containment of these systems, metallic tungsten has excellent molten zinc-halide salt resistance [LAWROSKI-1963]. However, tungsten is known to be very difficult to fabricate [WINSCH-1967] and has a high DBTT (ductile-brittle transition temperature) and a high cost. Molybdenum and its alloys are fabricable and have a useful DBTT and a lower cost. A molybdenum-30% tungsten alloy (Mo-30% W) has been rated a close second to tungsten in corrosion resistance to molten zinc-halide systems [LAWROSKI-1963, HODGE, BURMAN-1963, KYLE]. Thus, there is a distinct possibility that molybdenum alloys could be alternatives to tungsten as PDPM container materials.

Earlier work on the molybdenum-zinc system is very sketchy. Some investigators [KOSTER] concluded that molybdenum and zinc do not alloy at 1200°C. Others observed definite and measurable solubility of molybdenum in zinc at temperatures as low as 440°C [LAWROSKI-1959].

The difference may be explained by the difference in behavior of molybdenum in static versus dynamic testing systems. The solubility of molybdenum in molten zinc was determined [MARTIN-1961, LAWROSKI-1963] in an essentially static system. Results indicate that between 550 and 750°C the solubility reaches a low but constant saturation value of about 0.022 wt % Mo. The solubility curve at 550°C shows a peritectic reaction. The phase in equilibrium with the melt at temperatures below the peritectic is an intermetallic phase, possibly $MoZn_6$. In a dynamic system, the solubility trend would be different because saturation at the interface between the liquid and the solid would be greatly decreased.

A corrosion test of Mo-30% W in a zinc-halide salt system at 800°C was performed under dynamic test conditions and argon cover gas [LAWROSKI-1963, NELSON]. Specimens were exposed as agitator blades, fastened to a tungsten shaft with tungsten wires. A recrystallized alumina crucible was used as the container. Results of the test are summarized in Table 2. The 3.5% weight loss suffered by the specimen is equivalent to 5% of the molybdenum in the original specimen and would result in a molybdenum concentration in the 1350-g zinc bath of 70% of the saturation limit of 0.022% molybdenum in zinc [MARTIN-1961]. The exposed surface parallel to the direction of swaging showed uniform molybdenum leaching to a depth of 4 mils. However, the exposed surface perpendicular to the direction of swaging appeared to be irregular, with molybdenum leached to a maximum depth of 8 mils. Chemical analysis indicated that the area of attack contained 40% Mo rather than the initial 70%.

*Materials Science Division, Argonne National Laboratory.

Table 2. Corrosion of Mo-30W by Molten Zinc and Molten $LiCl-MgCl_2-ZnCl_2$

Test material	Arc-cast and swaged Mo-30% W
Weight change of Mo-30 W specimen, %	-3.5 (400 h)
Thickness change, mils	0
Depth of attack, mils	4-8
Type of attack	Molybdenum leaching

Burman and Litchfield [BURMAN-1963] believed that the corrosion of Mo-30% W exposed to flowing zinc at temperatures up to 600°C can be tolerable. No corrosion rates were indicated. However, the corrosion resistance was demonstrated by the fact that a full-size zinc pump element made of Mo-30% W showed no visible signs of attack at about 550°C after handling more than 30,000 tons of molten zinc.

An ANL-fabricated marine-type propeller [LAWROSKI-1962] was exposed in two 500-h runs at 800°C and 525 rpm rotation speed in a Zn-5% Mg-4% U metal phase and a 47.5 mol % $MgCl_2$-47.5 mol % LiCl-5 mol % MgF_2 salts phase. The propeller suffered pitting attack to a depth of 10-20 mils. U-shaped transfer tubes fabricated from gun-drilled swaged molybdenum-30 wt % tungsten rods have also been used successfully in flowing molten zinc-halide salt systems [GROSVENOR]. Although the exact chemical composition, microstructure, and mechanical properties of the alloy before and after exposure were not documented, the performance of this material was impressive.

Molybdenum-30 wt % W and TZM (Mo-0.5% Ti-0.08% Zr) are two principal molybdenum alloys that are commercially available today. The latter alloy has been improved by changing the composition to TZC (Mo-1.25% Ti-0.3% Zr-0.15% C). Additional alloys such as Mo-1.2% Hf-0.1% C and Mo-0.6% Zr-0.1% C are in the final development stage [BURMAN-1977].

The last three alloys required special processing to achieve a fine, uniform matrix precipitation with an acicular dispersion that provides additional barriers to dislocation movement. The Mo-Hf alloy had superior strength, with measurable ductility at room temperatures [NELSON].

The hafnium-zinc constitutional diagram is not available at present. However, the molybdenum-hafnium phase diagram has been determined [TAYLOR-1961]. The body-centered-cubic alpha-molybdenum primary solid solution extends to about 16.5 at.% Hf at 1000°C and 28 at.% Hf at 2165°C, at which temperature it reacts peritectically with liquid to form epsilon-Mo_2Hf, a hexagonal Laves phase. Since hafnium is highly reactive and exhibits a higher melting point than the other two Group IV members in the periodic table

(titanium and zirconium), hafnium may act as a deoxidation agent in alloys with molybdenum. Thus, there is a possibility that preferential penetration of the new alloy in the molten zinc-halide system will be reduced.

A PDPM corrosion evaluation program for metallic materials has been previously formulated [HAFSTROM]. This information, combined with literature information available and some experimental results recently obtained (see Section b below), provides a basis for recommending that molybdenum alloys be given the highest priority within the test program.

b. Experimental

(1) PDPM Environmental Test Facility (PETF)
(R. M. Arons* and D. J. Dorman*)

Interruption of a corrosion test as a result of seizure of the middle pump bearing was reported in the preceding report in this series [STEINDLER-1979B]. However, careful posttest examination revealed that rotation of the drive shaft was halted by solidified salts in the pump tube, not by bearing seizure. Molten salt had seeped through the bearing, driven by the pressure head of the pump itself. As the molten salt contacted the colder parts of the pump tube (above the hot zone of the furnace), the salts froze, binding the shaft. The pump design was subsequently modified by feeding argon gas into the top of the pump tube and blowing any stray salt out through drain holes machined just above the middle bearing.

A pump modified in the manner described above was run successfully for a complete run of 120 h. Posttest examination showed that the tube was free of residual salts and that the bearings were only slightly worn.

Other modifications had the objective of increasing pump life by selecting different materials of fabrication to allow extended test runs and multiple runs on a single pump. Use of a diamond-polished alumina-bearing journal and graphite bearings has been very successful in reducing bearing wear. This should increase both bearing lifetime and reliability.

An attempt was made to substitute a molybdenum pump housing for the tantalum pump housings used in previous tests. A pump so constructed was run for about 60 h, at which time the pump failed. Contrary to our expectations (based on the good performance of a molybdenum test coupon), the molybdenum tubing was more severely attacked than was the tantalum used in previous runs. Considerable intergranular attack had occurred, weakening the metal and resulting in fracture of the pump housing. The poor corrosion properties of this tube may be a result of fabrication history and should not be construed as indicative of the corrosion properties of molybdenum in general. The tube in question was fully recrystallized prior to use, resulting in poor intergranular corrosion resistance. (All molybdenum tubing must be heat treated, which results in such recrystallization.)

*Materials Science Division, Argonne National Laboratory.

A second and much more successful materials substitution was the use of a graphite pump housing. A graphite-housed pump with graphite bearings, polished alumina journals, and tantalum shaft and impellers was operated for 120 h with no visible material degradation. Except for routine cleaning, no work will be required for use of this pump in a second test run. We expect this type of pump to provide much longer service, to cut pretest time and costs considerably, and to permit extended lifetime testing (>120 h).

(2) Metallic Materials

(J. Y. N. Wang,* R. M. Arons,* D. J. Dorman,* and L. J. Marek†)

Refractory alloys Mo-30% W, TZM (Mo-0.5% Ti-0.08% Zr), W-25% Re, and Ta-10% W, and their respective pure metals were exposed to molten zinc and $CaCl_2$-KCl salt mixture at about 800°C under argon cover gas for 110 to 120 h.

Materials as-received from suppliers include recrystallized and as-rolled structures. Chemical analysis of alloying constituents revealed that the Mo-30% W contained 28.0% W, that W-25% Re contained 25.26% Re, and that Ta-10% W contained 9.73% W. All pure metals were commercial grades with purities greater than 99.95%. Results for carbon, oxygen, and hydrogen analyses of the material are not available at this time.

Figure 1 is a micrograph showing intergranular penetration of a recrystallized molybdenum specimen after about 120 h of exposure at about 800°C. The average corrosion rate, based on about 120-h exposure, was 19.2 mils per year.

An as-rolled Mo-30% W alloy, fabricated below the recrystallization temperature, had a corrosion rate of about 7.7 mils per year upon exposure to zinc and molten $CaCl_2$-KCl. No preferential attack was detected. A micrograph of the posttest surface of this alloy is shown in Fig. 2.

Posttest TZM specimen examination was not conclusive because mechanical damage occurred during the experiment.

The behavior of molybdenum differs from that of most common metals. Nonmetallic impurities in commercial molybdenum (99.95% Mo) migrate toward the grain boundaries and decrease the grain-boundary strength. If these grains are equiaxial, the material is prone to intergranular penetration and stress cracking. Alternatively, if the molybdenum is fabricated so that the grains are elongated, they interlock and the metal is ductile and consequently more resistant to corrosion attack in molten zinc-molten $CaCl_2$-KCl mixtures. Separate tests to examine the implications of various grain morphologies are in progress.

---

*Materials Science Division, Argonne National Laboratory.

†Accelerator Research Facilities, Argonne National Laboratory.

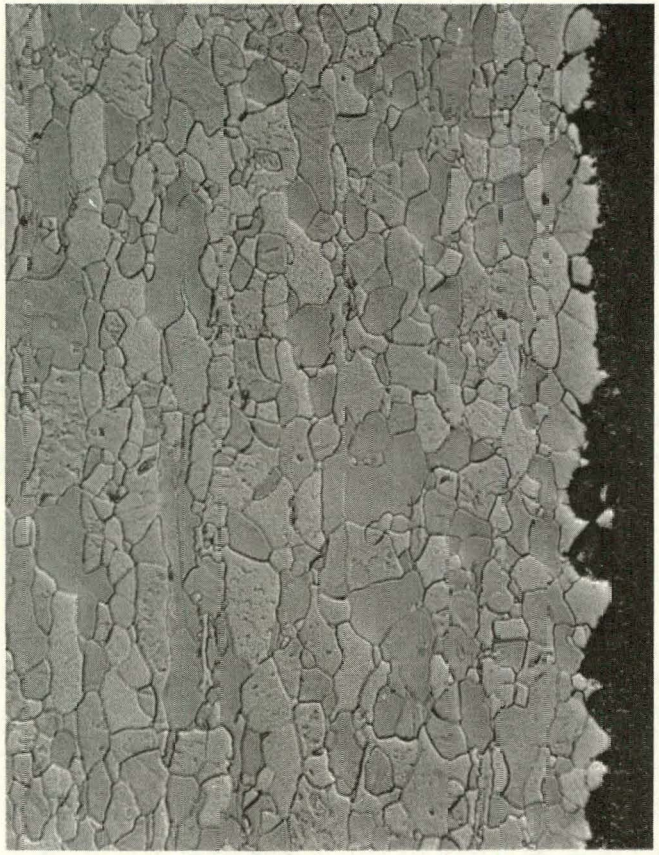

Fig. 1. Micrograph of a Recrystallized Mo-30% W Alloy after about 120 h Exposure to Zinc and Molten $CaCl_2$-KCl Salt System at about 800°C. Magnification, 200X. ANL Neg. No. 306-79-423

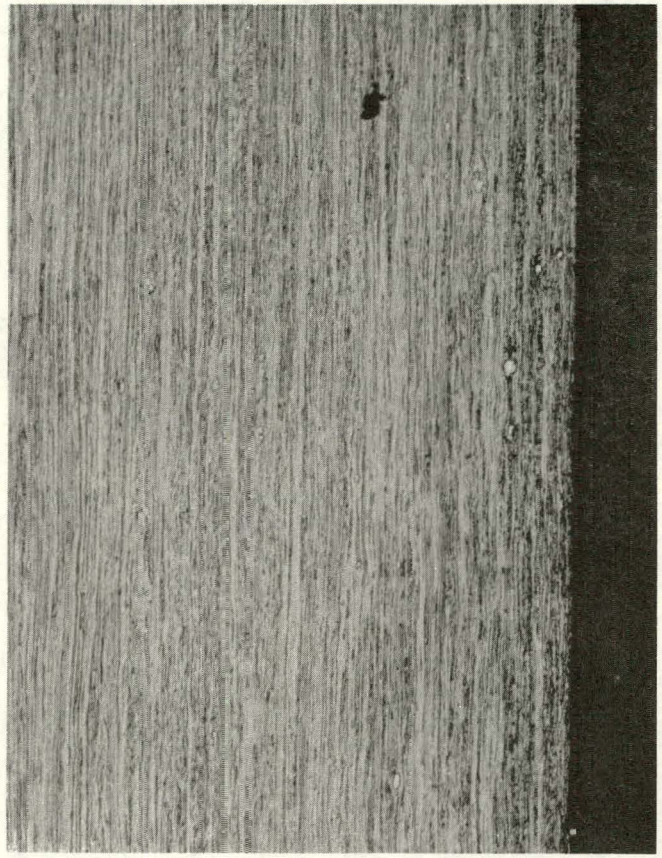

Fig. 2. Micrograph of an As-rolled Mo-30% W Alloy after about 120 h Exposure to Zinc and Molten $CaCl_2$-KCl Salt System at about 800°C. Magnification, 200X. ANL Neg. No. 306-79-423

On tantalum and Ta-10% W alloys, an adherent and nonuniform black surface coating formed upon exposure to the metal-salt system. Microhardness measurements showed Vicker's hardness values (HV) of the coating and the underlying material of 843 and 416 (each an average of four numbers), respectively. The materials were embrittled but not visibly attacked.

As expected, tungsten and W-25% Re alloys were unaffected.

(3) Ceramic Materials
(R. M. Arons* and D. J. Dorman*)

Screening of proposed materials for process containment was done for about 60 h at 800°C in a mixture of pure zinc and a eutectic $KCl-CaCl_2$ salt. Test specimens included pyrolytic boron nitride (BN), hot-pressed boron nitride, titanium diboride (TiB_2), titanium nitride (TiN), titanium carbide (TiC), and graphite (CGW grade).

A second screening test was run in a similar environment for 120 h on five grades of silicon carbide (SiC) (including one pyrolytic grade) and one specimen of silicon oxynitride (Si_2ON_2).

In the first test, both BN specimens suffered considerable corrosion. Based on weight loss, the pyrolytic BN lost 0.64 mil per 60 h or the equivalent of 93 mils/y (mpy). The hot-pressed sample was covered with a black corrosion product which spalled off in some areas. Despite the existence of this poorly adherent film, a net weight loss equivalent to 2.5 mils per 60 h or 365 mpy was observed. It is worthwhile to note that pyrolytic BN is the purest available form of BN and is therefore expected to be the most corrosion-resistant form. On the basis of these results, BN is being removed from the candidate list.

The TiN sample was of low density and low strength. It crumbled during posttest cleaning and no weight change could be determined. TiB_2 and TiC both experienced weight gains and were covered with a thin, black, poorly adherent film. Figure 3 shows representative corrosion product observed on all Ti-base ceramics. The SEM micrograph shows the corrosion product (right) adhering to the substrate (left). The associated X-ray images show the corrosion layer to be a calcium-rich product, evidently a result of attack by the $CaCl_2$ salt. Use of this salt should be avoided when Ti-base materials are used for hardware.

Graphite experienced a small weight gain, which was probably due to some infiltration of process fluids into the partially porous structure. SEM examination showed no attack of the material, and no corrosion products could be found. On this basis, graphite is still considered to be a promising material.

---

*Materials Science Division, Argonne National Laboratory.

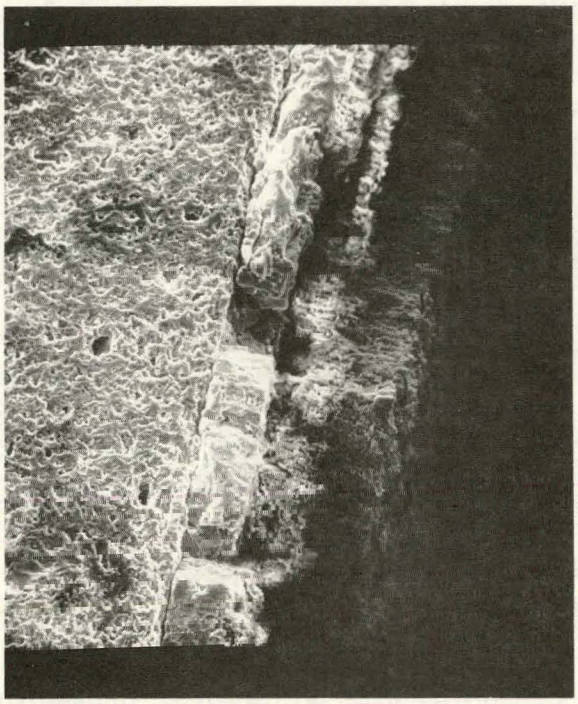

TiB_2

TEST #4

800°C

Zn, KCl-$CaCl_2$

120 H

33 μM

SEM

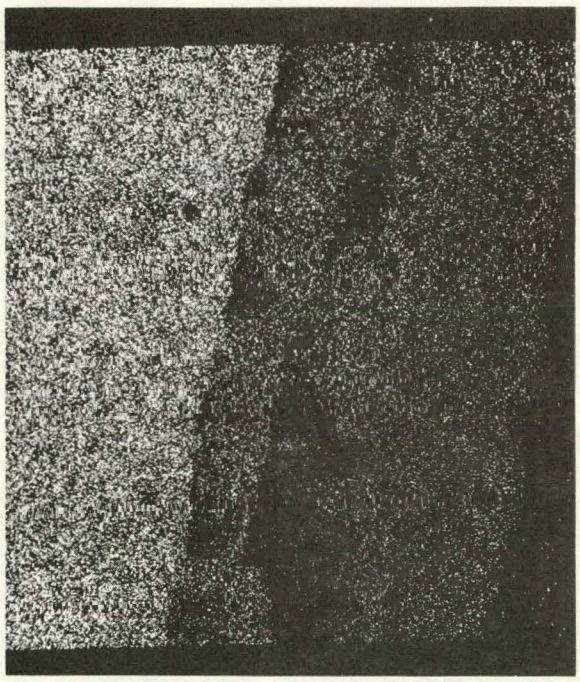

Ti SCAN

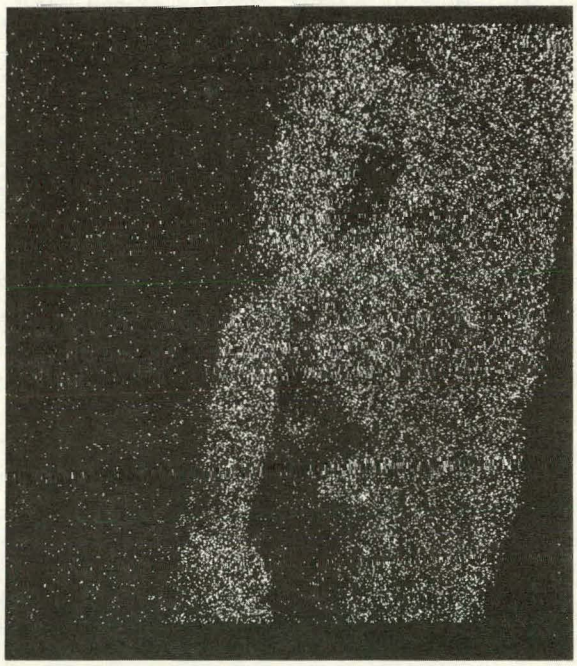

Ca SCAN

Fig. 3. Scans of Titanium Diboride After Exposure to a Mixture of Zinc and KCl-$CaCl_2$ Eutectic for 120 h at 800°C. Test 4. ANL Neg. No. 306-79-422.

A preliminary investigation of the SiC samples showed almost no weight change for four of five samples. The fifth sample had a slight weight gain. However, low-power light microscopy showed no observable attack or corrosion products on any of the samples. SEM microscopy is planned to confirm this absence of attack. SiC appears to be very promising.

Si_2ON_2 showed some attack and appeared to be pitted. The nature of this attack is not yet determined.

(4) Plasma-sprayed Tungsten
(R. M. Arons*)

Nickel infiltration and subsequent heat treatment of a plasma-sprayed tungsten tube was very successful in consolidating the tungsten microstructure. In this work, a plasma-sprayed tube was infiltrated under vacuum with an aqueous $NiCl_3$ solution returned to atmospheric pressure, and dried. It was then fired in pure hydrogen for 1 h at 1000°C and for 3 h at 1300°C. Figure 4 shows pre- and post-treatment micrographs of the tungsten. It is evident from these micrographs that virtually all porosity existing in the as-sprayed material was eliminated by the heat treatment, and that considerable grain growth occurred. Density was measured to be 18.4 g/cm^3 or 95% T.D.

Heat treatment resulted in a 3.3% shrinkage on the OD of the tube and a 17.0% shrinkage of the wall thickness of the tube. This anisotropy of shrinkage indicates that most consolidation occurs in the direction of prior spraying.

Chemical analysis of the heat-treated tube shows that the tungsten contains only 0.04% nickel, indicating that only small nickel additions are necessary to promote sintering. It is unlikely that such a small nickel content will affect the corrosion properties.

(5) Tungsten Metallization
(R. M. Arons* and J. T. Dusek*)

Three additional tungsten-metallized Al_2O_3-3% Y_2O_3 crucibles have been fabricated, using either brush coating or air brushing for tungsten application. All crucibles appear to have good, crack-free, dense adherent coatings on the inside. (Outside coatings on two of the crucibles are cracked, possibly due to proximity to heating elements in the furnace during firing.) One crucible which had been brush coated with the tungsten slurry before firing cracked during cooling. This crucible was sectioned for metallographic examination, and a coupon was cut for corrosion testing. The other two crucibles were air brushed (a paint-spraying technique) with tungsten slurry, then fired. One of these crucibles is shown in Fig. 5. One crucible is being service-tested for durability of the coating and to prove out the concept of tungsten-coated ceramic crucibles.

*Materials Science Division, Argonne National Laboratory.

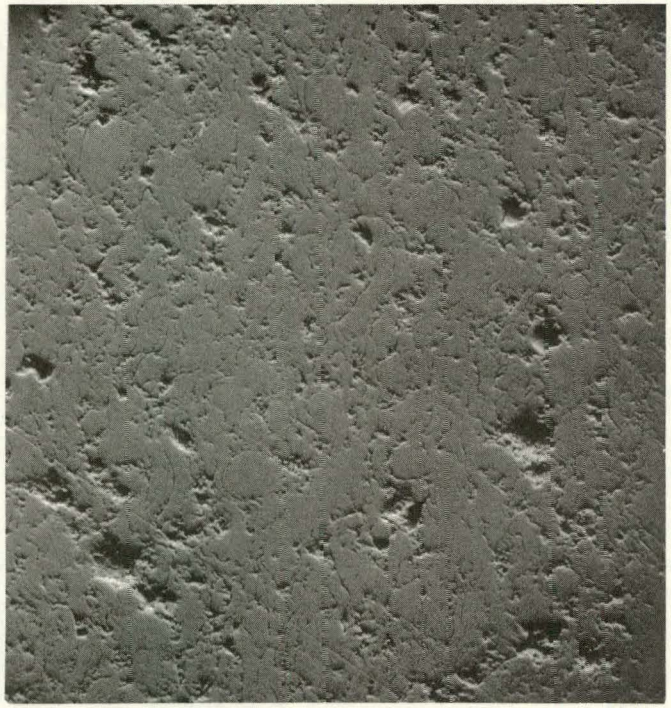

(a)

(b)

Fig. 4. Micrographs of Plasma-sprayed Tungsten. (a) As-sprayed condition, polished, and (b) nickel-treated, sintered, polished, and etched. Magnification, 600X. ANL Neg. No. 306-79-421

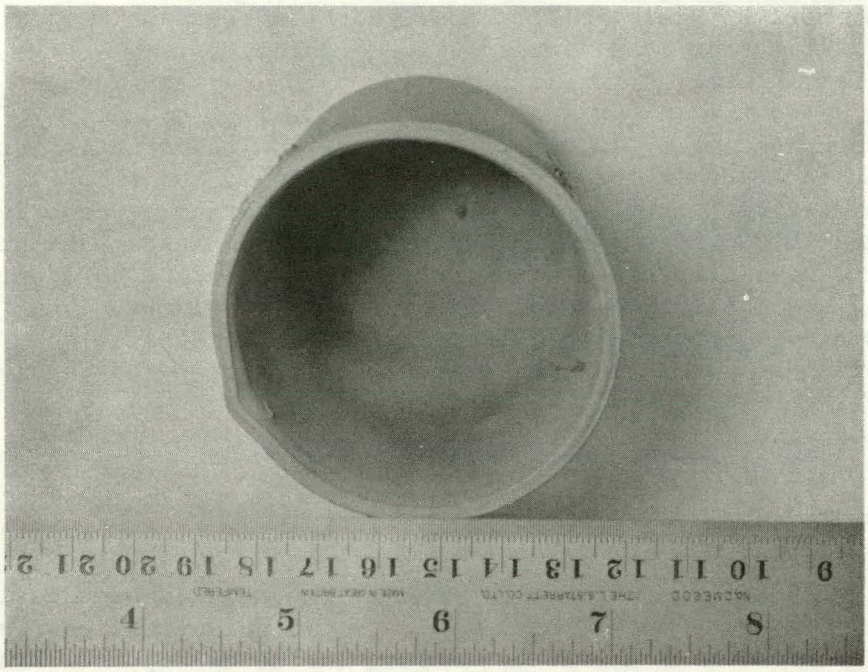

Fig. 5. Tungsten-coated Alumina-Yttria Crucible.
ANL Neg. No. 306-79-424

(6) Publication

R. M. Arons, J. T. Dusek, and J. W. Hafstrom, Development of Tungsten Coatings for the Corrosion Protection of Alumina-based Ceramics, submitted for publication in the Proceedings of the International Conference on Metallurgical Coatings at the Sixth International Vacuum Metallurgy Conference, San Diego, CA, April 23-27, 1979; to be published in Thin Solid Films.

2. Carbide Fuel Reprocessing
(Milton Ader)

Equipment assembled for evaluating the reaction of carbides with $CdCl_2$ was checked by measuring the solubility of thorium in cadmium-magnesium alloys. These data are reported in the thorium-uranium salt-transport processing section.

Because of the termination of funding for the PDPM program for FY 1980, it has been decided to concentrate the remaining effort on those portions of the program that had progressed further than had the carbide fuel work.

3. Thorium-Uranium Salt-Transport Processing
(Michael Krumpelt, Milton Ader, R. E. Barletta, J. K. Bates, T. J. Gerding, L. J. Jardine, D. K. Kroeck, O. C. Linhart, and J. H. Meisenhelder)

The objective of this program is to examine concepts for the selective transfer of spent fuel constitutents between molten alloys and/or molten salts and to develop process flowsheets for the thorium-based oxides and metal fuels. Initial flowsheets will be based on published data and thermodynamic evaluations. These flowsheets will be analyzed in detail to identify potential problem areas and missing data as part of an engineering analysis subtask. Laboratory-scale experiments will be instituted as a separations processes subtask in order to generate data required to establish the feasibility of selected flowsheets.

a. Thorium Salt Transport

Pyrochemical processes involving salt-transport and metal precipitation steps are currently being investigated for use in projected thorium-based fuel cycles. The reference flowsheet (Fig. 6) has been designed to meet proliferation standards and is applicable to plutonium-thorium transmuter and undenatured thorium-uranium breeder fuels. The necessary criteria are that the fissile streams be coprocessed (Th:Pu-U ratio of 4:1) and be diversion-resistant as a result of inclusion of some fission products. A paper entitled "A Nonaqueous Reprocessing Method for Thorium Based Fuels," which describes this process along with some experimental highlights, is to be presented at the ACS/CSJ meeting in Hawaii, April 1-6, 1979.

(1) Solubility Studies

(a) Cadmium-Magnesium-Thorium System

In solubility studies on the cadmium-magnesium-thorium system, it is necessary to identify the solid phase in equilibrium with the liquid because if thorium precipitates as an intermetallic compound, there might be simultaneous coprecipitation of plutonium, rendering the process separation ineffective. Initial attempts [STEINDLER-1979B] to identify this phase involved electron microprobe and X-ray diffraction techniques, but the results were inconclusive. It was evident, however, that in all metal samples, two separate regions are clearly identifiable. Region 1, comprising the upper portion of the ingot, has a metallic appearance, whereas region 2, the lower portion, is much darker. After leaching with ammonium nitrate, a black powder can easily be scraped from region 2. This black powder has been identified as having the Th_6Mg_{23} structure, but with a lattice parameter that varies with the magnesium and cadmium content of the melt.

Additional electron microprobe results of improved reliability have been obtained which aid in clarifying the situation. Results are reported for two samples 5-4 and 5-6. These ingots were prepared from Cd-Mg alloys (80:20 wt %) by saturating them with thorium, equilibrating, and quenching. Sample 5-4 was rapidly quenched, whereas sample 5-6 was slowly cooled.

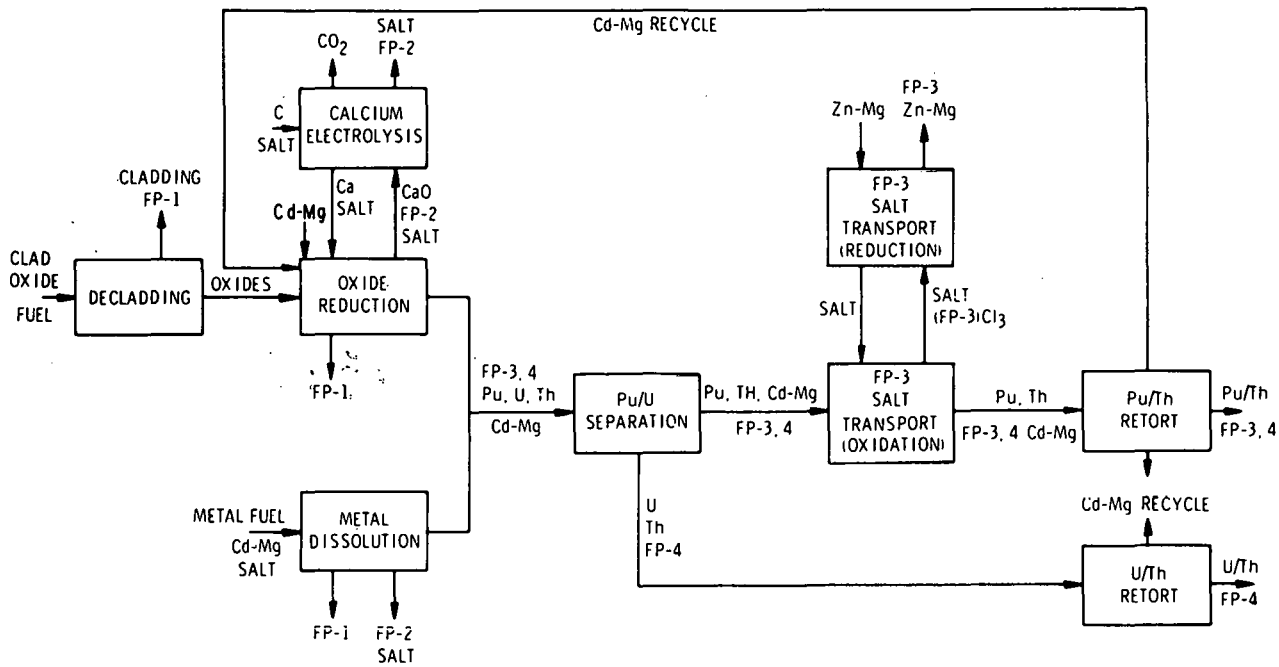

Fig. 6. Conceptual Flowsheet for Thorium-Based Fuels. FP-1: Xe, Kr, ^3H; FP-2: I, Br, Cs, Rb, Ba, Sr, Sm, Eu, Se, Te; FP-3: trivalent rare earths, Y; FP-4: Zn, Nb, Mo, Tc, Ru, Rh, Pd, Hg, Cd, In, Sn, Sb.

The results show that in both samples, region 1 consists of two phases. One phase ($ThX_{12.5}$) has the appearance of large granite blocks with the following composition (wt %): Cd(66.17), Mg(13.08), and Th(20.73). The atom ratio is Cd(6.5):Mg(6):Th:(1). The second phase is Cd-Mg having a composition (wt %) of Cd(75) and Mg(25).

Region 2 consists of both of the above phases, along with two additional phases. These additional phases consist of a primary phase and a solid precipitate that originates from the primary phase. This precipitated phase forms as the primary phase cools and is found only associated with the primary phase. The composition of the primary phase (wt %) is Cd(51.8), Mg(7.6), and Th(40.6), with an atom ratio of Th:Cd+Mg of 1:4.4. The precipitated phase is slightly enriched in cadmium and depleted in thorium. Surrounding this primary phase is the phase, $ThX_{12.5}$. The overall appearance of the alloy is that of a primary phase decomposing peritectically. The smallest primary phase crystals, which would be found near the top of the melt, would completely decompose, and this region (region 1) would consist of only $ThX_{12.5}$ and Cd-Mg. The larger primary phase crystals, found near the bottom of the melt, would decompose only partially, and in this region (region 2), four phases would be observed. The primary phase is probably a "pseudo" binary phase which, as suggested by the X-ray data, would have a composition

that varied as the initial Cd:Mg ratio of the melt changed. A more complete description of the ternary system will be given when the remaining samples have been analyzed.

(b) Cadmium-Thorium System

The solubility of thorium in cadmium has been determined over the temperature range from 325 to 600°C. The samples were taken in the standard manner. The results, which will be helpful in constructing the binary (Th-Cd) phase diagram, are presented in Fig. 7 and Table 3. Experimental conditions are also listed in Table 3. Included in Fig. 7 are the previous results obtained at ANL [MARTIN-1959]. Importantly, equilibrium was reached since samples taken with increasing and decreasing temperatures (not differentiated in the graph) give similar results.

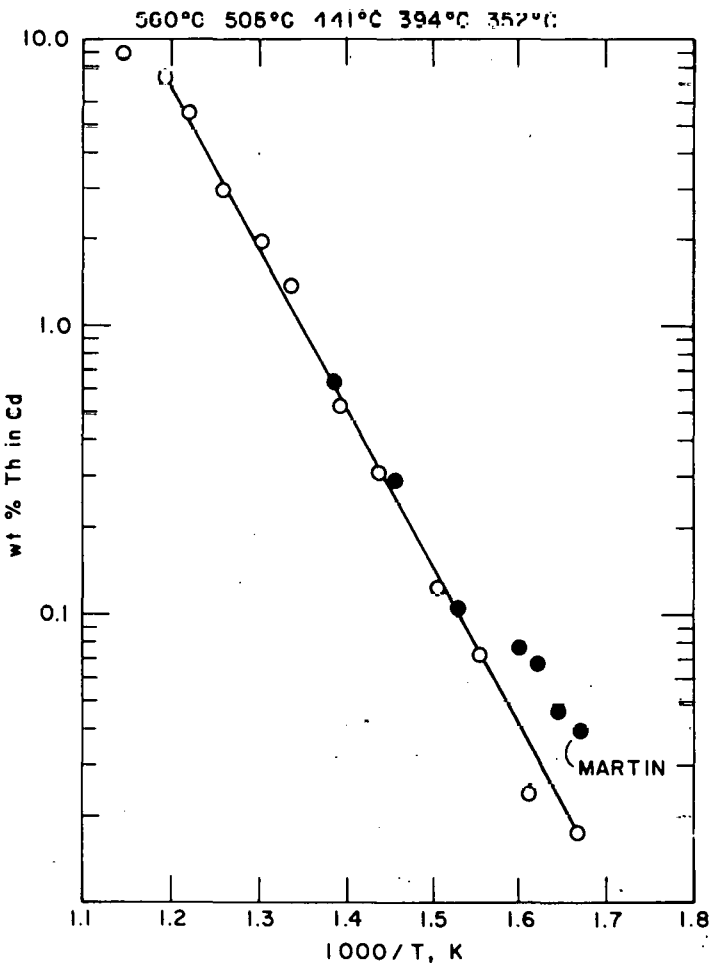

Fig. 7. Solubility of Thorium in Cadmium. Data represented by squares are from [MARTIN-1959].

Table 3. Solubility of Thorium in Cadmium at 325°C to 600°C

Temp, °C	1000/T, K	Thorium Solubility wt %	Thorium Solubility at.%
600	1.145	8.993	4.57
568	1.189	7.266	3.65
550	1.215	5.460	2.72
523	1.256	2.976	1.46
497	1.298	1.963	0.96
471	1.343	1.393	0.68
447	1.389	0.5626	0.27
423	1.437	0.3154	0.16
390	1.508	0.1255	0.06
371	1.552	0.07427	0.03
347	1.613	0.02465	0.01
327	1.666	0.01768	0.01

The present data form a straight-line plot ([x] vs 1/T) over the temperature range from 329 to 575°C. The point at 600°C is probably low since the alloy may not have been saturated. At the higher concentrations (>0.2 wt% Th), the data compare favorably with previous results [MARTIN-1959], but the values are lower than Martin's values at low thorium concentrations. This is not surprising considering that Martin reported difficulty in sampling and was not sure whether the filtering procedure used was effective. Further experiments (using the thermogravimetric/differential scanning calorimeter) have identified the peritectic decomposition temperature of $ThCd_{11}$ as 569 ± 2°C. Measurements of the heat of reaction are in progress.

(2) Reduction of Thorium Oxide

As indicated in the reference flowsheet for oxide fuels (Fig. 6), processing of oxide fuel constituents requires a reduction step. Pyrochemical reduction of UO_2, PuO_2, and ThO_2 has been demonstrated, but the process parameters have not been optimized for calcium reduction.

These parameters include alloy and salt composition, temperature, effect of mixing, CaO and metal loading in the salt and alloy, respectively, and type of oxide being reduced. Importantly, only the reduction of powdered ThO_2 has been demonstrated. A preliminary experiment to reduce high-fired ThO_2, which is the form that might be obtained from a reactor, was unsuccessful [STEINDLER-1979B]. Additional preliminary experiments designed to demonstrate this reduction have been performed.

Two types of high-fired thoria (1700°C) were used, 200-mesh microspheres and 1/4-in. pieces of irregular shape (Cerac, 99.9% pure). The other process variables were chosen to be compatible with the flowsheet and to optimize the conditions for reduction. A Cd-45 wt % Mg-10 wt % Ca alloy was covered with premelted salt ($CaCl_2$-20 mol % CaF_2) and equilibrated at 675°C. Enough ThO_2 was added so that if it was completely reduced, the resulting alloy would contain 5 wt % thorium. Upon addition of the ThO_2, the melt was mixed by stirring at 800 rpm with a flat impeller located at the salt-metal interface. The salt and alloy were sampled at the beginning of the experiment and at timed intervals up to four hours. For both types of starting material, there was a decrease in the calcium concentration and an increase in the thorium concentration in the alloy; the data indicated that reduction went to about 5% completion. No change larger than the experimental error could be detected in the CaO concentration in the salt.

These results indicate that the reduction of high-fired thoria is difficult and that a complete understanding of the reaction mechanism is necessary to identify optimum conditions. To this end, further reduction experiments are in progress.

b. Molten Salt Recycle, Electrolysis of CaO in Molten Salt
(R. E. Barletta, T. J. Gerding, and D. K. Kroeck)

Laboratory-scale studies of the fused-salt ($CaCl_2$·15% CaF_2) electrolysis of CaO using a molten-metal cathode* are continuing. Successful electrochemical reduction of calcium oxide would decrease the large volume of waste in pyro flowsheets.

The cathodic reaction in this proposed electrolysis would generate calcium metal for recycle, and the anode reaction on a graphic electrode would yield a waste stream of CO/CO_2 gas. The net cell reaction is

$$CaO(salt) + C_{anode} \xrightarrow{600\text{-}800°C} Ca\ (alloy/salt)_{cathode} + CO(g)$$

An electrolysis using a liquid-cadmium cathode and $CaCl_2$-15 wt % CaF_2 salt containing 5 wt % CaO was performed at 695°C and constant voltage (about 2.7 V). During this experiment, the voltage varied slightly between 2.74 and 2.68 V. Prior to electrolysis, a sample of the effluent gas was taken, and a current-potential curve was obtained. The cell was then operated for a total of 449 mins. During this time, the cell current remained

*Figure 4 of [STEINDLER-1979B] is a diagram of this cell.

roughly constant (2.7-2.3 A). If one assumes 100% cell efficiency, it should take roughly 5 h to electrolyze all of the 12.5 g of CaO present. Thus, during the course of the experiment, all of the CaO should have been electrolyzed and the cell current should have fallen substantially. The fact that it remained constant indicates a very low cell efficiency (about 10%).

Gas samples were taken after 314 min and at the end of electrolysis. The results of mass-spectroscopic analysis of these gas samples and of the initial gas sample are given in Table 4.

Table 4. Mass-Spectrometric Analyses of Gas Effluent from CaO Electrolysis

Conditions: 15 wt % CaF_2-$CaCl_2$; 2.5 V; graphite anode, cadmium cathode; 695°C

Component	Concentration, mol %		
	Initial	After 312 min	After 443 min
N_2[a]	8.0	69.2	2.8
CO[a]	0.4	1.9	6.6
O_2	0.2	18.8	0.4
Ar	91.4	10.0	89.8
CO_2	<0.01	0.7	0.4
Cl_2	ND[b]	ND	ND

[a]Best estimate
[b]Not detected

Although the 314-min sample is obviously contaminated with air and is therefore useless, the analysis of the final gas sample indicates that some CO and CO_2 were produced during the electrolysis. The absence of chlorine in these samples does not rule out chlorine production during electrolysis.

Decomposition of either CaO or $CaCl_2$ should result in the presence of calcium in the cadmium cathode. Analysis of samples of the cathode taken at the end of the experiment revealed that the cadmium contained roughly 1 at.% calcium, which indicated that some calcium had been reduced. Current/potential curves obtained for the system before and after electrolysis are shown in Fig. 8. The plot of current (I) vs. potential (E) before electrolysis began shows the presence of three materials with decomposition potentials of 0.7, 1.2, and 2.2 V, as indicated by the extrapolations of the slopes to zero current (x-axis). The theoretical decomposition potentials of CaO (to Ca and CO) is 1.7 V and that of $CaCl_2$ is 3.5 V. The observed values are

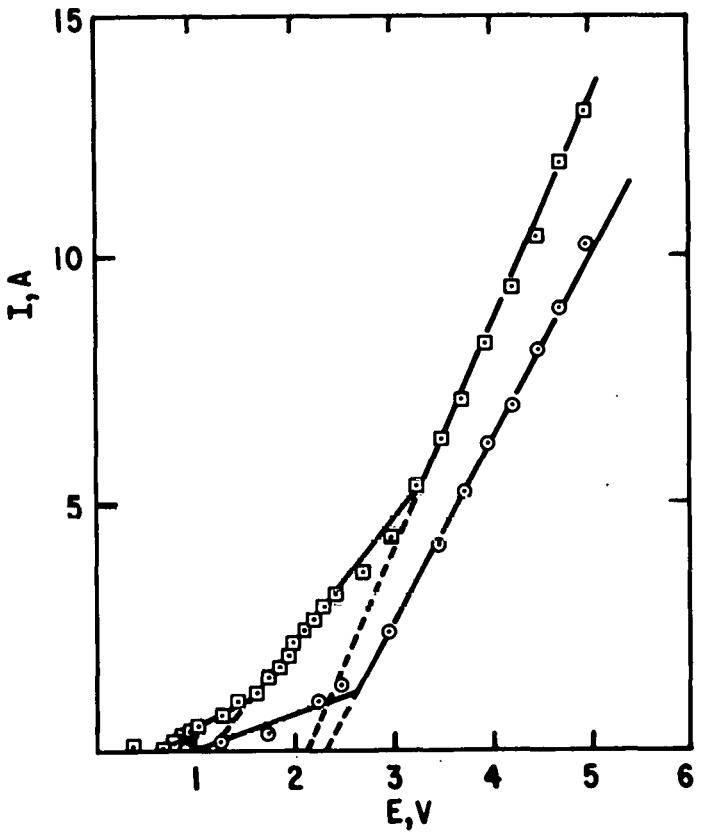

Fig. 8. Current vs. Potential Plots for Electrolysis of CaO in 15 wt % $CaF_2/CaCl_2$ at 690°C using a Carbon Anode and a Molten Cadmium Cathode. Squares denote data taken before electrolysis began; circles denote data after 449 min of electrolysis at 2.7 V.

substantially lower, which could perhaps be accounted for by solvation of calcium by cadmium. The I vs. E plot after electrolysis no longer contains the middle segment of the curve, giving further support to associating it with the decomposition of CaO.

Because of vaporization of cadmium during the experiment described above, the cadmium cathode was replaced with a 35 wt % Mg-Cu (58 at.% Mg-Cu) alloy in the next experiment. This alloy was chosen because of its low vapor pressure at the temperatures of interest and because, like cadmium, its use has been proposed in various pyro flowsheets. The alloy was prepared by heating a mixture of copper and magnesium to 800°C and holding the mixture at that temperature with occasional stirring for 4 h. The resulting alloy had an oxide layer, which was removed before use. The density of the alloy was found to be about 3.9 g/cm^3.

The electrolysis cell was loaded with the Mg-Cu alloy (about 100 g) and with a salt mixture (15 wt % CaF_2 - $CaCl_2$) containing 5 wt % CaO. As in the previous experiment, electrolysis was done at 690-695°C and constant voltage. This was done in two steps: (1) 110 min at 2.0 V (about 0.34 A); and (2) 433 min at 2.5 V (about 0.51 A). The second step was interrupted and the sample cooled to 570°C overnight. The cell was then warmed to 695°C and electrolysis was continued.

The progress of the experiment was monitored in several ways. Samples of effluent gas were taken before electrolysis and after 110 min. The results of a mass-spectrometric analysis of these samples show no reduction at the time the samples were taken. Samples of the alloy and salt phases were taken at the start and end of the experiment and analyzed (Table 5). Finally, current/potential data and cyclic voltammograms were taken at the start of the experiment, after 110 min, after 330 min, and after 567 min of electrolysis. Current/potential data were also taken after the overnight cooling period to ensure that no changes had occurred during cooling.

Table 5. Chemical Analyses of Materials from CaO Electrolysis

Conditions:
15 wt % CaF_2-$CaCl_2$; 2.0 to 2.5 V; graphite anode; 35 wt % Mg-Cu alloy cathode; 695°C

Material	CaO, wt %	Cl, wt %
Salt before electrolysis	4.2	50.9
Salt after electrolysis	3.1	51.6
Alloy after electrolysis[a]	1.8	—

[a]Alloy before electrolysis is not available for analysis.

The current/potential curves (Fig. 9) obtained in this experiment were quite similar to those obtained in the previous experiments with the cadmium cathode except that the first portion of the "before" curve in Fig. 8 (attributed to impurities) is absent. The decomposition potentials (1.2 V and 2.5 V) obtained by extrapolating to zero current the portions of the curve with different slopes are nearly the same as those previously obtained. Cyclic voltammograms of the system (Fig. 10) reveal two other broad peaks centered at 2 V and 2.5 V on the upsweep (increasing voltage) portion of the curve. The cause of these peaks has not yet been determined; however, these data point to at least three electrolytic processes occurring in the system.

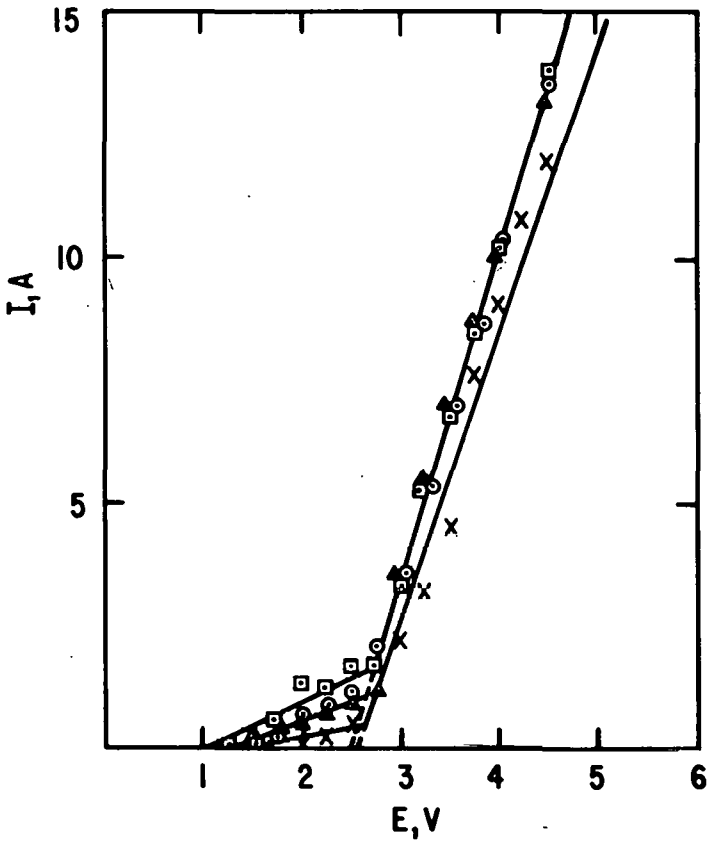

Fig. 9. Current vs. Potential Plots of CaO 15 wt % CaF_2-$CaCl_2$ in 15 wt % CaF_2-$CaCl_2$ at 695°C using a Carbon Anode and a Molten Cathode of 35 wt % Mg-Cu. Squares denote data taken prior to electrolysis; circles denote data taken after electrolysis for 110 minutes at 2.0 V; triangles after electrolysis for 303 minutes (193 minutes at 2.5 volts); and crosses after electrolysis for 543 minutes (333 minutes at 2.5 volts).

The results given in Table 5 appear to indicate that some reduction of the CaO initially present has occurred, and that there was little or no reduction of calcium chloride. It is difficult to determine the amount of reduction that took place since the CaO plus any dispersed or dissolved calcium are measured in the postelectrolysis analysis of the CaO concentration in the salt phase. There was very little change in current during the course of the experiment. If one assumes 100% cell efficiency during the experiment, then about 30% of the original 12.5 g of CaO should have been reduced, and a corresponding current drop produced. Thus, the observation of constant current in this experiment means that if the CaO is being reduced, the efficiency of the reduction is quite low, in agreement with results of the previous experiment. This conclusion is reinforced by the fact that CO and CO_2 concentations in the effluent gas samples increased only slightly.

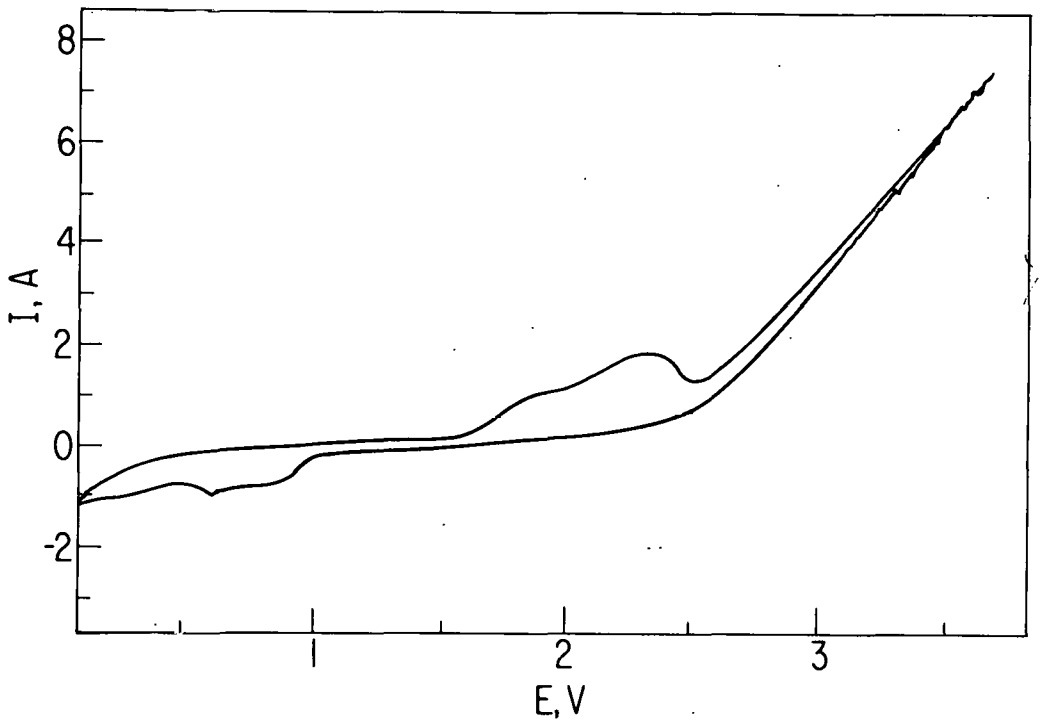

Fig. 10. Cyclic Voltammograms of CaO in 15 wt % CaF_2-$CaCl_2$ at 697°C after 543 Min of Electrolysis

Since both of these experiments produced such inconclusive results, there is a need to obtain a better understanding of the various electrochemical and chemical processes occurring in the system. In the absence of impurities, there are five possible reactions. The theoretical decomposition potentials of these reactions at 975 K have been calculated, based on free energy of formation data.

$CaO \rightarrow Ca + 1/2O_2(g)$	$E_d = +2.75$ V	(1)
$CaO + C \rightarrow Ca + CO(g)$	$E_d = +1.73$ V	(2)
$CaO + 1/2C \rightarrow Ca + 1/2CO_2(g)$	$E_d = +1.73$ V	(3)
$CaCl_2 \rightarrow Ca + Cl_2(g)$	$E_d = +3.41$ V	(4)
$CaF_2 \rightarrow Ca + F_2$	$E_d = +5.41$ V	(5)

Thus, in a cell with a molten-metal cathode and a graphite electrode, reactions 2 and 3 should occur first, reaction 4 next, and finally reaction 5. On graphite, reaction 1 should not occur; it would be expected to occur only when an inert anode is used.

To determine the potentials at which these reactions do, in fact, occur, a set of experiments was performed using either a carbon or a platinum anode. Current vs. potential data were taken for a system of 15 wt % CaF_2-$CaCl_2$ salt mixture, using a 35 wt % Mg-Cu alloy as a cathode. Data were

taken on a salt mixture in the absence of calcium oxide and on another salt mixture to which 12.5 g (5 wt %) of CaO had been added. The data were taken at various temperatures (from 675°C to 800°C); first, the voltage was set at the maximum potential and the potential was gradually reduced until a negative current was reached. The individual data points were taken after the current had stabilized at a given potential. This procedure would have the effect of minimizing contributions of any trace impurities to the current/potential data. It resulted in somewhat lower currents being observed at the lower potentials.

The current/potential data were plotted as shown in Fig. 11. In all experiments, it appeared as though only one electrochemical reaction was occuring, but at different potentials upon a change in electrode or upon the addition of calcium oxide to the system. The decomposition potential (E_d) for each of these reactions was obtained by fitting the upper portions of the curves to a straight line and extropolating this least-squares line to zero current. The decomposition potentials thereby obtained are given in Table 6.

Table 6. Decomposition Potential, E_d, for the $CaO-CaF_2-CaCl_2$ System. Temp: 675-800°C. Cathode: 35 wt % Mg-Cu.

Salt-Phase Composition	Anode Material	E_d, V					
		675°C	700°C	725°C	750°C	775°C	800°C
CaF_2-CaCl_2[a]	C	3.14	3.13	3.10	3.08	3.04	2.98
CaF_2-CaCl_2[a]	Pt	2.77	2.92	3.07	—	2.92	2.77
CaF_2-CaCl_2 + 12.5 g CaO	C	2.39	2.37	2.33	2.29	2.26	2.18
CaF_2-CaCl_2 + 12 5 g CaO	Pt	2.70	2.67	2.67	2.63	2.63	2.67

[a]15 wt % CaF_2-CaCl_2

Based on the species present in each of these experiments and by comparing the observed E_d with the calculated values for the possible reactions given above, it is possible to assign these observed decomposition potentials to specific chemical reactions. In the experiments with only $CaCl_2-CaF_2$ present, decomposition potentials at 700°C of 3.13 V and 2.92 V were observed with graphite and platinum, respectively. The theoretical value for $CaCl_2$ electrolysis is 3.41 V. The difference between 3.13 and 3.41 V may be attributed to the lower thermodynamic activity of calcium in the Cu-Mg alloy. The even lower value of 2.92 V on platinum is due to the anodic oxidation of the electrode material

$$Pt \rightarrow Pt^{2+} + 2e^-$$

Oxidation of platinum in chloride melts occurs typically at 0.2 to 0.3 V below the chlorine evolution reaction.

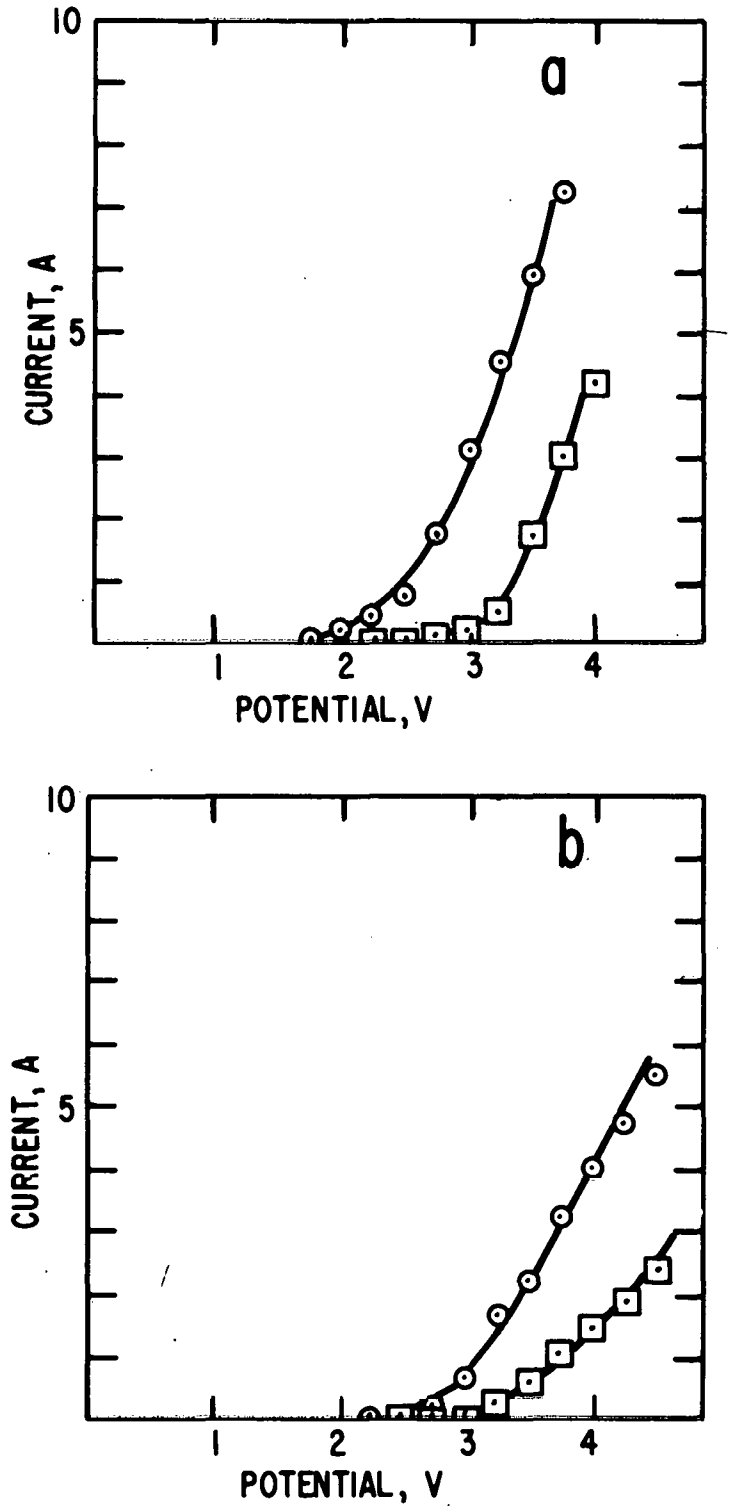

Fig. 11. Current-Potential Curves for the $CaO-CaF_2-CaCl_2$ System at 675°C. a. Carbon Anode. b. Platinum Anode. (Circles denote additional 5 wt % CaO; squares denote absence of CaO.)

The observed and theoretical decomposition potentials on graphite in melts at 700°C with CaO present are 2.37 V and 1.73 V, respectively, indicating an overpotential of 0.6 V; the observed decomposition potential on platinum is 2.67 V. The 2.37 V decomposition potential is attributed to reactions 2 and 3.

The overpotential observed in the CaO electrolysis on graphite may occur by a mechanism similar to that for electrolysis of Al_2O_3 in cryolite solution. When Al_2O_3 is electrolyzed in cryolite solution using a carbon anode, an overpotential of 0.2 to 0.5 V for CO_2 evolution is observed. This overpotential has been explained by Thonstead and Hove [THONSTEAD] in terms of the following mechanism:

transfer of oxygen through the electric double layers:

$$O^{2-}(\text{melt}) \rightarrow O^{2-}(\text{surface}) \tag{6}$$

discharge and chemisorption of oxygen:

$$O^{2-} + xC \rightarrow C_xO + 2e^- \tag{7}$$

formation of CO_2:

$$2C_xO \rightarrow CO_2(\text{adsorbed}) + C \tag{8}$$

desorption of $CO_2(\text{absorbed}) \rightarrow CO_2(g)$ (9)

They concluded that the slowness of reactions 6 and 8 accounts for the overpotential.

Finally, the potential of 2.67 V observed on platinum in CaO-containing melts at 700°C is attributed to reaction 1, which has a theoretical E_d of 2.75 V. The close agreement of observed and theoretical values is fortuitous, and may be owing to the lowering of the calcium potential in Cu-Mg canceling the well-known overpotential of the oxygen evolution reaction on platinum. A summary of the observed and theoretical potentials is given in Table 7.

On the basis of these experiments, it is possible to explain the low current efficiency of electrolysis described above. The experiments were run with potentials in the range of 2.0 to 2.5 V. At these potentials, one would expect little if any CaO electrolysis since the decomposition potential for CaO with a graphite anode is 2.4 V. Thus, electrolytic experiments on the system should be performed at a potential between the 2.4-V CaO decomposition potential and the 3.14-V $CaCl_2$ decomposition potential.

Such an electrolysis was performed at 695°C with a molten-salt mixture consisting of 12.5 g of CaO dissolved in 15 wt % CaF_2-$CaCl_2$. The cathode for the experiment was an alloy of 35 wt % Mg-Cu, and the anode was carbon. Prior to the start of electrolysis, samples of the salt and alloy

Table 7. Decomposition Potentials for the $CaO-CaF_2-CaCl_2$ System. Temp: 700°C. Cathode: 35 wt % Mg-Cu

Reaction	E_d, V Observed	E_d, V Theoretical
$CaCl_2 \rightarrow Ca + Cl_2$	+3.13	+3.41
$CaO \rightarrow Ca + 1/2O_2$	+2.67[a]	+2.75
$CaO + C \rightarrow Ca + CO$		
or	+2.37	1.73
$CaO + 1/2C \rightarrow Ca + 1/2CO_2$		

[a]Platinum anode.

phases and current vs. potential data were taken. A constant-voltage electrolysis was run at 3.0 V for 300 min. During that time, the current dropped steadily from 3 A to 1.28 A. After electrolysis, current vs. potential data and samples of the salt and alloy phases were taken again.

The current/potential curves taken before and after electrolysis (Fig. 12) reveal a striking change in the system behavior. Comparison of these data with those in Fig. 18a suggests that nearly all of the CaO had been electrolyzed. Indeed, the postelectrolysis E_d is 3.14 V, almost exactly that obtained for the E_d of $CaCl_2$ at 700°C (Table 6). This conclusion is reinforced by the condition of the carbon electrode after electrolysis (shown in Fig. 13). The smaller amount of carbon present after electrolysis is a further indication that extensive reaction involving the anode (i.e., reactions 2 and 3) occurred.

If current efficiency had been 100%, approximately 96% of the CaO should have been electrolyzed during the course of this experiment. However, the facts (1) that the current did not drop to zero or (2) that the residual CaO did not appear in the current/potential curve taken after electrolysis (as shown by comparison of Figs. 11a and 12) is puzzling. One possible explanation is that since the current/potential data were taken starting from the highest potential, the trace amount of CaO (less than 0.1 g total) which would still be present in the molten salt may be electrolyzed quickly in the vicinity of the carbon electrode. The area around the carbon electrode then would not reflect the bulk concentration since diffusion is slow on the time scale at which the data were obtained. True equilibrium data could be obtained only by increasing, instead of decreasing, the potential when obtaining current-potential data. Experiments to test this explanation are under way.

Chemical analyses of samples of salt and metal phases taken before and after the electrolyses are given in Table 8. The data show qualitatively a reduction of oxide concentration in the salt phase and the presence of calcium metal in the alloy. No reduction in the chloride ion content is indicated. This is consistent with the conclusion that only CaO was electrolyzed.

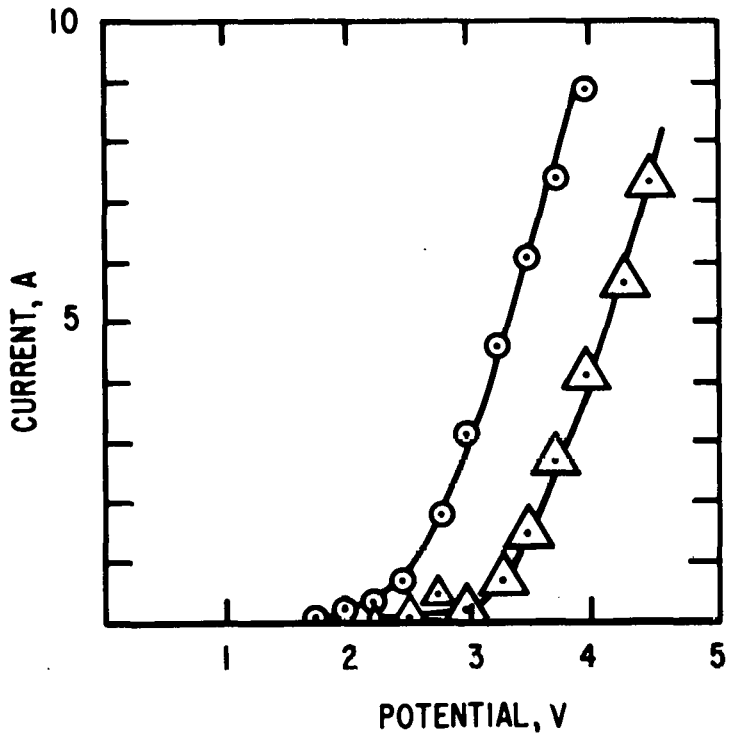

Fig. 12. Current vs. Potential Curves for Fused 15 wt % CaF_2-$CaCl_2$ Containing 5 wt % CaO at 695°C. (Anode is graphite. Circles denote data taken before electrolysis; and triangles denote data taken after 300 min of electrolysis at 3V.)

Table 8. Chemical Analyses of Solutions from CaO Electrolysis[a]

Salt Composition				Calcium Content of 35 wt % Mg-Cu Cathode
Before Electrolysis		After Electrolysis		
Ca, wt %	Cl, wt %	Ca, wt %	Cl, wt %	After Electrolysis[b], wt %
5.5	51.0	3.2	52.3	3.4
4.7	51.6	3.3	52.0	1.8
3.6	51.7			
3.6	52.0			

[a]Conditions: 15 wt % CaF_2-$CaCl_2$; 3.0 V; graphite anode; T = 695°C.
[b]The alloy analysis before electrolysis is not available.

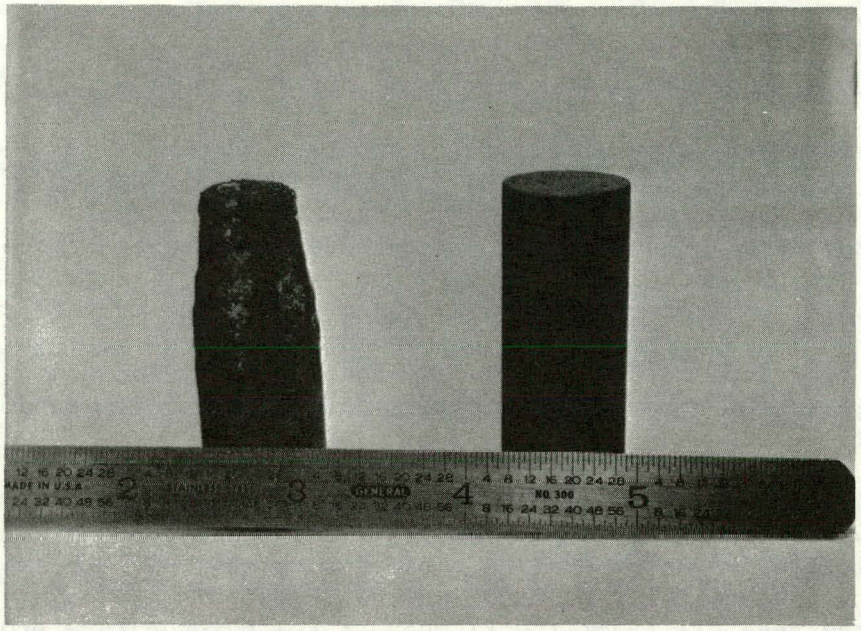

Fig. 13. Graphite Anodes Used in Molten Salt Electrolysis of CaO. On the right is the anode before electrolysis; on the left is the anode after 300 min of electrolysis at 3 V.

However, the analytical data are questionable since there were large differences between replicate samples. This made it impossible to calculate current efficiencies. It is difficult to reconcile these analytical data with the current/potential data curves obtained before and after the experiment, and with the current-drop observed during the course of the experiment. The analytical data indicate less reduction of calcium than do the electrical measurements obtained during electrolysis. It is important to note that the analytical procedure used to determine calcium oxide does not discriminate between calcium oxide and calcium metal, and so the post-electrolysis values for calcium oxide in Table 8 could be high owing to the presence of either dissolved or dispersed calcium metal in the salt. In future experiments, an effort will be made to obtain both the calcium oxide and calcium metal contents of the salt samples to resolve this ambiguity.

4. Uranium-Plutonium Salt Transport Processing

J. B. Knighton,* C. Baldwin,*, W. A. Averill,* M. Bracco,* M. F. Boyle,* S. J. Dyer,* J. E. Hicks,* G. A. Lambert,* T. D. Santa Cruz,* R. L. Sandvig,* S. P. Sontag,* and J. L. Zoellner*

a. Introduction

The purpose of this work package is to develop pyrochemical processes and associated hardware for coprocessing uranium and plutonium contained in spent FBR reactor fuels. The primary objective is to develop a process capable of producing a proliferation-resistant product suitable for reactor use. This proliferation resistance can be accomplished by coprocessing and/or by producing fission-product-contaminated plutonium. In addition, waste management of by-products for both interim and ultimate disposal will be explored.

The technical goals of this work package are (a) to develop a viable flowsheet for producing by pyrochemical means through coprocessing, a proliferation-resistant product suitable for reactor use; (b) to identify key problems and conduct early proof-of-principle experiments on key problems that challenge the feasibility of the flowsheet; (c) to prepare a process description and design criteria for a conceptual Pyrochemical Processing Facility (PPF); (d) to examine and integrate design concepts for the unit operations of the salt transport process; and (e) to evaluate containment of fission products and management of waste products.

b. Engineering Analysis

(1) Waste Management Studies

(S. P. Sontag*)

The Waste Awareness Meeting, presented on March 12, 1979, was attended by Rocky Flats PDPM personnel and several TRU Waste Systems Office personnel. An outline of the presentation, along with comments made during the meeting, is given in Appendix A. The meeting promoted an understanding, but mostly an awareness, of the importance, program size, and cost of dealing with nuclear waste.

Work on the "Preliminary Recycle and Waste Management Outline" [Table 19 of STEINDLER-1979B] is continuing. Correct material balances are being obtained by use of the salt transport computer program (see Section (3) below).

---

*Rockwell International - Rocky Flats

Work is also continuing on the scope-of-work document, with completion of a rough draft scheduled for April 13, 1979.

A rough draft of the Pyrochemical and Dry Processing Methods Annual Report - 1978, CRD-79-009, has been written and is being typed.

A Lindberg crucible furnace and controller will be used in performing the calcium oxide reduction experiments. An O.S.A. (Operational Safety Analysis) for use of the crucible furnace has been written and reviewed. Comments from the review are being incorporated into the O.S.A. Final approval will be obtained as quickly as possible. Maintenance personnel have started installing a 220 V power line and wiring the control console and furnace. Extension of an existing argon line to the hood side will start on March 26, 1979. High-purity (99.9%) U^{238} has been obtained for making UCl_4. Experimental work will begin after approval of the O.S.A. and electrical and argon line installation is completed.

The initial experiments will follow the outline given in Table 9. Since direct electrolysis of calcium oxide is being investigated by ANL, Rocky Flats work is being concentrated on alternative methods of calcium oxide reduction.

Chlorination of calcium oxide to calcium chloride, with subsequent electrolysis of the chloride to calcium metal and chlorine gas, will be the main experimental effort. Electrolysis of calcium chloride to produce calcium metal is an accepted industrial practice. One chlorination medium that will be tried is UCl_4, with the chlorination proceeding as follows:

$$2CaO + UCl_4 \rightarrow UO_2 + 2CaCl_2 \qquad (1)$$

The heat of reaction is -66.6 kcal/mol at 1000 K. Separation of UO_2 from $CaCl_2$ should occur as a result of density differences. The above reaction has the advantage of not introducing any new chemical species into the reprocessing system. A carryover of UCl_4 in recycling the salts would not be deleterious to the other fuel-reprocessing steps. Another chlorination reagent that will be tried is carbon tetrachloride. The reaction is:

$$2CaO + CCl_4 \rightarrow 2CaCl_2 + CO_2 \qquad (2)$$

The heat of reaction is -112.0 kcal/mol at 1000 K. This reaction is advantageous in that no residue of the chlorinating media is left. The newly formed calcium chloride would mix with the reduction salt, which is 80 wt % $CaCl_2$. It would then undergo electrolysis to produce calcium metal for the reduction of the oxide from the next fuel assembly, as would also be done with $CaCl_2$ produced by the chlorination of CaO with UCl_4.

A bleed stream of the reduction salt must be removed to prevent FP-2 buildup. One method of replacing the calcium salts lost in the bleed stream would be by carrying out either of the following reactions:

$$2CaO + CaC_2 \rightarrow 3Ca + 2CO \qquad (3)$$

$$4CaO + CaC_2 \rightarrow 5Ca + 2CO_2 \qquad (4)$$

Table 9. Initial Calcium Recycle Experiments

I. Furnace Checkout with CaO in Synthesized Reduction Salt

A. Furnace operating characteristics

B. Calcium oxide phase occurrence

1. Temperature range of 750 to 900°C

2. Oxide loadings will be increased until a multiphase system is reached

II. Chlorination of CaO to $CaCl_2$

A. Formation from UCl_4, i.e., $2CaO + UCl_4 \rightarrow UO_2 + 2CaCl_2$ derived from $2CaO + UF_4 \rightarrow 2CaF_2 + UO_2$ [CRIMES-1962]

1. Manufacture of UCl_4, i.e., $U + 2ZnCl_2 \rightarrow 2Zn + UCl_4$

a. Reaction kinetics
b. Optimum operating conditions

2. Reaction of $UCl_4 + 2CaO \rightarrow UO_2 + 2CaCl_2$

a. Reaction kinetics
b. Optimum operating conditions
c. Minimization of side reactions

B. Formation from CCl_4, i.e., $2CaO + CCl_4 \rightarrow CO_2 + 2CaCl_2$

1. Reaction kinetics

2. Optimum operating conditions

III. Direct Chemical Reduction of CaO with CaC_2, i.e.,
$2CaO + CaC_2 \rightarrow 3Ca + 2CO$
$4CaO + CaC_2 \rightarrow 4Ca + 2CO_2$

A. Reaction conditions required

B. Reaction kinetics

C. Optimum operating conditions

IV. Combination of Chlorination and Chemical Reduction of CaO, i.e.
$aCaO + bCCl_4 + dCaC_2 \rightarrow xCa + yCaCl_2 + zCO_2$

A. Reaction conditions required

B. Reaction kinetics

C. Optimum operating conditions

The heats of reactions 3 and 4 are +104.4 and +53.4 kcal/mol, respectively, at 1000K. The carbide-induced CaO reduction would produce the bulk of the required metallic calcium and would lessen the requirements for the chlorination reaction and subsequent electrolysis. Makeup CaF_2 and KCl would be added to the salt prior to recycle.

All of the above reactions can be experimentally performed with the equipment now available. When an atmospheric retort for the furnace is obtained, the experimental work will shift to electrolysis of $CaCl_2$ in mixed salts and the regeneration of UCl_4 from UO_2.

(2) Zinc/Cladding Separation (Literature Search)
(R. L. Sandvig,* G. A. Lambert,* S. J. Dyer*)

Available background material has been obtained and reviewed. A plan for developing a method for separating zinc from cladding has been developed. The plan concentrates on the recovery of suitable purity recycle zinc by high-temperature vacuum distillation of the zinc/cladding mixture. Other methods of recovering recycle zinc, such as electrorefining, will also be considered. However, methods which sharply increase process residue, such as aqueous treatment methods, will not be considered. Chemical Abstracts from 1908 to 1961 has been researched and yielded three extensive reports on low pressure zinc distillation. Several patents have been requested but not granted as yet. Zinc Abstracts from 1962 to 1978 has been researched. Four articles and two patents deemed to be of interest have been requested. The computerized index of references published between 1975 and 1978 has been reviewed. Dismissal of aqueous treatment methods has sharply reduced the number of references that are of interest. Very few of the indexed references are concerned with dry separations of metals and none involve the distillation separation of zinc from iron.

The computerized index of references published between 1967 and 1975 has been received and is being reviewed. Of the 2737 references listed in the first half of the index, eight items may be of interest. Material will continue to be reviewed and cataloged as it becomes available. Some requests for foreign, dated, or regional library materials have met with negative results. Also some delay in receiving requested copies of U.S. patents is expected.

A bibliography of useful works obtained to date is included as Appendix B.

A computer program to determine the vapor pressure of metals as a function of temperature has been developed and run. This program uses the upper three data points listed in the literature [STEINDLER-1978D], and fits these data points to the Antoine equation:

$$\log \text{Vapor Pressure} = A - \frac{B}{C + T}$$

*Rockwell International - Rocky Flats

where: T is in kelvins
Vapor pressure is in mm Hg
A, B, and C are empirical constants.

The values for zinc and iron are listed below.

	A	B	C
Zinc	7.651451	2563.722	-76.32259
Iron	9.61418	19880.38	-32.92745

The zinc-iron phase diagram has been studied for temperatures at and above 782°C. In this temperature range, there are three different phase regions at various zinc-iron concentrations. At high concentrations of zinc, a single liquid phase exists. At lower concentrations of zinc, two phases exist: a liquid phase and a solid-solution phase. At very low concentrations of zinc, only the solid-solution phase is present. The location of the boundaries between these three phases depends on the temperature of the melt. At higher temperatures, the solid-solution phase contains less zinc. The quantity of zinc that can be distilled from the liquid phase (to the point where only solid solution remains) appears to depend on the initial concentration of zinc and the temperature at which distillation is done. Zinc recovery from the two-phase region increases with an increase in temperature.

The zinc-iron phase diagram indicates that an intermetallic compound is present in the region being considered. A copy of a recent article on the thermodynamics of zinc-iron solutions at 700 to 900°C is being obtained [WRIEDT]. This article is expected to yield useful information about the vapor pressure and bonding of the zinc-iron solution in question.

Due to the wide varition in relative volatilities of metal constituents, batch distillation calculations will probably utilize a graphical solution for the zinc-iron binary system. This solution, when adapted to the computer, can be expanded to the five-component system for zinc and SS 316 cladding.

Rate of zinc evaporation from the melt surface, as well as the rate of zinc diffusion from the zinc-iron residue must be determined and correlated with vapor pressure and phase data in order to learn optimum operating conditions. Cycle times and the overall recovery of recycle zinc will be determined by the zinc evaporation and diffusion rates. Once the zinc-iron residue has been deposited in the disposal container, diffusion of the zinc to the surface of the residue for further evaporation is expected to be slow.

(3) Computer Model
(W. A. Averill*)

The base model for the salt transport process has been completed. The model simulates decladding, reduction, FP-3 removal, uranium-plutonium cotransport, and uranium transport. Several difficulties in the

*Colorado School of Mines

modeling process became apparent as the digital simulation was constructed. The problems that have been identified so far are described in the following.

The assumptions used in the previous calculations concerning the nature of the solid alloy phase produced during reduction were in error. The mass-balance calculations cannot converge correctly when UCu_5 is considered to be the only solid phase constituent. For correct computations, a combination of UCu_5 and copper metal must be present. This problem, which was not considered during manual calculation, was found only because an extensive amount of data was generated by the computer model during a simulation.

The importance of uranium solubility as a parameter in the process heretofore unknown, has been clearly demonstrated. This feature too was analyzed as a result of large amounts of data generated by the computer model.

The impact of variations in feed composition (core and axial blanket or radial blanket) on the operating parameters of the salt-transport process can be accurately assessed by computer modeling whereas it could only be approximated with hand calculations. The model can very quickly perform a simulation and identify the areas of the process that are particularly sensitive to feed changes.

As a result of analysis of the data generated by the computer, areas of future research critical to the development of the salt-transport process have been identified. For example, studies of the copper-uranium-magnesium ternary diagram have been shown to be absolutely necessary for the success of modeling and subsequent operation of the process. Furthermore, the need for data on the sensitivity of the solubilities of uranium, plutonium, FP-3, FP-4, and copper to the addition of various impurities has been shown.

It has been demonstrated that variations such as changes in the salt-to-metal ratio in various process stages impact upon the proliferation resistance of the process. The higher the ratio, the sooner the bulk of the uranium is transported. J. L. Zoellner of Rockwell International, is investigating details of this aspect.

The second generation of this modeling effort is "Salt II." Whereas the first program was written in basic computer language to facilitate modification during development, "Salt II" will be written in FORTRAN and will include all auxiliary operations performed off the rotating platform. FORTRAN will allow the ancillary steps to be included without a significant increase in the run time of the program. This will be important during optimization of the operating parameters ultimately to be used to control an operating system. The present model, though only describing the platform operations, has given the PDPM team an invaluable insight into the process and its intricacies, and has allowed the fundamental model to be changed and adapted to account for new information.

An updated version of the logic flow diagram and subsequent program listing is being prepared. The series of calculations previously used as a basis for the computer model was found to require some modification. This was due either to inherent weakness or inaccuracy in the nature of the calculations, discovered once data from the program could be analyzed, or to more accurate information on the system. These changes are being incorporated into the diagram and listing of the present base model, or "Salt I." The time and effort for developing this preliminary model were well spent, considering the benefits reaped from the data generated.

(4) Salt Transport Process Design
(J. E. Hicks*)

Extensive modifications of the baseline salt transport turntable design concept (Figs. 17-19, [STEINDLER-1979B]) have been made. As discussed below, the need for these modifications became readily apparent when preliminary plant layouts were done.

Translation of the original flowsheet into a facility design resulted in a layout which appeared unworkable or impractical for a variety of reasons. The most obvious defects in the facility design were (1) extremely long transfer tubes and (2) vessels connected by transfer tubes in a manner that prevented the pressure-transfer of liquids from one vessel to another.

An inability to pressure-transfer liquids was observed in several cases in which process vessels were connected to each other with open tubes in a manner similar to Fig. 14, so that a continuous loop of piping and vessels was formed.

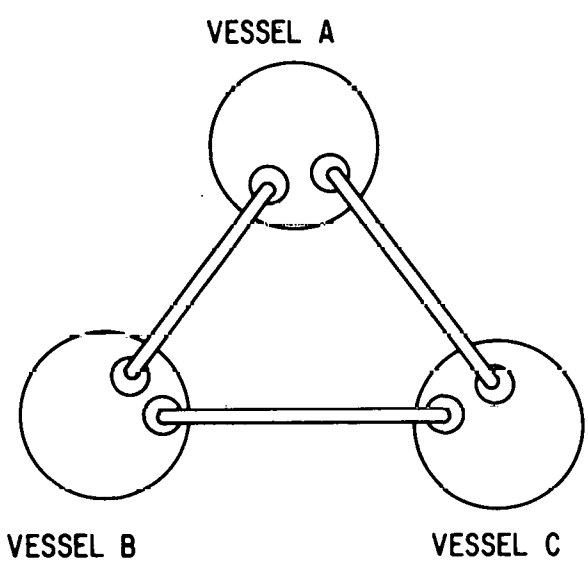

Fig. 14. Connection of Process Vessels

*Rockwell International - Rocky Flats.

This situation would make the transfer liquids between vessels by pressure-siphoning impossible unless valves or freeze collars were used. The pressure gradient required for transfer would not occur in a continuous loop--in Fig. 14, for example, the transfer of material from vessel A to vessel B would require that vessel A be pressurized and vessel B depressurized. However, if vessel A were pressurized, vessel C would also have to be pressurized in order to prevent undesired transfer of material from vessel A to vessel C. With vessel C pressurized, vessel B would have to be pressurized to prevent undesired transfer, contrary to the requirement that vessel B be depressurized for the desired transfer. Thus, no transfer would take place. If tube depth were shortened to prevent the undesired liquid transfers mentioned above, the vessels would be pressurized by gas flowing through the transfer tubes, resulting in the same difficulty.

The use of freeze collars or tungsten valves offers the possibility of overcoming the pressurization difficulties, but because the technology of neither is well developed, further development work would be required before use in a remote facility. In addition, the use of valves in molten-metal or molten-salt systems is generally not recommended [CHARNOCK]. Therefore, valves and freeze collars were not considered as a means of avoiding pressurization difficulties.

A third difficulty with the early layout was the large number of transfer tubes required. In some cases, the failure of a single tube would necessitate the removal of seven other transfer tubes before the failed tube could be replaced, due to access difficulties. All tubes removed would then have to be reinstalled or to be replaced if they had been broken in handling. Given the brittle nature of tungsten at low temperatures, it is likely that tubes would be broken in handling.

Because of these difficulties a redesign of the process was necessary. This was done in line with the general objectives and design criteria (Table 14, [STEINDLER-1979B]), and four subobjectives:

1. Minimize transfer tube lengths.
2. Minimize the number of transfer tubes.
3. Make the process as simple as possible to operate.
4. Locate as many of the ancillary operations as possible in canyons outside the main hot cell.

The new flowsheet for the turntable concept is given in Fig. 15 and the accompanying facility design in Fig. 16. Fission-gas collection and vacuum/vent and pressurization lines are not shown in either drawing. Vessel identification and stream numbers are kept consistent with all earlier drawings to facilitate comparisons and proliferation analysis.

The most noticeable change in the flowsheet is that the uranium-recovery operation (Table 10) is designated as optional and does not occur on the turntable.

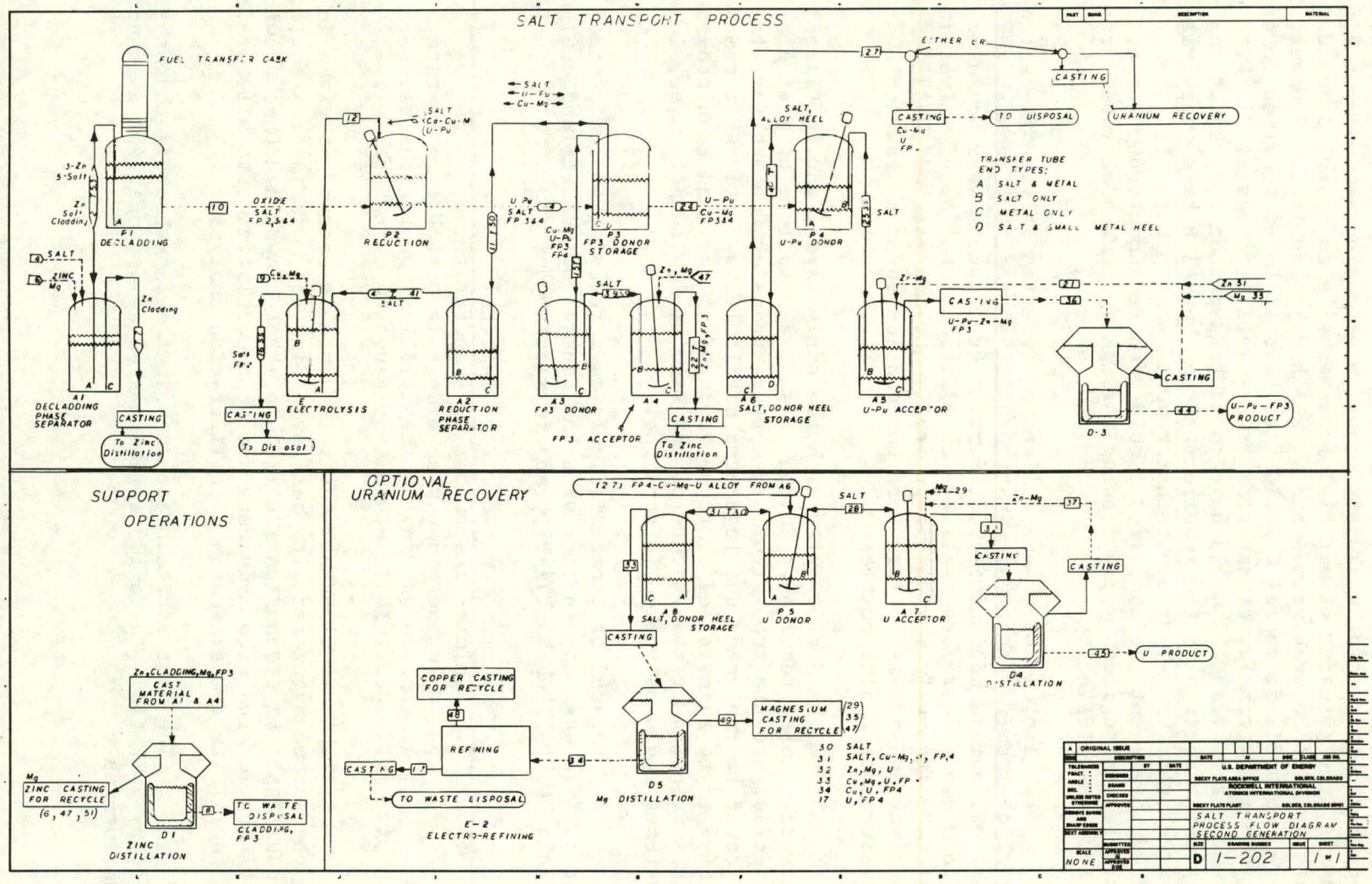

Fig. 15. Salt Transport Process Flow Diagram

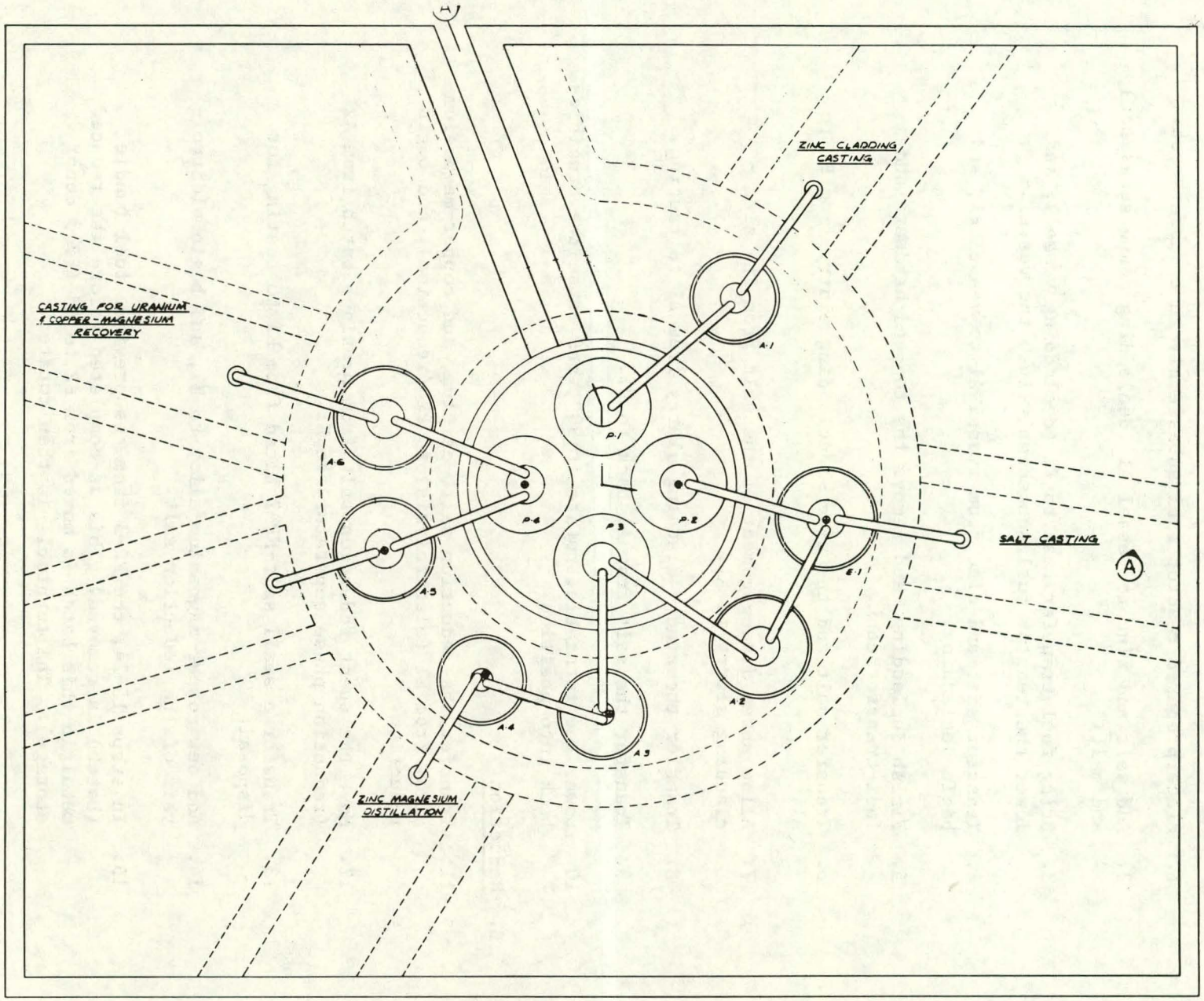

Fig. 16. Salt Transport Turntable Design

Table 10. Steps in Sequence of Events in Salt Transport Processing

A. Decladding

1. Place prepared reactor fuel subassembly in transfer cask.

2. Add salt and zinc to vessel A1 (decladding phase separator), and melt.

3. Bring fuel transfer cask to P1 (decladding vessel), and lower the reactor fuel subassembly into the vessel.

4. Transfer salt and zinc from vessel A1 to vessel P1, and begin decladding.

5. Finish decladding, and remove the top-end hardware and fuel-transfer cask.

6. Transfer salt and the zinc - decladding slurry from P1 to A1.

7. Allow phase disengagement of the salt from the zinc - cladding slurry in A1.

8. Transfer the zinc - cladding slurry from A1 to casting.

9. Transfer the salt from A1 back to P1.

10. Lower the turntable, rotate it 90°, and raise the crucibles back into position.

B. Reduction

11. Transfer the reduction salt, calcium, and copper-magnesium alloy from E1 (electrolysis) to P2 (reduction), and begin reduction.

12. Move the spent reduction salt from previous batch from A2 (reduction phase separator) to E1.

13. Transfer a small salt-FP-2 bleed from E1 to casting for disposal.

14. Add new copper-magnesium alloy to E1, and begin electrolysis of the reduction salt.

15. In steps 15-24, the FP-3 from the previous fuel bundle (batch) is removed. This is completed before the reduced metal in this batch is moved from P2 to P3 (FP-3 donor storage). The turntable is then rotated.

(contd)

Table 10. (contd)

C. FP-3 Transfer

16. Transfer a small quantity of metal heel from A2 to P3, thus keeping the alloy heel volume in A2 at a constant level.

17. Move a small amount of alloy from P3 to A3 (FP-3 donor).

18. Transfer salt from A4 (FP-3 acceptor) to A3.

19. Mix and equilibrate salt and metal phases in A3.

20. Disengage phases in A3, and transfer salt from A3 to A4.

21. Mix and equilibrate A4.

22. Transfer metal from A3 back to P3.

23. Transfer Zn/Mg/FP-3 alloy from A4 to casting (when necessary, A-4 can be sized to receive FP-3 elements from several subassemblies before being sent to casting).

24. Add fresh zinc and magnesium (solid) to A4.

25. Transfer salt and small metal heel from P3 to A2.

    a. Do steps 15-24 for the current batch.

26. Lower the turntable, rotate it 90°, and raise the turntable back into position. The fuel which we are following is now at P4 and ready for plutonium enrichment.

D. U/Pu Transfer

27. Transfer salt and a small metal heel from A6 (salt and donor heel storage) to P4 (U/Pu donor).

28. Transfer the U/Cu/Mg/FP-4 alloy from the previous batch from A6 to casting for disposal or uranium recovery.

29. Mix and equilibrate the salt and metal in P4.

30. Disengage phases, and transfer salt from P4 to A5 (U/Pu acceptor).

31. Mix and equilibrate salt and metal in A5.

32. Disengage phases in A5, and transfer salt back to P4.

(contd)

Table 10. (contd)

33. Repeat steps 30-32 until the desired enrichment is achieved.

34. Transfer U/Pu/Zn/Mg/FP-3 alloy product from A5 to casting and subsequent distillation, oxidation, and refabrication.

35. Add fresh Zn/Mg alloy to A5 for next batch.

E. Uranium Recovery Option

1. Transfer cast (or possibly liquid) U/Cu/Mg/FP-4 alloy into P5 (U donor) from A6, or storage (see Fig. 15).

2. Transfer salt and metal heel from A8, U-Salt and Donor Heel Storage, to P5.

3. Mix and equilibrate P5.

4. Disengage phases, and transfer salt to A7 (U acceptor).

5. Mix and equilibrate A7.

6. Disengage phases, and transfer salt from A7 back to P5.

7. Repeat steps 3-6 until the desired uranium transfer is achieved.

8. Transfer spent donor and salt from P5 to A8.

9. Transfer spent donor alloy from A8 to casting.

10. Transfer U/Zn/Mg alloy from A7 to distillation.

11. Distill Zn/Mg to separate it from uranium.

A number of casting operations are included in the flow diagram. These serve two purposes. First, they allow the removal of support operations from the main cell, and secondly, they provide a surge capacity so that the plant can continue operation if a breakdown occurs in one of the support operations.

Another simplification of the process is that the decladding cover salt remains in the reduction and donor storage crucibles in the reduction and the FP-3 removal steps. This eliminates several transfer tubes and transfers. This modification also allows the reduction salt to move in a loop, making the transfer lines one-way instead of two-way and thereby limiting any adjustments to the process.

The new flowsheet shown in Fig. 15 provides two options that will be examined after more data become available. These options, in order of importance are:

1. (a) Recover uranium, or
   (b) Dispose of spent donor and uranium.

2. Transfer material to uranium recovery as

   (a) Casting or
   (b) Liquid.

It is evident that option 2 is irrelevant if option 1.b is selected. Factors that will be considered in the selection of options are:

1. Proliferation resistance
2. Waste disposal costs
3. Reagent cost
4. Energy costs
5. Intangible factors

The flow of material through the system is described in Table 10. This table describes what happens as a given reactor fuel subassembly is processed through the system. The accompanying timing diagram (Fig. 17) shows the interrelation of these events in real time.

The fifth pot (formerly on the turntable) has been removed from the turntable to an optional auxiliary canyon. The four-pot turntable and drive mechanism are in a well in the center of the processing cell (Fig. 18).

The auxiliary crucibles are placed in individual shielded wells at the operating level of the turntable, and are serviced from beneath with a remote, rail-guided vehicle. The crucibles on the turntable can be removed and replaced, when the turntable is in its lowered position, by a walking beam carrying a winch and grappling hook.

The upper bay area will contain solids feed devices, pressure and vent lines, and electrical supply lines. It will be serviced by manipulators and a light-duty bridge crane.

The auxiliary canyon in which the U/Pu/Zn/Mg/FP-3 is cast will connect directly to its associated distillation canyon, which will in turn connect directly to the canyon where oxidation is accomplished, providing a smooth flow of product with minimal opportunities for diversion.

Figure 18 helps illustrate the workings of the process and the layout of the facility. The details of the mechanical support equipment are not included. The sealing of vessels, agitator entries, and shaft entries is illustrated, but not in great detail due to size constraints. An important

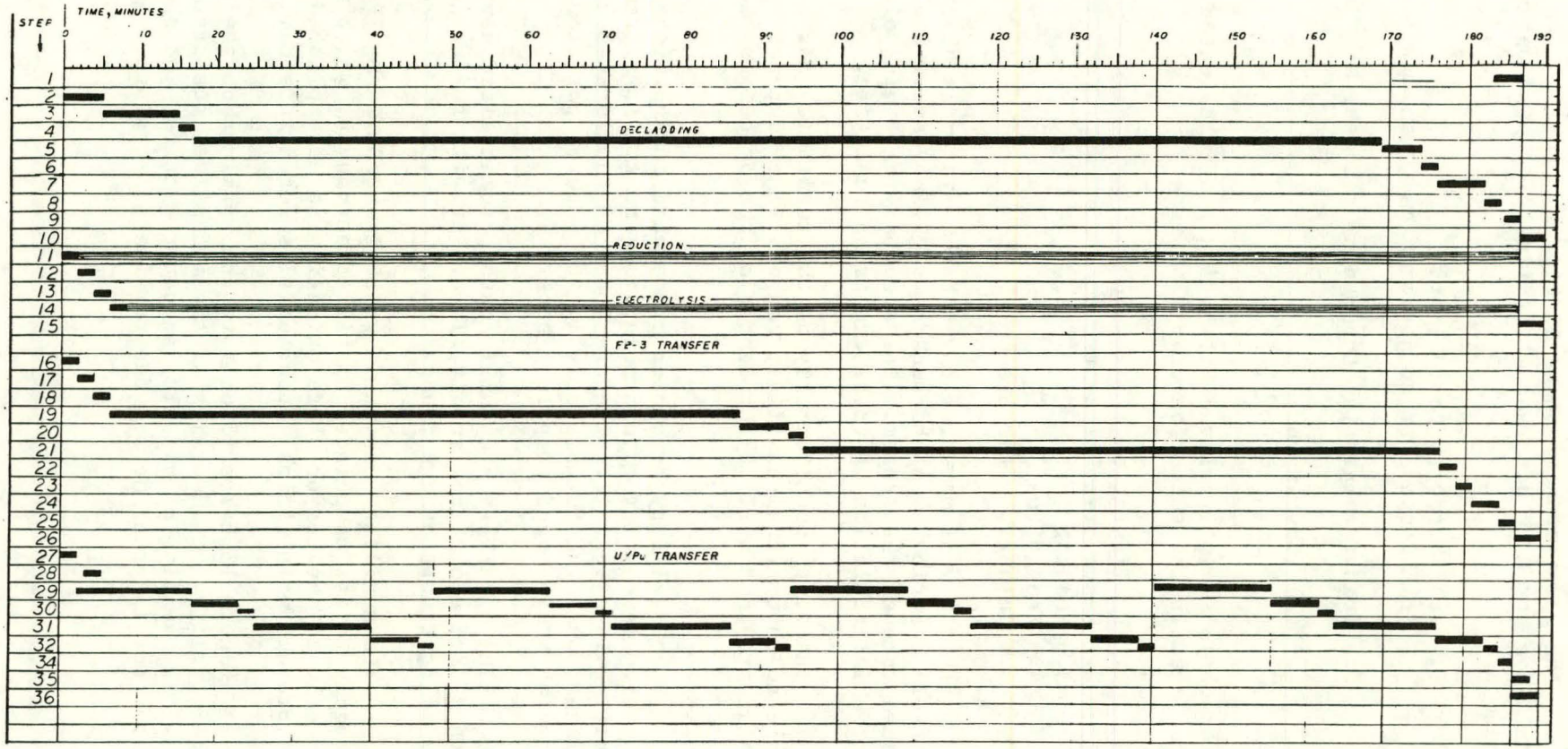

Fig. 17. Turntable Process Timing Diagram. Refer to sequence of events (Table 10) for step descriptions.

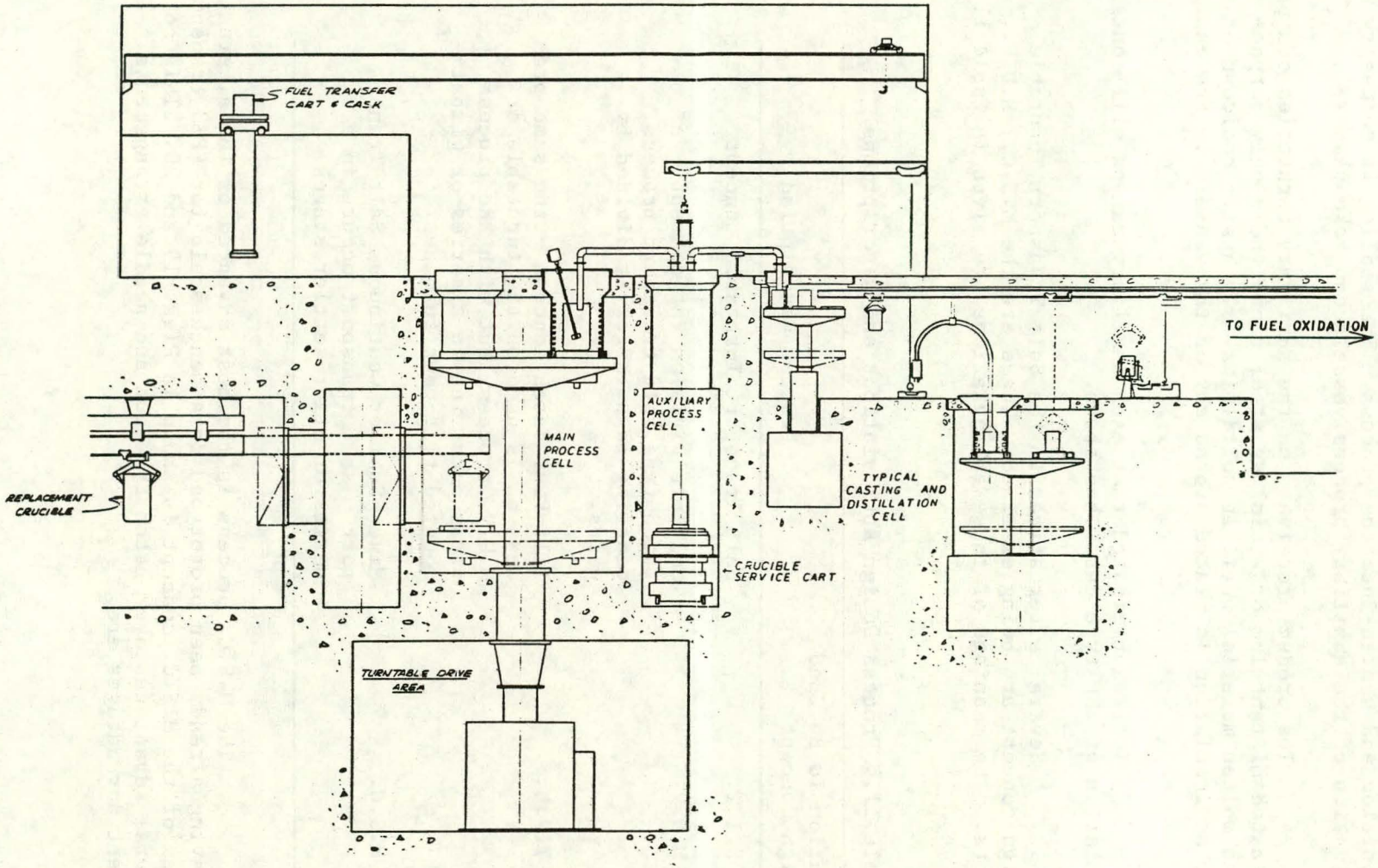

Fig. 18. Floor Layout for Salt Transport Turntable Concept

feature of this drawing is the small carousel to the right of the main turntable. The purpose of this small turntable is to allow casting vessels to be moved into position and sealed into the process. The sealing is necessary so that pressurization of the auxiliary process vessels can take place.

The product receivers on the auxiliary turntables can probably be fabricated of tantalum or stainless steel since their only purpose is to contain the molten material until it solidifies. To hasten cooldown of the cast product, no insulation is placed around any of the vessels in the casting cell.

It is anticipated that each auxiliary canyon will contain a casting operation of the type described above.

Several alternatives to the Salt Transport Turntable (S.T.T.) design concept are being examined. These are the M.S.C., M.D.V., and T.P.B. concepts. The meanings of these abbreviations are given in Table 11 below.

Table 11. Process Design Abbreviations and Descriptions

Abbreviation To Be Used For Design Concept	Process Description
S.T.T.	Salt Transport Turntable concept
M.D.V.	Multiple Division Vat concept - a batch-type salt transport process, ocurring in a large vat divided by weirs.
T.P.B.	Tilt-Pour Batch concept - the same process as is used on the turntable or M.D.V. process, but with the process steps occurring in a series of gimbal-mounted tilt-pour furnaces.
M.S.C.	Mixer-Settler Continuous Salt Transport - salt transport occurs in a series of mixer-settler stages.

The M.S.C. process is the most advanced of the alternative processes, having already been prototyped on a bench scale for FP-3 transport. A flow diagram of the M.S.C. concept is shown in Figs. 19 and 20. This concept has several advantages over batch-type pot and paddle arrangements. Some of the apparent advanatages are:

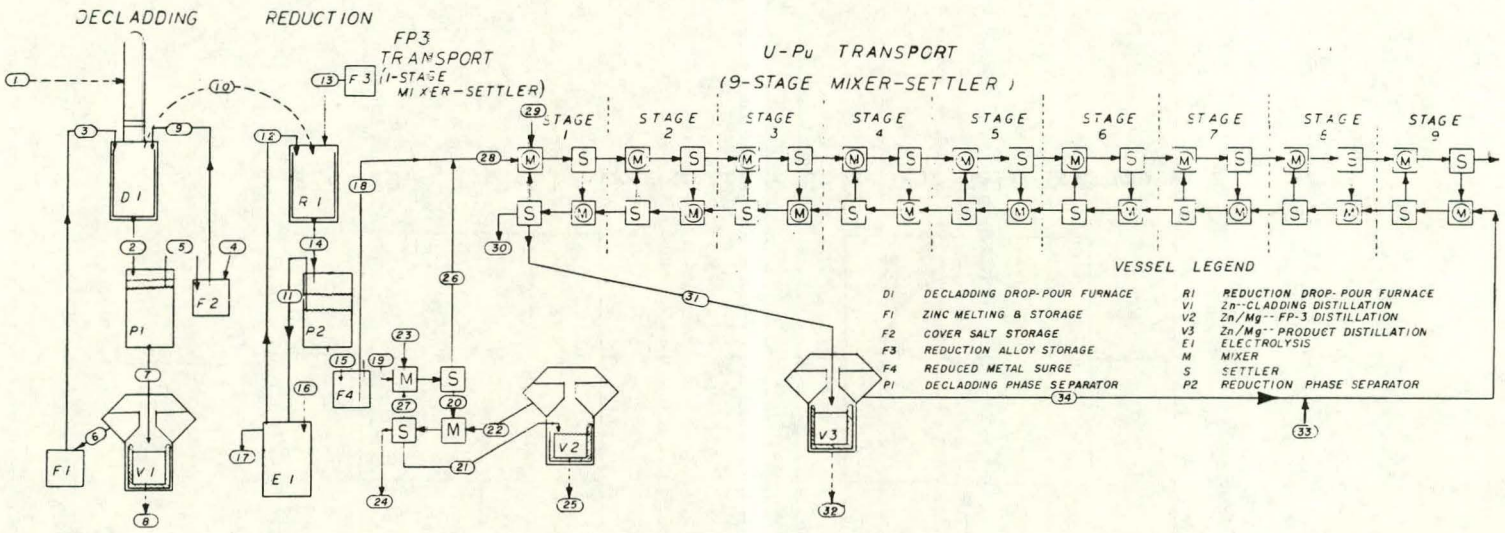

Stream No. →	1	2	3	4	5	6	7	8	9	10	11	12	13	14	15	16	17	18	19	20	21	22	23	24	25	26		27	28	29	30	31	32	33	34	35
Description / Component	Fuel Feed	Zn-Cladding Slurry	Recycle Zinc	Cover Salt Charge	Salt to Recycle	Zinc to Recycle	Zn-Cladding to Zinc Recovery	Cladding to Waste	Salt Recycle	Oxide to Reduction	Spent Salt to Electrolysis	Reduction Salt & Metal	Reduction Metal Makeup	Reduced Charge	Reduced Alloy to Processing	Salt Makeup	Salt Bleed	Spiked Alloy to U/Pu Transport	Alloy to FP-3 Removal	FP-3 Loaded Transport Salt	Loaded FP-3 Acceptor	Recycle FP-3 Acceptor	Salt Makeup	Salt Bleed	FP-3 to Waste	Alloy to U/Pu Transport		Recycle FP-3 Transport Salt	Loaded U/Pu Donor	Salt Makeup	Salt Bleed	Loaded U/Pu Acceptor	U/Pu/FP-3 Product	Acceptor Makeup	Recycle Acceptor	Spent Donor
Cladding	P						P	P																												
PuO_2	P									P																										
UO_2	P									P																										
CaF_2											P	P		P		P	P																			
FP1	P									P																										
FP2	P	T			T			T	T	P	P	P		P			P																			
FP3	P	T						T		P				P	P			P	P	P	P	T		T	P	P		T	P		T	P	P		T	T
FP4	P	T						T		P				P	P			P	P	T	T	T		T	T			T			T		T		T	T
Zn		P	P			P	P															P										P		P	P	
$ZnCl_2$																																				
Mg													P	P	P			P	P		P	P				P			P			P		P	P	P
$MgCl_2$											P	P		P			P			P			P	P				P		P	P					
Ca											P	P		P																						
CaO											P			P																						
$CaCl_2$		P		P	P				P		P	P		P		P	P			P			P	P				P								
KCl		P		P	P				P		P	P		P		P	P			P			P	P				P								
Cu													P	P	P			P	P							P			P							P
U														P	P			P	P		T	T			T	P		T	P		T	P	P		T	T
Pu														P	P			P	P		T	T			T	P		T	P		T	P	P		T	T
MgF_2																														P	P					

P = Process Quantity T = Trace Quantity

Fig. 19. Flow Diagram, Mixer-Settler Continuous Salt Transport

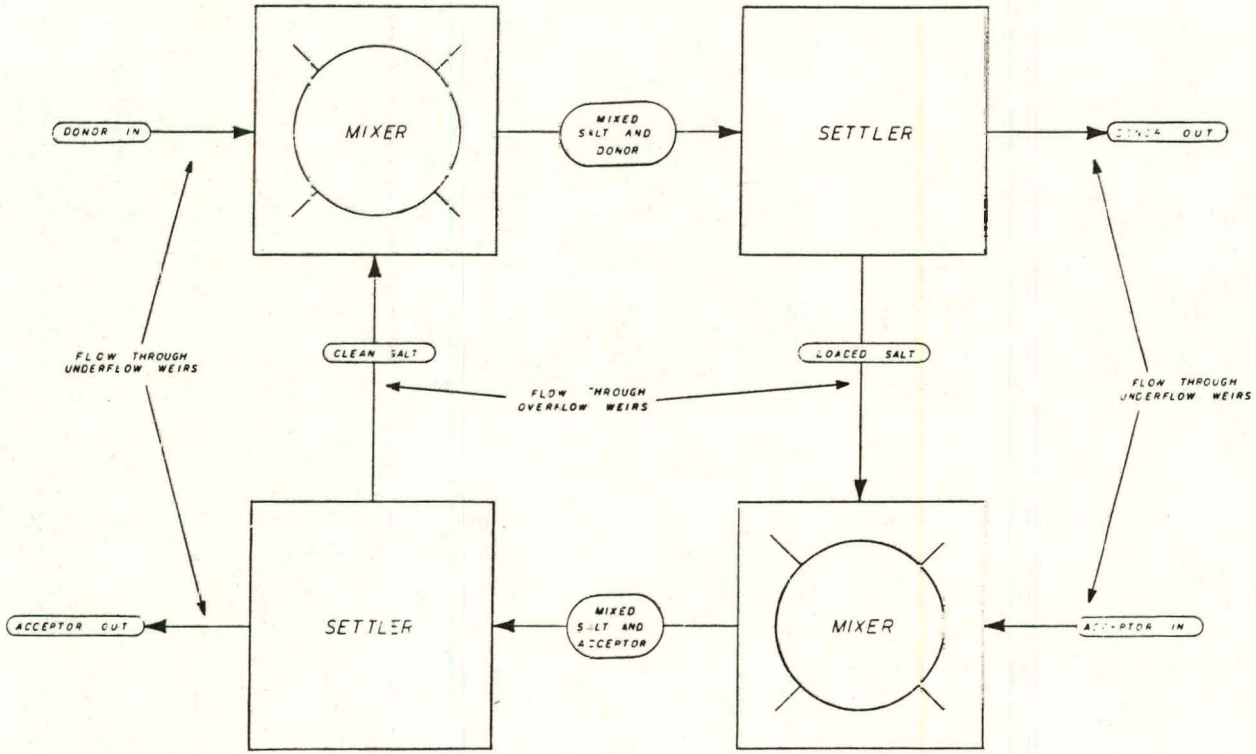

Fig. 2C. Typical Mixer-Settler Stage For Salt Transport

1. Higher throughput per unit hot cell volume.
2. Greater adaptability to a canyon-type situation.
3. Fewer opportunities for product diversion since material moves through weirs integral to the process equipment.
4. Fewer complicated mechanical equipment items.
5. Reduced number of transfer lines and thus fewer failure points.

The impact of these apparent advantages is discussed more thoroughly in the following paragraphs.

1. Higher throughput per unit hot cell volume:

Higher throughput is due to the basic advantages of continuous processing over batch-type processing and semi-batch processing. Continuous operation at steady state produces a more uniform product than batch operation because start-up and shut-down effects are minimized. The latter is quite beneficial since product quality and uniformity are critical in the manufacture of oxide fuel pellets. A possible disadvantage is that a continuous process must be run continuously in order to make best use of the process.

Another possible advantage is that continuous processes are often more cost-effective than comparable batch processes.

2. Greater adaptability to a canyon-type situation:

The mixer-settler stages can be placed either in a compact square array or in a linear array. A linear array is more suitable for canyon operation than is the circular cell demanded by the S.T.T. process.

The use of a narrow canyon, rather than a large circular cell, allows operational techniques and equipment already developed in U.S. facilities to be used. There is the possibility of retrofitting existing canyons if, the advantages of pyrochemistry over existing processes are great enough.

3. Fewer opportunities for diversion since material flows through weirs integral to the process equipment:

This advantage is a result of material flow in the mixer-settler through underflow and overflow weirs in common vessel walls, so that removal and replacement of a major portion of the process train would be necessary in order to change the flow pattern. This would probably be much more difficult than replacing transfer tubes.

4. Fewer pieces of complicated mechanical equipment: Complicated equipment in the turntable concept includes mainly the crucible replacement devices and the turntable and its associated drive mechanisms, which are not needed in the M.S.C. process.

5. Reduced number of transfer lines and thus fewer failure points:

The potential difficulty in fabricating transfer lines is a major problem with the turntable design at present. This difficulty is compounded by the general brittleness of tungsten and the need for heat tracing on all transfer lines. The risk of blockage or breakage of a transfer line appears to be great enough to warrant the elimination of transfer lines where feasible.

c. Separation Processes

(1) Proof-of-Principle Studies
(M. F. Doyle*)

The Operational Safety Analysis (O.S.A.) for the resistance-heated stationary furnaces for the uranium-plutonium salt transport process was given final approval January 3, 1979.

The vacuum-purge system, used to evacuate and pressurize the stationary furnaces during sampling operations, has been installed and is now operational.

The proof-of-principle experiments to evaluate controlled FP-3 removal and the feasibility of coprocessing uranium and plutonium by salt transport have begun.

The sampling techniques were first evaluated by attempting to obtain molten-salt and liquid-metal samples at 900, 820, and 750°C. The salt sampled had a composition of 24.1 mol % KCl, 69.1 mol % $CaCl_2$, and 6.8 mol % $MgCl_2$. A salt sample was successfully obtained in two tests, using a pressure of 11 psig. The alloy had a composition of 94 wt % Cu and 6 wt % Mg. This composition was changed in the next test run to 92 wt % Cu and 8 wt % Mg since it was closer to the eutectic composition and was a lower melting, less viscous alloy. Viscosity was of concern owing to the difficulty encountered in drawing a metal sample through the medium-porosity tantalum frits on the sampling tube openings used in the first test.

*Rockwell International - Rocky Flats.

Our major concerns pertaining to sampling were:

(a) Whether the porosity of the tantalum frits was of acceptable size. [K. M. Myles and J. K. Bates of Argonne National Laboratory suggested the purchase of type KL-308-30 tantalum frits (density, about 10), from the Tantalum Pellet Company, Phoenix, Arizona.] Successful sampling was achieved by using these frits and a pressure differential of 15 psi.

(b) Whether the pressure imposed on the stationary furnace cell would have to be increased. The restriction now limits the pressure to a maximum of 15 psig, accomplished with an adjustable relief valve. With KL-308-30 tantalum frits, the 15-psig maximum was found to be adequate for obtaining salt and alloy samples.

When time permits, a rigorous evaluation needs to be made of tantalum frits. Specifications need to be set to prevent future problems.

A brief description of the sample techniques follows. A salt of the same composition as given above was used--24.1 mol % KCl, 69.1 mol % $CaCl_2$, and 6.8 mol % $MgCl_2$. In the initial run, the salts were of reagent-grade quality. The alloy composition was 94 wt % copper and 6 wt % magnesium. The copper, zinc, and magnesium compositions are given in Table 12.

The alloy and salt were charged to a high-density MgO crucible (3.3 ± 0.1 g/cm^3) 2 in. in diameter by 6 in. tall. The amount of alloy used in this crucible gave a button about 0.75 in. thick after melting and the amount of cover salt gave a cake about 1.50 in. thick, after melting.

The charge in a crucible was heated under an argon atmosphere (about 5 psig) from ambient temperature to 890°C; a 300°C per hour heating rate was used. At 800°C, a tantalum stirrer was inserted into the melt and the melt was agitated until the temperature reached 890°C (about 20 min). The temperature was measured by a chromel-alumel thermocouple (range, -185°C to 1250°C) which was inside a tantalum thermowell immersed in the molten mixture. Stirring was done at low speed (about 50 to 100 rpm) to avoid splattering.

When the melt reached 890°C, mixing was terminated, the melt was allowed to equilibrate and the phases allowed to separate. Thirty minutes was allowed for phase separation. At this point, sampling of the molten alloy and molten salt was done by pressurizing the reaction vessel to 15 psig. to force the sample through the tantalum frits into press-fitted 1/4-in.-dia tantalum sample tubes [WINSCH-1965, STEINDLER-1979B].

Table 12. Compositions of Metals used in the Proof-of-Principle Experiments

Element	Copper, ppm	Zinc, ppm	Magnesium, ppm
C	30	50	50
Al	2000	5	100
As	<100	<50	<100
Ca	10	5	5
Cd	<10	<50	<10
Cu	major	200	200
Fe	1000	200	800
Mn	10	50	150
Mg	30	20	major
Ni	<30	100	20
Pb	<1	<10	<10
Si	<5	20	20
Sn	<10	<10	<10
Sb	<10	<10	<50
Zn	<100	major	<50

The sample tubes were allowed to cool above the melt, with the reaction vessel still pressurized to 15 psig to prevent any back-filtering of the samples. After cooling, the sample tubes were removed, the outside surfaces were polished to free the tubes of extraneous salt and alloy, then the tube was cut open with a pipe cutter. The tantalum frit was discarded to ensure that no solid phase was included with the liquid phase. The remainder of the sample was put into a glass vial for analysis. The analytical results will be included in the next report.

A supply of depleted uranium (D-38) which is to be used in the experimental work has been analyzed. The results of the analyses are presented in Table 13. This uranium will be used in the partitioning coefficient determinations.

Table 13. Impurity Content for Depleted Uranium (D-38)

Element	Concentration, ppm	Element	Concentration, ppm
Al	20	B	<1
Be	<1	Ca	<5
Cr	<14	Cu	2
Fe	<14	K	<10
Mg	<2	Mn	2
Mo	<3	Ni	<6
P	<25	Pb	2
Si	12	Sn	<2
V	<5	Zn	<20
C	221	U	0.9876[a]

[a]Weight fraction uranium.

Table 14 presents the zirconium metal analysis. Zirconium will function as a stand-in for FP-4 fission products.

The plutonium for the study will have a quantity of americium in it as a decay product. (The americium is to function as the FP-3 stand-in.) The plutonium will be analyzed as soon as it is obtained to determine the content of americium and other impurities.

Work on salt transport using the tilt-pour induction-heated furnace will begin as soon as approval from O.S.A. is received. Operationally, the tilt-pour furnace is ready.

Waste generated in the experimental studies will be dealt with by the Special Recovery Group.

Table 14. Impurity Content for Zirconium Metal

Element	Concentration, wt %
C	0.006
N	<0.003
O	0.038
Si	0.026
Zr	99.75 (by diff.)

(2) Salt Purification Laboratory
(T. D. Santa Cruz*)

The Salt Purification Laboratory [STEINDLER-1979B] is now operable. The various safety requirements have been met, and permits to operate major equipment items have been granted. Nuclear material safety limits have been written and established for the laboratory area. The operational safety analysis was completed, reviewed, amended, and authorized. An initial draft of the operating concepts was written and is discussed below. A design for the spectrophotometer furnace is also discussed.

On January 9, 1979, the UV-Vis-NIR spectrophotometer was serviced by a Varian service engineer. The servicing involved completion of an installation checklist, which covered operational, photometric, and accessory checks. The only item outside specifications was the wavelength calibration, which was corrected to ±0.5 Å. The spectrophotometer now meets factory specifications.

The ion selective electrodes (calcium chloride, divalent cation, fluoride, potassium, sodium, pH, and the reference) are now in service.

The argon ion laser for the Raman spectroscopy system has arrived. The spectrometer is not expected until April.

A survey of furnace designs for high-temperature spectroscopy has been completed. The basis of furnace designs will be the findings of the survey. The survey was based on the published literature [BLANDER, BOSTON, CORBETT, GRUEN, JANZ, MORREY, QUIST, YOUNG], designs supplied by Spex Industries [SPEX], and on conversations with Dr. G. N. Papatheodorou [PAPATHEODOROU] of Argonne National Laboratory, who has experience and expertise in spectroscopy at high temperatures. The furnaces described varied in size, temperature range, sample capacity, sample type, and other aspects.

*Rockwell International - Rocky Flats.

The furnace is to be electrothermally heated and controlled by thermocouples. The central core of the furnace will be a machined rod of copper wound with an electrically insulated heating wire covered by asbestos tape. The core section will be covered with a water-cooled stainless steel container. The core will have two compartments, one for the sample cell and one for the reference cell. The use of interchangeable inserts in the compartments will allow samples of various shapes and sizes to be held. A drawing illustrating the specifics of the furnace's construction is being prepared.

The term "black salt" is used generically in some pyrochemical operations to describe the material found in the salt-to-metal interface; this material differs in composition from that of the bulk salt. Since black salts are undesirable in the pyrochemical process, there is a need to understand why black salts are formed, what they are, what effects they have on the process, and how they can be eliminated. Three sources of black salts have been examined. These are graphite carbon, metal nitrides, and metallic fogs.

Graphite from containment vessels is one source of black salt. The carbon, because of its density and insolubility in both the salt and alloy, locates at the salt-to-alloy interface. Three problems might arise from this situation. The carbon might react with the metal solutes or solvent to form an insoluble carbide, the solutes might be sorbed by the carbon particles, or the carbon might collect as a residue in process vessels. The formation of this kind of black salt can be prevented by not using graphite vessels but if the use of graphite vessels is necessary graphite can be removed by filtration.

Another suggested source of black salts is nitride formation owing to the nitrogen atmosphere in the crucible. Actinide nitrides are easily formed in the laboratory by either of two methods: by heating the metal in a nitrogen atmosphere to a high temperature, or by heating the metal hydride in a nitrogen atmosphere at a lower temperature [BROWN-1955, CARROLL, KELLER, PARDUE, POTTER, SAMSONOV, TAGAWA]. In our pyrochemical operations, the molten-salt cover offers no protection against the nitridation of the actinides; instead, it provides a rather good mechanism for the formation of nitrides and has been suggested as a method for forming the actinide nitrides [ERVIN]. As in the case of black salt from graphite the actinide nitrides locate at the salt-to-alloy interface by virtue of their densities and insolubilities. As a result of the formation of actinide nitrides, there might be loss of accountability of the uranium, plutonium, and FP-3 elements. The solutes may be sorbed by the nitride particles, and the nitrides might build up as a residue in the process vessels. The formation of actinide nitrides can be prevented by using a noble gas, such as argon, instead of nitrogen. Metal nitrides can be eliminated by filtration, if nitrogen is used.

A third suggested source of black salt is the entrainment and dissolution of metal in the salt. These phenomena have been termed metallnebels (metallic fogs) or pyrosoles. This portion of the survey is very preliminary, and many of the pertinent publications have not yet been recieved.

The salt mixtures needed by various Rocky Flats Plant task teams have been tabulated (Table 15).

Table 15. Compositions of Major Salt Mixtures

Salt Mixture	Composition, mol %	Composition, wt %
$CaCl_2$:KCl	74.0:26.0	80.9:19.1
$CaCl_2$:CaF_2:KCl	74.0:24.6:1.4	80.2:18.8:1.0
$CaCl_2$:KCl:$MgCl_2$	69.1:24.1:6.8	75.8:17.8:6.4
$MgCl_2$:MgF_2	78.0:22.0	84.4:15.6

In a preliminary phase of the work (shown schematically in Fig. 21), the criteria and goals for salt purification will be established. Each of the salt compositions defined by the task teams (Table 15) will be prepared by weight. These salt mixtures will then be melted and thoroughly mixed. Samples of these salt mixtures will be analyzed--primarily to confirm the salt compositions, but also to identify impurities such as oxygen, sulfur, and heavy metals. The criteria and goals for the purification studies can be established from these results.

The next work phase (shown schematically in Fig. 22) encompasses the modes of purification. Each salt mixture will again be prepared by weight as defined by the salt composition. At this point, the decision must be made as to which of two modes of purification is to be applied: liquid alloy contacting [JOHNSON] or active gas purging [SHAFFER]. After use of the selected purification step, a sample of the salt mixture will be analyzed for composition and impurities. If the salt meets the criteria for purity, it will be sent to a task team for laboratory use in experiments. Otherwise, it will either be resubmitted for another purification run or submitted to the alternative purification route. Eventually, this process of experimental recursion will lead to a standard method for purifying the salt.

(3) Proliferation Study
(J. L. Zoellner*)

An outline and preliminary time schedule for the proliferation study have been developed; these are shown in Tables 16 and 17,

*Rockwell International--Rocky Flats.

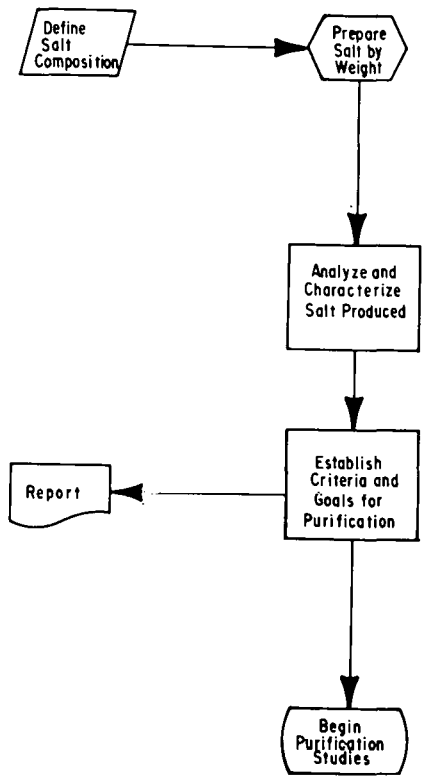

Fig. 21. Preliminary Phase of the Experimental Work Plan

respectively. This outline will be followed for each conceptual process design based on salt such as that shown in Fig. 15.

The first step in the proliferation study is to establish the general proliferation criteria to be used in the study. These criteria will be expanded and updated as more data become available. The following proliferation-related criteria were developed during the Proliferation-Resistant Pyrochemical Process which was performed for ORNL during October and November, 1978. These criteria will form the basis for the proliferation study of the Salt Transport Process at Rocky Flats. The following is a basic list of the criteria (presented in [STEINDLER-1979B]) and the manner in which they will be interpreted and used in the study.

1. The fissile materials produced should be sufficiently radioactive and diluted with fertile material so that diversion is difficult, detection of the material is easy, and conversion into weapons-usable material is difficult.

Sufficient radioactive contamination will be defined as 500 rads/h at 1 m from a mass of the material containing 8 kg of plutonium. This dose is considered to be sufficient to discourage diversion of unshielded material. The fissile material should be diluted with a minimum of 80 %

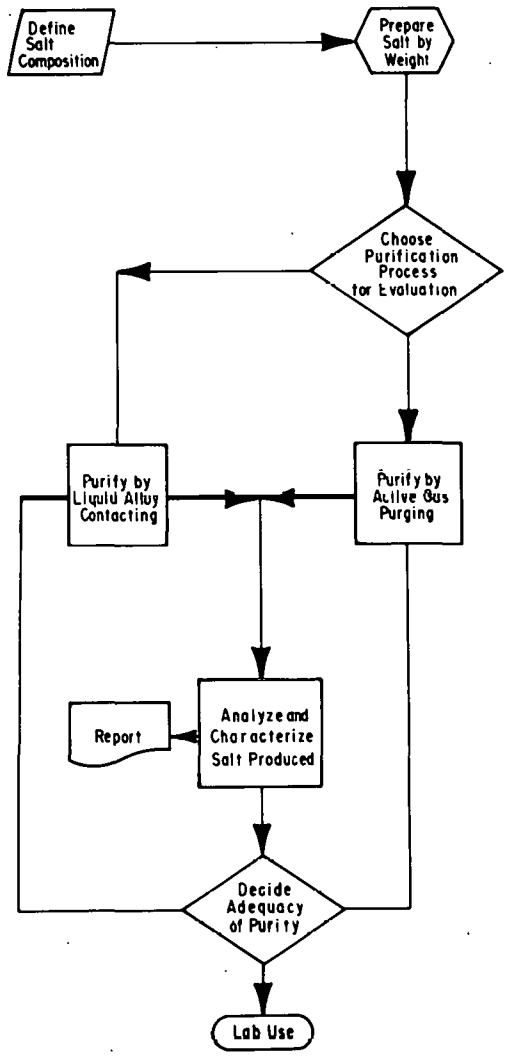

Fig. 22. Major Phase of the Experimental Work Plan

fertile material. Converting this material into weapons-usable material would be difficult since transport, storage, and concealment of the material would require heavy shielding. Processing any sizable quantity would require extensive facilities, reducing the opportunity for clandestine operations.

2. The process should not be capable of producing highly decontaminated or enriched fissile materials, through simple process adjustment, reagent substitution, or equipment modification.

This requirement is the main focal point of the proliferation study. The process must be so designed that in all operations the material remains at or above the radiation levels described in item 1 above. In

Table 16. Single Process Proliferation Study Approach

I. Analysis of Proliferation Resistance of the Base Case

A. Establish definitions and proliferation-resistance criteria

B. Establish base-case operating parameters

1. Mass balance

2. Vessel volumes

3. Thermal heating

4. Gamma radiation

5. Feed and bleed streams

6. Product streams

7. Process throughput

C. Proliferation resistance of the normal process and equipment

1. Methods of proliferation

2. Proliferation defense methods

a. Sufficient radiation
b. dilution
c. Other

II. Analysis of Proliferation Resistance After Modifications to the Process Control

A. Methods of Producing an enriched decontaminated product

1. Change in process temperatures

2. Change in type of fuel to be reprocessed (Substituting blanket for core and vice versa)

3. Recycle of processed material

4. Change in time allotted for process operations

5. Clandestine side stream and process stream confiscation

(contd)

Table 16. (contd)

6. Other methods

B. Proliferation defense methods against process control modifications

III. Analysis of Proliferation Resistance After Modifications in Process Control and Process Reagents

A. Methods of Proliferation

1. Substitution of reagents, including concentration changes

2. Addition and reduction of extra reagents

3. Other methods

B. Proliferation defense methods for modifications to process materials

IV. Analysis of Proliferation Resistance after Modifications in Process Control, Materials and Equipment, and Facilities

A. Methods of Proliferation

1. Rearrangement of piping

2. Reordering process steps

3. Substitution or rearrangement of other equipment

4. Facilities modification

5. Other methods

B. Proliferation defense methods for changes in plant piping and equipment

V. Examination of Possible Outcome and Defense Against Overt Political or Terrorist Plant Takeover

VI. Analysis of Recovered Product as a Fuel for Power Plant Use and Proliferation Resistance

Table 17. Preliminary Time Schedule for the Proliferation Study

Task		Estimated Completion Date
I.	Turntable Design[a]	
	A. Initiate base case evaluation	2/26/79
	B. Process control modifications	3/23/79
	C. Process material modifications	3/21/79
	D. Equipment and facilities modifications	4/9/79
II.	Mixer-Settler[a] or CSTR[b] Technology	
	A. Base case evaluation	4/30/79
	B. Process control modifications	5/14/79
	C. Process material modifications	5/27/79
	D. Equipment and facilities modifications	6/11/79
III.	Analysis of overt takeover for Cases I and II	7/11/79
IV.	Evaluation of fuel acceptability and proliferation effectiveness for cases I and II	8/11/79
V.	First alternative concept	
	A. Base case evaluation	6/1/79
	B. Process control modifications	6/15/79
	C. Process material modifications	7/11/79
	D. Equipment and facilities modifications	7/27/79
	E. Fuel acceptability evaluation	8/3/79

[a]See Section I.C.3b (4) of this report.
[b]Constant Stirred Tank Reactor.

addition, no simple modification of the equipment or chemical reagents should result in a process stream containing high percentages of (weapons grade) fissile materials.

3. Any modification of the process equipment should require facilities and components not normally on site and should require either plant decontamination or entry into areas of extremely high radioactivity.

This criterion is self-explanatory and further complicates attempted changes or modifications to the process facility.

4. The length of time required to divert fissile materials should be adequate for appropriate national and/or international responses.

Appropriate national and/or international responses are assumed to occur within eight weeks of discovery of a diversion incident. Thus, the plant must be so designed that any modifications necessary to produce the desired product must take eight weeks or longer to accomplish.

5. The process must permit real-time accountability of fissile material.

A method must be developed for accountability of the fissile material in the process at any given time. However, this criterion is not considered to be within the scope of the present proliferation study and will not be discussed at this time.

6. The facility must be operated remotely and must be maintained remotely, using only dedicated equipment.

Because of the radioactivity of the materials in the process, remote handling will be mandatory. Use of dedicated equipment only in such a remote handling area will further ensure maximum difficulty in making machinery and process equipment modifications.

Note that the above criteria are not restricted to any particular salt transport process design concept (i.e., turntable, mixer-settler, etc.) but are general in nature and will be used for all design concepts.

Based on predicted methods of construction and operation, preliminary heel volumes have been calculated for the salt transport process turntable* concept. The present design employs 24-in.-dia crucibles on the turntable, and most secondary process vessels; the FP-3 donor vessel and the FP-3 acceptor vessel are also 24 in. in diameter. The calculated heel volumes represent the minimum amounts of material remaining in the vessels after processing and removal from the vessel. These volumes will be included with the

*See Section I.C.3.b(4) of this report.

process volumes to establish the base case for the turntable concept (Table 18). It should be noted that these heel volumes are estimates only. In some cases, they will be varied to determine the effects on proliferation. The computer program modification presently being developed by Dr. W. A. Averill will incorporate the effects of heel volumes, which will be examined later for their influence on proliferation and diversion.

Table 18. Heel Volumes in Salt Transport Process - Turntable Concept

Vessel	Assumptions	Heel, L (ft^3)
Decladding (24-in. dia.)	5% of total zinc and stainless steel remains with fuel pellets (see design parameters)	3.73 (0.132)
Reduction FP-3 Donor Storage (24-in. dia.)	1/4-in. layer of alloy taken with the salt	1.85 (0.066)
FP-3 Donor A3 (14-in. dia.)	Assume 1/4-in. alloy layer remains in vessel bottom	0.63 (0.022)
	All salt taken except 1/4-in. layer	0.63 (0.022)
FP-3 Acceptor A4 (14-in. dia.)	1/4-in. salt layer remains on alloy	0.63 (0.022)
	1/4-in. alloy layer remains in vessel bottom	0.63 (0.022)
U-Pu Donor (24-in. dia.)	1/4-in. salt layer remains on alloy	1.85 (0.066)
	1/4-in. alloy layer transferred to storage vessel with salt	1.85 (0.066)
U-Pu Acceptor A5 (24-in. dia.)	All but 1/4-in. salt layer is transferred and 1/4 in. alloy remains in vessel bottom	1.85 (0.066)
		1.85 (0.066)
Salt Donor Heel Storage A6 (24-in. dia.)	1/4-in. layer of alloy remains after transfer	1.85 (0.066)

(contd)

Table 18. (contd)

Vessel	Assumptions	Heel, L (ft^3)
U-Donor (24-in. dia.)	1/4 in. alloy 1/4 in. salt	1.85 (0.066)
Salt Donor Heel Storage A8 (24-in. dia.)	1/4 in. alloy	1.85 (0.066)
U-Acceptor (24-in. dia.)	1/4 in. alloy 1/4 in. salt	1.85 (0.066) 1.85 (0.066)
Decladding Phase Separator A1 (24-in. dia.)	1/4 in. alloy 1/4 in. salt	1.85 (0.066) 1.85 (0.066)

The base-case salt transport mass balance has been developed, and analysis for proliferation resistance was started during January and February. However, the distribution coefficients and solubility values for several of the materials in the process have been reevaluated and were modified by process-design personnel to conform better to the process conditions. During February, the base process model was transferred from the DEC-10 computer at the Colorado School of Mines to the Apple II microcomputer at Rocky Flats. Several problems encountered during the transfer caused a delay in data analysis. These problems have been resolved, however, and the program is now running.

(a) Selection of Base-Case Operating Parameters

As mentioned above, the distribution coefficients and solubility values changed upon reevaluation. These changes affected the mass balances of the salt transport process being examined for proliferation potential. Since many different combinations of operating temperatures in the various operation steps exist, two tables were developed which list the various alloy and salt compositions under consideration (Table 19) and the metal solubilities and distribution coefficients for the conditions under consideration (Table 20).

Table 21, developed using these inputs and the SALT I computer model for each combination of donor and acceptor temperatures, shows calculated salt transport results. Also, two different masses of salt were evaluated. These cases were examined to determine the salt transport mass balance for a "base case." From Table 21, it can be seen that increasing the mass of the uranium-plutonium transport salt greatly reduces the number of passes (which refers to the number of times the transport salt is transferred from the donor to the acceptor and back again). It is desirable to reduce the number of passes in order to reduce operation time and the number of process steps.

Table 19. Salt Transport Operating Parameters

		Liquid Alloy Composition								Salt Composition									
		wt %				mol %				wt %					mol %				
Operation	Temp, °C	Zn	Cu	Mg	U	Zn	Cu	Mg	U	$CaCl_2$	KCl	CaF_2	$MgCl_2$	MgF_2	$CaCl_2$	KCl	CaF_2	$MgCl_2$	MgF_2
Decladding	800	100				100				80.9	19.1				74.0	26.0			
Reduction	800		89.4	6.5	4.1		83.2	15.8	1.0	80.2	1.0	18.8			74.0	1.4	24.6		
FP-3 Donor	800		89.4	6.5	4.1		83.2	15.8	1.0	75.8	17.8		6.4		69.1	24.1		6.8	
FP-3 Acceptor	750	88.0		12.0		73.2		26.8		75.8	17.8		6.4		69.1	24.1		6.8	
U-Pu Donor	850		87.9	4.6	7.5		86.2	11.8	2.0				84.4	15.6				78.0	22.0
	800		89.4	6.5	4.1		83.2	15.8	1.0				84.4	15.6				78.0	22.0
U-Pu Acceptor	750	88.0		12.0		73.2		26.8					84.4	15.6				78.0	22.0
	700	88.0		12.0		73.2		26.8					84.4	15.6				78.0	22.0
U Donor	850		87.9	4.6	7.5		86.2	11.8	2.0				84.4	15.6				78.0	22.0
	800		89.4	6.5	4.1		83.2	15.8	1.0				84.4	15.6				78.0	22.0
U Acceptor	800	88.0		12.0		73.2		26.8					84.4	15.6				78.0	22.0
	750	88.0		12.0		73.2		26.8					84.4	15.6				78.0	22.0
	700	88.0		12.0		73.2		26.8					84.4	15.6				78.0	22.0

Table 20. Salt Transport Distribution Coefficients and Solubilities

Operation	Temp, °C	Distribution Coefficient			Solubility in Appropriate Alloy, wt %					
		FP-3(Ce)	Pu	U	FP-3(Ce)	Pu	U	Fe	Cu	Ni
Decladding	800	0.005	2.8×10^{-5}	low	3.98	9.29	5.47	7.90	1.85	10.6
Reduction	800	0.005	2.8×10^{-5}	low	high	high	4.1	-	-	-
FP-3 Donor	800	10.7	0.037	0.0015	high	high	4.1	-	-	-
FP-3 Acceptor	750	0.0127	1.7×10^{-4}	7.06×10^{-5}	12.0	12.0	5.0	-	-	-
U-Pu Donor	850	600	2.1	0.41	high	high	7.5	-	-	-
	800	600	2.1	0.29	high	high	4.1	-	-	-
U-Pu Acceptor	750	0.70	0.01	0.004	12.0	12.0	5.0	-	-	-
	700	0.50	0.005	0.0014	5.5	5.5	1.9	-	-	-
U-Donor	850	600	2.1	0.41	high	high	7.5	-	-	-
	800	600	2.1	0.29	high	high	4.1	-	-	-
U-Acceptor	800	1.00	0.015	0.005	high	high	16.0	-	-	-
	750	0.70	0.01	0.004	12.0	12.0	5.0	-	-	-
	700	0.50	0.005	0.0014	5.5	5.5	1.9	-	-	-

Table 21. Calculated Salt Transport Results for Core/Axial Blanket

Case	Donor Temp, °C	Acceptor Temp, °C	Weight of Salt, kg	No. of Passes	Pu Enrichment	Pu Recovery, %
1	800	700	270	15	0.191	98.9
2	800	750	270	15	0.193	98.2
3	850	700	270	8	0.203	99.3
4	850	750	270	7	0.200	98.9
5	800	700	540	8	0.199	98.9
6	800	750	540	5	0.189	98.9
7	850	700	540	5	0.189	99.3
8	850	750	540	5	0.189	98.9

It is also a general design criterion that the recovery of plutonium must exceed 99% and that the plutonium enrichment* must be adequate for a fuel cycle, i.e., 20% enriched with plutonium (see General Design Criteria, [Table 14, STEINDLER-1979B]). From Table 21, it can be seen that the uranium-plutonium transport performed at 850°C donor and 700°C acceptor temperatures with 540 kg of transport salt (Case 7) yields the best combination of plutonium recovery and plutonium enrichment. This case will be referred to as the "base case" since initially, it appears to be the best combination of parameters for the process. However, all cases will be evaluated for proliferation resistance as a function of various parameters.

(b) Proliferation Resistance of the Normal Process and Equipment

In the uranium-plutonium salt transport step, the donor alloy (86.2 mol % Cu, 11.8 mol % Mg, 2 mol % U) is equilibrated with the transport salt (78.0 mol % $MgCl_2$, 22 mol % MgF_2) at 850°C. After equilibration is complete, the phases are permitted to separate and the salt phase containing uranium, plutonium, and fission products is transferred to another vessel. In the second vessel, the salt is equilibrated with the acceptor alloy (73.2 mol % Zn, 26.8 mol % Mg) at 700°C, resulting in the transfer of the bulk of the uranium, plutonium, and fission products originally in the salt to the acceptor alloy. After equilibration, the phases are permitted to separate and the salt is returned to the vessel containing the donor alloy. The completion of these two equilibrations is termed one pass. These two

*Percent plutonim in the actinides.

equilibrations may be repeated for a second pass and for as many additional passes as are deemed necessary to achieve the desired end product.

Table 22 shows the uranium, plutonium, and FP-3 contents in the uranium-plutonium transport steps for the base-case core/axial blanket fuel. The table shows the material content from the start of transport through pass five, at which time enrichment was less than 20% and plutonium recovery was greater than 99%. Note that the percent plutonium recovered is adequate after the third pass, but that two additional passes are required to reduce the enrichment level to the required 20%.

The FP-3 elements are retained in the uranium-plutonium acceptor alloy to provide diversion resistance. The FP-3 content of the alloy after the fifth pass is approximately 0.44 kg. The data in Tables 22 and 23 show that the mass of FP-3 releases about 360.8 gamma rads/h at 3 ft. This is less than the 500 rads/h limit defined in the proliferation criteria. However, the case under examination was run with a FP-3 concentration of zero initially in the uranium-plutonium transport salt. Table 24 shows the estimated concentration of FP-3 in the FP-3 acceptor and the uranium-plutonium acceptor alloy as several successive core/axial blanket fuel subassemblies are processed. The FP-3 quantity in the uranium-plutonium acceptor increases to a steady-state level after seven assemblies have been processed. As can be seen, the acceptor alloy is sufficiently contaminated after the second assembly has been processed. This indicates that in a new processing plant, the first runs should be made using artifically spiked salts to provide diversion resistance for the fuel alloy.

The plutonium/plutonium + uranium ratio (enrichment) is highest at the end of the first pass, as shown in Table 22. In subsequent passes, this ratio steadily decreases to the desired 20%. Since enrichment is never greater than 65% and since the plutonium is dissolved in both the acceptor and donor, a large quantity of material would need to be diverted to obtain a substantial quantity of plutonium. After the first pass, for instance, approximately 171.5 kg of acceptor alloy would need to be diverted to obtain 8.9 kg of plutonium. Also, such a quantity of material would contain most of the FP-3 fission products originally present in the irradiated fuel, resulting in a highly contaminated mass. Table 25, the mass balance for the base-case Salt Transport Turntable Process, demonstrates that no highly decontaminated process streams exist.

(c) Proliferation Resistance after Modifications of Process Control

There are modifications of the process control that may affect resistance to diversion of fissile material. Such modifications are (1) changes in time and temperature of operation, (2) changes in feed material, (3) recycle of material, and (4) diversion of process materials without changes or modifications of the process equipment or reagents.

Table 21 shows the relationship between temperature in the uranium-plutonium transfer steps and the enrichment of the uranium-plutonium acceptor alloy. The highest enrichment in the acceptor alloy occurs

Table 22. Core/Axial Blanket Reference Fuel - U-Pu Transport Steps (850°C Donor, 700°C Acceptor) with 540 kg Transport Salt[a]

Pass	Donor Alloy, kg			Salt, kg			Alloy Acceptor			Enrichment, Pu/U + Pu	Pu Recovery, %	Gamma Radiation, rad/h at 3ft for U-Pu Acceptor Alloy Containing FP-3	Gamma Radiation, rad/h at 3ft for Mass Containing 8 kg Pu[b]
	U	Pu	FP-3	U	Pu	FP-3	U	Pu	FP-3				
Start	11.045	10.075	1.019	0	0	0	0	0	0	0	0		
1	15.47	1.05	4.2×10^{-4}	0.030	0.138	0.619	6.88	8.88	0.40	0.563	89.07	327.9	295.4
2	17.72	0.178	3.8×10^{-4}	0.063	0.146	0.609	14.96	9.75	0.41	0.395	97.84	336.1	275.8
3	19.92	0.054	4.3×10^{-4}	0.095	0.142	0.600	23.63	9.88	0.42	0.295	99.08	344.4	278.9
4	22.22	0.036	4.7×10^{-4}	0.127	0.137	0.590	32.78	9.90	0.43	0.232	99.27	352.6	284.9
5	21.93	0.036	5.2×10^{-4}	0.157	0.131	0.580	42.38	9.91	0.44	0.189	99.27	360.8	291.3

[a]Transport salt was initially free of FP-3 contamination.

[b]Developed from Table 23.

Table 23. Radiation Data for AI Reference LMFBR Oxide Core + Axial Blanket Fuel Subassembly (at 90 days cooling, 8% core burnup) [ORNL]

Group	Wt Fuel Subassembly, kg Total	Wt Fuel Subassembly, kg Radioisotopes	Curies per Fuel Subassembly	Thermal Watts per Fuel Subassembly	Total Gamma Radiation, rad/h, at 3 ft
FP-1	0.567	0.003	1400	2.04	17.7
FP-2	0.963	0.422	1.05×10^5	306.7	1521
FP-3	1.122	0.088	2.96×10^5	1596	920
FP-4	1.659	0.305	6.11×10^5	3522	13950
Cladding	56.67	0.005	3.57×10^5	344.3	1081
Fuel	74.576	74.576	8.47×10^4	50.7	0
Np, Am, Cm	0.125	0.125	7450	19.6	0

Table 24. The FP-3 Fission Product Concentration in FP-3 and U-Pu Transport Alloys upon Recycle of Salt and Alloy

Number of Core/Axial Blanket Sub-Assemblies Processed	Residual FP-3 Content (in Alloy), kg After FP-3 Acceptor Step	Residual FP-3 Content (in Alloy), kg After U-Pu Acceptor Step	Gamma Radiation, rads/h at 3 ft
1	0.095	0.44	360.8
2	0.101	0.71	582.2
3	0.102	0.826	677.3
4	0.102	0.908	744.6
5	0.102	0.972	797.0
6	0.102	0.991	812.6
7	0.102	1.001	820.8
8	0.102	1.001	820.8

Table 25. Material Balance for Materials in Solution in Salt Transport Process for a Core/Axial Blanket Assembly (Base Case)

Vessel	Content, kg	Fission Product Decay Heat, W	Total Gamma Radiation, rad/h at 3ft	Material of Construction	Operating Conditions	Chemical Volume 270 kg U-Pu Transport Salt[a]	Chemical Volume 540 kg U-Pu Transport Salt[b]
Decladding	73.131 UO_2 11.466 PuO_2 0.567 FP-1 0.963 FP-2 1.122 FP-3 1.66 FP-4 226.68 Zn 56.67 SS 12.14 $CaCl_2$ 2.86 KCl 1.305 Excess O	5840	17,500	Tungsten	800°C Ambient Pressure	52.06 L 1.84 ft^3	52.06 L 1.84 ft^3
Phase Separator, A1	226.68 Zn 56.67 SS 12.14 $CaCl_2$ 2.86 KCl	344	1080	Tungsten	800°C Pressurized	46.01 L 1.62 ft^3	46.01 L 1.62 ft^3
Vacuum, D1	228.56 Zn 56.67 SS 0.225 Mg 0.095 FP-3 0.037 Pu 0.0017 U	479	1160	Tantalum-Carbide Coated Graphite	1000°C Vacuum	39.33 L 1.39 ft^3	39.33 L 1.39 ft^3
Phase Separator, A2	0.963 FP-2 204.67 $CaCl_2$ 2.86 KCl 41.66 CaF_2 39.87 CaO	307	1520	Tungsten	800°C Pressurized	122.2 L 4.32 ft^3	122.2 L 4.32 ft^3

(contd)

Table 25. (contd)

Vessel	Content, kg	Fission Product Decay Heat, W	Total Gamma Radiation, rad/h at 3ft	Material of Construction	Operating Conditions	Chemical Volume 270 kg U-Pu Transport Salt[a]	Chemical Volume 540 kg U-Pu Transport Salt[b]
Reduction	11.05 U 10.112 Pu 0.963 FP-2 1.122 FP-3 1.66 FP-4 6.78 Mg 2.85 Ca 116.58 Cu 204.67 $CaCl_2$ 2.86 KCl 41.66 CaF_2 39.87 CaO	5490	16,400	Tungsten	800°C Ambient Pressure	142.6 L 5.04 ft^3	142.6 L 5.04 ft^3
Electrolysis	0.963 FP-2 39.87 CaO 2.85 Ca 204.67 $CaCl_2$ 2.86 KCl 41.66 CaF_2	307	1520	Haynes 25	700°C Ambient Pressure	122.2 L 4.31 ft^3	122.2 L 4.31 ft^3
FP-3 Donor Storage	11.05 U 10.112 Pu 1.122 FP-3 1.66 FP-4 6.78 Mg 2.85 Ca 116.58 Cu	5190	14900	Tungsten	800°C Pressurized	20.36 L 0.72 ft^3	20.36 L 0.72 ft^3
FP-3 Donor, A-3	1.105 U 1.011 Pu 0.112 FP-3 0.166 FP-4 0.678 Mg 0.285 Ca 11.66 Cu 11.38 $CaCl_2$ 2.67 KCl 0.96 $MgCl_2$	519	1490	Tungsten	800°C Pressurized	9.08 L 0.32 ft^3	9.08 L 0.32 ft^3

(contd)

Table 25. (contd)

Vessel	Content, kg	Fission Product Decay Heat, W	Total Gamma Radiation, rad/h at 3ft	Material of Construction	Operating Conditions	Chemical Volume 270 kg U-Pu Transport Salt[a]	Chemical Volume 540 kg U-Pu Transport Salt[b]
FP-3 Acceptor A4	0.0017 U 0.037 Pu 0.095 FP-3 0.225 Mg 1.876 Zn 11.38 $CaCl_2$ 2.67 KCl 0.95 $MgCl_2$	135	87.9	Tungsten	750°C Pressurized	7.46 L 0.26 ft^3	7.46 L 0.26 ft^3
U-Pu Donor, P4	11.045 U 10.075 Pu 1.019 FP-3 1.66 FP-4 6.808 Mg 2.85 Ca 116.58 Cu 455.86[b] $MgCl_2$ (227.93)[a] 84.14[b] MgF_2 (42.1)[a]	5040	14,800	Tungsten	850°C Pressurized	131.34 L 4.63 ft^3	242.34 L 8.56 ft^3
U-Pu, Acceptor A5	42.534 U 10.038 Pu 1.018 FP-3 10.84 Mg 138.89 Zn 455.1[b] $MgCl_2$ (227.42)[a] 84.14[b] MgF_2 (42.07)[a]	1520	835	Tungsten	700°C Pressurized	139.29 L 4.91 ft3	250.31 L 8.83 ft3
Vacuum Still D3	42.38 U 9.908 Pu 0.438 FP-3 10.84 Mg 138.89 Zn	673	359	Tantalum Carbide Coated Graphite	1000°C Vacuum	28.52 L 1.01 ft^3	28.52 L 1.01 ft^3
Salt, Donor Heel Storage, A6	455.1[b] $MgCl_2$ (227.4)[a] 84.1[b] MgF_2 (42.1)[a] 0.157[b] U (0.086)[a] 0.131[b] Pu (0.068)[a] 0.58[b] FP-3 (0.413)[a]	826	476	Tungsten	800°C Pressurized	110.86 L 3.92 ft^3	221.79 L 7.83 ft^3

(contd)

Table 25. (contd)

Vessel	Content, kg	Fission Product Decay Heat, W	Total Gamma Radiation, rad/h at 3ft	Material of Construction	Operating Conditions	Chemical Volume 270 kg U-Pu Transport Salt[a]	Chemical Volume 540 kg U-Pu Transport Salt[b]
U Donor, P5	21.93 U 0.036 Pu 1.66 FP-4 15.1 Mg 279.4 Cu 227.9 $MgCl_2$ 42.07 MgF_2 2.85 Ca	3520	13,950	Tungsten	850°C Pressurized	154.1 L 5.44 ft^3	154.1 L 5.44 ft^3
U Acceptor, A7	21.36 U 0.036 Pu 37.95 Mg 302.3 Zn 227.9 $MgCl_2$ 42.07 MgF_2	0.20	0	Tungsten	700°C Pressurized	176.3 L 6.2 ft^3	176.3 L 6.2 ft^3
Vacuum Still, D4	21.36 U 0.036 Pu 37.95 Mg 302.3 Zn	0.20	0	Tantalum Carbide Coated Graphite	1000°C Vacuum	65.3 L 2.3 ft^3	65.3 L 2.3 ft^3
Salt, Donor Heel Storage, A8	279.4 Cu 18.38 Mg 0.583 U 1.66 FP-4 227.9 $MgCl_2$ 42.07 MgF_2	3520	13,950	Tungsten	800°C Pressurized	154.9 L 5.5 ft^3	154.9 L 5.5 ft^3
Vacuum Still, D5	279.4 Cu 18.38 Mg 0.583 U 1.66 FP-4	3520	13,950	Tantalum Carbide Coated Graphite	1000°C Pressurized	43.9 L 1.6 ft^3	43.9 L 1.6 ft^3
Electrorefine	279.4 Cu 0.583 U 1.66 FP-4	3520	13,950	Tantalum Carbide Coated Graphite	1000°C Pressurized	33.1 L 1.2 ft^3	33.1 L 1.2 ft^3

[a]The contents marked indicate the amounts present when 270 kg of U-Pu trnasport salt was used.

[b]The contents marked indicate the amounts present when 540 kg U-Pu transport salt was used.

when the donor alloy temperature is 850°C and the acceptor alloy temperature is 700°C, which are the temperatures used in the base case. If the donor alloy temperature is lowered from the base-case conditions, enrichment tends to decrease. If the acceptor alloy temperature is increased, the result is a tendency to lower plutonium recovery. Thus, altering the temperature in the 700 to 850°C range appears to produce material that is less desirable to divert. (Effects of temperatures outside this range will be examined later.)

The numerous side streams containing small amounts of plutonium going to waste storage or casting might be targets for confiscation over a long period of time. However, Table 26 shows that these streams would be sufficiently dilute and/or contaminated to make this technique for diversion undesirable.

Table 26. Product and Side Stream Enrichment and Radioactivity (Core/Axial Blanket Base Case)

Stream	Stream Description	Enrichment, Pu(U+Pu)	Gamma Radiation, rad/h at 1 m for a Quantity of Alloy Containing 8 kg Pu
8	Cladding to waste. Stream contains small amounts of U, Pu	0.96	2.51×10^5
22	FP-3 acceptor alloy to casting, stream contains small amounts of U, Pu	0.96	2.51×10^5
45	U product. Stream contains a small amount amount of Pu	0.0017	0

The effects of recycling process material, such as the uranium-plutonium product, have not yet been evaluated.

Currently, running a radial blanket fuel assembly through the process using the standard flowsheet on a once-through basis would give a product having a 12.4% enrichment and 59.9% plutonium recovery with one uranium-plutonium transport pass. Further uranium-plutonium transport passes would increase plutonium recovery but would severly decrease enrichment, which is already too low to make it attractive for diversion.

Recycle of processed radial blanket fuel material is being analyzed as a possible method of bringing its relatively low enrichment up to

the desired 20% enrichment. However, a method must be devised that would prevent enrichments greater than 20% by repeated recycle of processed fuel. The effects of blanket fuel recycle will be discussed in future reports.

(d) Proliferation Resistance after Modifications of Process Control and Process Reagents

The effects of modifying the quantity or concentration of process reagents have not yet been studied. These effects will be discussed in forthcoming reports. The salt transport computer model currently being revised by Dr. W. A. Averill will include provisions for easily determining the effects of modifying process reagent quantities and types.

(e) Proliferation Resistance after Modifications of Process Control, Equipment, and Facilities

Several areas in the salt transport process may be somewhat attractive for diversion. In one scenario, if process vessel volumes were large enough, sufficient alloy could be transferred to the FP-3 donor vessel (A3) from the FP-3 donor storage vessel (P3) to permit the FP-3 fission products to be removed to the FP-3 acceptor alloy, leaving the alloy protected only by contamination with FP-4 fission products and by dilution with uranium. The plutonium-to-uranium ratio in solution in the uranium-plutonium donor alloy ranges between 0.9 and 1.0 (45 to 50% enriched). This could easily be increased to approximately 60 to 70% enrichment in the uranium-plutonium acceptor alloy following the first uranium-plutonium transport pass. After distillation, the highly enriched material could be removed from the process. It would be almost totally free of fission products (both FP-3 and FP-4), and would contain only uranium and plutonium. Enough of this enriched product possibly could be recycled through the uranium-plutonium transport portion of the process to further enhance enrichment.

The defense against such a method of diversion is built into the current system design. First, the FP-3 donor vessel is sized to accept only the desired portion of alloy from which the FP-3 is to be removed. (This value is currently approximately one-tenth of the volume of the alloy in the FP-3 donor storage vessel, and represents the amount of FP-3 generated in a fuel subassembly during each full nuclear reactor fuel cycle.) The FP-3 donor and acceptor vessels are located in the pyrochemical facility in special, small-sized canyons in the auxiliary cell circle. These cell locations are in a high radiation area, which would have to be decontaminated prior to entry. The piping to these vessels will be sized and dedicated only for these vessels. In addition, the overhead cranes and equipment located in the area of the FP-3 transfer vessels will be sized so that they cannot handle these vessels.

Therefore, a diversion scenario which provided for the replacement of FP-3 vessels would also require blatant overt action, including initial ouster of the international inspection team. The facility would then have to be modified. This would require decontamination of the upper bay area. The sequence panel for operating the turntable, which is located in the contaminated, highly radioactive upper bay area, would have to be rewired or

bypassed. A new, larger FP-3 donor vessel would have to be brought into the upper bay area. A method of transfer of molten alloy to the donor vessel would have to be devised, since the vessel would be at a higher elevation and adequate pressure to transfer the molten metal would be required. A method of returning the molten metal to the FP-3 donor storage vessel would have to be devised also. Since the material must be returned from the FP-3 removal step to the salt transfer vessel for the uranium-plutonium transport step and since no capabilities for construction would be present in the upper bay area, most of these modifications would have to be made manually, necessitating total plant cooldown and removal of most of the (highly contaminated) material from the turntable and auxiliary vessels. These operations most likely would require more than eight weeks to complete, providing sufficient time for international response.

In a similar scenario, the FP-3 might be completely removed by repeated recycle of the FP-3 donor alloy between the FP-3 donor storage vessel and the FP-3 donor vessel. Each pass would be contacted with the transport salt to remove FP-3. However, if only that process step were changed, this method would require a very large number of steps since after each pass, the "clean" alloy would have to be reintroduced into the donor storage vessel with the remaining contaminated alloy. After ten passes, 34.8% of the FP-3 would still be in the donor alloy. (The number of passes required to reach a certain percent of fission products in the alloy can be controlled by changing the size of the FP-3 donor vessel and thus the quantity of metal. This affects the amount of FP-3 transferred to the FP-3 acceptor alloy during each pass. More passes would be required as vessel size is decreased. The effects of varying the FP-3 donor vessel volume will be evaluated in the future.)

It has been suggested that the enriched, yet contaminated, fuel alloy itself might be a target for diversion as it is being transferred to the oxide conversion operation. To discourage such action, distillation of the zinc-magnesium alloy from the uranium-plutonium and FP-3 fission products (in vessel D3) could be deferred until refabrication. The fuel alloy would then be combined with a zinc-magnesium alloy of great volume while enroute to the refabrication facility. This would permit easier detection of diverted material due to the large volume of a shipment and would further discourage diversion since further remote processing of the alloy would be required before any plutonium could be extracted.

5. Fabrication of Process-Size Refractory Metal Vessels

(C. M. Edstrom,* C. E. Baldwin,* L. D. Johnson,* and A. G. Phillips*)

a. Introduction

The pyrochemical processing of nuclear fuels requires crucibles, stirrers, and transfer tubing that will withstand process temperatures and

*Rockwell International - Rocky Flats.

chemical attack by the molten salts and metals used. Being able to fabricate the necessary hardware is critical to pyrochemical processing. For economics and safety in the pyrochemical process a crucible that is large enough to contain the entire fuel subassembly is needed. Tungsten, a material known to withstand the process temperatures and chemical attack, is presently not available in sheet size large enough to provide the surface area of large crucibles. This dictates the development of joining, coating, and/or forming processes to obtain a crucible of the desired shape and size.

b. Engineering Analysis

Conversations with Fred Bydash, Metalwerk Plansee's U.S. representative, confirm that riveted tungsten crucibles 20 in. in dia by 48 in. high can be fabricated with only one circumferential seam to join the spun bottom to the layered wall. Palnisil 10 (89.5% silver, 0.5% palladium, 10% nickel) braze alloy strips can be inserted between the layers of tungsten sheet before riveting. This should provide stronger joints and promote uniform thermal-expansion movement to improve adherence of the plasma-sprayed or CVD (chemical vapor deposited) tungsten coating. Ordering of riveted crucibles, 5 in. in dia. by 10 in. high, in Sept. 1979 is planned, if funding is available. Delay to that time was precipitated by budget restraints; however, meanwhile, there will be time to evaluate plasma-sprayed and CVD tungsten as protective coatings.

Fixturing for brazing a tungsten crucible becomes a major problem because of the requirements for Palnisil 10 braze. This braze requires a brazing temperature of about 1150°C, which prevents use of the former fixture material (Macor glass). The fixture material should not be wetted by the braze, should not react with the tungsten, and should have a thermal expansion coefficient similar to that of tungsten. This limits the fixture material to silicon carbide or mullite (aluminum oxide - silicon oxide). Silicon carbide is reasonably priced and easy to maintain; however, delivery dates exceed four months. Because silicon carbide is difficult to machine, it must be obtained in a shape close to the fixture dimension.

A piece of mullite is currently being ground as the mandrel for the brazing fixture. If there are no delays in the grinding, the fixture should be ready for brazing trials in April 1980.

As a possible stopgap, we are experimenting with coated graphite as fixture material. Graphite would make an excellent fixture material because it is easily machined and its thermal expansion matches the thermal expansion of tungsten. The only shortcoming of graphite is the tungsten-carbon reaction which, hopefully, will be eliminated by coating.

c. Separation Processes

Chemetal has completed the chemical vapor deposition (CVD) of tungsten on two molybdenum crucibles. The molybdenum crucibles had been spun and inside-machined by Metalwerk Plansee. The two CVD crucibles, therefore, had different surface finishes before coating. The surface finish on one crucible was better than 64 RMS and that of the other was rougher, approximately 125 RMS. Both crucibles were coated at the same temperature (approximately 550°C.).

This was a change from the original plan to coat one crucible at 350°C to obtain equiaxed grains in the tungsten coating and to coat the second at 700°C to better match the 800°C crucible operating temperature and minimize tensile stresses on the coating caused by thermal-expansion differences of molybdenum and tungsten. These two coating conditions were recommended by Chemetal, based on their experience with tungsten carbide coating; however, the experiments with pure tungsten did not produce the anticipated results. No coating temperature could be found that provided equiaxed grains, and at 700°C, large columnar (length equal to the coating thickness) grains formed. The coating temperature of about 550°C was selected because the compromise provided a thin columnar high-density grain structure in the coatings.

The CVD-coated crucibles look promising. Each has been cut to a 10-1/2-in. height. This cutting by an abrasive wheel serves as a good test for the bond between the CVD tungsten and the molybdenum. A dye penetration test of the crucible lip, using Zyglo ® showed no bond separation that might have been caused by the force of the abrasive cutting. In addition, one crucible was thermally cycled by heating to 850°C at 50°C/h and then cooling down at the same rate; no signs of bond separation were observed.

Sintering of plasma-sprayed tungsten crucibles that had been impregnated with nickel nitrate is partially complete. The three small crucibles and tube purchased by Argonne National Laboratory have been sintered. However, the large crucible, which is 5 in. in dia. by 10-1/2 in. high, has not been sintered because the Coors Porcelain Company does not have a large enough furnace operating with a dry 100% hydrogen atmosphere to accommodate the crucible. The only furnace available for a crucible of this size operates with 25% hydrogen and 75% nitrogen, with a 70°F dew point. Samples have been sintered in each atmosphere. Argonne National Laboratory will determine whether the 25% hydrogen atmosphere fully reduces the nickel nitrate and provides the desired density. If so, the large crucible will be sintered in 25% hydrogen - 75% nitrogen.

Sintering of the impregnated, plasma-sprayed tungsten for Argonne National Laboratory caused shrinkage and loss of weight. The weight loss was approximately 0.1% and dimensional shrinkage was 3% for each of the sintered pieces. The shrinkage must be controlled in order to maintain a round tube or crucible. To maintain roundness of the tube, it was laid on ceramic tubes to provide two lines of contact (support) the full length of the tube. An alumina tube was placed over the tungsten crucibles to maintain their roundness during sintering. The two crucibles and tube remained round within 0.030 in. after sintering.

The 1-1/2-in. dia rod of mullite needed for the continuation of the impregnation experiments has been received. This rod is approximately 60% dense. Several oxides and combinations of oxides have been selected as possible substances for impregnation. The selection of oxides was made using Argonne National Laboratory's free-energy guidelines and knowledge of the structures formed when oxides are combined. The binder in most impregnation trials will be chromium oxide. This program was discussed with R. M. Arons of Argonne National Laboratory during his visit to Rocky Flats on Feb. 6, 1979. Promising candidates will be corrosion-tested in zinc by Dr. Arons.

Two molybdenum crucibles, 5 in. in dia. by 10 in. high, were easily fabricated using the same drawing and spinning practices as those used for tungsten crucibles. Molybdenum is formed at 800°C, as compared with 1150°C for tungsten. Molybndenum also forms an oxide which serves as an excellent lubricant. One of these crucibles will be used to establish the procedure for testing the service life of crucibles. The other will be held for future coating investigations.

The spinning of three additional 5-in. dia. by 10-in. high tungsten crucibles has been postponed as a result of a cut in project funding and the lack of an immediate need for the crucibles. Three drawn cups, made from tungsten supplied by Metalwerk Plansee, are ready for spinning; thus, the production of spun crucibles can be completed shortly after funding becomes available.

We have tried to spin one tungsten crucible since the last successful spinning in Nov. 1978. This crucible cracked during the second spinning operation. The cause of the crack is unknown, but machining damage is suspected. The crucible was pulled out of the lathe chuck by the cutting tool during machining to remove lip roughness created during the form spinning and first extrusion spinning passes. No crack was seen visually, but a microcrack might have been present prior to the final spinning operation.

6. Chloride Volatility Processing of Thorium-Based Fuels

(R. L. Bennett*)

a. Introduction

The objective of the research and development being conducted under this contract is to determine the feasibility and proliferation resistance of (a) a chloride volatility coprocess for the recovery of irradiated thorium-based fuels and (b) a zinc distillation coprocess for the recovery of irradiated uranium-based fuels.

An evaluation of prior work was performed to obtain data and information about the current status of technology for the chloride volatility coprocess. A report was prepared which describes the existing data and information and a conceptual block diagram. The report is organized to permit evaluation of the technical feasibility, safety, and proliferation-resistance attributes of the chloride volatility coprocess. Tests are being conducted with simulated fuel and fission products to establish bases for technical feasibility and proliferation resistance.

Tests will be conducted to determine the phase relationships in the zinc-uranium-plutonium ternary alloy system at 1000°C and to determine the coprecipitation coefficients for zirconium, niobium, molybdenum, ruthenium, rhodium, and palladium with $(U, Pu)_2Zn_{17}$ from liquid zinc solutions at 470°C.

*Babcock and Wilcox

b. Engineering Analysis

(J. E. Bullard,* L. A. Smith,* and T. A. Thornton*)

(1) Proliferation Resistance Analysis of Chloride Volatility Coprocess

Evaluation of the block flow diagram (Fig. 23) for the chloride volatility coprocess was initiated to determine its proliferation resistance. The coprocess is being evaluated for the following six criteria:

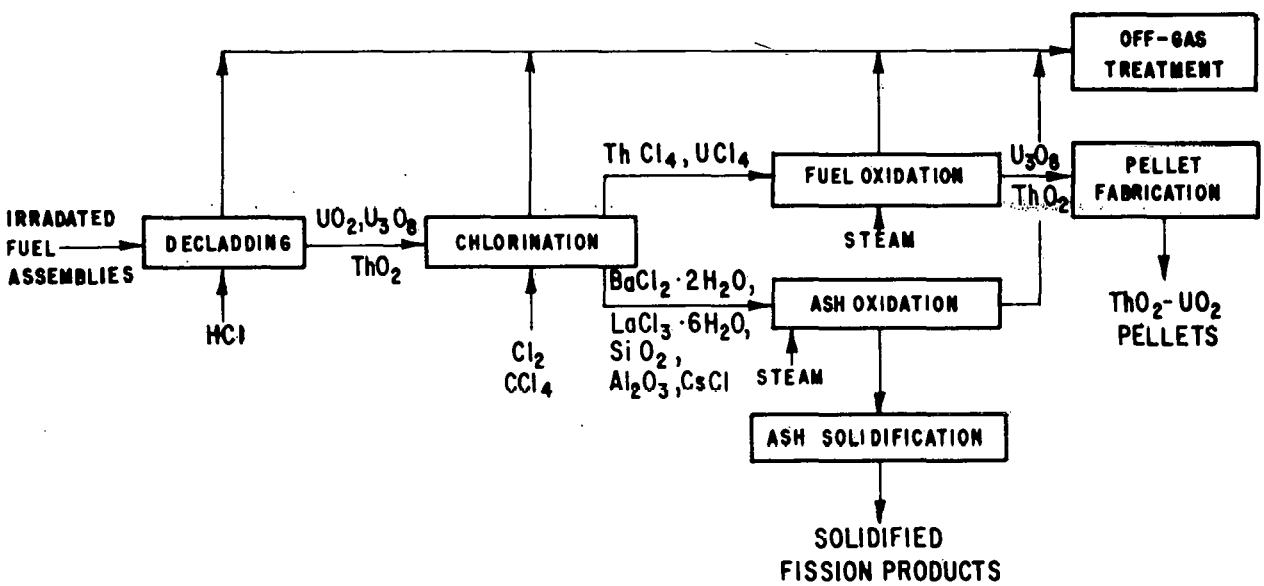

Fig. 23. Chloride Volatility Coprocessing of Thoria-Urania Spent Fuel

1. The fissile materials produced should contain gamma radiation >500 roentgens/h at 1 m from a sphere containing 8 kg of fissile material in fuel that had been cooled for 100 days and must retain a radiation level of 25R/h when cooled 500 days. The fissile materials produced should be diluted with at least 80% fertile material. These levels make diversion difficult and easily detected and make conversion into weapons-usable material difficult.

2. The process should not be capable of producing, by simple process adjustment or slight equipment modification, highly decontaminated fissile materials.

3. For modification of the process equipment, facilities and components should be required that are not normally on site, and plant decontamination or entry into very highly radioactive areas should also be required.

*Babcock and Wilcox

4. The minimum time in which weapons-usable metal can be produced by simple process modification or by additional processing in an external facility should be eight weeks. This would be adequate time for appropriate national and/or international responses.

5. The process must permit real-time accountability of fissile material.

6. The facility must be operated remotely and must be maintained remotely, utilizing only dedicated equipment.

The radioactive elements that could give proliferation and diversion resistance to the chloride volatility coprocess were identified as zirconium, ruthenium, antimony, cesium, and thallium. Fission products and actinide daughters were evaluated for level of gamma activity, neutron absorption cross section, and oxidation state and chemical form in the spent fuel. The behavior of these elements in the chloride volatility coprocess was also analyzed, based on their vapor pressures and heat of reaction. The physical and chemical states of the selected elements are shown in Table 27. Their chlorination reactions and their free energies of reaction are shown in Table 28. The gamma energies of the selected isotopes and their daughters are shown in Table 29.

Table 27. Physical and Chemical States of Elements Used to Provide Proliferation Resistance for the Chloride Volatility Coprocess

Element	Physical State	Chemical State
Zr	oxide in fuel matrix	ZrO_2, $BaZrO_3$, $SrZrO_3$
Ru	metallic inclusions	Ru
Sb	metallic inclusions or oxide in fuel matrix	Sb, Sb_2O_3
Cs	precipitate	Cs_2O, Cs_2UO_4
Tl	metallic inclusions	Tl

This information was used to select the elements and compounds for bench-scale testing of their behavior during chlorination. The results of these tests, discussed in subsection c(1) below, will be used in evaluating the proliferation resistance of the chloride volatility coprocess.

(2) Analytical Determination of U-Pu-Zn Phase Diagram

To obtain data needed for a zinc distillation coprocess for the recovery of irradiated uranium-based fuels, thermodynamic analysis

Table 28. Free Energies of Reaction for Chlorination of Radioactive Species

Element	Form	Reaction	ΔG_r°, kcal/mol
Zr	ZrO_2	$ZrO_2 + CCl_4 = ZrCl_4 + CO_2$	-49(1000 K)
	$BaZrO_3$	$BaZrO_3 + \frac{3}{2}CCl_4 = BaCl_2 + ZrCl_4 + \frac{3}{2}CO_2$	No data
	$SrZrO_3$	$SrZrO_3 + \frac{3}{2}CCl_4 = SrCl_2 + ZrCl_4 + \frac{3}{2}CO_2$	No data
Ru	Ru	$Ru + \frac{3}{2}Cl_2 = RuCl_3$	-31(298 K)
Sb	Sb	$Sb + \frac{3}{2}Cl_2 = SbCl_3$	-66(1000 K)
	Sb_2O_3	$Sb_2O_3 + \frac{3}{2}CCl_4 = 2SbCl_3 + \frac{3}{2}CO_2$	-181
Cs	Cs_2O[a]	$Cs_2O + CCl_4 = 2CsCl + CO + Cl_2$	-196(1000 K)
Tl	Tl	$Tl + \frac{1}{2}Cl_2 = TlCl$	-34(1000 K)

[a]Cesium probably exists in numerous other forms.

of the phase relationship of U-Pu-Zn was initiated, with emphasis on the low-plutonium region at 1000°C. This analytically generated phase diagram will serve the following objectives:

(a) Generation of crude phase relationship data.
(b) Increased technical familiarity with both the actual ternary U/Pu/Zn system and the methodology of determining thermodynamic phase relationships.
(c) Creation of a data base to be used in designing experimental phase relationship determinations [see subsection c.(2) below].

The prediction of phase relationships from basic electronic, thermodynamic, and crystal configuration data for the individual metals is too complex, tentative, and theoretical for the purpose of this project. Therefore, the three binary phase diagrams (U-Pu, U-Zn, and Pu-Zn), along with other germane thermodynamic data available in the literature, will be the basic data used in the analytical determination of the ternary phase diagram.

Table 29. Gamma Radioactivity Provided by Selected Elements for Proliferation Resistance

Element	Isotope	Principal Gamma Energy, MeV	Yield, %
Zr	^{95}Zr	0.724	49
		0.756	49
	^{95}Nb	0.76	100
Ru	^{106}Rh	0.51	21
		0.62	11
Sb	^{125}Sb	0.43	31
		0.60	24
Cs	^{134}Cs	1.3	3
		0.80	99
		0.60	98
	^{137}Cs	0.66	85
Tl	^{208}Tl	2.62	100
		0.58	80

Two general methods for the determination of ternary phase diagrams are being considered at this time, each involving the assumption of regular solution theory for the ternary system. The regular solution theory assumption, however, essentially disregards the existence of a ternary compound of U/Pu/Zn in the composition region over which the appropriate activity coefficients (or free energies) of the system are averaged. Since this system study is not beginning with the basic electronic and thermodynamic data for the individual metals, the existence of a possible ternary compound of the metals can be accounted for and incorporated into the ternary phase diagram only in the experimental phase of the program.

The two methods for determining the ternary phase relationships being used in this program are those elaborated by [BREWER] and by [KAUFMAN-1970]. Although each uses regular solution theory as a starting point, the Brewer method seems to be simpler in its estimation of average system properties such as activities and activity coefficients. The Brewer method may be utilized with the simple HP-67 or 97 programs, using activity, solubility, and free energy data derived from the three binary phase diagrams.

The Kaufman method [KAUFMAN-1970, 1975] is at present not completely understood by project personnel since it comprises proprietary computer simulation techniques which are purchased on a time-sharing basis from Man Labs, Inc., of Cambridge, Massachusetts. In this method, the excess free

energies of mixing for the binary solutions and compound phases are expressed as temperature-dependent functions of the lattice stability and other thermochemical parameters obtained from binary phase diagram data. The excess free energy of the ternary system is then formulated from the binary functions, using the Kohler equation. The Brewer and Kaufman methods thus differ in that the Brewer method uses averaging techniques for the binary phases to generate activities for the ternary system, whereas the Kaufman method deals directly with free energies which are more complexly extracted from the binary data.

Appropriate thermodynamic data, including the binary phase diagrams, for the binary systems U-Pu, U-Zn, and Pu-Zn have been and continue to be collected to provide a data base for the analytical determination of the ternary phase diagram. Figures 24a, 24b, 24c, 25, and 26 present the respective binary phase relationships for the U-Zn, U-Pu, and Pu-Zn systems. The three diagrams shown for the U-Zn systems denote the phase diagram changes due to differences in pressure.

Extensive thermodynamic data for the binary system, uranium-zinc, has been compiled by [CHIOTTI]. Since in the present study, the low-plutonium region of the ternary diagram at 1000°C is to be emphasized, extrapolation and averaging of appropriate binary U-Zn data with plutonium data into the ternary range might be expected to be more likely successful than study of the low-U or low-Zn region of the ternary system. The lack of extensive thermodynamic data for the U-Pu and Pu-Zn systems (aside from the binary phase diagrams themselves) could compromise the accuracy of an analytically determined total ternary diagram, but to little extent in the region of interest.

(3) Work Plans for April-June, 1979

Evaluation of the proliferation resistance of the chloride volatility coprocess will be completed. Work will continue on preparation of the U-Pu-Zn phase diagram using the Brewer method and the Kaufman method.

c. Separation Processes

(J. J. Petchul* and C. F. Stafford*)

(1) Fission Product Behavior in Cochlorination of Uranium and Thorium

Seven experiments were performed to evaluate the behavior of fission products under conditions suitable for cochlorination of uranium and thorium. The conditions are 700°C reaction temperature, 100cm^3/min Cl_2 flow rate, and 150 cm^3/min CCl_4 flow rate. Uranium and selected fission products were chlorinated in three experiments, and selected fission products were chlorinated in four experiments. The results of these experiments are shown in Tables 30 and 31. Material accountability was good in all experiments except the experiment in which antimony was chlorinated. It is believed that the loss of antimony was associated with the formation of an organic polymer.

*Babcock and Wilcox.

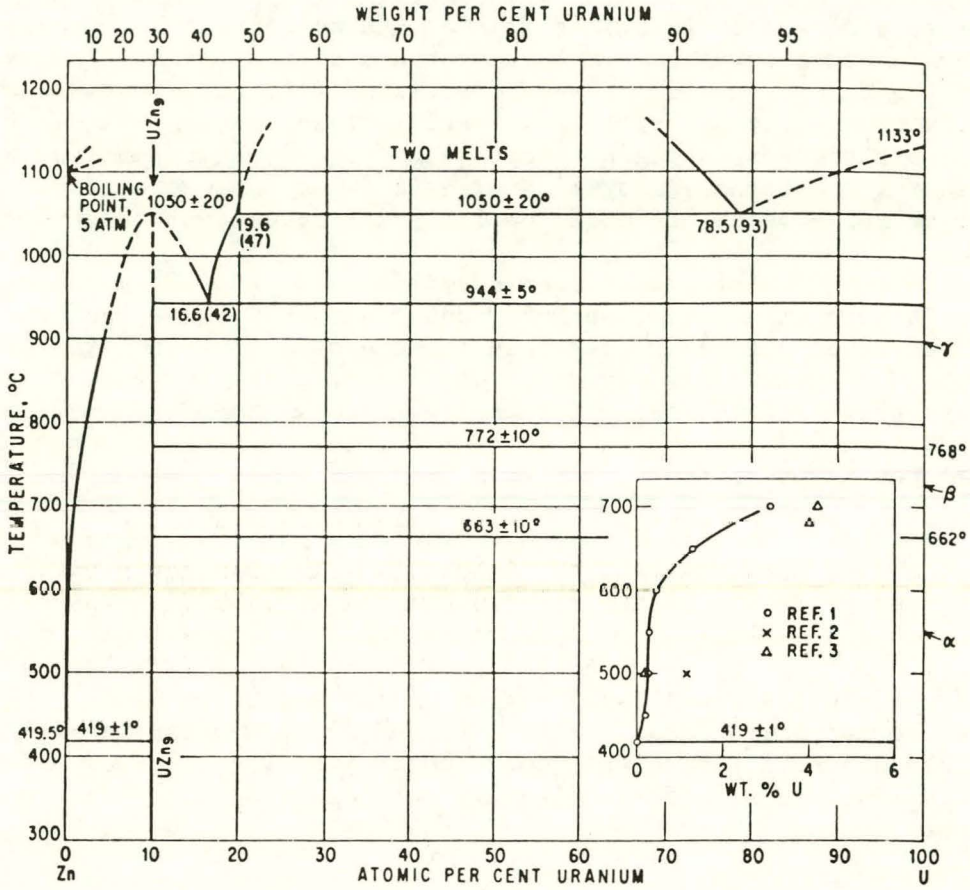

a. [HANSEN]

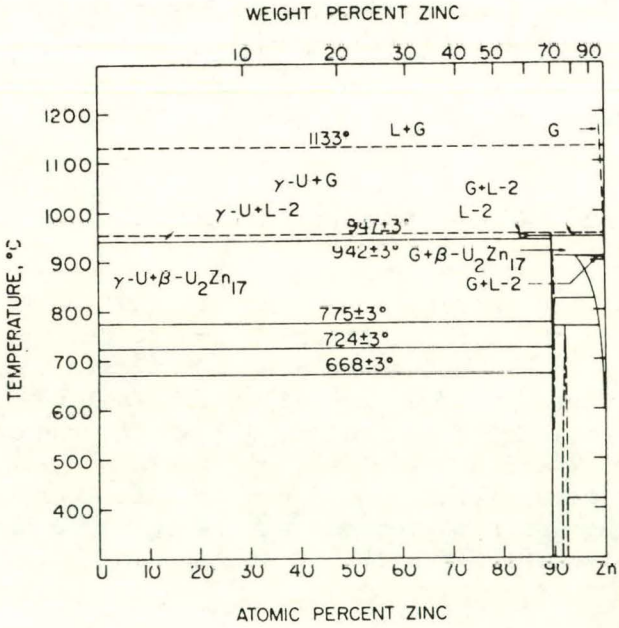

b. U-Zn system under one-atmosphere pressure

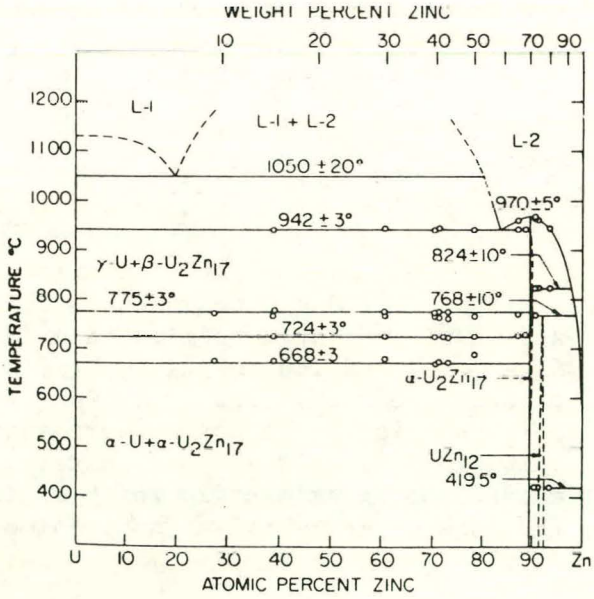

c. U-Zn system under constrained vapor conditions

Fig. 24. U-Zn Phase Diagrams

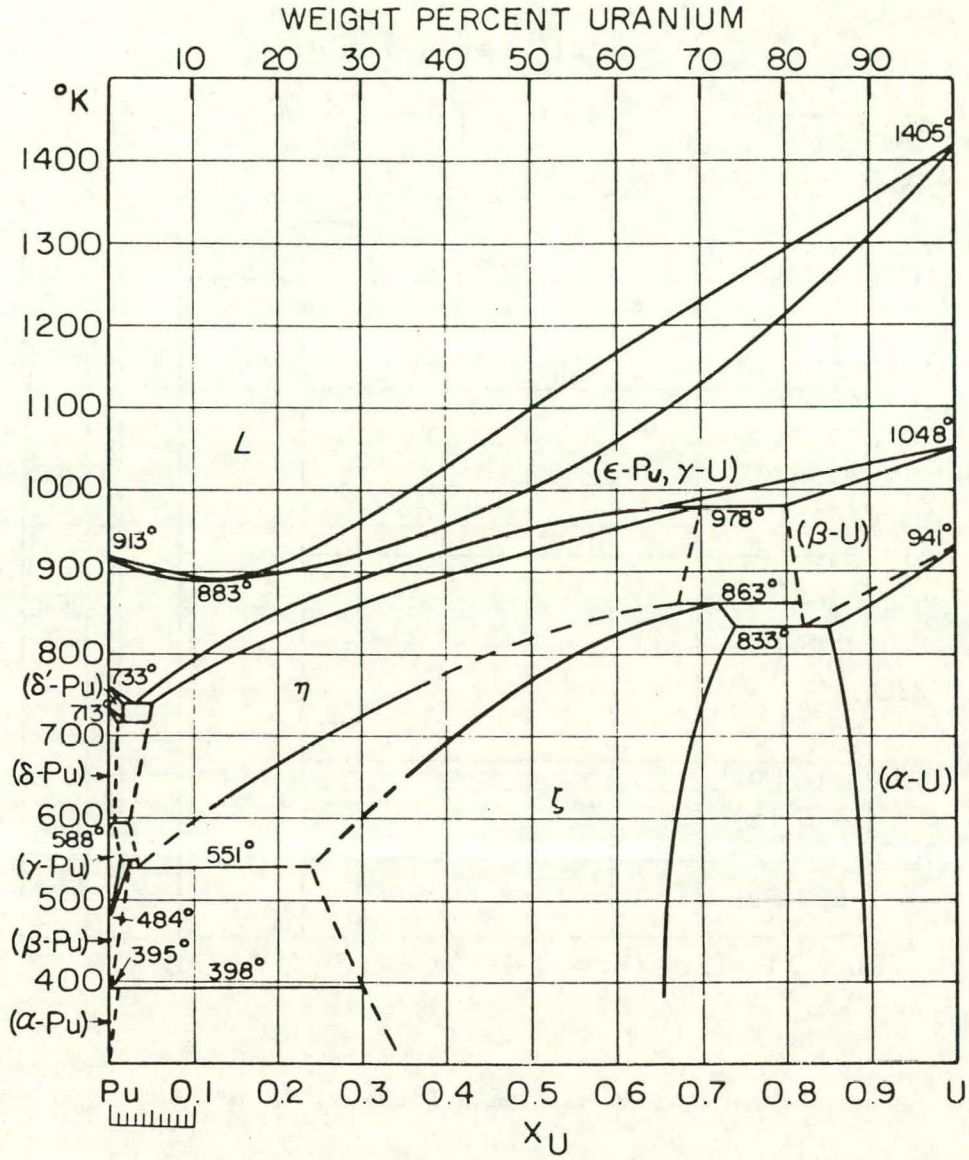

Fig. 25. U-Pu Phase Diagram [HULTGREN]

A carbon tetrachloride polymer formed during chlorination. We believe polymerization was caused by the dissociation of CCl_4 at very high temperatures and the recombination of radicals, which is favored by the high CCl_4 concentration. Approximately 25 g of hexachloroethane solids has been isolated. We believe that much more was formed. The presence of polymers which would cause problems in process development and operation, will have to be investigated in future process development work.

(2) Determination of U-Pu-Zn Phase Diagram

An experimental procedure for the determination of the U-Pu-Zn phase diagram at 1000°C has been selected. We will test the procedure with U-Zn in a hands-on situation before moving it into a glovebox. After the procedure has been demonstrated with U-Zn in and out of the glovebox,

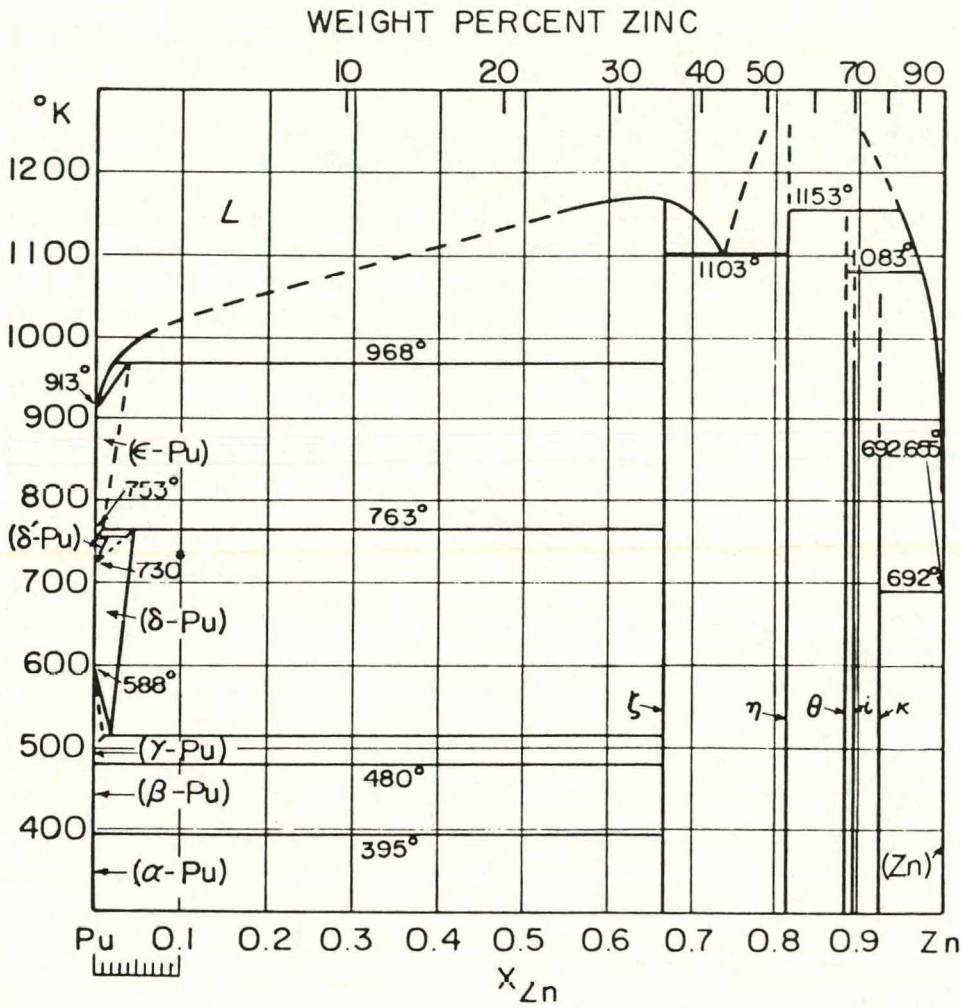

Fig. 26. Pu-Zn Phase Diagram. [HULTGREN]

plutonium will be added. The preliminary U-Zn experiments will not only provide experience, but will also provide samples for verification of analytical results that can be compared with existing U-Zn phase diagrams.

Uranium turnings and zinc granules will be cleaned in dilute nitric acid, rinsed with water and acetone, and immediately placed in a desiccator under an argon atmosphere. Desired quantities of the uranium and zinc will be placed in a tantalum crucible, which will then be heated under vacuum to remove sorbed gas. A preformed, threaded plug will be screwed into the crucible (Fig. 27) and sealed with a TIG weld under inert atmosphere and partial vacuum.

In the next step, the tantalum crucible containing the U-Zn mixture will be held at 1100°C for several hours. Since the tantalum crucible will be sealed, the melt will be under the pressure of the argon gas and

Table 30. Distribution of Products from Chlorination of UO_2 and Fission Products. Reaction temperature, 700°C; Cl_2 flow rate, 100cm^3/min; CCl_4 flow rate, 150 cm^3/min

Experiment No.	Starting Material	Residue in Boat	Cold Trap, 200°C	Scrubber
11	UO_2, ZrO_2	ZrO_2, UCl_4	$ZrCl_4$, UCl_6 UCl_5	$ZrCl_4$, UCl_6 UCl_5
12	ZrO_2	ZrO_2	$ZrCl_4$	$ZrCl_4$
13	$SrZrO_3$	$SrCl_2$, ZrO_2	$ZrCl_4$	$ZrCl_4$
14	$BaZrO_3$	$BaCl_2$, ZrO_2	$ZrCl_4$	$ZrCl_4$
15	Sb	Sb	$SbCl_3$	$SbCl_3$
16	Ru, UO_2	$RuCl_3$	$RuCl_3$, UCl_6 UCl_5	$RuCl_3$, UCl_6 UCl_5
17	Cs_2O, UO_2	CsCl, Cs_2UCl_6	CsCl, UCl_6 UCl_5	CsCl

Table 31. Elemental Mass Balance For Chlorination Experiments

Experiment No.	Starting Material, g	Residue in Boat	Cold Trap, g	Scrubber, g	Not Accounted For,%
11	U 5.19	U 0.52	U 3.47	U 0.46	U 14
	Zr 3.66	Zr 0.11	Zr 2.94	Zr 0.39	Zr 6
12	Zr 7.11	Zr 0.30	Zr 5.80	Zr 0.58	Zr 6
13	Sr 3.55	Sr 3.27	Sr <0.001		Sr 8
	Zr 3.70	Zr 0.65	Zr 2.96	Zr 0.04	Zr 1
14	Ba 4.23	Ba 3.87	Ba <0.001	Ba <0.001	Ba 9
	Zr 2.81	Zr 0.10	Zr 2.34	Zr 0.33	Zr 1
15	Sb 8.67	Sb 3.40	Sb 2.10	Sb 0.22	Sb 34
16	Ru 1.28	Ru 0.81	Ru 0.29	Ru <0.02	Ru 13
	U 3.91	U 0	U 2.89	U 0.68	U 9
17	Cs 3.98	Cs 3.39	Cs 0.060	Cs 0.01	Cs 13
	U 2.07	U 1.84	U 0.03	U <0.002	U 10

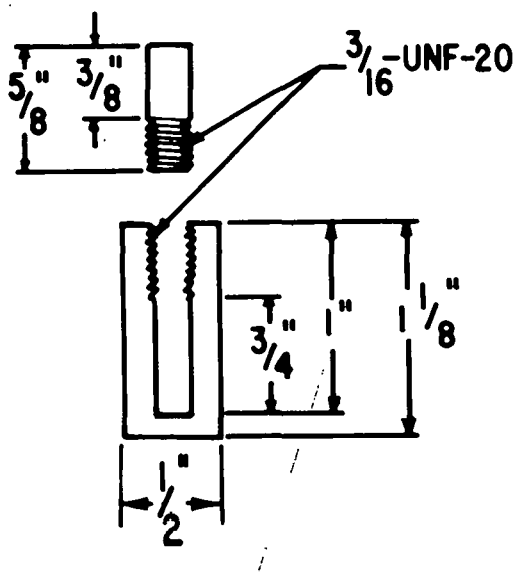

Fig. 27. Tantalum Crucible

zinc vapor. The pressure will not exceed 10 atm and will probably be lower. The U-Zn phase diagram indicates that at this temperature, under constrained vapor conditions, melting will be complete. However, if the solution contains about 20% uranium, a second immiscible liquid phase will form. This may cause homogeneity problems if careful temperature control is not maintained.

The samples will undergo heat treatment in their tantalum crucibles at 1000°C. To reach phase equilibrium, holding times of 2 to 3 h should be sufficient; however longer holding times will be tested to verify that this is true. At low uranium concentrations and 1000°C, no primary crystal phases are expected. At about 20% U, a uranium precipitate can be expected to form. (We will briefly study the system at 900°C and examine the U_2Zn_{17} phase formed at that temperature for more complete verification of our procedures.)

The tantalum crucibles, after heat treatment of their contents, will be removed from the furnace and immediately quenched in oil or water. They will then either be prepared for sample analyses as described below or saved for future annealing.

Metallographic, X-ray, and chemical techniques will be coordinated to determine phase structure and chemical compounds in each phase of a sample.

After proper sectioning, mounting, grinding, polishing, and etching, the samples will be subjected to energy-dispersive or wavelength-dispersive examination. These will identify, at least qualitatively, the elements in the different phases of a sample. Quantitative measurements would require standards. Therefore, quantitative evaluations by chemical techniques should probably be preferred.

Chemical analysis is expected to be a difficult, time-consuming task. If a procedure can be found to selectively dissolve amorphous or secondary crystal phases from the primary phase, the primary and secondary phases can be chemically analyzed for uranium and zinc content and X-rayed for structure.

The procedure described above will enable us to construct the solidus curve and liquidus-solidus tie lines in the ternary system by studying many compositions of U-Pu-Zn at 1000°C. DTA studies, in conjunction with these results, will provide a reasonable approximation of the liquidus curve.

Tantalum stock has been ordered to be used for fabrication of the needed crucibles. Uranium metal has also been ordered. A preliminary experimental plan and schedule have been submitted to the analytical groups to allow them to properly allocate manpower needs during the next several months.

(3) Work Plans for April-June, 1979

The uranium-zinc studies will begin in mid-May, and U-Pu-Zn studies are planned for August.

7. Material Characterization and Process Analysis
(L. J. Jones,* L. F. Grantham,* and R. C. Hoyt*)

a. Introduction

This program was redirected, for GFY 1979, from AIROX,† CARBOX,† and RAHYD† processing systems to material characterization and process analysis. The primary objectives are: (1) to perform an engineering and cost analysis of the FBR fuel cycle, utilizing a reference proliferation-resistant pyrochemical process, and (2) to prepare facilities to support the characterization of product material and data needed for fuel refabrication of product material obtained from the candidate PDPM processes.

The reference proliferation-resistant process of interest is called the Zinc Distillation Process. Fuel cladding is dissolved in molten zinc. After zinc removal, the fuel oxide is reduced by calcium and dissolved in molten zinc. The gaseous and volatile fission products are separated from the fuel during these steps. Partial removal of the rare earth fission products is effected by titrating the zinc with a molten salt. A limited increase in the concentration of the plutonium is accomplished by a high-temperature zinc distillation step. In the initial stage of this step, the concentrations of both uranium and plutonium in the zinc are increased as a result of removal of the zinc by distillation. As the solubility of uranium in zinc is exceeded,

*Rockwell International - Atomics International

†The AIROX process consists of multiple oxidation-reduction cycles of oxide fuels, the CARBOX process of multiple oxidation-reduction cycles of carbide fuels, and the RAHYD process of multiple hydride-dehydride cycles of metal fuels. In these processes, gaseous fission products are released, the fuel is pulverized, and the fuel is separated from the cladding.

about one-half of the uranium precipitates from the liquid zinc. The remaining liquid zinc, which contains the plutonium, the remainder of the uranium, and the noble metal fission products, is then transferred to a retort where it is diluted with zinc and cooled to precipitate the uranium, plutonium, remaining rare earths, and about one-half of the noble metals. After the bulk of the liquid zinc is removed, the remaining zinc is removed by distillation. The solidified and cast product from this step is then oxidized for use as proliferation-resistant fuel.

Several minor tasks also in the GFY 1979 contract are: closing out AIROX, CARBOX, and RAHYD reprocessing, decommissioning of the processing facilities, and the preparation of topical reports.

b. Engineering Analysis of a Fuel Cycle Utilizing the Zinc Distillation Process

The Zinc Distillation Process is being reviewed, and an engineering analysis has been started for the overall Zinc Distillation fuel cycle economic analysis. As part of this study, a literature search has been initiated on fuel cycle costs, including those associated with transportation, waste treatment, waste storage, fuel element fabrication, and plant decommissioning. These costs will be applied with the engineering analysis to the Zinc Distillation processing costs, which are being evaluated by another contractor.

Analysis of the conversion of uranium-plutonium-fission product metal mixture to the oxide for recycle to the reactor is continuing. A literature search of Nuclear Science Abstracts and Energy Data Base on the conversion of uranium-plutonium alloys to oxides has been completed. Two of the most thorough studies of UO_2 preparation and properties, including the preparation of UO_2 from metallic uranium, were made by [CLAYTON] and by [BELLE]. Some data from their papers are reproduced below (Table 32) to illustrate the properties of UO_2 powder prepared from metallic uranium. Two of the powders whose preparation conditions are shown in Table 32 were tested for sinterability. Their sintering characteristics are shown in Table 33. In addition, a table (Table 34) from [STEINDLER-1978D, Table 34] is reproduced, showing the specifications for several fuels. Comparison of the data in these three tables indicates that the physical properties required to meet fuel specifications are similar.

[BELLE] indicated that the UO_2 powder produced by steam oxidation has poor sinterability characteristics in comparison to UO_2 powders produced by other methods. However, data shown in Table 33 indicate that UO_2 powders produced by steam oxidation of uranium metal and of uranium powder from uranium hydride were sintered to produce UO_2 pellets having densities 79.2% and 94.7% of theoretical, respectively. Although experimental evidence is lacking, it is conceivable that higher pellet densities might be achieved by subjecting to an AIROX oxidation-reduction cycle the UO_2 powder produced by steam oxidation of metallic uranium. Such a procedure might produce a powder consisting of smaller and more porous particles. This would improve powder sintering characteristics and increase UO_2 pellet density. In the past, powders produced by AIROX reprocessing have produced high-density pellets which have been recycled to the reactor, AIROX-processed a second time, and then refabricated a second time into high-density pellets [GUON, BODINE].

Table 32. Properties of UO_2 Prepared from Uranium Metal[a]

Method of Preparation	Reaction Conditions	O/U	Density g/cm^3[b] He Method[c]	Density g/cm^3[b] CCl_4 Method[c]	Density g/cm^3[b] Bulk	Surface Area,[d] m^2/cm^3 BET Sg	Surface Area,[d] m^2/cm^3 Permeability Porosity	Surface Area,[d] m^2/cm^3 Permeability Sp	Roughness Factor Sg/Sp
High-pressure steam oxidation of uranium	72-h oxidation at 343°C and 2200 psig	1.97	10.92 ± 0.1	10.75	2.76	12.9	0.645	3.1	4.2
Controlled low-pressure steam oxidation of uranium	24-h oxidation at 150°C and 5 psig; dried 8 h in vacuo at 700°C	2.02	10.85 ± 0.1	10.91	1.75	2.4	0.645	3.2	0.8
Uncontrolled low-pressure steam oxidation of uranium	5-h oxidation at 350°C and 5 psig; heated in hydrogen 5 h at 900°C	2.03	10.92 ± 0.05	10.85	2.47	9.0	0.645	2.7	3.3
Steam oxidation of uranium from uranium hydride	4-h oxidation at 400°C and 5 psig; heated in hydrogen 15 h at 700°C	2.03	10.98 ± 0.1	10.67	1.75	22.6	0.686	5.6	4.0
Air pyrolysis of uranium metal to U_3O_8; hydrogen reduction to UO_2	15-h oxidation at 800°C; 16-h reduction at 800°C	2.01	10.02 ± 0.1	10.07	-	5.8	-	-	-
Hydrided-air oxidized uranium; hydrogen reduction of U_3O_8 to UO_2	24-h oxidation at 740°C; 16-h reduction at 800°C	2.02	10.32 ± 0.15	10.46	1.10	9.4	0.739	5.4	1.7

[a]Data taken from [CLAYTON] and [BELLE].

[b]Theoretical density = 10.96 g/cm^3.

[c]Method described by [ROSSMAN, SMITH-1942]

[d]Sp - surface area by permeability method
Sg - surface area by BET method

Table 33. Sintering Characteristics of UO_2 Powders Produced from Uranium Metal[a]

Powder	Compact Condition after Sintering of Pellets Having Indicated Pressed Densities	Highest Sintered Density[b]	Density Reached in 8 h in H_2 at 1700°C		Dependence of Sintered Density on Pressed Density	Rank of Preparation Method Based on	
			Pressed Density	Sintered Density		Surface Area	Density
Steam oxidation of uranium from uranium hydride	Cracks (55% TD) Good (65% TD)	94.7% TD	55.3% TD	79.2% TD	Marked	1	1
High-pressure steam oxidation of uranium	Flaky (55% TD) Good (65% TD)	79.2% TD	55.2% TD	58.1% TD	Marked	2	2

[a]Data taken from [BELLE].

[b]Before sintering at 1700°C in H_2 for 64 h, density was 65% TD.
TD= theoretical density (10.96 g/cm^3)

Table 34. Typical Fuel Powder Specifications and Characteristics

Spec. Source	FBR Specifications			LWR Specification	LWR Fabrication Data			
	RDT E13-2T	RDT E13-1T	RDT E13-6T	ASTM C-753				
User Reactor					Surry 1 & 2	Zion 1, Region 3	Oyster Creek Cycle 7	Peach Bottom-2 Cycle 2
Fuel Material	UO_2	PuO_2	$(U, Pu)O_2$	UO_2	UO_2	UO_2	UO_2	UO_2
Particle Size, μm, Max.	79	90		850		--	850	--
Avg.	10(Max)	10(Max)				2.82 to 0.79	6.84	
Surface Area, m^2/g	2.5	2.5				2.80 to 2.10	2.04 to 3.09	--
Bulk Density, g/cm^2				0.75(Min)		1.64 to 1.81	2.07 to 2.28	--
Sintered Density, % TD	92(Min)[a]	90(Min)[a]	90.4 (nominal)	92(Min)[a]	93.1 to 96.0	92.9 to 95.4	93.2 to 94.6	94.0 to 96.7

Spec. Source	E13-2T	E13-1T	ASTM C-753	
			Dry	Wet
Binder Type A Addition (max)	4% Carbowax 20-M	0	0	1.5% PVA
Lubricant Addition (max)	Optional	Optional	0	0.4% Sterotex
Pressing Pressure (pascals x 10^7)	20.7 to 34.5	20.7 to 34.5		
Green L/D	1.0 to 1.5	1.0 to 1.5	≥1	≥1
Green Density, % TD	--	--	45 to 55	50 to 60
Sintering Atm	6 to 8% H_2 in Inert Gas	Wet Air or Inert Gas	H_2 or NH_3	H_2 or NH_3
Sintering Temp, °C	1600		1625	1625
Sintering Time, h	2 h 15 min (Max)	1 h (Min)	4(Max)	4(Max)
Sintering Density, % TD	92(Min)	90(Min)	92(Min)	92(Min)
Theor. Density, g/cm^3	10.97	11.46	10.96	10.96

[a]Sinterability test parameters.

It is well known that physical properties are usually not an adequate measure of sinterability. Therefore, sintering tests must be made on powder produced by any method to determine sintering suitability. Some general trends have been established, however, with respect to the dependence of UO_2 properties on the method of preparation. The work of [CLAYTON] illustrated many of these relationships, and the following summarizes some of their conclusions.

Physical properties, such as particle size and distribution, microstructure, porosity, crystallite size, surface area, and density, can be controlled by judicious choice of variables in the preparation procedure. To a first approximation, the crystallite size of UO_2 powders depends more on the temperature than on the method of preparation. Low-temperature preparation produces the smallest crystallite sizes. (UO_2 crystallite size ranged from about 200 Å at 350°C to about 1000 Å at 800°C.) The particle size distribution and total BET surface area of a UO_2 preparation depend upon (1) the particle size distribution and surface area of the higher oxide from which it has been prepared by reduction and (2) the reduction temperature itself. Particle growth occurs at high temperatures (temperatures above 500°C), and some particle breakdown can occur at lower temperatures. This suggests that fracturing occurs in U_3O_8 particles when they are reduced to UO_2 at low temperatures; at higher temperatures, the strains are annealed out or sintering takes place.

[CLAYTON] indicated that there is no correlation between powder density and total BET surface area; a high surface area can be associated with either a high or a low density; a low-surface-area powder can have either a high or a low density. The real density of a UO_2 preparation depends upon its oxygen-to-uranium ratio and on the density of its parent higher oxide. The density is not dependent on reduction temperature up to 1200°C. However, heating of low-density UO_2 above its temperature of preparation can cause an increase in its density.

Work is continuing on the development of fuel powder and pellet specifications necessary to evaluate the fuel product from proliferation-resistant pyrochemical processing. The optimum particle size distribution to achieve the most efficient packing of particles (highest pressed density) has been studied by [ADWICK] who reported that, for a three-component particle mixture having the relative particle sizes, 1.000:0.091:0.015, the highest pressed density is achieved when the particle volume fractions are 0.40:0.20:0.40, respectively. The highest density of sintered UO_2 has been reported [JANOV] to occur in UO_2 pellets having small grains (< 3 μm). To prevent in-reactor pellet densification, it has been reported, the fuel pellet structure should have a median pore volume diameter greater than 1 μm [FRESHLEY] and the pores should be 1.3 times as large as the grains [MARLOWE]. These porosity and grain size distributions will be determined by the particle size distribution, surface area, morphology, density of the UO_2 powder, and presintering treatments, such as pelletization, poreformer additive, and preslugging techniques.

Preliminary results from the literature review of the conversion to oxide of uranium-plutonium-fission product metal mixture indicate that irradiation and the pressure of alloying elements may significantly affect oxidation rates. [ANTILL] reported that alloys of uranium may oxidize at significantly lower rates than pure uranium. Some of the data of Antill and Peakall is shown in Table 35.

Table 35. Oxidation Rates of Uranium and Binary Uranium Alloys in Air at 500°C [ANTILL]

Alloy	Oxidation Rate, $mg/cm^2 \cdot h$
Base Uranium	90
10% Mo	0.48
5% Mo	0.66
15% Mo	2
5% Nb	18
10% Nb	21
5% Ti	22
10% Zr	45
10% Ti	50
1% Cu	64
6% Zr	70
3% Zr	80
1% V	100
5% V	100
7.3% Si	110
3.8% Si	126

These data suggest that oxidation problems may be encountered in converting uranium-plutonium-fission product metal mixtures to oxide fuel. However, [BENNETT-1974] reported that irradiation may enhance oxidation rates by factors as large as 2000. These phenomena will be investigated more thoroughly as the literature review continues. This information is necessary to help establish areas where oxidation difficulties may be encountered and to establish areas where further experimental work is necessary.

c. Characterization of PDPM Product for Recycle

Fabrication of the remotely operated alpha boxes by Stainless Equipment Company will be complete in the near future. It is expected that both boxes will be delivered in April 1979. Additional stiffeners (3/16 in. thick by 2 in. deep) have been tack-welded to the outside of the glove boxes around the window areas. These stiffeners will not increase the cost of the alpha boxes.

d. Closeout of AIROX, CARBOX, and RAHYD Processes

(1) Dry Processing Literature Review

All sections of the AIROX, CARBOX, and RAHYD literature review have been completed, and the first internal review is complete. A summary of this literature review is given below.

The complete dry processing cycle has been demonstrated with oxide fuel, and oxidation and pulverization have been demonstrated for both UO_2 and UO_2-PuO_2 fuel.* Oxidation of UO_2 occurs by a two-stage reaction--first to U_3O_7 or U_4O_9 and then to U_3O_8. Fission product content equivalent to 100,000 MWd/MTU does not affect oxidation and pulverization of UO_2; however, PuO_2 concentrations of 20% or above do retard oxidation. Fuels containing high concentrations of PuO_2 can only be oxidized and pulverized by successive oxidation-reduction cycles or by the use of high oxygen pressures (3.43 MPa). However, it is not necessary that oxidation of UO_2 to U_3O_8 be complete for fuel pellet pulverization, and particles smaller than 37 μm in diameter can be readily attained by successive oxidation-reduction cycles. The degree of pulverization has been shown to be greatest for oxidation temperatures near 400°C; oxidation is most rapid at about 480°C.

Decladding of both unirradiated and irradiated UO_2 has been demonstrated. Punched fuel rods have been declad about three times faster than unpunched rods having open ends. During dry processing of oxide fuel, the maximum decladding rate occurs at 480°C at an oxygen pressure of about 79.8 kPa. Oxidation of Zircaloy cladding can be avoided by using oxidation temperatures below 600°C, and Zircaloy hydriding can be avoided by keeping reduction temperatures above 800°C. The declad fuel is pulverized to 98% less than 74 μm diameter and contains no cladding corrosion products.

Two complete cycles of oxide dry processing have been demonstrated, including remote refabrication and reirradiation. The only major fission products released were the fission gases, cesium, and some ruthenium. Dusting was not a problem, and an economic evaluation showed that dry processing has a cost advantage over aqueous reprocessing methods.

The hydriding and dehydriding of metal fuels has been demonstrated with uranium, thorium, and plutonium. Reaction rates depend upon both temperature and hydrogen pressure, and there are induction periods when small quantities of oxygen are present. Uranium is observed to hydride

*For the UO_2, the experiments involved 100 g of oxide. The UO_2-fissia experiments were on the killogram scale, and the UO_2-PuO_2 experiments were on the gram scale.

most rapidly at 225 to 250°C, and its trihydride dissociates at temperatures above 450°C when hydrogen pressures are near 1 atm.

Very little work has been done on the hydriding-dehydriding of plutonium. Plutonium begins to hydride in 1 atm of hydrogen at 150 to 200°C, but the reaction is most rapid at 200 to 270°C. Plutonium dihydride dissociates at temperatures above 800°C.

Most of the dry processing of carbide fuel has been done with UC, although some work has been done with UC-PuC and ThC. Small- and large-scale experiments have demonstrated oxidative decladding, carbothermic reduction, and repelletization of UC fuel. Oxidation of UC proceeds by the formation of an intermediate oxide (UO_2) and then U_3O_8. Oxidation begins at about 257°C in oxygen and at about 350°C in air; peak oxidation rates occur at 850°C in oxygen. During oxidation, the pellets are pulverized to a powder in which >70% of the particles have diameters smaller than 74 μm; this pulverization occurs for both unirradiated and irradiated UC.

Carbothermic reduction has been demonstrated with UO_2, U_3O_8, PuO_2, and ThO_2 powders. Carbon content of the final pellets is controlled by making allowances for (1) the effects on carbon volatilization of the binder and arc-melting and (2) the carbon content of the oxidized fuel, since some carbon is present after oxidation.

Large quantities of fission products can be volatilized during arc-melting (about 75%); however, plutonium losses are high (>90%). This means that low-temperature pelletization techniques must be developed if plutonium is to be recycled.

For both oxide and carbide fuels, the fission products volatilized during dry processing will be primarily the fission gases and cesium and ruthenium. However, during the dry processing of metal fuel, fission product release will depend primarily upon the vapor pressure of the elements during the dehydriding and fuel pelletization steps. At temperatures of about 900°C for dehydriding and >1600°C for pelletization, significant quantities of samarium, cesium, europium, cerium, and gadolinium will be released in addition to fission gases.

Treatment of wastes from dry processing of oxide, carbide, and metal fuels can be accomplished by techniques which are either in use at aqueous processing facilities or are currently under development. Waste treatment will be easier and less costly at a dry processing facility than at an aqueous facility. This is because large-scale liquid solidification is not necessary and because many of the problems associated with NO_x vapors will not be present. All wastes leaving the facility could be either solids packaged in containers for disposal at a federal repository or gases stored in compressed-gas cylinders.

Although many significant areas of dry processing have been demonstrated, additional work must be completed before its commercial application is demonstrated. Optimization studies are needed on reaction rates, decladding rates, and pulverization. The behavior of fission products must be

more thoroughly established, and complete multicycle processing-refabrication-reirradiation experiments must be performed with oxide, carbide, and metal fuels. Dry processing reenrichment requirements must be determined, and fuel cycle cost studies must be updated and expanded to include metal fuel. Process conditions must be established for oxide fuels having high plutonium concentrations, and carbothermic reduction conditions need to be established for powder containing fission products. Large-scale decladding demonstrations should be done on metal fuel, and methods should be developed for the pelletization of metal powders that contain fission products.

(2) AIROX Topical Report

Analysis of data from the AIROX verification tests has been completed; that information which has not been previously reported is summarized below. The AIROX topical report is complete and is undergoing internal review.

Pulverization data on the remainder of the AIROX verification tests has been obtained and analyzed. Process conditions for the tests are listed in Table 36, and the particle size distributions of the products are listed in Table 37.

It can be seen by examination of Table 37 that (1) 70 to 99% of the product is smaller than 297 μm in particle size, (2) only 10 to 25% of the product is within the size range, 37 to 297 μm, and (3) the amount of material smaller than 5 μm is negligible. These data are consistent with previous results and indicate that once pulverization begins, the fuel pellet pulverizes readily to a powder. Pulverization is adequate for decladding to be complete, and dusting will not be a major problem since 97 to 100% of the product is larger than 5 μm.

Pellet pulverization is decreased when oxygen is added after the fuel has been heated to the desired reaction temperature. This is shown in Fig. 28, in which data are given for two samples heated in argon before reacting with oxygen. In Test 26, oxygen was added to the system when the oxidation temperature, about 300°C, was reached, whereas in Test 28, no oxygen was added to the system until the temperature reached 415°C. A marked decrease in pulverization was observed for Run 28.

During a second oxidation-reduction cycle pulverization is enhanced when the oxygen concentration of the second cycle (and thus the reaction rate) is low, as shown in Fig. 29. These data indicate that oxygen concentration in the second cycle must be reduced significantly to enhance pulverization. Second-cycle oxidation rates are very rapid because of the high surface area of the powders produced during the first oxidation-reduction cycle. Therefore, to maximize pulverization, it is necessary to use a low oxygen concentration during the second-cycle oxidation.

Table 36. Pulverization Test Conditions

Run No.	Form of Charged Sample	Sample Wt g	Oxidation[a]		Reduction[a]	
			Temp °C	O_2, vol %	Temp °C	H_2, vol %
V-O-P-14[b]	Powder	7	-	-	625	21
V-O-P-22[c]	Powder	7	-	-	625	50
V-O-P-23[d]	Powder	7	-	-	625	4
V-O-P-25[d]	Powder	7	-	-	850	50
V-O-P-26	Pellet	27	415 to 436[e]	50	850	15
V-O-P-27	Pellet	27	412	50	850	15
2nd Cycle	Powder[f]	27	410 to >500[e]	50	850	15
V-O-P-28	Pellet	27	412 to 436[e]	50	850	15
V-O-P-29	Pellet	27	415	50	852	15
2nd Cycle	Powder[f]	27	412 to 570[e]	21	852	15
V-O-P-30	Pellet	27	412 to 429[e]	50	850	10
2nd Cycle	Powder[f]	27	412 to 460[e]	8	850	15

[a]System pressure was about 122 kPa.

[b]Feed material was powder produced during oxidation in Run V-O-P-13 (480°C, 50 vol % O_2)

[c]Feed material was powder produced during oxidation in Run V-O-P-18 (486°C, 50 vol % O_2)

[d]Feed material was powder produced during oxidation in Run V-O-P-12 (410 to 457°C, 100 vol % O_2)

[e]Exothermic reaction caused the temperature to increase above the lower temperature for about 10 min.

[f]For particle size distribution of powders, see Table 37.

Table 37. Particle Size Distribution of Product[a]

Run No.	Size Distribution, wt %								
	>297 μm	<297 to >210 μm	<210 to >125 μm	<125 to >74 μm	<74 to >37 μm	<37 to >20 μm	<20 to >10 μm	<10 to >5 μm	<5 μm
V-O-P-12	21.4	10.3	6.6	5.6	8.8	16.1	29.2	2.0	0.01
V-O-P-13	23.2	4.5	4.1	5.4	9.1	30.5	21.5	1.6	0.01
V-O-P-14	20.0	1.6	3.0	5.1	8.9	16.5	35.4	9.5	0.00
V-O-P-18	23.2	1.7	3.1	4.9	9.2	37.3	19.3	1.3	0.00
V-O-P-22	9.9	1.8	6.5	4.6	10.6	19.7	26.8	20.0	0.10
V-O-P-23	9.0	2.3	6.9	5.1	11.0	20.7	25.4	17.4	2.3
V-O-P-25	10.5	3.2	6.8	4.5	10.5	17.6	26.7	18.5	1.7
V-O-P-26	1.1	0.1	0.3	1.0	8.3	59.7	12.4	17.0	0.07
V-O-P-27	26.3	1.3	4.3	5.1	7.1	15.3	19.2	21.4	0.06
V-O-P-28	19.2	0.9	3.7	5.8	8.5	18.2	23.8	19.8	0.11
V-O-P-29	18.8	1.2	3.3	5.9	8.0	36.5	19.8	6.5	0.00
V-O-P-30	0.6	0.3	1.0	2.4	13.0	72.3	8.6	1.8	0.03

[a]Size distributions were obtained with five Standard Sieves (No. 50, 70, 120, 200, and 400) and with three Precision Mesh Subsieves (20, 10, and 5 μm).

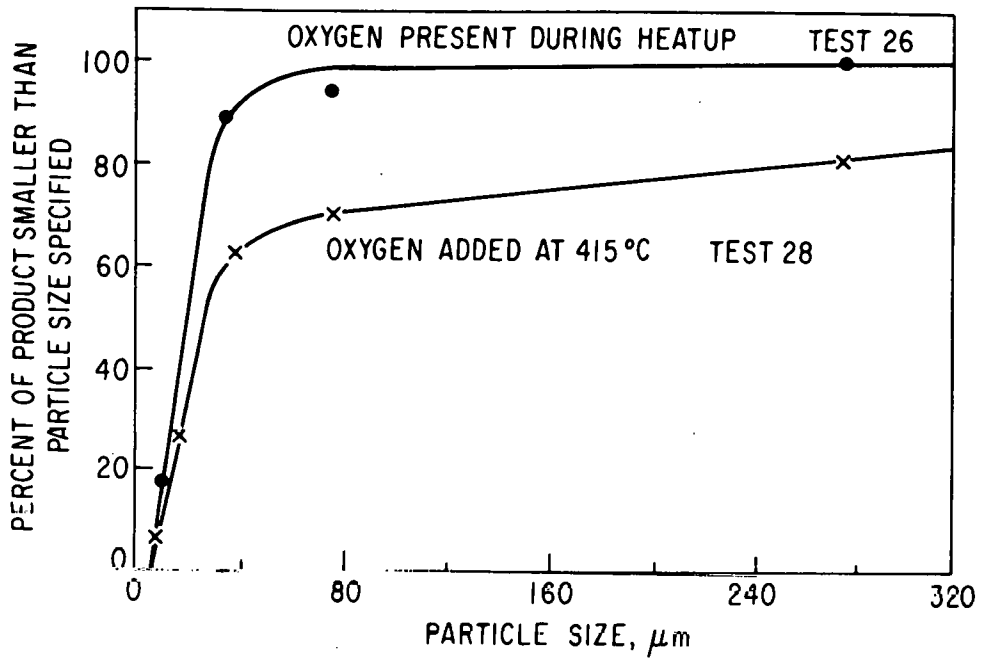

Fig. 28. Pulverization when Oxygen was Added after Fuel Reached Oxidation Temperature. Oxidation, 415°C, 50% O_2; Reduction, 850°C, 15% H_2

The hydrogen concentration used during reduction does not affect size distribution in pulverization, as shown in Table 38. Previous results [HOYT] have shown that: (1) high reduction temperatures slightly enhance pulverization and (2) inclusion of the reduction step significantly increases the pulverization achieved during oxidation. These results indicate that although reduction is beneficial for pulverization, the exact conditions used have only a small effect and reduction conditions can be chosen without consideration of pulverization. Thus, reduction conditions can be based on minimizing the reaction time and preventing the hydriding of Zircaloy when Zircaloy-clad fuels are processed.

Most of the verification tests on unirradiated UO_2 have been concerned with optimizing reaction rates and the degree of pulverization. A preliminary examination of the ability to comminute the processed powder into finer particles indicates that the large particles are readily reduced to smaller particles--even after only partial oxidation. This can be seen by examination of the sieve data presented in Table 39 and Fig. 30 for powder produced during oxidation in Run 18. This powder was sieved three times--first for 15 min, then for an additional 30 min, and finally for an additional 30 min with a steel ball placed on each sieve. Note the significant increase in the amount of particles smaller than 37 μm when the material was sieved with a steel ball on the sieve. These data tend to indicate that all of the powder produced during AIROX processing will readily be comminuted to a small

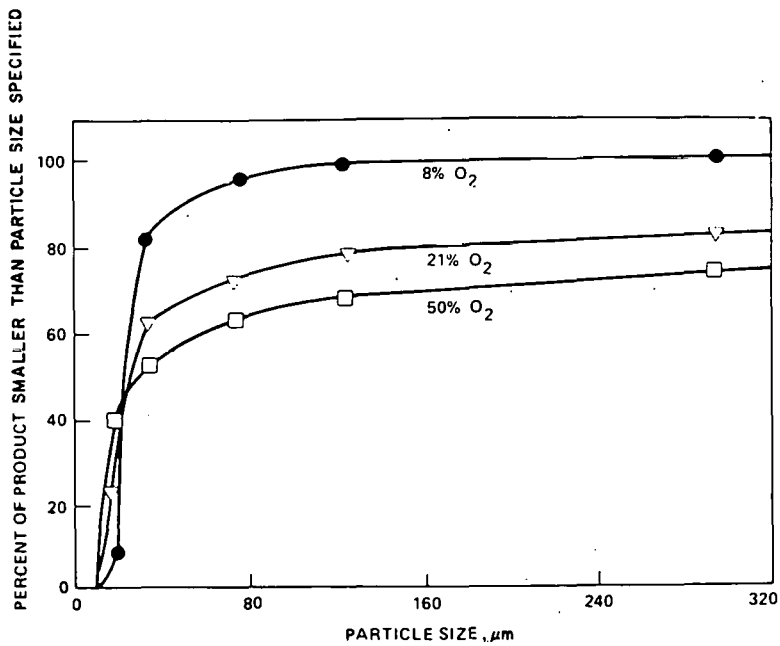

Fig. 29. Degree of Pulverization after the Second Cycle at Various Oxygen Pressures

	Oxidation	Reduction
1st Cycle	420°C, 50% O_2	850°C, 12% H_2
2nd Cycle	415°C, curve callouts give oxygen levels	850°C, 15% H_2

Table 38. Effect of Hydrogen Concentration during Reduction

Run No.	Hydrogen Concentration, Vol %	Size Distribution of Product, wt %			
		>297 μm	<297 to >37 μm	<37 to >20 μm	<20 μm
V-O-P-23	4	9.0	25.3	20.7	45.1
V-O-P-25	50	10.5	25.0	17.6	46.9
V-O-P-14	21	20.0	18.6	16.5	44.9
V-O-P-22	50	9.9	23.5	19.7	46.9

size during AIROX ball-mill blending operations. Thus, if pulverization is sufficient for complete decladding, optimization of AIROX processing can be based primarily upon reaction rates.

Table 39. Effect of Continued Sieving on Particle Size Distribution of Oxidized UO_2 Powder

Sieving	Size Distribution of Product,[a] wt %			
	>297 μm	<297 to >74 μm	<74 to >37 μm	<37 μm
1st Sieving (15 min)	23.2	9.7	9.2	57.9
2nd Sieving (30 min)	2.6	4.4	2.6	83.4
3rd Sieving (gentle sieving for 30 min with steel ball on each sieve)	0.01	0.1	1.0	99.9

[a]Product from Run V-O-P-18 (oxidation at 486°C with 50% O_2, but no reduction was performed).

There is some evidence of sintering of fine powder when rapid oxidation occurs. This is shown in Fig. 31, which indicates that when the second oxidation occurs rapidly, some powder produced during the first oxidation is sintered into larger particles. Although the oxidations (first and second) were carried out at similar conditions, the much greater surface area during the second oxidation permitted the reaction to proceed much more rapidly (about 4 min instead of about 30 min). In fact, the reaction was so rapid that the powder surface temperatures may have approached 600°C, even though the thermocouple in the vessel detected a much lower thermal spike of <50°C.

The degree of pellet pulverization has been found to be very sensitive to oxidation temperature, with higher temperature yielding less pulverization. Maximum pellet pulverization occurred for oxidation temperatures near 400°C in air, and even small 25 to 50°C temperature excursions for about 10 min significantly reduced pulverization. This was particularly noticeable during a second oxidation in which temperatures increased momentarily due to rapid exothermic reaction. This reduction in pellet pulverization is believed to be a result of partial sintering of the oxide particles. Thus, controlled oxidation is necessary and is much more important than complete oxidation to obtain pulverization and decladding. It is not surprising that pulverization was not good (i.e., that cyclic oxidation-reductions were required to obtain pulverization) in previous work under conditions in which rapid sodium oxidation was the primary goal [GOODE].

Although the reduction step has been found to enhance pellet pulverization, the specific reduction conditions have only a minor effect. Pulverization increased only slightly with increased reduction temperature and was relatively independent of hydrogen concentration.

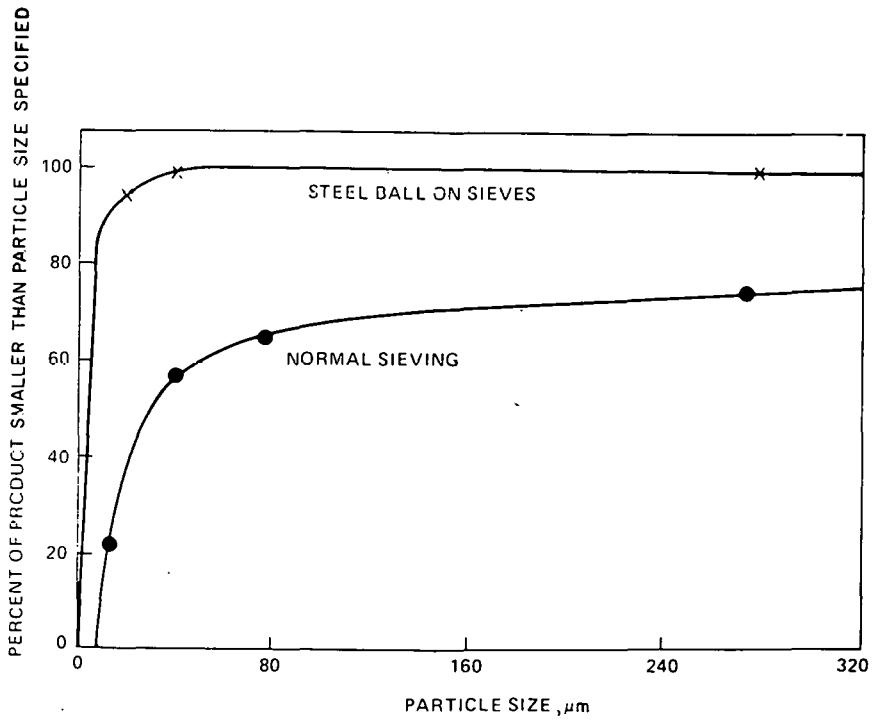

Fig. 30. Fuel Not Completely Pulverized during Oxidation but Readily Pulverized by Pressure Sieving. 486°C, 50% O_2; O:U = 2.6

The product produced by the AIROX process has been shown to be very friable and to be readily comminuted into finer particles. Thus, the degree of pellet pulverization is not a limiting factor for choosing dry processing conditions when pulverization is sufficient to declad the fuel. The fuel product will be free of any contamination from Zircaloy cladding, since process conditions favorable for fast reaction rate or pellet pulverization are the same conditions which prevent Zircaloy oxidation and Zircaloy hydriding.

Although many significant areas of AIROX reprocessing have been demonstrated, additional work must be completed before its commercial application. Optimization studies need to be performed on decladding rates, and process conditions must be established for oxide fuels having high concentrations of elements other than uranium. The behavior of fission products should be more thoroughly established, and demonstration tests need to be done involving complete multicycle processing-refabrication-reirradiation. Process analysis with computer codes should also be continued in order to determine fuel management strategies in relation to fuel cycle costs.

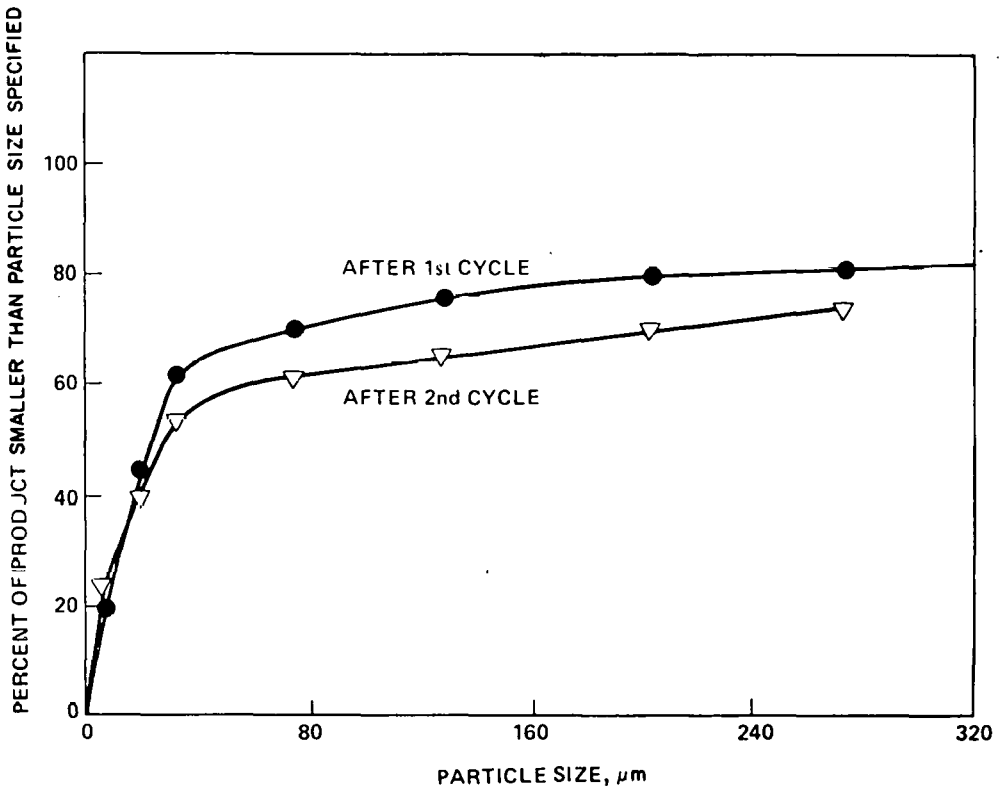

Fig. 31. Rapid Oxidation during Second Cycle Reduces Pulverization of Finely Divided Product. 430°C, 50% O_2; 850°C, 15% H_2

8. Molten Nitrate Salt Oxidation Processes
(L. L. Burger,* L. G. Morgan,* and R. D. Scheele*)

The objective of this work is to identify chemically feasible nonaqueous reprocessing methods that fall within the framework of nonproliferation. In this study, treatment of ceramic fuels with molten salts is examined and the use of molten nitrate systems is emphasized. Incorporation of other nonaqueous steps to develop a conceptual process will be considered where applicable.

a. Engineering Analysis

No engineering analysis studies were scheduled or conducted during this reporting period.

*Pacific Northwest Laboratory

b. Separations Processes

(1) Behavior of Plutonium Dioxide in Molten Alkali Metal Nitrates

Additional studies of the behavior of plutonium dioxide in molten equimolar sodium nitrate-potassium nitrate have been completed. These experiments were conducted by a procedure equivalent to that in the earlier experiments utilizing only uranium dioxide [STEINDLER-1979B].

A mass ratio of plutonium dioxide to nitrate melt of 1:100 was used in these studies. Plutonium dioxide did not react with the nitrate melt at the temperature range studied (up to 525°C). The temperature of the melt was then reduced to 275°C, and nitric acid vapor was added by sparging the melt with nitrogen that had bubbled through 100% HNO_3 contained in a heated vessel. As in previous experiments, at no time were there visible indications of solubility or reaction of the plutonium dioxide in the melt.

Analytical results were based on alpha energy analysis of samples of the molten phase taken throughout the experiment. Analytical results of the study of the behavior of plutonium dioxide in equimolar sodium-potassium nitrate show that, under the conditions cited, plutonium dioxide did not react and did not form a soluble species either with the original melt or with the addition of 100% nitric acid vapor. Additional analytical tests utilizing plutonium gamma energy analysis in both molten salt phase samples and the remaining plutonium dioxide solids are in progress. The results of these additional tests will be reported upon their completion.

(2) Behavior of Mixed Uranium Dioxide-Plutonium Dioxide in Equimolar Sodium Nitrate-Potassium Nitrate

Mixed uranium dioxide-plutonium dioxide has been obtained in two compositions. The first composition, designated material A, consists of 5.44% PuO_2-94.56% UO_2. The second composition, designated material B, consists of 27.56% PuO_2-72.44% UO_2. Both materials were acquired as pellets that had been sintered at 1700°C. Further documentation of the history of these materials exists but is not reported here.

The behavior of the lower-plutonium-content material (material A) in equimolar sodium nitrate has been studied in a manner analogous to that utilized in previous experiments. The reaction of material A was similar to the reaction of uranium dioxide, although a higher temperature of 400°C was required to initiate reaction. Reaction of material A was completed at 450°C.

The temperature of the melt was reduced to 275°C after the completion of the oxidation reaction, whereupon nitric acid vapor was added as in previous experiments. Most of the solids dissolved in the melt, producing the characteristic uranyl color, but not all of the solids could be dissolved by this treatment. Preliminary analyses of samples of the molten

phase (taken throughout the experiment) indicate that plutonium dioxide remained insoluble at all times. Quantitative analytical tests to determine the quantitative partition of uranium and plutonium are in progress. These results will be reported as they become available.

Material B, which is typical of that scheduled for use in the Fast Flux Test Facility (FFTF), has also been studied in preliminary experiments. This higher-plutonium-content material requires an even higher melt temperature, 500°C to 550°C, to initiate the oxidative reaction. The reaction rate of this material also appears to be much lower than that noted in previous studies--even at temperatures as high as 700°C.

Subsequent reduction of the melt temperature to 275°C and addition of nitric acid vapor to the melt containing Material B produced results similar to those reported for material A. Quantitative analytical tests for these experiments are also in progress, and their results will be reported when available.

Further studies of the behavior of both materials are in progress. Addition of peroxide to the melt to oxidize the plutonium dioxide will be investigated. The insolubility of plutonium dioxide must certainly be investigated further since its solubility in the molten phase upon addition of nitric acid vapor has been claimed in various patents [BRAMBILLA-1973, 1976A, 1976B]. It must also be remembered that the behavior of irradiated uranium dioxide-plutonium dioxide may differ from the behavior of material utilized in our experiments.

(3) Fission Product Behavior in Molten Nitrate System

Several experiments were performed in which selected fission products were exposed to the conditions expected during treatment of irradiated fuels. A simulated fission product mixture consisting of Eu_2O_3, CsI, and Sb_2O_3 was prepared by: (1) dissolving Eu_2O_3 in 2M HNO_3, adding ^{154}Eu tracer, and calcining at 500°C; (2) adding ^{137}Cs tracer in aqueous CsI, and adding Sb_2O_3 with ^{125}Sb tracer to the Eu_2O_3; and (3) evaporating the total mixture to dryness.

This simulated fission product mixture was added to equimolar sodium-potassium nitrate, and the salt phase was melted and brought to a final temperature of 450°C. During this time, some iodine was evolved. Preliminary analysis of samples indicates that after 2 h, 60% of the europium, 100% of the cesium and 25% of the antimony dissolved in the melt. The temperature was then lowered to and maintained at 270°C for 1 h while 100% HNO_3 vapor was sparged through the melt. Nearly all of the europium, 100% of the cesium, and 30% of the antimony were found in the melt. The temperature was then increased to 450°C for 2 h. Analysis showed that 73% of the europium, 100% of the cesium, and 17% of the antimony remained in the melt. No activity was found in the caustic offgas scrubbers nor in the offgas lines.

The concentrations of the three fission products in the melt were determined from samples of the molten phase taken throughout the experiment. The salt samples were dissolved in 0.5 M nitric acid, and the resulting solutions were analyzed by gamma energy analysis.

(4) General

Dissolution of sodium diuranate in the melt is accomplished by adding nitric acid vapor in the sparge gas. Initial studies utilized 100% HNO_3, but recent tests have demonstrated that commercial white fuming nitric acid (90% HNO_3) is equally effective. Concentrated nitric acid does not produce complete dissolution of the sodium diuranate.

9. Molten Salt Processes Applied to Nuclear Fuels
(D. H. Smith* and E. C. Douglas,*)

The purpose of this program is to establish chemical bases for proliferation-resistant methods utilizing molten salts and/or metals for reprocessing nuclear reactor fuels.

a. Progress

(1) Engineering Analysis

In the current flowsheet, oxide fuels are dissolved in lithium chloride with the aid of aluminum chloride. The uranium and plutonium are transferred next to a bismuth phase by reductive extraction. Finally, the actinides are removed from the bismuth by oxidative extraction into NH_4AlCl_4 [SMITH-1978].

As a culmination of our examination of possible alternatives for the ammonium chloroaluminate recovery step [STEINDLER-1979B], we have studied the possibility of a recovery of the actinides without the use of salt. In this scheme, HCl gas would be bubbled through the molten bismuth solution of the actinides in order to oxidize the actinides to chlorides. The bismuth would then be cooled, and the actinide chlorides (which are less dense than bismuth) would be leached out with water and sent through the sol-gel process.

Scouting studies with uranium/bismuth solution, however, have failed to demonstrate significant recovery of uranium chloride by this method. This finding supports the continued inclusion of ammonium chloroaluminate in the reprocessing flowsheet.

We have attempted this quarter to obtain specifications for reprocessed fuel and the composition of a reference spent fuel, so that detailed mass balance calculations for the various fission products could be carried out for the lithium chloride-bismuth extraction steps of our process.

*Oak Ridge National Laboratory

Apparently, no accurate calculations (utilizing fast neutron cross sections for the fission products and other appropriate parameters) have been reported for the composition of the spent fuel from a standard UO_2-PuO_2 breeder reactor [CROFF, GRIMES-1979, KRUMPELT, MYLES, WACHTER]. In particular, the fission product distribution expected from the Clinch River Breeder Reactor oxide core (our first choice for a reference fuel) has never been calculated [CROFF]. Further mass balance calculations have been suspended pending resolution of these questions [MYLES]. However, during this report period, the reference temperatures for the extractions of uranium and the coprocessed stream have been established, and a set of heuristic mass-balance calculations has been made for uranium and for plutonium.

The chemistry of the extraction was reviewed in earlier reports. Briefly, the reductive extraction reaction for element M between lithium chloride and the bismuth-lithium alloy may be written

$$MCl_n \text{ (salt phase)} + nLi \text{ (metal phase)} = M \text{ (metal phase)} + nLiCl \text{ (salt phase)} \quad (1)$$

where n is the oxidation state of M in the salt phase at equilibrium. (Although uranium is present in LiCl as U^{4+} before contact with the alloy, only U^{3+} and U^0 are present at equilibrium; hence n = 3.). The equilibrium constant for this reaction may be written.

$$K = \frac{a_M \; a_{LiCl}^n}{a_{MCl_n} \; a_{Li}^n}$$

$$= \frac{X_M \; X_{LiCl}^n}{X_{MCl_n} \; X_{Li}^n} \cdot \frac{\gamma_M \; \gamma_{LiCl}^n}{\gamma_{MCl_n} \; \gamma_{Li}^n} \quad (2)$$

where a_M is the activity of the actinide, M
X_M is the mole fraction of M in the metal phase
γ_M is the activity coefficient of M in the metal phase

The distribution coefficients for M (actinide) and for lithium are defined as follows:

$$D_M = \frac{X_M}{X_{MCl_n}} \quad (3)$$

$$D_{Li} = \frac{X_{Li}}{X_{LiCl}} \quad (4)$$

If the activity coefficients are assumed to be constant, the equilibrium constant from Eq. 2 becomes K'.

$$K' = \frac{X_M \; X_{LiCl}^n}{X_{MCl_n} \; X_{Li}^n} \tag{5}$$

Combining Eqs. 3, 4, and 5 and using the logarithmic form yields the following equation:

$$\log D_M = n \log D_{Li} + \log K_M' \tag{6}$$

The reductive extraction consists of two stages, an extraction of one-half of the uranium for separate processing, and a coprocessing extraction of the plutonium, the remaining uranium, and other actinides.

In both stages the uranium-plutonium separation factor is independent of the reductant metal (lithium) concentration, but increases as the equilibration temperature is decreased. Since it is desired that the uranium-plutonium separation factor for the first stage be as large as possible, the temperature selected is determined by the freezing point of the salt solution, which is 605 ± 5°C. The reference temperature for this step has been set at 640°C to allow a reasonable margin for temperature gradients and fluctuations.

The temperature for the second stage, the extraction of the coprocessed stream from LiCl into bismuth, is set by the requirement that the distribution coefficients of uranium and plutonium be equal. From the various data for the distribution coefficients of uranium and plutonium [SMITH-1979], this temperature was calculated to be 688°C.

The mass balance calculations assume that the uranium oxide/plutonium oxide fuel has been dissolved in lithium chloride with the aid of aluminum chloride and that any excess aluminum chloride from the dissolution step has been removed [e.g., by the reaction, $NH_3(g) + AlCl_3\ (\ell) = NH_3AlCl_3(g)$]; hence, the dissolution step leaves uranium in the oxidation state U^{4+} [MOORE] and plutonium in the state Pu^{3+} [LYON]. The uranium and plutonium are assumed to be present in an 8:1 ratio, and the solvent masses given are per 100 kg of uranium (see Table 40).

A minimum amount of metal solvent is used, governed by the solubility of uranium in bismuth. Since the solubilities of uranium and plutonium chlorides in lithium chloride are quite large [LEVIN], generation of lithium chloride by Eq. 1 places a lower limit on the quantity of solvent salt present. The solubility of uranium in bismuth at 640°C is about 1.5% [ELLIOTT]; we have chosen a weight of bismuth that will give a maximum uranium concentration in the process of 1.0 at. %. The salt volume was chosen to be somewhat less than the volume of the metal phase. Solvent volumes calculated from compiled density equations for bismuth [WASHBURN] and lithium chloride [JANZ] are listed in Table 40.

Table 40. Weights and Volumes of Solvents for Reductive Extractions at 640[a] and 688°C[b] per 100 kg of Uranium

Element	Atomic Weight, kg/mol	Weight, kg	Volume, L	moles	T, °C
Bi	0.209	4389	457	21,000	640
		2195	230	10,500	688
LiCl	0.0424	445	273	9,430	640
		445	304	10,500	688

[a] $D_{Li} = 1.43 \times 10^{-4}$; $D_U = 1.0$; $D_{Pu} = 0.077$.
[b] $D_{Li} = 1.84 \times 10^{-3}$; $D_U = D_{Pu} = 100$.

(2) Separations Processes

The initial rates of dissolution of various sized UO_2 sol-gel microspheres in 39.9 ± 0.1 mol % LiCl/60.1 ± 0.1 mol % $AlCl_3$ mixtures have been measured at 120°C and 220°C and various degrees of stirring by previously reported methods [STEINDLER-1979B]. The postulated reaction for these temperatures,

$$UO_2 \text{ (solid)} + 2AlCl_3 \text{ (salt phase)} = UCl_4\text{(salt phase)} + 2\ AlOCl\text{(solid)},$$

was supported by the green color of the salt phase and by the free energies calculated for this and for alternative reactions [SCHAEFER, BROWN-1968].

Figure 32 shows log-log plots of the concentrations of uranium dissolved in the melt vs. reaction time for microspheres of 150 ± 10 μm (6-mil) diameter. Linear regression fits to the equation

$$\log [An] = A \log t + B, \tag{7}$$

where [An] is the concentration in wt % of the dissolved actinide, and t is the time in hours, gave the values A = 0.22 at 120°C and A = 0.4 at 220°C (see Tables 41 and 42).

These rate expressions were quite different from those measured for 350 ± 50 μm diameter ThO_2 beads under similar conditions [STEINDLER-1979B]; in particular, at 220°C, the slope of a plot of log [Th] vs. log t for ThO_2 was 1.37. However, similar experiments with 1190-μm UO_2 beads gave the value A = 1.406, in striking agreement with the value of A for ThO_2.

In an attempt to clarify these findings and to obtain kinetic data for all three sizes (coarse, medium, and fines) of microspheres which are used in the sphere-pac process of fuel-rod fabrication, the measurements were extended to include four sizes of UO_2 microspheres. The diameters

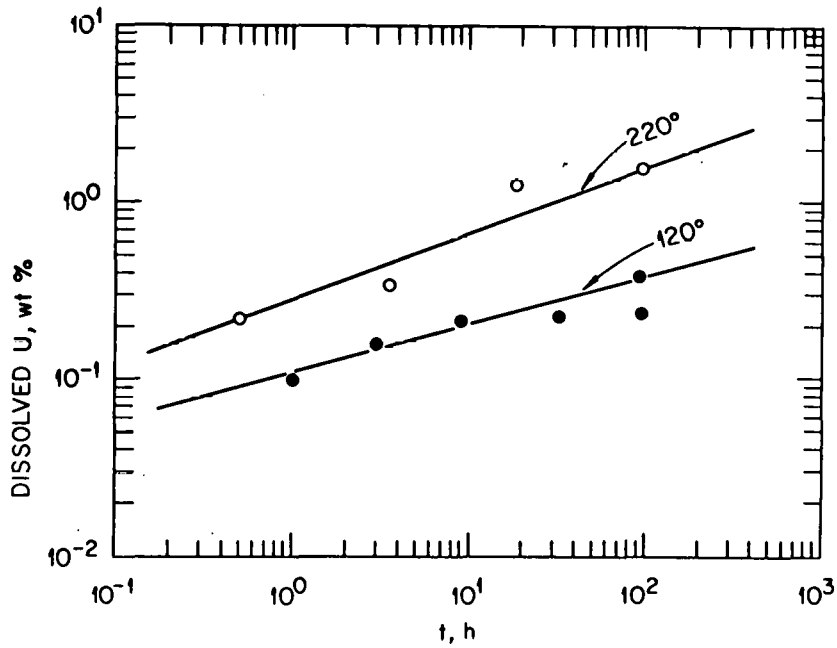

Fig. 32. Dissolution of UO_2 Microspheres in $LiCl/AlCl_3$. Microspheres, 150 μm Diameter; 39.9 mol % LiCl/60.1 mol % $AlCl_3$

Table 41. Initial Rate of Dissolution of UO_2 Microspheres in $LiCl/AlCl_3$ (60:40 mol %) at 120°C

Diameter, μm	Δt, h	[U], wt%	A	Stirring[a] Method
150 ± 10	1	0.10	0.223	1
(6 mil)	3	0.161		1
	9	0.215		1
	96	0.395		1
	32	0.230		1
	96	0.242		1
	0.25	0.0411	∿1.0 ± 0.2[b]	3
	0.5	0.0982		3
	1.16	0.33		3
	2.16	0.20		3
	4.16	0.23		3
	7.41	0.88		3

[a]1 represents "convective" stirring; 3 represents magnetic stirring rod.
[b]An accidental loss of UO_2 occurred between 1.16 and 2.16 h.

Table 42. Initial Rates of Dissolution of UO_2 Microspheres in $LiCl/AlCl_3$ (60/40 mol %) at 220°C

Diameter, μm	Δt, h	[U], wt %	A	Stirring Method[a]
25 ± 12	0.33	0.462		1
(1-mil)	0.5	0.480		1
	1	0.626	0.283	1
	4	1.09		1
	16	1.25		1
	0.5	0.380		2
	1.5	0.580	0.058	2
	4.4	0.430		2
150 ± 10	0.5	0.233		1
(6-mil)	3.5	0.348	0.404	1
	18	1.28		1
	93.5	1.57		1
250 ± 75	0.33	0.099		1
(10-mil)	1	0.120	0.313	1
	4	0.214		1
	3	0.088		2
	6.5	0.113	0.664	2
	16	0.117		2
	64	0.706		2
1190 ± 140	16	0.0439		2
(47 mil)	32	0.0996	1.406	2
	64	0.539		2
	100	0.420		2

[a]1 represents "convective" stirring; 2, rocking furnace.

studied were d = 25 ± 12 μm, d = 150 ± 10 μm, d = 250 ± 75 μm, and d = 1190 ± 140 μm (see Tables 41 and 42). This series of experiments has apparently shown that this rate difference is not a chemical one--that is, the different time dependencies are not produced by different reaction mechanisms. Rather, the value of A is a function of the microsphere diameter, d, and of the rate of agitation of the melt.

Our conclusions can be summarized as follows: At very low rates of stirring, such as might be produced by convection currents in a large process vessel, A = 1.37 for d $\geq$ (350 ± 50) μm and A = 0.264 for d $\leq$ (250 ± 75)μm. (These values are based on about 25 data on UO_2 and ThO_2 for d $\geq$ 350μm and 14 data on UO_2 for d $\leq$ 250μm.) The smaller value of A is caused by "clumping" of the microspheres; this "clumping" has been visually observed.

Stronger agitation provided by a rocking furnace was still inadequate for breaking down the clumps of UO_2 fines (d = 25μm) and gave intermediate results for 250-μm spheres (A = 0.66). However, the strong agitation provided by a magnetic stirring rod did prevent clumping of 150-μm microspheres (Table 41) and probably would do the same with fines.

The force which holds the spherical, nearly uniformly sized particles together in the hexagonally closed-packed clumps is believed to be interfacial tension between the salt (which because of the chemical attack wets the solid) and the spheres. Apparently, the clumping forces and the resulting diffusion-controlled reaction rate could be accurately modeled, although this is outside the scope of the present study.

For experiments with strong stirring (A = 1.37), one might expect the reaction rate to be proportional to the macroscopic surface area of the solid phase, i.e., with all other parameters held constant, $B \propto d^2$. Data to test this hypothesis are not yet available. However, it is interesting to note that the value of B for 1190-μm UO_2 spheres and the value of B for 350-μm ThO_2 spheres were found to be equal, even though the specific surface area of the UO_2 spheres was ten times that of the ThO_2 spheres.

10. Molten Tin Process for Reactor Fuels

(O. Krikorian,* J. Grens,*
M. Coops,* and W. Parrish*)

The objective of this work is to identify chemically feasible pyrochemical reprocessing methods within the general frame of nonproliferation. Specifically, this effort is aimed at the decomposition and dissolution of spent fuel elements and the formation of thorium, uranium, and plutonium nitrides in molten tin solutions. Separation of fission product elements and other impurities by the use of various physical and chemical processes is anticipated.

a. Scope of Work Package

Lawrence Livermore Laboratory will provide program management, studies and analyses, fuel reprocessing flowsheet development, and general support for the research and development of molten tin processes for the

*Lawrence Livermore Laboratory.

removal of fission products and other impurities from spent uranium-plutonium and thorium-uranium (plutonium) fuels in oxide, metal, or carbide form. Initial effort should be on oxide fuel, followed by metal, and then carbide.

More specifically, effort will be directed in FY1979 to determining the technical feasibility of a selected process flowsheet. Laboratory experiments will be performed with small-scale simulated fuel specimens to refine process parameters and to test process performance. A topical report will be prepared containing a review of thermodynamic and kinetic data relevant to the process, and a proliferation analysis will be made for the process according to guidelines established by Argonne.

b. Process Description

Molten tin is used as a solvent and reaction medium in the Molten Tin Process to separate actinide fuels from fission products and other materials by precipitating out the actinide nitrides, which are insoluble in molten tin. The process is applicable to uranium-plutonium and thorium-uranium (plutonium) breeder fuels in oxide, carbide, or metallic form. If the fuel is an oxide, it is first declad, then introduced directly into molten tin at about 1900 K contained in a graphite crucible. Under these conditions, carbon will dissolve in the molten tin and react with the actinide and fission product oxides, converting them to a metallic solution in tin and releasing CO gas. Carbide or metallic fuels would be dissolved directly in molten tin.

After dissolution of the fuel, gaseous nitrogen is introduced and actinide nitride precipitate is formed by a nitriding reaction at about 1900 K. We also expect that under these conditions, some of the fission products such as the lanthanides will form mixed crystals with the actinide nitrides and precipitate out with them. A significant fraction of the fission products should remain in the molten tin. The actual partitioning behavior of the fission products between the actinide nitride and molten tin phases needs to be experimentally established. Retention of a certain amount of highly radioactive fission products within the actinide fuel is consistent with the nonproliferation goal, since a highly radioactive fuel material provides a deterrence to theft. After nitriding, the molten tin is filtered away from the fuel nitride and the fuel nitride is further processed to convert it to the chemical form required for a new fuel element.

c. Engineering Analysis

We are developing new flowsheets for the molten tin process for separating ^{238}U,/^{239}Pu and ^{232}Th/^{233}U in breeder fuels. Initially, we are looking at oxide systems, but we expect to follow up with carbide and metallic fuel options. For this initial analysis, about 1-2% ^{239}Pu or ^{233}U is assumed to be in the blanket region and we expect to attain about 20% fissile material for the core fuel.

We do not yet have analytical data on the separation factors between plutonium and uranium upon nitriding from molten tin, although a nitriding run was completed recently (see below). Complete data are not yet available on separation factors between uranium and thorium either, but we have found that thorium will nitride at approximately one-fourth the rate of uranium at 1900 K (see below). Thus, we are proceeding on the assumption that uranium can be preferentially enriched relative to thorium by nitriding because of uranium's faster kinetics. As more definitive results become available, this assumption may be modified.

d. Separations Processes

(1) Nitriding of U/Pu Mixtures in Tin

We have completed a nitriding run on a U^{238}/Pu^{239} mixture in molten tin to examine the extent of separation, but no results are yet available. The reaction mix had the composition:

50.168 g tin
1.513 g calcium metal shot
7.99 g D-38 uranium, 3.2-mm-dia. rod
1.738 g plutonium, WR grade

All metals were well cleaned and shiny. Nitriding was done in a graphite reactor at 1900 K under about 680 torr nitrogen pressure for 2 h. The product was a solid brittle metallic ingot that was very adherent to the graphite walls. Our next step will be to use a filtration technique (described below) to separate the nitride precipitate from the molten tin in preparation for analysis. The method of analysis we plan to use for the U-Pu nitride experiment is (1) to separately dissolve the tin and nitride portions, (2) to spike the two portions separately with known amounts of ^{233}U and ^{242}Pu mass tracers, and (3) to analyze for uranium and plutonium by mass spectrometry.

(2) Nitriding of Th/U Mixtures in Tin

We have begun experimentation to explore the separation of thorium from uranium by preferentially nitriding out ThN from Th/U mixtures dissolved in molten tin. Nitriding seems to be a reasonable approach for separation since ThN is substantially more stable than UN (e.g., ΔH°_{f298} = -90.6 kcal/mol for ThN compared with -70.4 kcal/mol for UN).

In the preceding report in this series [STEINDLER-1979B], we reported on a nitriding experiment with uranium and another nitriding experiment with uranium and thorium.

The first run, reported previously, used a composition of 50 g Sn, 1 g U, and 1 g Ca (calcium was included as a catalyst) at 1900 K under stagnant nitrogen and a sequence of nitrogen pressures namely, 304, 432, 507, 608, and 704 torr. Uranium did not nitride.

In the second experiment, also previously reported, 9 g of thorium was added to the mixture of 50 g Sn, 1 g U, and 1 g Ca from the earlier experiment, and nitriding was continued under 395 torr nitrogen for 2 h at 1800 K. From the results, we conclude that thorium will nitride in molten tin under conditions where uranium will not, although the reaction rate is low. We have now made a third run to determine the nitriding rate of thorium in tin with no uranium present. We used a mixture of 9 g Th, 1 g Ca, and 50 g Sn and nitrided at an initial nitrogen pressure of 674 torr and 1900 K. From the rate of nitrogen uptake, the nitriding rate was found to be nearly linear with time at 4-5 torr/h (19%/h). Nitriding was complete in 5 h and 20 min, compared with 1 h and 20 min for uranium under identical conditions. Thus, the nitriding rate for uranium was four times that for thorium. Next, we expect to explore the relative nitriding rates of uranium and thorium in U/Th mixtures in tin at about 675 torr nitrogen to see if uranium can be enriched relative to thorium because of a faster nitriding rate.

II. Engineering Support for the PDPM Program
(K. M. Myles and E. D. Creamer)

The objective of this work is to assist the PDPM Program management in evaluating proliferation resistance, process equipment designs, conceptual process scoping designs, and materials applications of all other work packages in the program. This assistance will be provided by reviewing various reports, participating in the technical information exchange meetings, utilizing other appropriate means of interaction with others in the program, and performing exploratory experimental engineering projects.

Several mass transfer unit operations incorporating agitation were evaluated. Extrapolations of existing correlations tentatively fit the liquid metal-fuel pellet data. The correlations predict that alternative means of agitation to impeller mixing, such as pulsed columns, can be effective in mass transfer operations. These dimensionless correlations also may permit scale-up based on predictions from small-scale laboratory experiments, provided that the necessary variables have been measured.

a. Pulsed-Liquid, Packed-Bed Mass Transfers
(E. D. Creamer)

Various modes of agitation are being investigated as more reliable alternatives to mechanical impeller mixing. In a literature search, dimensionless correlations were found relating the Sherwood number to the Reynolds and Schmidt numbers for operations involving mass transfer in an agitated solution. Since a reciprocating pulsed liquid through a packed bed will be used for fuel decladding and oxide reduction experiments, the correlation for pulsation was investigated in initial work.

(1) Experimental

The dissolution of brass in an aqueous iodine-sucrose solution was utilized as an investigative technique. The rate of dissolution of brass in aqueous iodine solutions is controlled by the rate of transport

of iodine to the metal surface. Although this was determined with systems containing an impeller, the basic technique can be used as a tool to characterize mass transfer in other mechanical systems [MADDEN]. The kinematic viscosity and the diffusion coefficient (diffusivity) can be varied by adding sucrose to the iodine solutions to give a range of Schmidt numbers, Sc, from 800 to 30,000 at room temperature. Operation at elevated temperatures (45°C) decreases the Schmidt number to 300. This Schmidt number appears to be slightly higher than that of the pyrochemical process mixtures of interest, but diffusivity and viscosity data are scarce. For uranium in cadmium, the Schmidt, number varies from 90 to 150 [TRAYLOR]. From available viscosity and diffusivity data [RICHARDSON], similar values are expected for salt mixtures. Oxide mixtures in the reduction step have higher viscosities and therefore higher Schmidt numbers than the studied range. The iodine system was chosen to first characterize the pulsed liquid, packed bed, in spite of the limited range of Schmidt numbers, because of the availability of viscosity and diffusivity data and ease of analysis.

The apparatus was constructed having the smallest dimensions which permit scaling-up. The brass pellets (in a fixed bed resting on a screen) were contacted with the aqueous iodine solution which was pumped up through the pellets and then allowed to drain. For scale-up, the bed diameter must be at least eight times the pellet diameter and must be at least three pellets deep.

Initially, the bed was lowered into a 4-L glass beaker filled with an accurately known volume of solution. The solution was pulsed and also was stirred magnetically at 120 rpm to provide a uniform iodine concentration. Samples were withdrawn periodically during the run and analyzed for iodine by titration with thiosulfate [FURMAN]. It was quickly observed that the magnetic stirring overwhelmed the desired effects of pulsation, and so the procedure was modified.

The same bed was lowered into a 1-L glass beaker filled with 0.650 L of solution. No measurable reaction or evaporation were observed in the absence of pulsation. Runs 4-11 were then conducted at various pulsing rates or frequencies and various Schmidt numbers (Table 43).

The lower solution level was always adjusted to be slightly above the top of the pellets. Thereby, most of the solution was expelled into the bulk solution in the beaker. This helped to avoid depletion of the iodine solution in contact with the pellets and made the bulk concentration more representative of the actual driving force.

(2) Results

The results from a series of experiments are assembled in Table 43. These data were calculated using the following relationships.

Table 43. Pulsed Liquid Mass Transfer[a] m/(s x 10^6)

Run	Pulse Amplitude, m	Pulse Frequency, Hz	Sucrose Conc, mol/L	D, $m^2/(s \times 10^{12})$	ν, $m^2/(s \times 10^6)$	Re	k, m(s x 10^6)	Av. I_2 Conc, mol/m^3	Sh	Sc
4	0.031	0.32	0	1130	0.874	140	31.1	4.6	175	773
5	0.027	0.05	0	1130	0.874	19	10.5	5.6	59	773
6	0.022	0.10	0	1130	0.874	32	14.6	5.5	82	773
7	0.018	0.11	0.5	685	1.36	19	11.5	24.9	107	1990
8	0.021	0.03	0.5	685	1.36	5.0	5.8	22.4	53	1990
9	0.025	0.29	0.5	685	1.36	67	11.1	20.6	103	1990
10	0.026	0.29	1.0	380	2.45	39	12.3	24.3	205	6450
11	0.024	0.03	1.0	380	2.45	4.0	3.8	23.7	63	6450

[a]See text for definitions of symbols.

$$Re = \frac{2 \cdot A(m) \cdot W(1/s) \cdot d_p(m)}{\nu(m^2/s)}$$

$$k = \frac{\text{iodine reacted per unit time (mole/Ms)}}{(I_e \text{ conc., mol/m}^3)\ (\text{surface area, m}^2)}$$

$$Sh = \frac{k(m/Ms) \cdot d_p\ (m \times 10^{-3})}{D(m^2/Ms)}$$

$$Sc = \frac{\nu(m^2/Ms)}{D(m^2/Ts)}$$

where

Re, Reynolds number $= \frac{2A\omega d_p}{\nu}$

Sh, Sherwood number $= kd_p/D$

Sc, Schmidt number $= \nu/D$

k = mass transfer coefficient, m/s

d_p = pellet effective diameter, m

ν = kinematic viscosity, m^2/s

D = Diffusivity, m^2/s

C = iodine concentration, mol/m^3

ω = pulse frequency, 1/s

A = pulse amplitude, m

In comparison, studies with oscillating cylinders in fluids were correlated dimensionlessly [JAMESON] with

$$Sh = 0.746\ Re^{1/2}\ Sc^{1/3}\ (A/R)^{1/6}$$

Thus, in analyzing the dissolution of brass in iodine solutions, as a first approximation, the data were plotted with $Sh/Sc^{1/3}$ as the ordinate and Re the abscissa (Fig. 33), yielding the following correlation

$$Sh = 1.6\ Re^{1/2}\ Sc^{1/3}$$

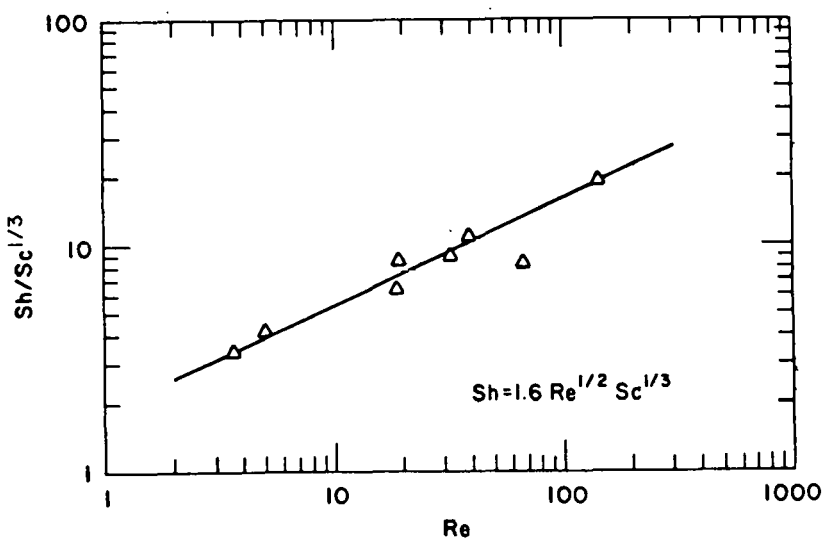

Fig. 33. Pulsed Liquid Mass Transfer Dimensionless Correlation

(3) Conclusions

Within the range of Reynolds numbers (4 → 140) and Schmidt numbers (773 → 6450) examined, pulsed-liquid, packed-bed mass transfer can be correlated dimensionlessly. The pulse frequency range examined is typical of what can be practically achieved with present pulsation apparatus. It is planned to use the same apparatus for the oxide reduction studies. The results, however, are valid only for systems with bulk solution reservoirs in which the pulse amplitude and frequency are sufficiently large to avoid depletion or saturation of the solution and therefore loss of a driving force of mass transfer.

b. Oxide Reduction Mechanism

The dimensionless correlation for the pulsed-liquid, packed-bed system was confirmed experimentally, as described above. This mode of agitation is planned for oxide reduction studies because of its ease of operation and control. However, the overall rate of reduction can not be predicted or scaled up to production size from such correlations with a reasonable degree of certainty until the mechanism of at least the rate-limiting step (if there is one) is known. Proposed mechanisms can be investigated with a known, characterized method of agitation by adjusting the rate-controlling parameters, such as the driving force, surface area, and rate coefficients, which are functions of temperature, pressure, viscosity, mixing,etc.

A dual-level pulser is being constructed to determine under which conditions either oxide-salt phase transport or oxide-metal phase transport is rate-limited. The pulser is capable of contacting the oxide alternately with the salt and metal phases for different time periods and under

different agitation conditions. It is expected that the overall reduction rate will be faster when the oxide is in contact with the salt phase for a greater fraction of the total time than it is in contact with the metal phase. The optimum actual rates are, however, unknown.

Before experimentation could begin it was learned that funding for FY1980 is not available. Since it was estimated that no definitive results would be forthcoming from this project before the end of the fiscal year, work on this project was terminated.

II. ENCAPSULATION OF RADIOACTIVE WASTE IN METAL

(L. J. Jardine, K. F. Flynn, W. J. Mecham and R. H. Pelto)

The major objective of this program is to identify the advantages and disadvantages of encapsulating solidified radioactive waste forms in a metal matrix. The net attributes of metal encapsulation, if any, are to be identified by comparisons of waste form properties and fabrication methods with those of other well-developed solidification alternatives--i.e., calcination and vitrification in the special case of high-level radioactive wastes.

Laboratory-scale investigations are in progress specifically aimed at generating data required to further assess probable or unresolved problem areas. Experimental studies have continued to focus upon the determination of leach rates of simulated waste forms. A study aimed at assessing the impact resistance of metal-encapsulated waste forms in comparison to glass waste forms has continued during this period.

A. Leach Rates of Simulated Radioactive Waste Materials

1. Introduction

Measurements of leach rates are necessary to evaluate the rate at which specific hazardous radionuclides will migrate from the waste if the waste form should come in contact with an aqueous medium. Much of the leach rate data for nuclear waste materials are based on measurements at room temperature (about 25°C) with distilled water. Since this leaching medium is atypical of any natural environment, preliminary work has been done on the effect on leach rate of changing the various parameters associated with the leaching medium. Neutron activation analysis (NAA) techniques [FLYNN] have been used predominantly in these studies.

2. Experimental Materials, Procedures, and Results

The solid waste material chosen for these studies was a simulated high-level waste (HLW) glass obtained from Battelle Pacific Northwest Laboratories (PNL) and identified as 76-68 PNL-glass. The composition of this material has been defined by PNL [McELROY]. Previous experiments with this waste form using 25°C quiescent distilled water as the leaching medium [STEINDLER-1978D] showed this PNL-glass to be relatively homogeneous, with the fission product elements incorporated uniformly (presumably by encapsulation in the vitreous phase).

Leach rates were measured for a series of tests using the following leaching media:

(1) Distilled water (about 25°C, pH 5.8)
(2) Tap water (about 25°C, pH 9.7)
(3) Carbonate-saturated distilled water (about 25°C, pH 3.9)
(4) WIPP* brine-saturated distilled water (about 25°C, pH 7.6)
(5) WIPP* brine-saturated distilled water (about 109°C, pH 7.6)

*A salt core from the proposed Waste Isolation Pilot Plant (WIPP) was used to saturate distilled water. This leaching medium corresponds to an aqueous solution that could be formed in a salt repository.

Each pH measurement was made using a calibrated Sargent-Welch model NX pH meter at the indicated temperature. The low pH (5.8) of the 25°C distilled water is attributed to dissolved carbonate from equilibration with air. The high pH (9.7) of the tap water is attributed to the site-specific water treatment process used at ANL. Groundwaters typically cover a pH range of about 5 to 9. The variation in pH of the leaching media listed above adequately covers this range.

Results of the sequential leach tests for the leaching media identified above (Tables 44-48; previously published Table 44 is included to permit comparison with other leaching media) are reported in units of grams per square centimeter of surface area per day (g/cm^2-d). These units represent the equivalent grams that would have been leached if the entire glass

Table 44. Sequential Leach Tests for 76-68 PNL-Glass[a] in 25°C Quiescent Distilled Water[b]

	Leach Rate,[c] g/cm^2-d						
Isotope Analyzed	1st Test (5.8 d)[d]	2nd Test (21.0 d)[d]	3rd Test (32.0 d)[d]	4th Test (29.1 d)[d]	5th Test (48.9 d)[d]	6th Test (49.0 d)[d]	7th Test (54.1 d)[d]
^{51}Cr	1.9 E-6	3.0 E-7	4.2 E-7	e	e	e	e
^{60}Co	4.8 E-6	1.4 E-6	1.2 E-6	4.1 E-6	1.8 E-7	1.2 E-7	5.2 E-7
^{65}Zn	5.4 E-6	8.7 E-7	6.5 E-7	1.8 E-7	1.5 E-8	1.5 E-8	3.5 E-7
^{85}Sr	5.8 E-6	1.1 E-6	9.6 E-7	1.5 E-6	6.6 E-7	1.3 E-6	2.1 E-6
^{95}Zr	4.5 E-7	1.1 E-7	1.0 E-7	e	e	e	e
^{134}Cs	7.8 E-7	2.9 E-7	6.1 E-7	4.4 E-7	5.2 E-8	1.3 E-7	4.2 E-7
^{141}Ce	6.0 E-7	7.1 E-8	1.2 E-7	1.2 E-7	e	e	e
^{152}Eu	5.1 E-7	6.5 E-8	8.4 E-8	3.1 E-8	3.2 E-9	2.7 E-9	3.5 E-7
^{237}U	1.5 E-7	e	e	e	e	e	e
^{239}Np	1.5 E-6	e	e	e	e	e	e

[a]Composition 76-68 as defined in [McELROY]. The initial sample weight was 0.47 g, and the initial surface area (calculated apparent geometric surface) was 2.3 cm^2.

[b]Laboratory distilled water, air-equilibrated (pH 6.0).

[c]The unit of grams per cm^2-day represents the equivalent grams that would have been leached had the entire matrix leached at the same rate as the specific isotope studied.

[d]Duration (in days) for each sequential leach test.

[e]The gamma rays for these isotopes were no longer resolvable from the gamma spectrum because of radioactive decay.

Table 45. Sequential Leach Tests for 76-68 PNL-Glass[a] in Tap Water[b] (25°C)

Isotope Analyzed	Leach Rate,[c] g/cm^2-d			
	1st Test (6.8 d)[d]	2nd Test (37.0 d)[d]	3rd Test (49.0 d)[d]	4th Test (54.1 d)[d]
^{22}Na	7.1 E-7	5.2 E-8	e	e
^{51}Cr	1.7 E-6	e	e	e
^{60}Co	6.2 E-6	1.0 E-6	e	2.4 E-6
^{65}Zn	1.0 E-6	2.4 E-7	2.1 E-8	6.6 E-7
^{85}Sr	e	9.6 E-7	e	e
^{95}Zr	1.4 E-6	1.2 E-7	e	2.0 E-7
^{103}Ru	3.3 E-6	e	e	e
^{110}Ag	7.6 E-6	e	e	1.2 E-6
^{134}Cs	2.3 E-6	1.4 E-6	6.5 E-7	7.4 E-7
^{141}Ce	6.4 E-7	1.0 E-7	e	3.1 E-7
^{152}Eu	2.9 E-7	1.1 E-7	e	1.2 E-7

[a]Composition 76-68 as defined in [McELROY]. The initial sample weight was 0.23 g, and the initial surface area (calculated; apparent geometric surface) was 1.1 cm^2.

[b]ANL tap water (pH 9.7).

[c]The unit of grams per cm^2-day represents the equivalent grams that would have been leached if the entire matrix had leached at the same rate as the specific isotope studied.

[d]Duration (in days) for each sequential leach test.

[e]These values were not determined because the gamma rays were not resolved from the spectrum.

matrix had leached at the same rate as the specific isotope measured. These leach rates are calculated [STEINDLER-1978B] from the following equation:

$$L = \frac{A_t W_o}{A_o St} \quad (1)$$

where A_t = amount of material A removed in time t
A_o = initial amount of material A in solid
S = surface area of the solid material (cm^2)
W_o = initial weight of the solid material (g)
t = leaching period (d)
L = leach rate (g/cm^2-d)
A_t/A_o = fraction leached.

Table 46. Sequential Leach Tests for 76-68 PNL-Glass[a] in Carbonate Water[b] (25°C)

Isotope Analyzed	Leach Rate,[c] g/cm^2-d			
	1st Test (6.8 d)[d]	2nd Test (37.1 d)[d]	3rd Test (49.0 d)[d]	4th Test (54.1 d)[d]
^{22}Na	e	e	e	e
^{51}Cr	e	e	e	e
^{60}Co	7.5 E-6	8.4 E-7	9.8 E-7	5.2 E-7
^{65}Zn	3.6 E-6	2.1 E-8	2.1 E-8	4.8 E-8
^{85}Sr	1.7 E-5	e	2.9 E-6	e
^{95}Zr	e	e	e	e
^{103}Ru	1.8 E-6	e	e	e
^{110}Ag	1.9 E-6	e	e	e
^{134}Cs	2.5 E-6	4.9 E-7	8.6 E-7	1.0 E-6
^{141}Ce	3.4 E-7	e	9.9 E-8	e
^{152}Eu	2.1 E-7	4.1 E-8	2.2 E-8	3.0 E-8

[a]Composition 76-68 as defined in [McELROY]. The initial sample weight was 0.22 g, and the initial surface area (calculated; apparent geometric surface) was 1.1 cm^2.

[b]Distilled water saturated with CO_2 (pH 3.9).

[c]The unit of grams per cm^2-day represents the equivalent grams that would have been leached if the entire matrix had leached at the same rate as the specific isotope studied.

[d]Duration (in days) for each sequential leach test.

[e]These values were not determined because the gamma rays were not resolved from the spectrum.

Table 47. Sequential Leach Tests for 76-68 PNL-Glass[a] in WIPP Brine[b] (25°C)

Isotope Analyzed	Leach Rate,[c] g/cm^2-d				
	1st Test (7.0 d)[d]	2nd Test (10.9 d)[d]	3rd Test (36.2 d)[d]	4th Test (54.1 d)[d]	5th Test (53.9 d)[d]
^{22}Na	9.1 E-7	e	e	e	e
^{51}Cr	7.2 E-7	4.1 E-7	e	e	e
^{60}Co	9.2 E-6	4.1 E-6	2.3 E-5	1.7 E-5	1.6 E-6
^{65}Zn	1.2 E-6	3.1 E-7	4.7 E-7	4.0 E-7	1.1 E-7
^{85}Sr	3.1 E-6	6.9 E-6	e	e	1.9 E-6
^{95}Zr	3.1 E-6	4.9 E-7	e	e	4.4 E-7
^{103}Ru	2.4 E-6	e	e	e	e
^{110}Ag	1.7 E-5	3.9 E-6	2.6 E-6	e	1.3 E-6
^{134}Cs	3.1 E-6	2.9 E-7	1.6 E-7	1.7 E-7	1.9 E-7
^{141}Ce	8.9 E-7	4.4 E-7	1.4 E-7	e	2.2 E-7
^{152}Eu	6.0 E-7	1.2 E-7	4.4 E-8	4.8 E-8	7.8 E-8

[a]Composition 76-68 as defined in [McELROY]. The initial sample weight was 0.33 g, and the initial surface area (calculated; apparent geometric surface) was 2.3 cm^2.

[b]Waste Isolation Pilot Plant (WIPP) salt core was used to saturate distilled water (pH 7.6). This leaching medium corresponds to an aqueous solution that could be found in a salt repository.

[c]The unit of grams per cm^2-day represents the equivalent grams that would have been leached if the entire matrix had leached at the same rate as the specific isotope studied.

[d]Duration (in days) for each sequential leach test.

[e]These values were not determined because the gamma rays were not resolved from the spectrum.

The surface area used in these determinations was the calculated geometric surface area of the solid samples. Leach rates for about a dozen different elements have been determined in these studies. The results (Table 44 through 48) indicate a relatively small variation (i.e., about an order of magnitude) in leach rates for the different elements studied as well as little change in leach rate with time (again a variation of about an order of magnitude or less). These studies, which have been in progress for about six months, are continuing since changes in leach rate with time are of concern when extrapolating results to longer time scales.

Table 48. Sequential Leach Tests for 76-68 PNL-Glass[a] in WIPP Brine[b] (109°C)

Isotope Analyzed	Leach Rate,[c] g/cm^2-d				
	1st Test (7.0 d)[d]	2nd Test (11.0 d)[d]	3rd Test (36.1 d)[d]	4th Test (49.0 d)[d]	5th Test (54.0 d)[d]
^{22}Na	1.1 E-6	4.1 E-7	2.3 E-7	e	e
^{51}Cr	3.4 E-6	1.2 E-6	e	e	e
^{60}Co	2.2 E-6	4.8 E-7	2.5 E-6	1.3 E-7	8.2 E-8
^{65}Zn	4.4 E-7	7.0 E-7	6.5 E-7	9.3 E-8	6.9 E-8
^{85}Sr	7.6 E-6	2.2 E-6	8.7 E-6	e	e
^{95}Zr	2.1 E-6	5.5 E-7	e	e	8.2 E-8
^{103}Ru	4.3 E-6	1.1 E-6	e	e	4.3 E-7
^{110}Ag	2.4 E-5	8.1 E-6	2.7 E-6	9.6 E-7	8.4 E-7
^{134}Cs	9.0 E-6	3.6 E-6	6.9 E-7	4.9 E-7	5.8 E-7
^{141}Ce	1.2 E-6	5.3 E-7	2.3 E-7	8.4 E-8	e
^{152}Eu	8.3 E-7	5.1 E-7	1.7 E-7	2.8 E-8	2.5 E-8

[a]Composition 76-68 as defined in [McELROY]. The initial sample weight was 0.24 g, and the initial surface area (calculated; apparent geometric surface) was 2.3 cm^2.

[b]Waste Isolation Pilot Plant (WIPP) salt core was used to saturate distilled water (pH 7.6). This leaching medium corresponds to an aqueous solution that could be found in a salt repository.

[c]The unit of grams per cm^2-day represents the equivalent grams that would have been leached if the entire matrix had leached at the same rate as the specific isotope studied.

[d]Duration (in days) for each sequential leach test.

[e]These values were not determined because the gamma rays were not resolved from the spectrum.

Results from the initial leach tests (of about 1-week duration) using the five leaching media identified above are compared in Table 49. These results indicate no significant effect of pH on the leach rate for this particular waste form over the pH range of 3.9 to 9.7. Furthermore, the leach

Table 49. Initial (about 7-day-duration) Incremental Leach Rates (g/cm^2-d) for 76-68 PNL-Glass[a] Using a Variety of Leaching Media

Isotope	Distilled Water, 25°C, pH 5.8	Tap Water, 25°C, pH 9.7	Carbonate Water, 25°C, pH 3.9	Brine, 25°C, pH 7.6	Brine, 109°C, pH 7.6
^{60}Co	4.8 E-6	6.2 E-6	7.5 E-6	9.2 E-6	2.2 E-6
^{65}Zn	5.4 E-6	1.0 E-6	3.6 E-6	1.2 E-6	0.5 E-6
^{85}Sr	5.8 E-6	1.0 E-6	2.9 E-6	3.1 E-6	7.6 E-6
^{134}Cs	0.8 E-6	1.4 E-6	2.5 E-6	3.1 E-6	9.0 E-6
^{141}Ce	0.6 E-6	0.6 E-6	0.3 E-6	0.9 E-6	1.2 E-6
^{152}Eu	0.5 E-6	0.3 E-6	0.2 E-6	0.6 E-6	0.8 E-6

[a]Composition 76-68 as defined in [McELROY]. Initially, a sample typically weighed about 0.3 g and had about 2.3 cm^2 geometric surface area.

rates for saturated brine solution were only marginally greater than those for the nonsaline aqueous media, and raising the temperature of the brine solution to its boiling point (i.e., 109°C) resulted in at most only a small increase in the leach rate for cesium and the rare earths. Although these measurements are based on initial leach rates for one particular waste formulation (76-68 PNL-glass), it can be inferred from these data that pH (in the range, 4 to 10), salinity, and temperature (below 110°C) can have minimal effects on the leach rate of this vitrified radioactive waste form.

The temperature of the leaching medium in a waste repository will depend to some extent on the decay heat generated by the waste. Although this temperature will probably be relatively low (i.e., below 100°C) for existing defense wastes, future commercial reprocessing wastes having higher heat generation rates might generate considerably higher temperatures. Three temperatures have been chosen for studies of the effect of this variable on leach rate. These temperatures are (1) ambient room temperature (about 25°C), (2) boiling aqueous temperature (about 100°C), and (3) high pressure autoclave temperatures (up to about 300°C). These temperatures should adequately span the range of possibilites for both present and future high-level wastes destined for geologic storage.

Preliminary measurements have been made using distilled water as the leaching medium and the 76-68 PNL-glass [McELROY] discussed above as the solid waste material. Results from initial leach tests (of about 1-week duration) at the three temperatures identified above are given in Table 50. These leach rates, as in (Eq. 1), are reported in units of g/cm^2-d.

Table 50. Initial (about 7-day-duration) Leach Rates for 76-68 PNL-Glass[a] in Distilled Water

Isotope Analyzed	Leach Rate, g/cm^2-d		
^{134}Cs	7.8 E-7	8.8 E-5	3.4 E-3
^{152}Eu	5.1 E-7	1.0 E-6	6.0 E-6
Wt. Loss	b	1.1 E-4	3.8 E-3
Temperature, °C	25	100	286
$\frac{1}{T(K)}$	3.36×10^{-3}	2.68×10^{-3}	1.79×10^{-3}

[a]Composition 76-68 as defined in [McELROY]. The initial samples weighed about 0.4 g and had surface areas of about 2 cm^2.

[b]This value could not be determined because of difficulties associated with evaluating small differences between large numbers.

Leach rates are reported in Table 50 for the elements, cesium (the most leachable radionuclide element in HLW) and europium (among the least leachable radionulcide elements in HLW), along with total weight loss. Weight loss values could not be determined for the very low leach rates at 25°C. However, at 100°C and 286°C, the leach rate had increased sufficiently so that this determination could be made with reasonable accuracy.

The leach rates reported in Table 50 have been plotted as a function of the reciprocal of the absolute temperature (Arrehenius plot) in Fig. 34. Within the uncertainties associated with these preliminary measurements, these data can be fitted to straight lines (log-log plot). Although more experimental data must be accumulated before definitive statements regarding the shape of the leach rate vs. temperature functions can be made, these data suggest that the leach rates for cesium and europium differ significantly at high temperatures. In fact, at 286°C, this difference is about three orders of magnitude. As shown in Fig. 34, the leach rates for cesium at 100°C and 286°C are in agreement with the total weight losses at these temperatures. The much lower leach rate for europium, particularly at 286°C, indicates that a significantly different mechanism operates for europium than for cesium. This may be because europium oxide has a much lower solubility than does cesium oxide and/or because the coefficients of diffusion of europium and cesium differ. Leach rates as a function of time at the above temperatures continue to be measured. Tests results will establish the significance of the initial results reported here.

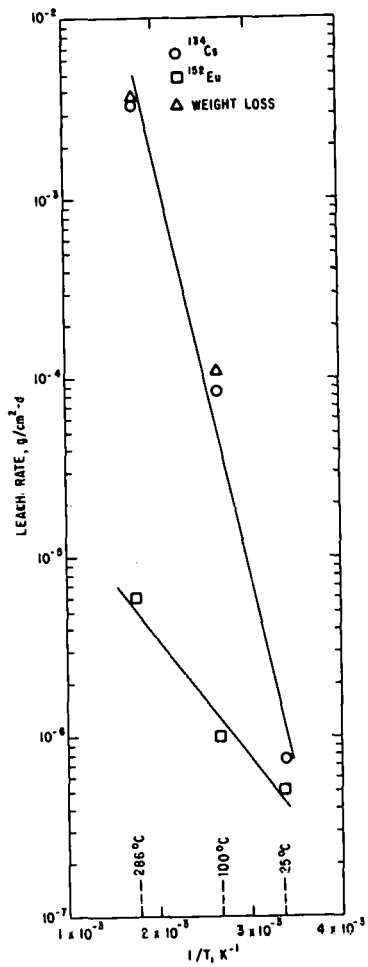

Fig. 34. Effect of Temperature on Leach Rate of 76-68 PNL Glass in Distilled Water for Initial 7-day Leaching Period

Studies have been initiated of the leaching characteristics of other potential nuclear waste materials, including metals. In the current series of experiments, samples of copper, lead, aluminum, porcelain beads, soft glass, and zinc glass have been neutron-irradiated. (In the preceding quarterly report [STEINDLER-1979B], experiments on the leaching of borosilicate Pyrex glass are reported.) After suitable cooling periods, the residual gamma-emitting nuclides have been determined by GeLi spectroscopy. These results are summarized in Table 51. The data in this table verify that the neutron activation technique [FLYNN] is suitable for preliminary study of all of these candidates for leach rate studies.

Initial leach rates (based on one 48-day leach test) for the above-mentioned materials are tabulated in Table 52. The leaching medium for these studies was 25°C quiescent, air-equilibrated, distilled water (pH 5.8). The leach rates are given in units of grams per square centimeter per day,

Table 51. Activation Products in Potential Materials for Application to Nuclear Waste Disposal

Matrix Material	Activated Species	Specific Activity[a]
Copper	^{182}Ta	1.3 E+6
	^{124}Sb	2.0 E+5
	^{110}Ag	2.7 E+5
	^{65}Zn	1.6 E+5
	^{60}Co	1.8 E+5
	^{75}Se	1.1 E+5
Aluminum	^{182}Ta	5.7 E+5
	^{59}Fe	4.4 E+5
	^{65}Zn	2.3 E+5
	^{51}Cr	5.2 E+5
Lead	^{124}Sb	4.1 E+8
Zinc borosilicate glass	^{65}Zn	1.0 E+8
	^{124}Sb	3.5 E+6
Soft glass	^{65}Zn	2.3 E+6
	^{124}Sb	1.0 E+6
	^{110}Ag	1.1 E+5
Porcelain beads	^{46}Sc	1.2 E+7
	^{51}Cr	4.0 E+6
	^{152}Eu	4.0 E+5
Pyrex (borosilicate) glass	^{124}Sb	7.2 E+7

[a]Specific activity in units of disintegrations per minute (corrected to time at end of irradiation) per gram of matrix material.

representing the equivalent grams that would have been leached if the entire matrix leached at the same rate as the isotope studied.

Weight loss data are based on small differences between large numbers and hence are subject to considerable uncertainty. In most cases, this difference was not even measureable. Perhaps, longer term studies of larger samples would result in more reliable weight loss data.

Table 52. Initial (about 48-day-duration) Incremental Leach Rates[a] for Various Materials Associated with Nuclear High-Level-Waste

Matrix Material	Species Measured	Leach Rate, g/cm^2-d[b]
Soft glass	^{65}Zn	2.5 E-7
	^{110}Ag	2.4 E-6
	^{124}Sb	9.7 E-7
	Wt loss[c]	2.8 E-6
Zinc borosilicate glass	^{65}Zn	7.0 E-8
	^{124}Sb	2.7 E-7
	Wt loss[c]	3.3 E-6
Porcelain beads	^{46}Sc	1.2 E-8
	^{134}Cs	5.5 E-6
	^{152}Eu	6.7 E-7
	Wt loss[c]	N.D.[d]
Pyrex (borosilicate) glass beads	^{134}Cs	6.3 E-5
	^{124}Sb	1.4 E-6
	Wt loss[c]	N.D.[d]
Copper	^{182}Ta	1.2 E-6
	Wt loss[c]	6.2 E-5
Aluminum	^{182}Ta	1.5 E-6
	Wt loss[c]	N.D.[d]
Lead	^{124}Sb	2.0 E-5
	Wt loss[c]	N.D.[d]

[a]Leaching medium was 25°C quiescent distilled water (pH 5.8).

[b]These units of grams per cm^2 per day represent the equivalent grams that would have been leached if the entire matrix leached at the same rate as the isotope studied.

[c]Weight loss data are based on small differences between large numbers and hence are subject to considerable uncertainty.

[d]N.D. means not determined.

Physical measurements of this type, particularly measurements of metals, are continuing.

The results of the preliminary measurements reported in Table 60 indicate that under the conditions of these tests, the leach rates for copper and aluminum* are comparable i.e., about one order of magnitude lower than the leach rate for lead. [KBS] suggested using these metals as potential canisters or barriers in HLW disposal concepts. Continued study of these metals will establish their potential as barriers to dispersal by aqueous leaching of the solidified waste.

The leach rates for the three glasses studied are similar to those for metals. Hence, future studies will be based on the use of Pyrex (borosilicate) glass when a "stand in" for waste glass is required. At best, the porcelain bead leach rates were only marginally greater than those for borosilicate glass beads.

Leach rates of these materials will continue to be studied in order to reduce uncertainties in the results and to establish leach rates as a function of time and temperature for each material.

3. Conclusions

Changing of various parameters associated with the leaching medium can significantly affect leach rates. The effects of the pH and the salinity of the leachant, though small, were measurable for the waste form studied here (i.e., PNL 76-68 glass). However, the effect of temperature on leach rate was dramatic--particularly at the possible high temperatures (e.g., 286°C) associated with future geologic repositories for commercial wastes. Large differences in leach rate can exist for different chemical elements such as cesium and europium at temperatures of about 250°C. The initial rate at which europium is absorbed into the aqueous leachant is markedly less than the rate of dissolution of the matrix (Table 50). This difference could be explained in part by a conversion of the glass to a mixture of crystalline phases under these hydrothermal conditions, an effect observed by [WESTSIK]. Continued testing as a function of time at these high temperatures may shed some light on this phenomenon and its ramifications.

Preliminary measurements by the neutron activation technique [FLYNN] of the leach rates of a host of potential materials for application to nuclear waste disposal have established their suitability for further leach rate studies.

B. Evaluation of Impact Resistance of Waste Forms

Resistance of solid radioactive waste forms to dispersion by mechanical impacts during in-plant storage and transportation is likely to be a property of great concern. The effects of mechanical impacts on waste forms are being analyzed and evaluated.

---

*Other metals (e.g., titanium) are also being analyzed.

In this report period, further literature reviews were made (1) of relevant engineering experiments in brittle fracture made from 1949 to 1962 and (2) of the recent(1973) state of the art of a new field of materials science, fracture mechanics of ceramics. These literature reviews are summarized below.

A major accomplishment in our evaluation of impact resistance has been the development of descriptive and calculational models relating deformation measures to material properties and to impact conditions. This work has been summarized in a paper, The Effect of Impact Energy on Solid-Waste Composites of Brittle and Ductile Materials (see also [STEINDLER-1979B]). The paper has been accepted for presentation at and publication in the proceedings of the International Symposium on Ceramics in Nuclear Waste Management in conjunction with the annual meeting of the American Ceramics Society, April 30 - May 2, 1979, at Cincinnati, Ohio.

1. Engineering Studies of Brittle Fracture: A Chronological Review

Although there has always been practical interest in the behavior of brittle materials, both as to their performance as load-bearing structural materials and the resistance of minerals to comminution, the process of brittle fracture has been sufficiently complex that no satisfactory theory has emerged from academic research; the early incomplete and tentative theories came from research laboratories of chemical industries [TAYLOR-1947, ROESLER].

Brittle behavior is defined as inelastic deformation by fracture (rather than by plastic flow) with the breaking of chemical bonds and the formation of new surface area. The fracture process, in general, varies with the rate of application of stress and its duration, and varies also with the temperature and the chemical environment. In particular, the fracture behavior of glass varies markedly with moisture. Also, even normally ductile materials may show brittle behavior in the very short term (i.e., under sharp impacts), and brittle materials may fracture at unpredictably low stress levels if loading is maintained for a long enough time [TAYLOR-1947]. An explantion has been made which related fracture to critical tensile strain and to a rate-controlling factor, an activation energy for orientation of the atomic network under the stress. Moisture on glass (or moisture plus oxygen on certain metals) appears to have a catalytic function in this (hypothetical) rate process. The energy threshold for fracture and the energy released per unit surface area formed is estimated in terms of a tensile elastic-energy model [TAYLOR-1947]. This is essentially the same as our brittle-fracture model mentioned above [MECHAM].

Conical indentation fractures of silicate glass (i.e., window glass) are sufficiently reproducible that their sizes can be controlled and measurements made of the fracture-surface area under specific conditions. From such an approach, the minimum fracture-surface energy (J/m^2) approaches the thermodynamic equilibrium surface free energy, which was estimated to be about 2 J/m^2 [ROESLER].

Experimental investigation of the energy consumption in the crushing of quartz was improved by the use of gas adsorption methods for measurement of total surface area formed [PIRET-1949]. Surface areas measured by gas adsorption were about a factor of two higher than those measured by the gas permeability (flow) technique; the adsorption method was believed to measure surface area not accessible to gas in the flow method. The quartz used was natural crystalline mineral (from Arkansas), sized in the 10/14 mesh fraction, and washed free of dust. For crushing, batches of about 1000 particles (5 g) were placed in a steel cavity and were covered with a steel plunger, onto which a steel ball was dropped up to 32 times, each impact being about 10 J. The sample was wetted before impact with carbon tetrachloride to prevent dust losses, and the same liquid was used to transfer crushed material to the adsorption sample tube. It was found that 40% greater surface was measured when impacted samples were degassed at 555°C rather than at 200°C; the explanation and general significance was not reported. The adsorption was of pure ethane at low temperature (-183°C) and appeared to be reproducible within 2% [PIRET-1949].

Special precautions were taken to determine the energy actually absorbed in the brittle material by subtracting the energy dissipated in metal components of the impact apparatus from the gross impact energy. It was found that the fracture surface energy increased from about 87 J/m^2 for single impact and relatively low energy input to about 123 J/m^2 for the higher energy inputs (28.5 J/g)--indicating a lower efficiency of energy use with higher energy input.

In comparison, slow-compression crushing of similar batches of particles gave fracture surface energies of about 80 (±8%)J/m^2 for both single crushing and multiple crushing (energy inputs up to about 17 J/g). Thus it was believed that slow compression is more energy efficient than are impacts (especially multiple impacts) in producing new fracture surface [PIRET-1949].

This work was continued by refined measurements of slow-compressive crushing of single particles of crystalline quartz (1 to 2 g). Particles were crushed in a crushing device made of high-speed steel hardened to 58 Rockwell [PIRET-1950]. The energy input was calculated from force and displacement measurements of the loading device; the surface areas (before and after) were determined by gas adsorption. In 17 experiments, the energy density in the material at fracture varied from 0.030 to 4.4 J/g. The surface fracture energy ranged from 3.7 to 58 J/m^2. The surface fracture energy (J/m^2) increased linearly with the energy density (J/g) at the time of fracture of single particles under slow compression.

The energy efficiency of fracture of single particles was calculated for an assumed equilibrium (thermodynamic) surface-formation free energy of 1.0 J/m^2 for quartz: the range of energy efficiencies in the experiments was 1.7% to 26.5%. The higher efficiencies of fracture were statistically rarer (Fig. 35). In comparison, a nearly constant 1.4% energy efficiency was obtained over a range of energy inputs in the multiple-particle measurements reported above. It was suggested that the low energy efficiency

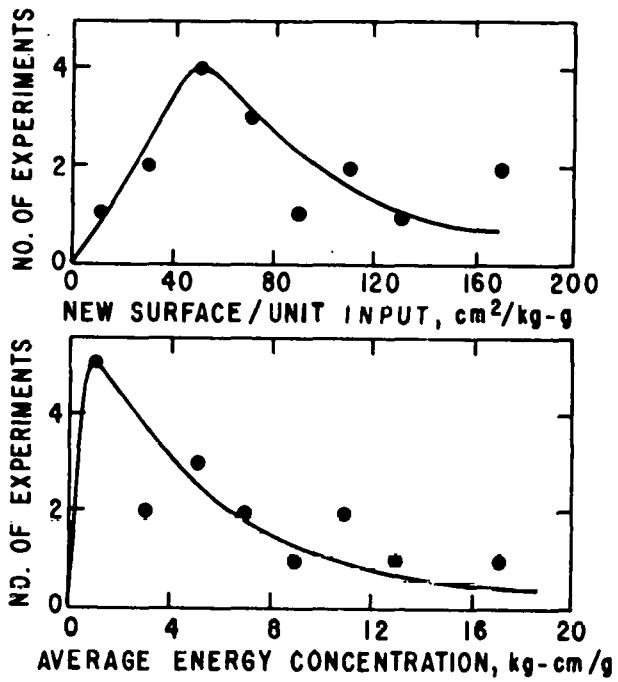

Fig. 35. Frequency Curves of (1) New Surface Produced per Unit of Energy Input and (2) Average Energy Concentration at Fracture for Single Particles [PIRET-1950]. (Note: 1kg-cm = 0.098 J)

in multiple-particle crushing was due to a shearing action rather than the shattering action of single crystals. In single-particle crushing, the higher energy density (J/g) produces more (and therefore shorter) cracks, while for multiple-particle contact, there is more opportunity for the elastic energy to change into heat [PIRET-1950].

A calorimetric method was applied [SCHELLINGER] to the determination of the fracture surface energy for ball-milled quartz sand, in conjunction with surface-area measurement by gas adsorption. Measurement of the heat and the surface area generated with and without quartz sand present in the ball-milling apparatus indicated a net fracture surface energy of 107 J/m^2; this value was constant within 10% for energy inputs of up to 700 J/g glass [SCHELLINGER]. However, the net fracture surface energy included energy absorbed by the metal balls.

A drop-weight crusher (similar to that reported previously) was used to investigate the effect of temperature (in the range of -58°C to 400°C) on the fracture surface energy of several brittle materials: taconite, quartz, magnetite, hematite, and glass. There was very little effect of temperature (in the range of 25 to 400°C) in any of the materials tested. For all materials other than glass, there was a peak resistance to crushing (i.e., an especially high value of fracture surface energy in J/m^2) at -32°C,

but this peak declined to previous levels at yet lower temperatures (-58°C). No visible effect of particle shape etc. was observed. When gamma-irradiated to about 4.0 x 10^6 R/g, glass (Ford Motor Company single-strength glass for auto windows) showed no marked change in fracture surface energy [PIRET-1957]. These were practical empirical tests, and there was little attempt at theoretical explanation.

A calorimetric technique (see above) was adapted to the slow-compression crushing of single particles of glass in order to make a detailed determination of the energy-dissipation paths. A hydraulic press provided a controlled-energy source. As reported above for single-particle slow-compressive crushing of quartz, there is a wide scatter, both of (1) the stored elastic energy per gram of glass at time of fracture (0.030 J/g to 9.8 J/g), and (2) the surface fracture energy (6.1 J/m^2 to 65 J/m^2) associated with the new surface area of glass formed. As described in more detail below, the principal results were that solid Pyrex glass specimens of different sizes and shapes showed different fracture behaviors [PIRET-1961].

Pyrex glass was fabricated into specimens of three types: small cylinders (0.365-in. dia. by 0.355 in. high); large cylinders (0.50 in. by 0.50 in.); and spheres (0.05-in. dia.). The specimens were uniform in size and shape, smooth, and had been annealed 3 h at 560°C. A gas adsorption measurement was used. Calorimetric measurements and analysis of the energy feed-in from the hydraulic press were used to confirm the effect of size and shape on the results of crushing, which can be summarized statistically as follows: (1) there is a 90% probability that fracture at low energy density (J/g) yields more new surface per unit of stored elastic energy (i.e., low J/m^2); (2) for cylinders crushed on the round, there is a 95% probability of a lower fracture surface energy (J/m^2) when fracture occurs at low energy density (J/g); (3) effects of energy density similar to the above were shown for quartz particles (previously reported) but not for glass spheres or for glass cylinders crushed on the flat (as in this study). The principal quantitative results are summarized in Table 53.

As shown in Table 53, for a given energy absorbed, more fracture results when cylinders have force applied to their rounded side than to their flat end; also, in such cases, the larger cylinders are less energy efficient than are smaller cylinders [PIRET-1961]. It is notable that slow compression allows fracture to take place at much lower levels of stored elastic energy than when energy input is by impact.

Impact fracture of solid-glass specimens was measured calorimetrically [PIRET-1962] in order to verify the energy dissipation in comparison with slow crushing. A previous calorimetric impact (ball-milling) study [SCHELLINGER] did not correct for partitioning of energy between metal and glass. Borosilicate glass cylinders (1.27-cm dia. by 1.27 cm high) and spheres 1.27-cm dia.) were made to precise dimensions and were fully annealed (verified by an absence of internal strain as determined by polarized light). Natural quartz crystals were cut and polished to rectangular prisms (parallelopipeds, 0.7 x 0.8 x 1.1 cm) [PIRET-1962]; they were not annealed. Two quartz prisms were aligned and crushed together in a test.

Table 53. Fracture Surface Energy of Slow-Compression Crushing of Small Pyrex Glass Cylinders and Spheres [PIRET-1961]

Specimen	Side of Applied Force	Average Fracture Surface Energy,[a] J/m^2	Range of Stored Elastic Energy at Fracture, J/g
Cyl, Small[b]	Round[c]	9.6 (±25%)[d]	0.072 to 0.21
Cyl, Large[e]	Round	17 (±30%)	0.033 to 0.21
Cyl, Small	Flat[f]	36 (±30%)	2.5 to 9.8
Cyl, Large	Flat	36 (±25%)	3.4 to 4.8
Sphere[g]	-	44 (±27%)	0.15 to 0.31

[a]For a given amount of energy, the new fracture surface area is inversely related to the fracture surface energy.

[b]Dia., 0.927 cm; Ht, 0.902 cm.

[c]Force applied on round side.

[d]Error band at 95% confidence level.

[e]Dia, 1.27 cm; Ht, 1.27 cm.

[f]Force applied on flat side.

[g]1.27-cm dia.

These specimens were fractured within a small calorimeter by impacting with a dual pendulum device. The energy input and the heat produced were calculated from hammer height and weight and from temperature measurements. The relatively small amount of heat generated in the metallic device was estimated in obtaining the net energy input to the specimens. Most of the energy input to the specimens was dissipated to heat; the surface energy for brittle fracture was shown by these measurements to be certainly less than 5.0 J/m^2, and the best estimate of the actual nonequilibrium (minimum) surface energy was believed to be very near the theoretical surface free energy about 1.0 J/m^2.

A 24-fold range of energy density (up to 16 J/cm^3) was used in these experiments [PIRET-1962], and it was found that up to 50% of the impact-energy input was dissipated by plastic deformation of the hardened steel crusher surfaces (the balance went to the specimens). At all conditions measured, the net fracture surface energy to the specimens was nearly constant at 77.0 J/m^2 for the new surface formed. The uniformity of this result is attributed to the uniformity of the specimens and the reproducibility of the impact conditions. Similarly to slow-compression crushing (reported above), when cylinders are impacted on their flat surfaces rather than on their round side [PIRET-1962], the stored elastic energy at the point of fracture is higher.

The above engineering studies were principally made under the direction of Edgar J. Piret and were discontinued 17 years ago. The studies establish a useful energy analysis, identify the controlling features of brittle fracture, and demonstrate effective experimental techniques. Apparently, work of this sort has not been continued. This work was not cited in previous studies of waste-form impacts.

2. Mechanics of Ceramics: A Current Summary

Academic research on fracture mechanics of ceramics has grown out of practical concerns with establishing controls on structural material to minimize structural failure, which is principally by rupture, i.e., fracture under load. Because practical problems tend to have particular solutions, the knowledge in this field was marked by specialized applications without a common vocabulary, let alone a systematic theory. Only since about 1966 has a major effort been made to overcome the systematic difficulties and make the mechanics of materials sufficiently interdisciplinary to meet the challenges of dealing effectively with brittle materials and metals. This new study of strength of materials includes macro and micro process mechanisms, properties and testing thereof (including QA), and theoretical analysis of structures under stress, including dynamic systems [PEARS].

Although most practical emphasis is on metals and on methods of preventing brittle fracture of metals, recently, attention has also been paid to fracture mechanics of ceramics [BRADT].

Fracture mechanics is focused on the processes of the formation and extension of cracks, i.e., mechanisms of fracture involving the microstructure of materials under stresses. The properties of materials and energy transformations are principal concerns [LANGE].

In the past, misinterpretation of test data on ceramics has contributed to confusion of the concepts needed for understanding the behavior of materials. Because conventional test procedures are so well established, it is important to use them as a basis for the study of ceramics. In a review of methods and concepts for testing the strength of ceramics, the main difficulties (in comparison to the testing of ductile metals) are identified as the critical parasitic stresses that can develop in rigid brittle bodies as a result of undetected localized imperfections (e.g., a lack of geometric uniformity of the presence of microcracks) in either the test specimen or the test apparatus. Such parasitic stresses make behavior less predictable [MARSCHALL].

When a damage-free glass fiber is subjected to tension, maximum stresses of the order of 3×10^9 Pa (about 400,00 psi) can be measured. Such high stresses, of course, represent very high energy densities (about 10^6 J/cm^3). When fracture occurs, the glass does not break into two pieces as in ordinary tensile tests, but explosively shatters into a cloud of dust. High-speed cine-microscopic photography was used to observe the tensile fragmentation of 30μm-dia fibers of alumino-borosilicate glass. The fragments mostly

were of the order of 1.0 μm and were not measured in this work, which was focused on the velocity of the elastic waves in the fragmentation. The velocity of the fragmentation waves was about 180 m/s and depended on the stress. This work, only a small effort, was done at the University of Tokyo [HYODO].

A review has been reported of the effects of microstructure on the strength of ceramics in terms of the key variables of fracture mechanics: the critical flaw size, the surface energy, and the stress intensity. (The use of energy relationships is essentially the same as our macro model [STEINDLER-1979B], but attention is here focused on the microstructure and on crack propagation.) Material properties and environments are considered for single crystals, simple polycrystals, multiphase materials, and ceramic-based composites. The scope is limited to ambient temperature and pressure and to simple bend tests, which tests are equivalent to uniaxial tension tests. Time-dependent effects and statistical variations of strength are not included in this particular review paper [DAVIDGE]. The discussion of grain and pore size in relation to strength and surface energy is relevant to our work.

In fracture tests made on MgO, it was shown that the mode of fracture shifts from transgranular to intergranular with increasing grain size of MgO; the indifference (50%) point is at about 30 μm.

Glass always shows higher strength in dry air than in moist air. Under extreme conditions, such as in vacuum or liquid nitrogen, its strength is high and the dependence of strength on the time rate of loading tends to disappear. A study of glass that was coated with acrylic, epoxy, and silicone polymers showed that the coating limited the availability of water to the glass surface and hence the short-term strength of abraded glass was increased. However, the coatings did not affect the stress corrosion susceptibility of abraded and acid-polished soda-lime glass. As part of this study, a mathematical analysis was made of the two-point bend test of strength. [RITTER]

One concept that has been confusing in earlier work on brittle fracture is the failure to distinguish properly between the reversible thermodynamic surface free energy and the nonreversible catastrophic fracture, which requires an energy expenditure in excess of the surface free energy of the new crack surfaces--even in the absence of other mechanisms of energy dissipation, such as plastic flow at the crack tip. This nonreversible energy is termed the apparent surface energy, γ_F (we have called it the fracture surface energy). The "excess" of fracture surface energy goes into acoustic and vibrational energy and heat. In this analysis, two critical stress levels for a brittle material having a microcrack correspond to the reversible and nonreversible surface energies. (For impacts, the higher nonreversible stress is most important) [HASSELMAN].

Porous ceramics are relatively weak, but they can be infiltrated with metals to increase their strength. Tests with graphite showed increased fracture resistance upon infiltration with aluminum alloys. The increased strength is believed to be a result of several effects: (1) amelioration of high local stresses near voids when the voids are filled; (2) the filled pores

may be reinforcements; (3) the ductility of the metal may allow strain energy to be absorbed in crack propagation; and (4) chemical reaction at the interface may enhance bonding of the phases. This work is preliminary. [QUEENEY]

III. TRANSPORT PROPERTIES OF NUCLEAR WASTE IN GEOLOGIC MEDIA

(M. G. Seitz, R. A. Couture, P. Rickert,*
A. M. Friedman,* Jacqueline Williams,† and
M. J. Steindler)

A. Introduction

A large number of experiments of various types have been performed to quantify the migration of radionuclides present in nuclear waste by groundwater flow and their immobilization by reaction with rock. The experiments are geared to evaluating the safety of geologic repositories for the disposal of nuclear wastes. Unfortunately, many of the simpler types of experiments are abstractly related to nuclide migration in groundwater, and results from these experiments may not be appropriate for safety evaluations. An experimental approach, termed leach-migration, described in a quarterly report in this series [STEINDLER-1979A], was developed to simulate repository and geologic conditions more accurately than experimental designs previously used.

The migration of cesium in limestone observed in leach-migration experiments was found to differ from migration of cesium in limestone observed in conventional infiltration experiments [STEINDLER-1979B]. Partitioning values for cesium on limestone that are related to migration cannot help resolve this discrepancy since partitioning values measured in batch experiments in six different laboratories varied by more than two orders of magnitude [RELYEA].

During in this quarter, we resolved these discrepancies by demonstrating that cesium concentration affects the results obtained from the various types of experiments.

B. Concentration Dependence of Trace-Element Migration--A Theoretical Treatment

The concept of the partition coefficient, K_d, to express the distribution of a solute between a solution and a solid phase is widely used to predict the migration velocity of a radionuclide through rocks, sediments, and soils. Here, the adsorption behavior expected at very low trace-element concentrations will be examined. Nonlinear behavior will be shown to be a feature expected for many water-rock systems, showing that the concept of a single K_d value is inappropriate to represent adsorption which might not be linear with trace-element concentration.

We have developed general concepts that may be applicable to cesium in oolitic limestone and which also allow us to identify other systems in which there may be nonlinear concentration dependence of trace-element adsorption at very low concentrations of the trace elements.

---

*Members of the Chemistry Division.

†Member of the Analytical Group of the Chemical Engineering Division.

The partition coefficients express the amount of solute partitioned onto a solid phase per unit of substrate and per unit of concentration of the solute in solution. For ion-exchange, there is a region at low trace-element concentrations in which the partition coefficient is constant. Under certain conditions, provided the solute concentration lies within this region of constant partition coefficient, the mean velocity of a solute through a rock or mineral column relative to the velocity of solvent can be predicted approximately by knowing the partition coefficient, the porosity of the column, and the densities of the solution and the solid. A principle is that the relative velocity is equal to the fraction of the solute in solution (which is constant in this region of constant partition coefficent). Essential conditions are that the reaction velocity is fast compared to the residence time in the column and that the streaming potential is not large (or that uncharged species are being considered). Fulfillment of the last condition is favored by high ionic strength, low surface charge of the particles, and high porosity.

Of several possible reasons for failure of such a prediction of migration velocity, this discussion is concerned with nonconstant partition coefficients. In addition to the trivial case in which K_d is not constant because the solute has precipitated (for example, as PuO_2), K_d can vary with solute concentration if the solute populates a large fraction of the ion exchange or adsorption sites.

1. Exchange of Species With Like Charges

An example of simple ion exchange illustrates the basic principle. Consider Cs^+ - Na^+ exchange on a substrate whose exchange positions are denoted by "X".

$[CsX]$, $[NaX]$ = concentrations on the substrate.

$[Cs^+]$, $[Na^+]$ = concentrations in solution.

λ_{CsX}, λ_{NaX} = activity coefficients on the substrate.

γ_{Cs^+}, γ_{Na^+} = activity coefficients in the liquid.

K = equilibrium constant.

According to the mass action law, the equilibrium constant is expressed by

$$K = \frac{\lambda_{CsX}\,[CsX]}{\lambda_{NaX}\,[NaX]} \quad \frac{\gamma_{Na^+}\,[Na^+]}{\gamma_{Cs^+}\,[Cs^+]} \qquad (1)$$

By rewriting Eq. 1, the partition coefficient for cesium can be expressed by

$$K_d = \frac{[CsX]}{[Cs^+]}$$

$$= K \frac{\lambda_{NaX} \; [NaX] \; \gamma_{Cs^+}}{\lambda_{CsX} \; [Na^+] \; \gamma_{Na^+}} \qquad (2)$$

Cesium is a rare element, and so in most natural systems the ratio of cesium to sodium is small. Thus [CsX] << [NaX], and most of the exchange sites will be occupied by sodium. Thus, [NaX] is nearly constant (and equal to the ion-exchange capacity), and λ_{NaX} and λ_{CsX} are constant. (The standard state is usually defined so that $\lambda_{NaX} = 1$, but this is not essential.) At a given ionic strength, $\gamma_{Cs^+}/\gamma_{Na^+}$ is constant and generally near unity. By combining all of the constants in Eq. 2 in a new conotant, K', Eq. 2 can be written as

$$K_d = \frac{[CsX]}{[Cs^+]} \approx K'/[Na^+] \qquad (3)$$

Thus, in this simple system, the distribution of cesium between solid and liquid depends on $[Na^+]$ but not on $[Cs^+]$.

2. Saturation of Exchange Sites

a. Equivalence of Adsorption Treatment and Ion-Exchange Treatment

Saturation of exchange sites leads to a breakdown of linearity of the isotherms. Adsorption is sometimes treated analytically by means of the Langmuir isotherm, which allows for saturation of the adsorption sites. It can be shown easily (but will not be derived here) that treatment with the Langmuir isotherm is exactly equivalent to an ion-exchange treatment in which ideal solid solution is assumed and the dissolved concentration of one ion is held constant. The Langmuir isotherm can be expressed by

$$[MX] = \frac{[MX]_\infty \; [M]}{K + [M]}$$

where [MX] is the amount of solute sorbed or exchanged, $[MX]_\infty$ is the capacity, K is a constant, and [M] is the solution concentration. The isotherm looks like this:

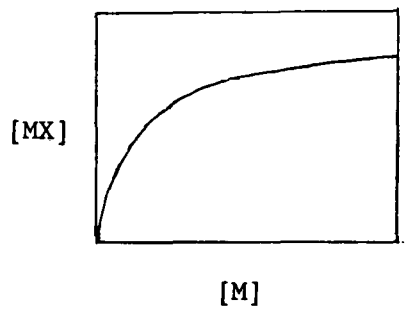

b. Cs^+-Na^+ Ion Exchange in Natural Systems

Some sample calculations are useful in assessing the likelihood of saturating clay surfaces with cesium from radioactive waste. Various values of the constant for cesium-sodium exchange calculated from data in the literature are shown below. The data are valid for trace concentrations of cesium.

Mineral	K/λ_{CsX}	Source
Kaolinite	1000	[COUTURE-1978]
Montmorillonite	130	[MEYER]
Palygorskite	1700	[BEALL]
Palygorskite	2500	[MERRIAM]

An additional estimate, based on the compositions of average shale and sea water, is 16,000. We will assume a conservative value of 130 in our sample calculations. $NaHCO_3$-dominated groundwaters from siliceous igneous rocks have sodium concentrations in the range, $5 \times 10^{-4}\underline{M}$ to $2.6 \times 10^{-3}\underline{M}$ [WHITE]. For the typical sodium concentration of $10^{-3}\underline{M}$ and for the cesium concentrations given below, the cesium to sodium ratios on the substrate are calculated.

For $$[Cs^+] = 10^{-6}\underline{M}, \quad \frac{[CsX]}{[NaX]} \approx 0.13$$

and for $$[Cs^+] = 10^{-5}\underline{M}, \quad \frac{[CsX]}{[NaX]} \approx 1.3.$$

Thus, in dilute groundwater solutions with $K/\lambda_{CsX} \geq 130$, cesium at concentrations of 10^{-5}M or lower (possibly much lower) could fill a large fraction of the exchange sites and the isotherm would be nonlinear.

c. Cs^+ - Ca^{2+} Exchange in Natural Systems

Because most groundwaters are dilute, and because Ca^{2+} is usually the most common dissolved cation in groundwater [WHITE], Ca^{2+} is usually the most abundant exchangeable ion. We have estimated the amount of exchangeable cesium in Ca-montmorillonite. Assuming a typical groundwater Ca^{2+} concentration of 2.5×10^{-4}M [WHITE] and using data on Cs-Ca exchange on montmorillonite from [MEYER], roughly 30% of the exchange sites would be occupied by Cs^+ at a Cs^+ concentration of 10^{-6}M, and so substantial nonlinear behavior would exist.

d. Nonequivalent Ion-Exchange Sites

Any rock may have two or more nonequivalent ion-exchange sites. The most obvious example is a multi-mineralic-rock in which each mineral is selective for a different solute. In fact, pure minerals and synthetic compounds are known to have nonequivalent bonding sites [GARRELS, KRAUS, SCHROEDER, LIESER]. The implication is that a trace element might saturate its bonding sites at concentrations far below the determined ion-exchange capacity.

e. Discussion of the Adsorption Isotherm in Relation to Waste Migration Studies

If the sorption isotherm for a trace element is nonlinear, calculation of migration rate from fluid flow is complicated since the migration rate depends on the concentration of the element. Past experimental and theoretical work in nuclear waste management to predict the migration of elements in radioactive waste has not taken this effect into account (see [SEITZ-1979A] for review of models). There are many substantial disagreements for adsorption parameters (spec. partition coefficients) measured in different laboratories [RELYEA] which are due in part to a lack of recognition of nonlinear isotherms. Even where there is agreement of measured adsorption parameters, the agreement may be fortuitous and the measured values may lead to erroneous predictions.

The theories presented here suggest that substantially more rigor is feasible in waste migration studies. The important point is that it is necessary to determine the entire isotherm on a case-by-case basis.

Examples of nonlinear isotherms are not hard to find. [GILLHAM] presented evidence that the rate of elution of radioactive cesium in soils depends on the amount of cesium naturally present. [SEITZ-1978B] presented a curve for elution of strontium from limestone that clearly represents nonlinear behavior. Nonlinear behavior of cesium in limestone is indicated elsewhere in this report. [SEITZ-1979C and COUTURE-1979] presented an isotherm

for sorption of iodate by Fe_2O_3 in which saturation was found at about 1.4×10^{-5} mol/g. In pure minerals, nonlinear isotherms are seen for cesium and strontium at concentrations of the trace elements that are of interest in nuclear-waste disposal safety evaluations [WAHLBERG-1962, 1965]. [SHIAO] gives evidence for nonlinear isotherms, but concludes, contrary to what is stated in this report, that differences between finite concentrations and true "trace" conditions for a trace element are not of concern in radionuclide adsorption on clays.

Leaching of neutron-irradiated simulated radioactive waste glass can give dissolved cesium concentrations as high as 3×10^{-7}M and possibly higher (as evidenced by neutron activation analyses). This is a concentration in which, it was deduced earlier, nonlinear behavior is expected. An earlier quarterly report in this series [STEINDLER-1979B] has documented a discrepancy between the behavior in limestone columns of (1) cesium leached from glass at high temperature and (2) cesium added from prepared solutions. This discrepancy is thought to be due to nonlinearity.

C. Concentration Dependence of Cesium Adsorption on Limestone

To establish the adsorption dependence on cesium concentration, batch partitioning experiments with cesium on limestone were performed with synthetic groundwater solutions containing seven different concentrations of cesium. The batch partitioning experiments were done using materials and procedures described in the Waste Isolation Safety Assessment Program (WISAP) Controlled Sample Program [RELYEA] for cesium adsorption on limestone.

The synthetic groundwater solution had a nominal composition of 92.5 mg $Ca(OH)_2$, 18 mg $MgSO_4$, 5.8 mg NaCl, and 0.8 mg KCl per liter of distilled water, as prescribed in the procedures. The solution was filtered through a 0.4-μm-pore membrane filter. The seven concentrations of cesium ranged from about 2×10^{-9} to 1×10^{-3}M. (Solutions were prepared containing radioactive ^{137}Cs or both radioactive ^{137}Cs and stable cesium).

The 20 to 50 mesh size aggregate of oolitic limestone supplied for the controlled-sample program was wet-sieved on a 60-mesh screen and dried prior to use in the batch experiments. Characteristics of this material are described by [AMES].

In each batch experiment, about 3.0 g of oolitic limestone was placed in a 15-mL polystyrene centrifuge tube and was washed three times with synthetic groundwater solution. Each wash was done with 10 mL of solution in the capped centrifuge tube. The tube was rotated end over end six times per minute for 24 h, after which the limestone was allowed to settle, and the wash solution was decanted. The centrifuge tubes containing limestone aggregate were each weighed before and after washing to determine the weight of residual wash solution remaining with the limestone (as prescribed in the Controlled Sample Procedure).

Triplicate batch-adsorption experiments were done with each of seven solutions having different cesium concentrations (Table 54) and containing radioactive ^{137}Cs. The cesium concentration of the synthetic groundwater solution before the addition of cesium was found by atomic absorption analysis to be below about 1.5×10^{-7} M.

Table 54. Cesium Concentrations and Activities of Solutions Used in the Batch-Adsorption Experiments

Solution	Concentration of Added Cesium,[a] M	Activity[b] from ^{137}Cs, c/s-mL
S-7	1.62×10^{-9}	131.1
S-6	1.20×10^{-8}	129.2
S-5	1.05×10^{-7}	131.1
S-4	1.05×10^{-6}	130.6
S-3	1.04×10^{-6}	131.5
S-2	1.05×10^{-4}	131.3
S-1	1.15×10^{-3}	128.7

[a]Stable cesium was added to the synthetic groundwater solutions as dissolved $CsNO_3$. The only cesium added to solution S-7 was carrier-free ^{137}Cs. Before the addition of cesium to the synthetic groundwater solution it was found, by atomic absorption analysis, to contain less than 1.5×10^{-7} M cesium.

[b]The efficiency for the counting geometry employed (5 mL of solution in a test tube placed in a NaI well crystal) was determined to be 0.18 for the 0.662-MeV gamma ray from ^{137}Cs decay.

Blank tests to evaluate cesium adsorption on the test tube wall were performed by placing solutions having the seven cesium concentrations (Table 54) in centrifuge tubes not containing limestone. This blank test was in accord with the batch-test procedures of the controlled-sample program. However, it is emphasized here that typically, absorption on test tube walls observed in the blank tests differs from the adsorption observed on test tube walls in the presence of rock material. These test tubes were rotated end over end six times a minute for three days. The seven tubes were centrifuged and the solutions filtered through a 0.4-μm-pore membrane filter and counted for cesium activity. The solutions in the blank tests were filtered and counted after the fourth day of rotation. The remaining tubes containing both cesium solution and limestone were agitated periodically (about twice daily) and centrifuged after seven or eight days of contact of the radioactive solutions with the limestone.

Results of the batch tests, listed in Table 55, show that cesium adsorption by limestone depends very strongly on the cesium concentration of the solution.

Table 55. Activities of Solutions and Partition Coefficients in Batch Experiments for Cesium Adsorption on Oolitic Limestone

Batch Experiment Number[a]	Initial Cesium Concentration in Solution, M	Volume of ^{137}Cs Bearing Solution,[b] mL	Volume of Residual Wash Solution, mL	Activity of Solution After Contact,[c] c/s-mL	Partition Coefficient,[d] mL/g
First Series (Contact for 3 days)					
1	1.6×10^{-9}[e]	9.93	1.14	2.43	170.
2	1.2×10^{-8}	9.95	1.22	5.58	74.
3	1.0×10^{-7}	9.94	1.18	38.3	7.6
4	1.0×10^{-6}	9.93	1.12	85.0	1.4
5	1.0×10^{-5}	9.97	1.21	100.0	0.6
6	1.0×10^{-4}	10.00	1.22	106.8	0.3
7	1.0×10^{-3}	9.94	1.18	113.5	0.1
Second Series (Contact for 7 days)					
8	1.6×10^{-9}[e]	9.65	1.19	1.53	265.
9	1.2×10^{-8}	9.98	1.12	3.82	104.
10	1.0×10^{-7}	9.92	1.18	33.0	9.4
11	1.0×10^{-6}	9.93	1.20	76.9	1.9
12	1.0×10^{-5}	9.90	1.17	99.8	0.6
13	1.0×10^{-4}	9.94	1.21	108.4	0.2
14	1.0×10^{-3}	9.92	1.28	112.9	0.1
Third Series (Contact for 8 days)					
15	1.6×10^{-9}[e]	9.92	1.15	1.55	268.
16	1.2×10^{-8}	9.91	1.21	3.55	119.
17	1.0×10^{-7}	9.94	1.18	35.50	8.5
18	1.0×10^{-6}	9.96	1.16	76.66	1.9
19	1.0×10^{-5}	9.99	1.17	100.8	0.6
20	1.0×10^{-4}	9.99	1.17	109.9	0.2
21	1.0×10^{-3}	9.94	1.22	123.7	0.0

(contd)

Table 55. (contd)

Batch Experiment Number[a]	Initial Cesium Concentration in Solution, M	Volume of ^{137}Cs Bearing Solution,[b] mL	Volume of Residual Wash Solution, mL	Activity of Solution After Contact,[c] c/s-mL	Partition Coefficient,[d] mL/g
Fourth Series (Blank Tests)					
22(s-7)	1.6×10^{-9}[e]	9.90	0.0	115.6	-
23(s-6)	1.2×10^{-8}	9.94	0.0	121.3	-
24(s-5)	1.0×10^{-7}	10.01	0.0	122.2	-
25(s-4)	1.0×10^{-6}	9.96	0.0	124.2	-
26(s-3)	1.0×10^{-5}	9.95	0.0	127.0	-
27(s-2)	1.0×10^{-4}	10.01	0.0	130.1	-
28(s-1)	1.0×10^{-3}	9.95	0.0	127.1	-

[a]Experiments No. 1 to 21 were each performed with about 3 g of 20-50 mesh oolitic limestone (the actual amount varied from 2.99 to 3.03 g). Experiments No. 22 to 27 were blank tests performed with no limestone. The solution numbers (Table 54) are in parentheses.

[b]The cesium-bearing solutions used are those listed in Table 54.

[c]Solutions were filtered through 0.4-μm-pore membrane filters before being counted.

[d]The partition coefficients were calculated assuming that no activity had been adsorbed by the centrifuge tube walls. This was verified, in some instances, by rinsing the tubes and counting for residual activity.

[e]The limestone in this experiment was prewashed with solution containing no cesium. After the batch test, the concentration of cesium in solution may have been different from 1.6×10^{-9}M. Cesium indigenous to the limestone could raise the cesium level to about 3×10^{-9}M (as estimated from the amount of cesium that can be leached for limestone with distilled water).

Partition coefficients, defined as the amount of activity on the rock (per gram of rock) divided by the amount of activity in solution (per milliliter of solution), were calculated for each batch test and are given in Table 55. Cesium is extensively adsorbed from solutions of low cesium concentrations (lower than about 10^{-7}M concentration), as indicated by the high values of the partition coefficients measured at low concentrations. Because the rock was prewashed with cesium-bearing solutions, the final cesium concentrations of the solutions are very nearly equal to the initial cesium concentrations (as evidenced by cesium analyses of the third wash solutions being equal to

their initial cesium levels). Little cesium is adsorbed from solutions containing about 10^{-5}M cesium or higher, as evidenced by the correspondingly low values of the partition coefficients. Nowhere in the range of cesium concentrations investigated does the partition coefficient appear to be independent of the cesium concentration.

As seen in Table 55, partition coefficients for solutions having 1.6×10^{-9} and 1.2×10^{-8}M added cesium differ. This suggests that before cesium addition, the cesium concentration in the synthetic groundwater solution must have been considerably below 1×10^{-8}M.

The partition coefficients measured after seven days of contact are plotted in Fig. 36 against the cesium concentrations in the radioactive solutions.

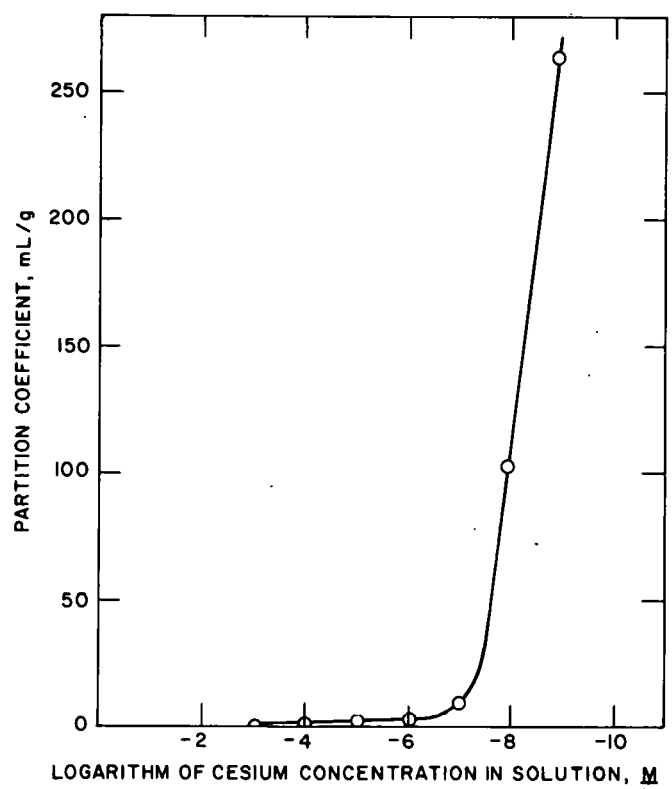

Fig. 36. The Partition Coefficient for Cesium on Limestone is Dependent on Cesium Concentrations as low as about 10^{-9}M.

D. Cesium Concentration as a Controlled Variable in Infiltration Experiments

Four infiltration experiments (148-49, 148-61, 157-14, and 148-66) were performed to measure the migration of cesium in limestone at different concentrations of cesium in solution. A limestone column, 1 cm in diameter and 3.8 cm long, mounted with epoxy in stainless steel tubing, was used in experiments. The column preparation and experimental techniques were comparable to those used in infiltration experiments with limestone reported previously [STEINDLER-1979B, SEITZ-1979D].

The oolitic limestone-groundwater solution used in the experiments was prepared by stirring water with powdered limestone for about 30 days and filtering the resulting solution (solutions prepared in this manner are unsaturated with respect to $CaCO_3$). Cesium concentrations were varied from $<10^{-8}$M* to about 1.4×10^{-3}M. The higher concentrations of cesium were obtained by adding $CsNO_3$ to the oolitic groundwater solutions. Each experiment was performed by injecting a small quantity (20 μL) of solution containing ^{134}Cs in the solution stream above the limestone column and monitoring the activity in the solution exiting from the column. The experiments were run sequentially, using the same limestone column and solutions of increasingly higher concentrations.

In experiments with the higher cesium concentrations, appearance in the new eluate of cesium activity (bound on the column) from the preceding experiment had to be prevented. Therefore, prior to each experiment, the column was washed with the inactive solution to be used in the experiment until the cesium activity of the wash solution was comparable to or below the counting background. Most of the released activity appeared in the initial 10 mL of eluate, but some appeared in subsequent eluate so that several hundred milliliters of solution was required for a wash. The groundwater solution was pumped through the column at a nominal rate of 0.1 mL/min (actual flow rate of about 0.07 mL/min, corresponding to a linear flow rate of 0.5 cm/min or about 2 km/y).

Conditions and results of the experiments are given in Table 56. Experiment 148-49 is similar to experiment 128-56 reported previously [STEINDLER-1979B].

The most striking change associated with a higher cesium concentration in solution is the greater amount of radioactive cesium eluted in a given volume of eluate. This change is evident in column 4 of Table 56, which gives the activity in the first 10 mL of eluate. The change is also illustrated graphically in Fig. 37, in which the cumulative amounts of activity for three experiments (Expts. 148-49, 148-61, and 148-66) using solutions having different cesium concentrations are plotted against the eluate volume. Results similar to those given in the figure were obtained from other experiments run under similar conditions.

---

*Estimated concentration in the oolitic groundwater solution. No cesium was detected by atomic absorption or neutron activation techniques.

Table 56. Conditions and Results of Experiments Used to Measure the Behavior of Cesium in a Limestone Column at Several Concentrations of Dissolved Cesium

Expt. No.	Cesium Concentration in Solution, M	Size of Each Fraction, mL	Activity of Cesium Recovered in the First 10 mL of Eluate, c/s[a]
148-49	3.6 x 10-8[b]	7.4	16
148-61	1.42 x 10-4	1.3	46
157-14	1.82 x 10-4	7.4	49
148-66	1.44 x 10-3	1.3	58

[a]Cesium recovered in the first 10 mL of solution was measured from the 605-keV gamma radiation present in 98% of cesium-134 decay and is a fraction of the 94.6 c/s introduced in each experiment. The activities either were counted on 1.3-mL samples or were activities of larger samples adjusted to reflect the counting of 1.3-mL samples.

[b]The cesium concentration was determined by neutron-activation analysis.

Figure 37 contains activities for only two solution fractions (out of a total of 56 fractions) from experiment 148-49. Also plotted in Fig. 37 is a region that is estimated to encompass the migration behavior of leachate containing 8 x 10^{-7}M cesium. This concentration of cesium was determined to enter the groundwater solution in leach-migration experiments during the leaching process. (The glass used in the experiments contained 1.03% CsO and had a ^{134}Cs activity of 1.38 x 10^{6} d/s·g of glass. The activity of the leachate was about 14 d/s·mL, giving a concentration of cesium in the leachrate of 0.10 μg/mL solution or 7.6 x 10^{-7}M cesium from the leached glass.)

E. Discussion of Concentration Dependence of Cesium Adsorption by Limestone

The results of static adsorption experiments and column-infiltration experiments clearly demonstrate the dependence of cesium adsorption and cesium migration on the cesium concentration in the groundwater solution. The very strong dependence of measured partitioning values on cesium concentration in the range from 10^{-6} to 10^{-10}M cesium (listed in Table 55 and illustrated in Fig. 36) can clearly account for some previously unexplained phenomena in our program, as well as unanticipated results in the larger WISAP task 4 program.

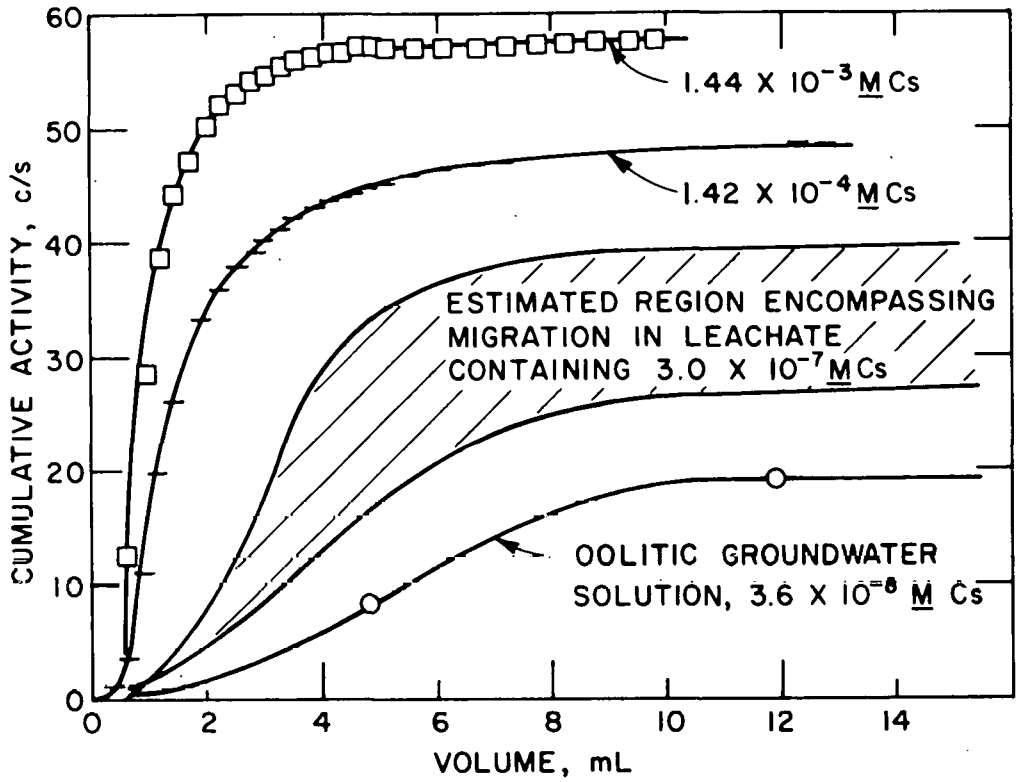

Fig. 37. Cumulative Activity of Cesium Eluted Through Limestone in Groundwater Solutions Containing Various Amounts of Cesium. The total activity applied in each experiment (and, therefore, for each curve) was 95 c/s.

The concentration dependence of adsorption is probably the origin of differences in cesium behavior seen in leach-migration and conventional infiltration experiments. In conventional infiltration experiments, small quantities of cesium (2.0×10^{-4} μg or about 1.5×10^{-12} mol cesium) are introduced into solution streams that are essentially devoid of cesium (cesium concentration was determined to be less than 4×10^{-7}M by neutron activation analyses). If cesium to calcium abundance ratios in BHVO-1 standard basalt are used [FLANAGAN] and if it is assumed that cesium and calcium are leached proportionately, we estimate that about 1×10^{-2} ng/mL or 8×10^{-11}M cesium may be present in the limestone groundwater solution. Another value is about 10^{-8}M, calculated using average crustal abundances [TAYLOR-1964]. At the higher estimate, cesium from the limestone would determine the cesium concentration in solution, and the injected radiocesium concentration would be insignificant. Because this concentration is low, the radiocesium would be expected (based on the results of the static adsorption experiments) to be strongly adsorbed. This is the result seen experimentally in the infiltration experiments.

On the other hand, in leach-migration experiments, leaching of the glass introduces about 3×10^{-7}M cesium into the solution. At this concentration,

based on the results illustrated in Fig. 36, most of the cesium would be expected to be transmitted through the limestone. Experimentally, we have seen that all but 1 to 2% of the leached cesium is transmitted through limestone [STEINDLER-1979B].

We can understand the results for other laboratories in the light of the results reported here. For example, in the controlled-sample program of the Waste Isolation Safety Assessment Program, task 4, investigators in nine different laboratories reported partitioning values for cesium on limestone of 1.3 to about 800 [RELYEA]. The cesium concentrations in the solutions from which these measurements were made were not reported. However, the cesium concentrations in solutions used at the different laboratories are likely to have been different. The concentration of carrier-free ^{137}Cs tracer is 1.9×10^{-9}M in the experiments reported here. In any set of experiments, additional cesium as a carrier or as an impurity in chemicals used to make the synthetic groundwater solution could produce cesium concentrations higher than 2×10^{-9}M so that measured partitioning values would be in the range from 1 to about 270 mL/g. Although changes in other experimental parameters may have contributed to the measured partition coefficients, most of the range in the partition coefficients reported for cesium with limestone in the controlled-sample program could be accounted for by concentrations of cesium in the range 10^{-6} to 10^{-10}M alone (the lower concentration was obtained by extrapolating the curve in Fig. 36).

From the isotherm depicted in Fig. 36, we would except that most cesium leached in concentrations of about 10^{-7}M from a waste form would move with the leachate away from the repository. However, as the concentration of the leachate is lowered by some adsorption of cesium on the rock and by dilution of the leachate with groundwater, cesium adsorption would increase , and eventually, almost all of the cesium would be removed from the groundwater (i.e., the velocity of cesium relative to flowing water, given by the fraction of cesium in solution, would be very low). Low cesium concentrations in solution would allow stronger adsorption which, in turn, would lead to still lower cesium concentrations in solutions until cesium would be adsorbed almost completely into the solid rock phase. This condition would result in a very low net migration rate for cesium.

The data in Fig. 37 showing the dependence on initial cesium concentration of cesium migration obtained in infiltration experiments reveal a phenomenon not suggested by the batch experiment data. Although the cesium migration rate is greater at higher cesium concentrations (as suggested by the batch tests), a significant fraction of the cesium (40% in a 1.4×10^{-3}M cesium solution, more at lower cesium concentrations) is held up in the limestone column after passage of the main cesium peak. This effect may be due to cesium binding at sites in the bulk of the limestone material (rather than at the surface as measured in the batch tests) and appears to be very significant in retarding cesium in flowing groundwater.

F. Effect of pH of Groundwater Solution on Cesium Migration in Limestone

Differences in the pH (nominally the negative of the logarithm of the hydrogen ion concentration) of solutions used in leach-migration and conventional infiltration experiments were studied because differences in pH are postulated to alter the behavior of cesium.

1. pH of Solutions

Measurements of the pHs of solutions used in leach-migration experiments and conventional infiltration experiments are reported in Table 57.

Table 57. pHs of Solution Used in Leach-Migration and Conventional Infiltration Experiments with Cesium

	Experiments in Which Solutions Were Used	Hydrogen Ion Concentration, pH
Groundwater Solution Made With Oolitic Limestone	128-56 128-95 148-1 148-22	8.96
Leachate From Groundwater Solution Reacted with a Solid Waste Form	128-95 148-1	9.11
Cesium-Spiked Groundwater Solution	148-22	9.05
Concentrated Cesium Solution Made with Groundwater Solution	128-56	7.36

One solution, the concentrated ^{134}Cs solution, has a pH distinctly lower than those of the other solutions. The lower pH value is presumably due to hydrochloric acid in the stock $^{134}CsCl$ solution used to make the concentrated cesium solution. Although only 20 μL of low-pH solution was used, nearly all of the cesium was retained by the limestone in experiment 128-56. Therefore, the different behaviors of cesium might be due to differences in the pH of the solutions.

2. Infiltration Experiments with Cesium in Limestone

Infiltration experiments were performed to examine the possibility that the pH of solutions affects the adsorption of cesium from solutions. One experiment (Expt. 148-41) was performed using a solution with a reduced pH. The solution, which had a pH of 3.47, was prepared by adding 1 meq HCl (0.02 mL of 0.05M HCl) to 900 mL of the cesium-spiked groundwater solution used in Expt. 148-22. The resulting solution was sparged with nitrogen. Prior to experimentation, a limestone column was prepared by eluting it with a solution produced by the addition of 0.33 meq HCl/L to groundwater solution having a pH of 7.79. For the experiment, the cesium-bearing solution was pumped from a reservoir flask through the limestone column, and the eluate was collected in fractions and analyzed for cesium activity and pH. A plot of the cesium activity vs. the eluate volume is given in Fig. 38.

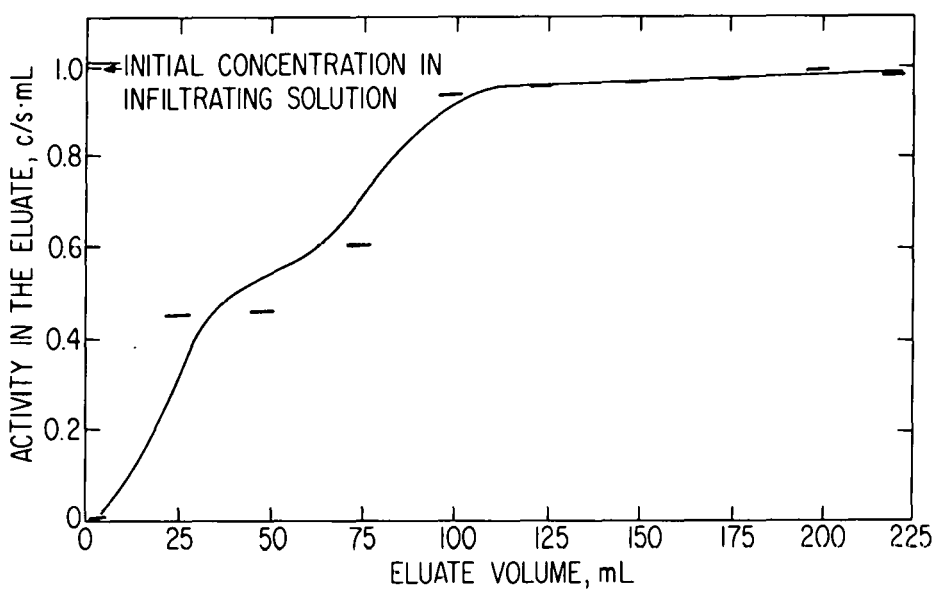

Fig. 38. Cesium Activity in the Eluate Versus Eluate Volume. The solution fed to the column had a pH of 3.5 and an activity of 0.98 c/s.mL. Experiment 148-41.

Cesium is depleted in the initial eluate but rises with increased volume of the eluate to the value in the initial cesium-bearing solution.

The eluate from the experiment had a pH of about 8.3 and contained a suspended red precipitate, presumably $Fe(OH)_3$. Both the elevated pH value and the precipitate were likely generated from reactions that occurred during the experiment.

A second experiment (Expt. 148-45) was performed using the same column after it had been washed with groundwater solution. The solution used in the second experiment was made by adding 0.3 meq HCl per liter of

cesium-spiked groundwater solution, which formed a solution having a pH of 7.79. The eluate was again collected in fractions and was analyzed for cesium activity. The cesium activity vs. the eluate volume is plotted in Fig. 39.

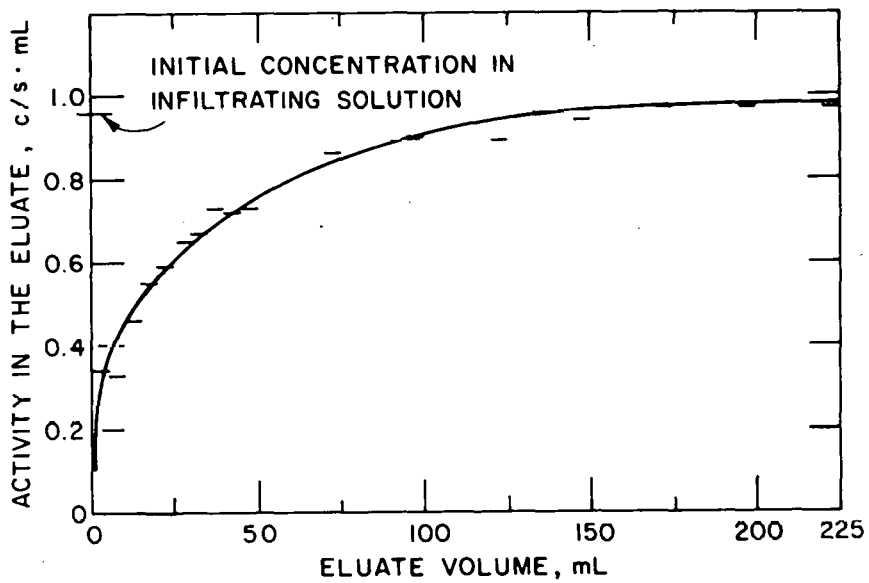

Fig. 39. Cesium Activity in the Eluate Versus Eluate Volume. The infiltrating solution had a pH of 7.79 and an initial cesium-134 activity of 0.96 c/s.mL. Experiment 148-45.

3. Discussion of Results Using Solutions of Different pH

The steady rise of cesium in the eluate to the level in the initial cesium-bearing solution, seen in the experiments reported here, is comparable to the behavior seen in other experiments (Expts. 128-95, 148-1, and 148-22, reported in [STEINDLER-1979B]) in which cesium was diluted in large volumes of solutions.

The pH of the solution used in experiment 148-41 was considerably below that used in any previous experiments; the results suggest that cesium behavior is not strongly dependent on the initial pH of the experimental solution (the pH value of the solution rose due to reactions that occurred during elution). It is very unlikely that differences in pH values of solutions contributed to the different behavior observed for cesium in leach migration and column-infiltration experiments.

Experiment 148-45 was run with a solution of high pH and a limestone column that had been exposed to the acid solution from experiment 148-41. This treatment might have sensitized the column and thus altered cesium behavior. However, the results are similar to those seen in previous experiments, and subjecting limestone to an acid solution has little effect on cesium migration.

4. Estimate of Cesium Loading on Limestone

a. Cesium Loading in Adsorption Experiments

From the data given in Tables 54 and 55, the amount of cesium adsorbed by the limestone can be estimated by assuming either (1) that the radioactive cesium exchanges with cesium already on the limestone or (2) that the radioactive cesium exchanges with another element such as sodium or hydrogen. The first assumption is valid for experiments preceded by washing of the limestone with solutions of high cesium concentration. The second assumption is valid for experiments preceded by washing of the limestone with solutions of low cesium concentration; this represents the maximum loading because only a limited mass of cesium was in the system prior to the adsorption step. To categorize a cesium concentration as high or low, we need to know the quantity of cesium adsorbed by the limestone. Therefore, mass loadings were calculated from the adsorption data (Table 55) for each assumption and are listed in Table 58.

During limestone washing with the two wash solutions having the lowest cesium concentrations, the amounts of cesium were insufficient to populate the exchange sites on the limestone; in subsequent contacting of the limestone with the radioactive solution, the radioactive cesium exchanged with sodium or other abundant cation on the limestone rather than with cesium from the wash solutions, as indicated by the mass loading calculated from assumption 2 (that all of the cesium from the wash solution was adsorbed) being lower than the mass loading calculated from assumption 1 (that the radioactive cesium exchanged with cesium already on the limestone). Therefore, in experiments using the two lowest cesium concentrations in solution, there may have been a net adsorption of cesium and a subsequent lowering of the cesium concentration of the solution--the final concentrations of cesium in solutions from experiments 1, 8, and 15 and from experiments 2, 9, and 16 were calculated to be 3.4×10^{-11} M and 2.2×10^{-9} M, respectively. No reduction of the cesium concentrations in the solutions in other experiments is postulated.

These calculations were substantiated, in part, by analyses of the cesium in the wash solutions, which showed all solutions to which cesium was added to have cesium concentrations equal to their cesium concentrations before contacting the limestone so that no reduction of the cesium concentrations in any experiments (except possibly experiments 1, 8, and 15) is expected. By considering cesium leached from the limestone, it is possible that, even in experiments 1, 8, and 15, the cesium concentrations of the solutions were not reduced significantly during the experiments.

Mass loadings obtained from the breakthrough curves of the infiltration experiments are consistent with those obtained with the granulated limestone (in batch experiments) in that the lowest mass loading was observed with the lowest cesium concentration. The amounts of stable cesium (1) in the chemicals used to prepare groundwater solutions, (2) available for exchange from limestone, and (3) in the solutions after contact with limestone are not known in sufficient detail to assess whether the mass loading of granulated limestone is higher than that of intact limestone (as can be postulated because of the presumed increased surface area of the granulated limestone).

Table 58. Calculated Mass Loadings of Cesium on Limestone, Using the Two Assumptions Described in the Text. The mass loadings calculated using assumption 2 are upper limits; therefore, the smaller of the two numbers calculated for an experiment is the more accurate estimate of mass loading.

Batch Experiment No.	Inital Cesium Concentration In Solution, M	Calculated Mass Loading, Mol/g	
		Assumption 1	Assumption 2
1		2.7×10^{-10}	5.3×10^{-12}
8	1.6×10^{-9}	4.3×10^{-10}	5.3×10^{-12}
15		4.3×10^{-10}	5.3×10^{-12}
2		8.9×10^{-10}	1.5×10^{-10}
9	1.2×10^{-8}	1.2×10^{-9}	1.5×10^{-10}
16		1.4×10^{-9}	1.5×10^{-10}
3		8.1×10^{-10}	9.3×10^{-10}
10	1.0×10^{-7}	9.9×10^{-10}	1.0×10^{-9}
17		9.0×10^{-10}	9.7×10^{-10}
4		1.5×10^{-9}	3.9×10^{-9}
11	1.0×10^{-6}	2.0×10^{-9}	4.8×10^{-9}
18		2.0×10^{-9}	4.8×10^{-9}
5		6.5×10^{-9}	2.0×10^{-8}
12	1.0×10^{-5}	6.7×10^{-9}	2.1×10^{-8}
19		6.2×10^{-9}	1.9×10^{-8}

(contd)

Table 58. (contd)

Batch Experiment No.	Inital Cesium Concentration In Solution, M	Calculated Mass Loading, Mol/g	
		Assumption 1	Assumption 2
6		3.1×10^{-8}	1.0×10^{-7}
13	1.0×10^{-4}	2.4×10^{-8}	8.2×10^{-8}
20		2.0×10^{-8}	7.0×10^{-8}
7		$0\text{-}1.4 \times 10^{-7}$[a]	$0\text{-}4.8 \times 10^{-7}$[a]
14	1.1×10^{-3}	$0\text{-}1.1 \times 10^{-7}$[a]	$0\text{-}4.2 \times 10^{-7}$[a]
21		0 - 0[a]	0 - 0[a]

[a]The lower value (e.g., 0) was calculated by subtracting the amount of cesium adsorbed on the test tubes (found in the blank tests) from the amount of cesium removed from the solution to give the amount of cesium adsorbed by the rock. The higher value (e.g., 1.4×10^{-7}) was calculated by assuming that there was no cesium adsorption by the test tube walls in these experiments.

G. Conclusions

For safety assessments of a nuclear-waste repository, it has been generally assumed that adsorption is proportional to trace-element concentration. The measurements here for cesium adsorption on limestone are believed to be the first documented record of nonlinear isotherms (adsorption not proportional to trace-element concentration) for trace-element adsorption on a rock at concentrations expected for radionuclides leached from a solid waste form. These studies show that linear behavior may not exist at concentrations below 10^{-6}M and possibly even below about 10^{-9}M. The reported results demonstrate that linear isothermal behavior (i.e., a constant K_D) cannot be assumed to exist at concentrations above about 10^{-9}M for nuclides on rocks. Because concentrations of elements with radionuclides greater than this exist in natural groundwaters or can be readily generated by leaching of solidifed nuclear waste, models of nuclide migration for repository safety evaluations need to consider the concentration dependence of radionuclide adsorption.

IV. TRACE-ELEMENT TRANSPORT IN LITHIC MATERIAL BY FLUID FLOW AT HIGH TEMPERATURE

(M. G. Seitz and R. A. Couture)

A. Introduction

In the preceding quarterly report [STEINDLER-1979B], the isotherm for adsorption of iodate by hematite (Fe_2O_3) was reported. The isotherm as a function of pH is reported here. This work, discussed in [STEINDLER-1979B], may have practical value in the disposal of iodine-129 from nuclear fuel reprocessing.

In [STEINDLER-1979B], the rates of transport of I^- and Na^+ through a kaolinite column at 25°C were reported. The experiments have now been repeated at 158°C and the same elution volumes were observed as at 25°C. This result is not further discussed in this report.

B. Adsorption of Iodate by Hematite (Fe_2O_3)

The pH dependence of iodate sorption by hematite was determined by titrating a mixture of hematite and solution, first with a base, then with an acid, and analyzing periodically for dissolved iodate. This method also gave information on the rate of equilibration.

In a second experiment, exchange isotherms were determined at three pH values by reacting Fe_2O_3 samples in buffer solutions and analyzing for dissolved iodate.

1. Experimental Methods

In the first experiment, a solution of 0.1M $NaClO_4$ and 0.001M $NaHCO_3$ was prepared and filtered through a Millipore membrane filter having 0.45μm pores. KIO_3 was added to bring the iodate concentration to 0.0012M. Reagent grade Fe_2O_3 (0.20-0.25 μm dia particles; surface area of $10m^2/g$, determined by nitrogen adsorption) was added to the solution, and the mixture was stirred continuously throughout the experiment. Measured quantities of of 0.979M Na_2CO_3 were added at intervals, and samples were taken after each addition. Then 1.00M $HClO_4$ was added to test the reversibility of the reaction. In several instances, samples were taken at intervals in order to determine the approximate time dependence of adsorption. The change in pH was also used as a measure of equilibration. Equilibration appeared to be virtually complete in as little as 3 min; times between addition of acid or base and final sampling ranged from 13 min to 21 h.

The pH was measured by means of a glass electrode and a calomel-saturated KCl reference electrode. An external salt bridge filled with 0.1M $NaClO_4$ solution was used to prevent contamination of the hematite-solution mixture. At one time, stirring was stopped and the Fe_2O_3 was allowed to settle below the liquid junction, but no difference was observed between

the pH determined at that time and that determined during rapid stirring. Thus, there was no "suspension" effect, which is sometimes reported in the measurement of the pH of mixtures.

Prior to analysis for iodate, the samples were filtered through polycarbonate membrane filters having 0.45-μm pores. Aliquots of 1 mL were titrated for iodate by immediately adding excess H_2SO_4 and NaI to produce I_2, and then titrating the I_2 with $Na_2S_2O_3$ solution, using a starch indicator near the end point. Except for the first few samples, duplicate titrations gave values within 0.5%. After analysis of the first few samples, it was discovered that significant reduction of iodate took place if the acid and NaI were not added immediately after pipetting the samples. Apparently, the iodate was reduced by an impurity in the distilled water or by residual starch in the titration vessels. The discrepancy is believed not to have affected the data used, and the analyses are believed to be accurate to within $\pm 10^{-5}$M, or 1% of the highest values.

In the second experiment, Fe_2O_3 was added to test tubes containing different quantities of KIO_3 in buffer solutions. The compositions of the buffers are given in Table 59. The samples were then mixed by rotation of the test tubes. The samples at pH 3.93 were rotated for about 62 h; the others were rotated for about 20 h. The samples were then centrifuged at high speed for 1/2 h, and 0.5-to 1-mL samples of solution were titrated for iodate. The method of titration was the same as in the first experiment. The pH was measured at the end of an experiment with a glass electrode-saturated KCl calomel electrode pair, and is expressed on the usual NBS scale.

Table 59. Compositions of Buffer Solutions

pH	Composition
3.93	50 mL 0.1M CH_3COOH 8.9 mL 0.1M CH_3COONa
5.77	2.8 mL 0.1M CH_3COOH 50 mL 0.1M CH_3COONa
8.67	0.1M $NaHCO_3$

Determinations were also made with no Fe_2O_3 present. Results showed that no detectable amounts of iodate were adsorbed by the test tubes.

2. Results

The results of the first experiment are given in Fig. 40.

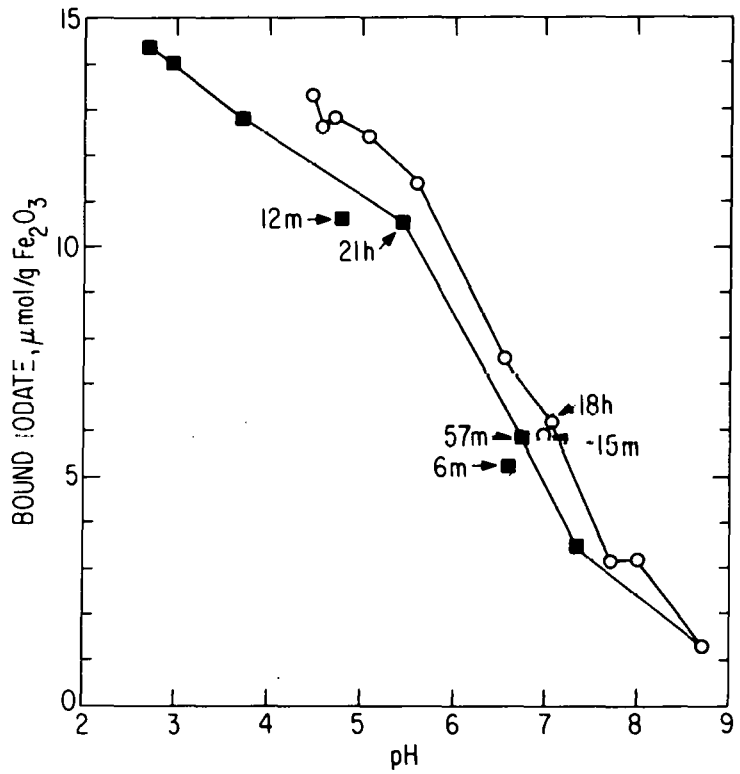

Fig. 40. Adsorption of Iodate by Hematite as a Function of pH in 0.1M $NaClO_4$ Solution. Circles represent consecutive additions of base; squares represent consecutive additions of acid. Numbers are the time intervals after addition of the acid or the base.

The reaction appears to be quite reversible, showing the expected dependence of iodate adsorption on pH. The pH dependence demonstrates that iodate substitutes for negative ions, probably OH^-, HCO_3^-, or CO_3^{2-}, on the surface of the hematite particles.

There is some indication, after initial equilibration, of a slow drift toward higher concentrations of bound iodate. In Fig. 40, three points are off the line. These represent analyses made shortly after the addition of the acid or the base. At two points (between pH 6.5 and 7), the solutions drifted toward higher pH values and higher bound iodate concentrations. The drift is in the opposite direction from what would be expected from drift in

pH (due, for example, to loss of CO_2). Since the drift is in the same direction after addition of either acid or base, the cause cannot be slow equilibration due to slowness of the ion-exchange reaction.

The drift appears to be due to a change in the properties of the solid. One strong possiblity is that new surfaces are exposed by abrasion during stirring. Another is that the surface may be hydrating (to form FeOOH or another hydrous oxide). The properties of the hydrated surface might differ from those of the unhydrated surface. Hydration would also cause a volume change, which might cause cracks or spallation of the surface and thereby increase the surface area.

In the acid region (pH about 5), there appears to be a slow drift of pH upward when acid is added. The mechanism is not clear, but the amounts of iodate adsorbed nevertheless appear to be nearly reproducible, not showing a great amount of hysteresis.

The results of the second experiment are shown in Fig. 41, which illustrates the effects of both pH and saturation of the exchange sites. Examination of the data has shown that a Langmuir isotherm does not apply and that therefore the surface phase does not correspond to an ideal solid solution. An attempt will be made to fit the data to a regular solution model.

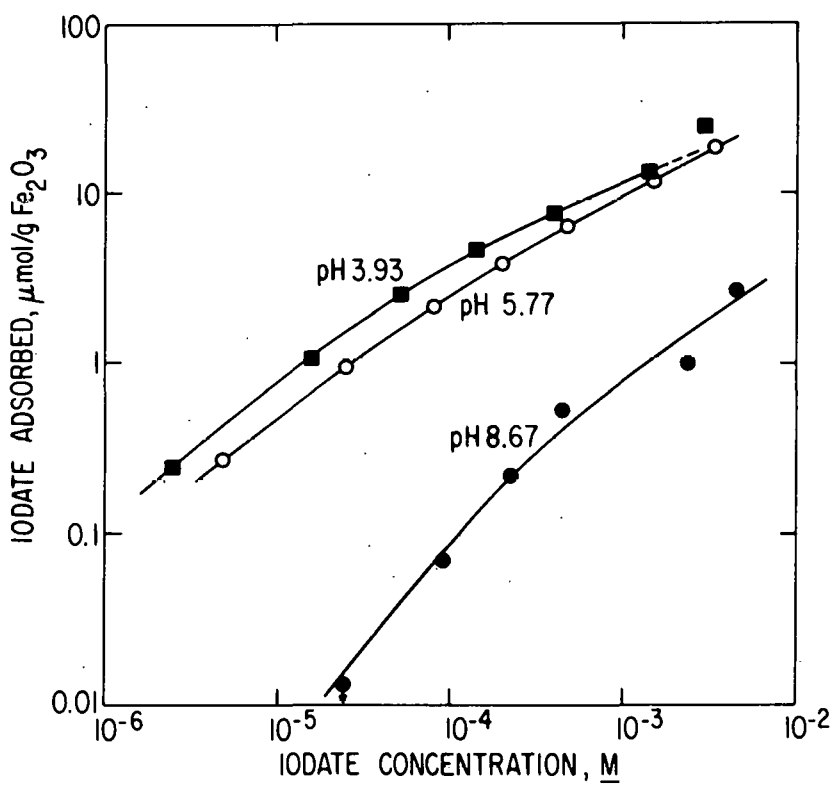

Fig. 41. Adsorption of Iodate by Hematite (Fe_2O_3).

C. Discussion

It is apparent from both experiments that hematite retains a significant capacity for iodate at pH values greater than 8. Thus, it is reasonable to expect that iron oxides, which occur in some rocks, sediments, and soils will retain an affinity for iodate in most rivers, lakes, groundwaters, and possibly in the oceans. However, the effect of competing ions such as phosphate and silicate has not yet been determined.

We suppose that the iodate is specifically adsorbed, i.e., bound to the surface by Fe-O bonds. This supposition is supported by the fact that $Fe(IO_3)_3$ is only slightly soluble. If iodate is specifically adsorbed, the ionic strength should have little effect on the isotherm. Thus, we would expect iodate to be adsorbed by hematite in solutions having high ionic strength, such as seawater.

Work is now in progress to answer the above questions, and a literature search is being continued. This report thus represents only the initial effort to evaluate iron oxides as adsorbers of iodine species.

Appendix A.

Outline for Waste Awareness Meeting

Note: Comments in parentheses discussed at the meeting

I. Waste Classification/Definition

A. TRU Waste

1. Definition [BENNETT-1978]

(a) It contains $\geq$10 nanocuries per gram of waste of ^{233}U, Pu, trans-Pu elements, and daughter products.

(1) ^{238}Pu, ^{241}Pu, ^{235}U, and ^{238}U are not considered "TRU actinides." (These must be pure isotopes to be non-TRU.)

(2) See Table A-1 for equivalent weights of 10 nanocuries.

(b) No recovery of the contained actinides for reuse is planned, but recovery may be required for waste management purposes.

Table A-1 Equivalent Weight of Ten Nanocuries

Isotope	Half-Life, y	Specific Activity, Ci/g[a]	Wt of 10 nCi, g[b]
Thorium-232	1.41×10^{10}	1.09×10^{-7}	9.17×10^{-4}
Uranium-233	1.62×10^{5}	9.48×10^{-3}	1.05×10^{-8}
Uranium-235	7.1×10^{8}	2.14×10^{-6}	4.67×10^{-5}
Uranium-238	4.51×10^{9}	3.33×10^{-7}	3.00×10^{-4}
Plutonium-239	2.44×10^{4}	6.13×10^{-2}	1.63×10^{-9}
Plutonium-240	6537.	0.228[c]	4.38×10^{-10}
Plutonium-241	14.7	101[c]	9.90×10^{-13}
Americium-241	432	3.44[c]	2.91×10^{-11}
Curium-242	0.45	3285[c]	3.04×10^{-14}
Curium-244	18.11	81.0[c]	1.23×10^{-12}

[a]Data from Radiological Health Handbook, Rev. Ed. U.S. Department of Health, Education, and Welfare (January 1970).

[b]Calculated from:
10×10^{-10} Ci/nCi ÷ specific activity in Ci/g = Value in g/10 nCi.

[c]Calculated from:
Curies/g = 3.578×10^{5} ÷ [(T1/2) (atomic mass)], where T1/2 = half-life in years. Equation from footnote (a) reference.

2. Classification

(a) Commercial fuel reprocessing produces no TRU waste, only reprocessing of DOE/DOD does.

(b) Value of I.A.I.(a) above is based on the upper range of radium-226 concentrations in the earth's crust (this value is under review).
(Examples of TRU waste are spent fuel cladding, soil contaminated by HLW tank leakages, and TRU-contaminated buildings only after reduction to rubble.)

B. High-Level Waste (HLW)

1. Definition [BENNETT-1978]

(a) The wastes from the first cycle of solvent extraction in the Purex Process.

(b) This waste contains the majority of fission products and some actinides, but is specifically not considered TRU waste. [It has been produced at Hanford, SRP, INEL, ORNL, and West Valley, N.Y. (commercial).]

C. Spent Fuel

1. Spent fuel isn't classified as HLW or TRU.

2. It defines itself.
(It may or may not be considered waste depending on politics.)

D. Uranium Mine/Mill Tailings

1. These are self-defining.
(Only recently has this been considered a radioactive waste.)

E. Mixtures

1. Some alpha, beta-gamma, and activation product mixtures exist, but they are historic.

F. Permanent Gases

1. They are defined as radioisotopes of hydrogen, krypton, and xenon.

2. Few regulations exist. (Limits on the quantities in Ci/day which can be discharged are the only regulations.)

G. Low-Level Waste (LLW)

1. Low-level waste is defined as being essentially all R/A wastes not classified above.

2. DOT has a classification of low-specific-activity waste (LSA) for waste containing <100 nCi/g of waste (applies to TRU & LLW). (This allows the use of lower "quality" or proven integrity shipping containers.)

II. Disposal and Storage Methods Used to Date

A. TRU Waste (waste is classified to be remotely handled if radiation levels are greater than 200 mR/h at contact, and to be contact-handled if less than 200 mR/h.)

1. Since 1970, all TRU waste has been put into retrievable storage.

(a) Waste must be solidified. In other words, no liquid, dust, or fine-particle-size material will be accepted. (This is to minimize the severity of any transportation accidents.)

(b) Retrievability period is 20 y.

(c) Only DOT-approved containers are used, such as plastic-lined 55-gal drums, Fiberglas-reinforced plywood boxes, or metal bins.

(1) Waste having high gamma radiation levels or >0.1 Ci TRU actinides is placed in concrete coffins.

2. Primary Storage Methods [NATIONAL RESEARCH COUNCIL]

(a) Waste containers are placed on concrete pads (150 x 2400 ft) in a tightly packed array; when the pad is full the containers are covered with plywood, plastic sheeting, and 1 m of dirt. (Hanford, INEL)
(Some old pads are being reinforced with a clay topping.)

(b) Some containers are stored in buildings. (ORNL)

(c) Some high-gamma TRU waste is drummed, placed in concrete casks, and buried in trenches. (ORNL, LASL, Hanford)
(Concrete is for radiation shielding.)

(d) INEL is the main repository in the U.S.

(e) Some conventionally buried TRU waste exists.

(1) They were generated and buried prior to 1970.

(2) This includes solids and liquid seepage basins. (ORNL, LASL, SRP)
(The fraction of the radioactivity attributed to TRU waste generally increases with age; radioactivity continues for 10^6 y.)

B. High-Level Waste (All HLW is remotely handled; HLW is radioactive for approximately 10^3 y.)

1. Most is liquid and is in semipermanent storage in large (1 million gallon) underground tanks. (Hanford, SRP)

2. Hanford is evaporating liquid by vacuum evaporation or self-heating to form in tank salt cakes without provisions for heat removal and condensation.

3. Hanford also separates cesium and strontium from the HLW stream, cans the cesium and strontium as halide salts for water pit storage, and returns the main HLW stream to the tank farm.

4. INEL is/has calcined its liquid HLW by adding carbonates and evaporating it in a fluidized bed.

5. Many other methods of converting HLW to solids are being investigated or are currently being used.

(a) Calcine is formed into glass. (Note that all operations are remote.)

(1) Pilot plants are operating at Hanford and W. Germany.

(2) This is the method used in France and Sweden.

(3) This method is undergoing development and testing in the U.S. now.

(b) Supercalcine is formed by phosphate additions (imitates natural minerals).

(c) Hot-pressed concrete forms are being investigated.

(d) ORNL mixes HLW with grout and them pumps the mixture into shale beds.

(e) Synthetic rock processes are being researched.

(f) Metal matrix encapsulation of calcines or glass beads is being evaluated.

6. All liquid waste is to be converted to solid within 10 y of generation.

   (a) As of July 1, 1978, shipment of liquid R/A waste is unlawful (DOT regulation).

   (b) Both of the above, 6 and 6(a), also apply to low-level waste.

   (c) Spent Fuel

      (1) Spent fuel is currently stored in water basins near reactors.

      (2) The future of spent fuel will be determined on the basis of political considerations.

   (d) Low-Level Waste (LLW) (LLW is radioactive for 10^2-10^3 y.)

      (1) Low-level waste is packaged in cardboard or plywood boxes or drums, then buried in trenches with 4 to 6 f of dirt overpack.

      (2) Every major laboratory has its own LLW burial sites. Also, several commercial sites exist.

   (e) Permanent Gases (Gases are radioactive for 10^2 y.)

      (1) Dilution, then dispersal is the most common disposal method.

      (2) Gases are stored (under pressure) to allow decay; then they are dispersed.

   (f) Associated Costs

      (1) The cost of shipping TRU from INEL to WIPP is $30/cu ft. Hanford reports a cost of $19/cu ft to box and store waste.

      (2) HLW - not known

      (3) LLW burial cost was $5/cu ft at Beatty, Nevada.

      (4) Spent Fuel

         i. Cost is $117/kg heavy metal for disposal only.

         ii. Cost is $232/kg heavy metal for storage and disposal [DOE].

III. Possible Future Disposal Techniques/Requirements

A. TRU Waste

1. Processing Techniques which are being considered are:

(a) Volume reduction

(1) Reduce the waste generation rate

(2) Compaction

(3) Incineration

(4) Surface cleaning (electropolishing, shot peening)

(5) Melt (arc melting, slagging purification)

(6) Separation of actinides

(b) Other Treatment

(1) Neutralize

(2) Reduce Flammability

(3) Solidify

2. Immobilization in an advanced solid waste form is being researched. (May or may not include volume reduction. The goal is an extremely long-life containment mechanism.)

3. Packaging is receiving much attention.

4. The processing site is assumed to be the generation site. (This is to reduce transportation risks.)

5. Disposal Techniques Being Considered: (Some uses for curium and americium exist.)

(a) Temporary/Interim Storage (Whether or not waste should be processed or left unprocessed has not been decided.)

(b) Permanent

(1) Transmuation

(2) Removal from earth

(3) Isolation
(Definition: waste is to be retrievable for 10 y, but is considered to have been disposed of after the 10-y period.)

B. High-Level Waste
(Some uses for ^{90}Sr and ^{137}Cs exist.)

1. Processing techniques can be similar to those for TRU waste.

2. Disposal techniques can be the same as for TRU.

(a) Container material/and design are important.
(This is due to the heat generation and radiation levels.)

C. Low-Level Waste

1. Radioisotope separation is being considered.

2. R & D on physical volume reduction (primarily by incineration and compaction) is under way.

3. Segregation can reduce waste volume.

4. Work to improve containers is aimed mainly at meeting DOT requirements.

D. Spent Fuel

1. Isolation with (or as) HLW is being considered.

(a) Experiments will be done at WIPP.

2. Away-from-reactor storage is losing favor due to transportation risk.

E. Permanent Gases

1. Encapsulation is being researched.
(This is accomplished by metal sputtering techniques.)

2. Improved storage materials and techniques are being tested.
(Separation methods are being improved constantly.)

IV. Future of Waste Disposal

A. DOE Approach

1. DOE has established decentralized offices.

2. Waste programs are separate from each other.

B. NRC + EPA + DOT Impacts

1. New standards are being proposed.

2. Stricter standards are probable in the future.

C. Major Research Areas

1. Repositories are receiving much attention.

   (a) Hard rock

   (b) Salt

   (c) Deep space

   (d) Sea bed

   (e) Deep sea trench

   (f) Aboveground

2. Transmutation has and is being researched.

3. New waste forms are being developed.

   (a) Synthetic Rock

   (b) Metal Matrix

   (c) Others

4. Making dismantling and decontamination an input to facility design is starting. (The choice of method will depend on the waste volume, the cost per unit volume, the capital cost, and political/social pressure.)

D. Controversies

1. The legacy to future generations must be considered.

2. Location is a major battle. (The "why-here-next-to-me" syndrome is prevalent.)

   (a) Benefit vs. location is one solution.

   (b) State's right to refuse waste disposal site is a major question.

      (1) States may claim this right themselves.

      (2) Proposition 15 type action is possible. (California)

3. Goals are difficult to establish.

   (a) What are acceptable risk levels?

4. Urgency should be considered.

   (a) A perfect answer will never be obtained.

   (b) An operating repository (for defense waste) will allow continued use of nuclear power.

   (c) Groups are specific to one cause. There are many groups. (Anti-war groups are anti-weapons but not necessarily anti-nuclear power plant.)

5. Who pays the cost is now much debated. (A WIPP type facility will add $0.15/kWh to electric bills.)

6. Risk must be considered.

   (a) The absolute risk is unknown.

   (b) Measurement is difficult.

   (c) Public is mainly over "mushroom cloud" fear, but now "genetic, poison, etc" fears are in forefront.

7. Nuclear power expansion is on "hold."

   (a) Stalling of waste management will stall nuclear power.

   (b) States can regulate nukes out of business.

V. Waste Management Notes Relevant to Salt Transport

A. Waste Stream Classification.

1. All primary waste streams, such as salt bleeds, stainless steel sponge, upper and lower hardware, and residue that contains FP-4 will be HLW.

2. Secondary wastes such as broken equipment, decontamination solutions, etc. will be either HLW or LLW.

3. A change in TRU waste definition may cause some salt streams to be classified as TRU waste.

B. Disposal Methods

1. Vitrification of salt streams may encounter problems due to the volatility of salt at the glass processing temperature of 1000°C.

2. Densification of spongy forms of metallic wastes may be required to decrease their high ratio of surface area to weight.

THIS PAGE

WAS INTENTIONALLY

LEFT BLANK

Appendix B

USEFUL WORKS ON ZINC/CLADDING SEPARATION

C. R. Brown and M. Templer, Method and Apparatus for Recovery and Refining of Zinc, U.S. Patent 3,778,044 (July 13, 1971).

R. F. Bunshah, Vacuum Metallurgy, Reinhold Publishing, New York (1958).

Fritz Hansgirg, Apparatus for Distilling Metals Such as Magnesium and Zinc, U.S. Patent 2,118,973 (May 31, 1938).

R. C. Krutenat, Vacuum Metallurgy, Science Press, Princeton (1977).

W. L. McCabe and J. C. Smith, Unit Operations of Chemical Engineering, 3rd Ed., McGraw-Hill, New York, Chapters 17, 19, 21 (1976).

Matthiessen and Hegeler Zinc Co., Metal Purifying Apparatus, U.S. Patent 3,437,331 (June 17, 1966).

J. C. Moulden and H. W. Webster, Zinc Distillation Process, U.S. Patent 1,030,676 (June 25, 1912).

Nafeizer et al., The Electroslag Melting Process, Bureau of Mines Bulletin 669 (1976).

H. W. St. Clair and M. J. Spendlove, Rate of Evaporation of Zinc at Low Pressures, J. Metals, Trans AIME 191, 1192-1197 (1951).

R. Speiser and J. W. Spretnak, Determination of the Vapor Pressure of Metals and Alloys, Vacuum Metallurgy Symposium, Electrochemical Society, pp. 155-191 (1954).

M. J. Spendlove, Experiments on Vacuum Distillation of Nonferrous Metals and Alloys, Vaccum Metallurgy Symposium, Electrochemical Society, pp. 192-212 (1954).

M. J. Spendlove and St. Clair, Rate of Evaporation of Zinc at Low Pressures, Bureau of Mines Report of Investigation 4710 (June 1950).

M. J. Spendlove et al., Low Pressure Distillation of Zinc from Zinc-Aluminum Alloy, J. Metals, Trans. 185, 553-560 (Sept. 1949).

J. E. Vivian, Principles of Vacuum Distillation of Metal Mixtures, Livermore Research Laboratory Report LRL-88 (March 1954).

S. Von Winbush et al., A Zinc Chlorine Molten Salt Cell, J. Electrochem. Soc. 123(5), 650-653 (May 1976).

W. J. Walsh and G. Burnet, Surface Concentration Changes During Distillation of Liquid Metals, Nucl. Sci. Eng. 25(3), 227-235 (1966).

O. Winkler and R. Bakish, Vacuum Metallurgy, Elsevier Publishing, New York, Chapter 1, 3 (1971).

M. Yasuda, Recent Operation of Electrothermic Distillation Process at Mikkaichi Smelter, TMS Paper A77-19, Metallurgical Society AIME (1977).

REFERENCES

Adwick

A. G. Adwick and R. J. Warmer, The Influence of Particle Size Distribution on the Sintering of Ceramic Powders, Proceedings of the Particle Size Analysis Conference, Society for Analytical Chemistry, 329, London, England (1966).

Ames

L. L. Ames, Controlled Sample Program; Publication No. 1, Characterization of Rock Samples, PNL-2797 (1978).

Antill

J. E. Antill and K. A. Peakall, Oxidation of Uranium Alloys in Carbon Dioxide and Air, J. Less-Common Met. 3, 239 (1961).

Beall

G. W. Beall, B. H. Ketelle and R. G. Haire, Sorption Behavior of Trivalent Actinides and Rare Earths, Radioactive Waste in Geologic Storage, ACS Symposium Series 100, p. 201 (1979).

Belle

J. Belle and B. Lustman, Properties of Uranium Dioxide, WAPD-184 (1957).

Bennett-1974

M. J. Bennett, B. L. Myatt, and J. E. Antill, The Oxidation Behavior of Highly Irradiated Uranium in Dry Carbon Dioxide at 375 to 500°C and in Dry Air at 200 to 300°C, J. Nucl. Mat. 50, 2 (1974).

Bennett-1978

W. S. Bennett, letter "Transmittal of Information to Albuquerque Lead Office, TRU Program", 78-RF-2062, October 27, 1978.

Blander

M. Blander et al., Chemical Engineering Division - Physical Inorganic Chemistry Annual Report - July 1974 - June 1975, Argonne National Laboratory Report ANL-75-46, p. 24 (1976).

Bodine

J. E. Bodine, J. Guon and R. J. Sullivan, Second Cycle AIROX Reprocessing and Pellet Refabrication of Highly Irradiated Uranium Dioxide, NAA-SR-11375 (1965).

Boston

C. R. Boston and G. P. Smith, J. Phys. Chem. 62, 409 (1958).

Bradt

R. C. Bradt, D. P. H. Hasselman, and F. F. Lange, Fracture Mechanics of Ceramics, Vol. I, Concepts, Flaws, and Fractography; Vol. 2, Microstructure Materials and Applications, Plenum Press, New York (1973).

Brambilla-1973

G. Brambilla, G. Caporali, and M. Zambianchi, Process for the Dissolution of Ceramic Nuclear Fuels, Ger. Offen. 2 319 717 (1973).

Brambilla-1976A
G. Brambilla and G. Caporali, Process for the Pyrochemical Separation of Plutonium from Irradiated Nuclear Fuels, Ger. Offen. 2 611 333 (1976).

Brambilla-1976B
G. Brambilla, G. Caporali, and M. Zambianchi, Reprocessing Method of Ceramic Nuclear Fuels in Low-Melting Molten Salts, U.S. Patent 3 981 960 (1976).

Brewer
L. Brewer, HP-67 Calculator Programs for Thermodynamic Data and Phase Diagram Calculations, LBL-5485 (May 25, 1978).

Burman-1963
R. W. Burman and G. Litchfield, Severe Molten Zinc Corrosion as Reduced by Improved Molybdenum-Tungsten Alloys, Eng. Min. J. 164(2), 88-90 (April 1963).

Burman-1977
R. W. Burman, Molybdenum - A Super Superalloy, J. Metals, 29(12), 1-6 (December 1977).

Brown-1955
F. Brown, H. M. Ockenden, and G. A. Welch, J. Chem. Soc. 1955, 4196 (1955).

Brown-1968
D. Brown, Halides of the Lanthanides and Actinides, John Wiley and Sons, New York (1968).

Carroll
D. F. Carroll, Synthesis and Properties of Plutonium Mononitride, HW-SA-2755 (1962).

Charnock
H. O. Charnock and H. B. Holz, Sodium Technology, Atomics International, North American Rockwell, p. IV-1-NA-113, (1970).

Chiotti
P. Chiotti and J. T. Mason, Phase Diagram and Thermodynamic Properties of the Uranium-Zinc System, J. Less-Common Met. 40, 39-55 (1975).

Clayton
J. C. Clayton and S. Aronson, Some Preparative Methods and Physical Characteristics of Uranium Dioxide Powders, J. Chem. Eng. Data 6(1), 43 (1961); also WAPD-178.

Corbett
J. D. Corbett and F. R. Duke, Techniques of Inorganic Chemistry, Vol. 1, H. B. Jonassen and A. Weissberger, Eds., Interscience Publishers, New York, p. 103(1963).

Couture-1978
R. A. Couture, M. G. Seitz and M. J. Steindler, Experimental Trace-Element Transport by Fluid Flow at Elevated Temperatures: Ion Exchange on Kaolinite, Symposium on Trace-Element Migration by Fluid Flow, 1978 Fall Meeting of the American Geophysical Union (1978).

Couture-1979
R. A. Couture, M. G. Seitz and M. J. Steindler, Adsorption of Iodate by Hematite, Abstract, Annual Meeting of the American Nuclear Society, in press (June 1979).

Croff
A. Croff, ORNL, personal communication (February 1979).

Davidge
R. W. Davidge, Effects of Microstructure on the Mechanical Properties of Ceramics in [BRADT], pp. 447-468.

DOE
Preliminary Estimates of the Charge for Spent Fuel Storage and Disposal Services, DOE/ET-0055, UC-70, Washington D.C. (July 1978).

Eisenman
G. Eisenman, On the Elementary Origin of Equilibrium Ion Specificity, Symp. on Membrane Transport and Metabolism, A. Kleinzeller and A. Kotyk (Eds.), Academic, New York (1962).

Elliott
R. P. Elliott, Constitution of Binary Alloys, First Supplement, McGraw-Hill, New York, pp. 191 and 205 (1965).

Ervin
G. Ervin, U.S. Patent 4029740 (1977).

Flanagan
F. J. Flanagan, Description and Analysis of Eight New USGS Rock Standards, Geological Survey Professional Paper 840 (1976).

Flynn
K. F. Flynn, L. J. Jardine, and M. J. Steindler, Method for Determining Leach Rates of Simulated Radioactive Waste Forms, American Chemical Society Symposium, Radioactive Waste in Geologic Storage, ACS Symposium Series 100, 115 (1979).

Freshley
M. D. Freshley, D. W. Brite, J. L. Daniel, and P. E. Hart, Irradiation-Induced Densification of UO_2 Pellet Fuel, J. Nucl. Mat 62, 138 (1976).

Fried
J. J. Fried, Groundwater Pollution, Elsevier, New York (1975).

Furman
N. H. Furman, Ed., Scotts' Standard Methods of Chemical Analyses, 6th Ed. Vol. 1, D. Van Nostrand and Co., New York pp.517-518 (1962).

Garrels
R. M. Garrels and C. L. Christ, J. Sci. 254, 372 (1956).

Gillham
Robert Gillham, Lecture, Seattle (October 1978).

Goode
J. H. Goode and V. C. A. Vaughen, Voloxidation Tests with Irradiated Fuels, Voloxidation - Removal of Volatile Fission Products from Spent LMFBR Fuels, J. H. Goode, Ed., pp. 100-120 ORNL-TM-3723 (1973).

Grimes-1962
W. R. Grimes, J. H. Shaffer, R. A. Strehlow, W. T. Ward, and G. M. Watson, Radioisotopes as Tracers for Reactions in Molten Fluoride Media, Radioisotopes in Physical Science and Industry, IAEA (1962).

Grimes-1979
W. R. Grimes, ORNL, personal communication (February 1979).

Grosvenor
D. E. Grosvenor, I. O. Winsch, W. E. Miller, G. J. Bernstein, and R. D. Pierce, Corrosion-Resistant Heated Transfer Tubes for Molten Metals and Salts, Nucl. Appl. 5, 329-332 (1968).

Gruen
D. M. Gruen and R. L. McBeth, J. Inorg. Nucl. Chem. 9, 290 (1959).

Guon
J. Guon, J. E. Bodine, and R. J. Sullivan, Refabrication and Encapsulation of Highly Irradiated Uranium Dioxide, NAA-SR-8213 (1964).

Hafstrom
J. W. Hafstrom, R. M. Arono, and J. Y. N. Wang, Materials Development, AO, Quarterly Progress Report, January-March 1978, Pyrochemical and Dry Processing Methods, B&R AG-02-01-2A, Advanced Fuel Cycle Research and Development, C. H. Bean, K. M. Myles, and M. J. Steindler, Eds. pp. I-3 to I-11.

Hansen
M. Hansen and K. Anderko, Constitution of Binary Alloys, McGraw-Hill, New York (1958).

Hasselman
D. P. H. Hasselman et al., The Griffith Criterion and the Reversible and Irreversible Fracture of Brittle Materials, in [BRADT], pp. 749-755.

Hodge
W. Hodge, R. M. Evans, and A. F. Haskins, Metallic Materials Resistant to Molten Zinc, J. Metals TRANSAIME, 825-832 (July 1955).

Hoyt
R. C. Hoyt, personal communication (August 1978).

Hulse
C. O. Hulse and J. A. Batt Fracture of Directionally Solidified $CaO \cdot ZrO_2 \cdot ZrO_2$ Eutectic in [BRADT], pp. 483-494.

Hultgren
R. Hultgren et al., Selected Values of the Thermodynamic Properties of Binary Alloys, ASM (1963).

Hyodo
Shin-ichi Hyodo and Masaki Kimura, Tensile Fragmentation of Virgin Glass Fibers, in [BRADT], pp. 431-443.

Jameson
G. J. Jameson, Mass (or Heat) Transfer from an Oscillating Cylinder, Chem. Eng. Sci. 19, 793-800 (1964).

Janov
J. Janov, P. G. Alfredson, and V. K. Vilkartis, The Influence of Precipitation Conditions on the Properties of Ammonium Diuranate and Uranium Dioxide Powders, J. Nucl. Mater. 44, 161 (1972).

Janz
G. J. Janz, Ed., Molten Salt Handbook, Academic Press, New York, pp. 39, 503, and 522, (1967).

Johnson
T. R. Johnson, F. G. Teats, and R. D. Pierce, A Method for the Purification of Molten Chloride Salts, Argonne National Laboratory Report ANL-7603 (1969).

Kaufman-1970
L. Kaufman and H. Bernstein, Computer Calculation of Phase Diagrams, Academic Press, New York (1970).

Kaufman-1975
L. Kaufman and H. Nesor, Treatise on Solid State Chemistry, V.5, Plenum Press, New York, p. 179, (1975).

KBS
Handling of Spent Nuclear Fuel and Final Storage of Vitrified High Level Reprocessing Waste, Karn-Bransle-Sakerhet Report, Stockholm, Sweden (1978).

Keller
C. Keller, The Chemistry of the Transuranium Elements, Verlag Chemie GmbH, Berlin (1971).

Koster
V. W. Koster and H. Schmid, Alloying Ability of Zinc with Molybdenum and Tungsten, Z. Metallkd. 46(2), 462-463 (1955) (in German).

Kraus
K. A. Kraus, H. O. Phillips, T. A. Carlson, and J. S. Johnson, Ion-Exchange Properties of Hydrous Oxides, Proc. Second United Nations International Conference on the Peaceful Uses of Atomic Energy, Vol. 28 United Nations, Geneva, pp. 3-16 (1958).

Krumpelt
M. Krumpelt, Argonne National Laboratory, personal communication (February 1979).

Kyle
M. L. Kyle, R. D. Pierce, and V. M. Kolba, Containment Materials for Pyrochemical Processes, Nucl. Met. Symp. on Reprocessing of Nuclear Fuels 15, 433-452 (1969).

Lange
F. F. Lange, Origin and Use of Fracture Mechanics in [BRADT], pp. 3-15.

Lawroski-1959
S. Lawroski, N. A. Rodger, R. C. Vogel, and V. H. Munnecke, Chemical Engineering Division Summary Report, October-December, 1958, Argonne National Laboratory Report ANL-5959.

Lawroski-1962
S. Lawroski, R. C. Vogel and V. H. Munnecke, Chemical Engineering Division Summary Report, July - September 1962, Argonne National Laboratory Report ANL-6596.

Lawroski-1963
S. Lawroski et al., Chemical Engineering Division Summary Report, October-December, 1962, Argonne National Laboratory Report ANL-6648 (May 1963).

Lawroski-1964
S. Lawroski and L. Burris, Jr., Processing of Reactor Fuel Materials by Pyrometallurgical Methods, At. Energ. Rev. 2(3), 3-69 (1964).

Levin
E. M. Levin, C. R. Robbins, and H. F. McMurdie, Phase Diagrams for Ceramists, The American Ceramic Society, Columbus, Ohio, p. 383 (1964).

Lieser
K. H. Lieser, E. Kluge, Abtrennung von Reinem Francium-223 aus Actinium-227 auf Eines Trennsäule, Sonderdruck aus Radiochim. Acta 7, 3-9 (1967).

Lyon
W. L. Lyon and E. E. Voiland, The Preparation of Uranium Dioxide from a Molten Salt Solution of Uranyl Chloride, HW-62431 (October 1959).

Madden
A. J. Madden and D. G. Nelson, A Novel Technique for Determining Mass Transfer Coefficients in Agitated Solid-Liquid Systems, AIChE J. 10(3), 428-429 (May 1964).

Marschall
C. W. Marschall and A. Rudnick, Conventional Strength Testing of Ceramics, in [BRADT], pp. 69-91.

Marlowe
M. O. Marlowe, In-Reactor Densification Behavior of UO_2, NEDO-12440 (1973).

Martin-1959
A. E. Martin, Argonne National Laboratory, personal communication (1959).

Martin-1961
A. E. Martin, J. B. Knighton, and H. M. Feder, Solubility of Zr, Nb, Mo, Pd, and Th in Liquid Zinc, J. Chem. Eng. Data 6(4), 596-599 (October 1961).

McElroy
J. L. McElroy, Quarterly Progress Report Research and Development Activities, Waste Fixation Program, October-December 1976, Battelle Pacific Northwest Laboratories Report PNL-2264 (November 1977).

Mecham
W. J. Mecham, L. J. Jardine, and M. J. Steindler, The Effect of Impact Energy on Solid-Waste Composites of Brittle and Ductile Materials, Proceedings of the International Symposium on Ceramics in Nuclear Waste Management (American Ceramic Society) April 30-May 2, 1979, Cincinnati, Ohio, CONF-790420 (1979).

Merriam
C. N. Merriam and H. C. Thomas, Adsorption Studies on Clay Minerals VI, Alkali Ions on Attapulgite, J. Chem. Phys. 24, 993-995 (1956).

Meyer
R. E. Meyer, Systematic Study of Nuclide Adsorption on Selected Geologic Media, App. D., Waste Isolation Safety Assessment Program Quarterly Technical Progress Report for Oct.-Dec. 1978, A. Brandstetter, Ed.

Moore
R. H. Moore and W. L. Lyon, Distribution of the Actinide Elements in the Molten System: $KCl-AlCl_3-Al$, HW-59147 (October 1959).

Morrey
J. R. Morrey and A. W. Madsen, Rev. Sci. Instrum. 32, 799 (1961).

Myles
K. M. Myles, Argonne National Laboratory, personal communication (February 1979).

NRC
The Shallow Land Burial of Low-Level Radioactively Contaminated Solid Waste, National Research Council, Library of Congress Catalog Card 76-56928 (1976).

Nelson
P. A. Nelson, M. L. Kyle, G. A. Bennett, and L. Burris, Jr., Corrosion of Refractory Metals by Zinc-Magnesium-Uranium and Halide Salt Systems, Electrochem. Technol. 3 (9-10), 263-269 (Sept.-Oct. 1965).

ORNL
Staff of Chemical Technology Division, Aqueous Processing of LMFBR Fuels - Technical Assessment and Experimental Program Definition, Oak Ridge National Laboratory Report ORNL-4436 (June 1970).

Papatheodorou
G. N. Papatheodorou, Argonne National Laboratory, discussion with T. Santa Cruz, Rockwell International (May 18, 1978).

Pardue
W. M. Pardue et al., Synthesis, Fabrication and Chemical Reactivity of Plutonium Mononitride, BMI-1693 (1964).

Pears
C. D. Pears, Strength-of-Materials for Brittle Materials as a Guide to Testing and Properties, Chapter IV, pp. 139-189, S. J. Acquaviva and S. A. Bortz, Eds., Structural Ceramics and Testing of Brittle Materials, Gordon and Breach Science Pulbishers, New York (1967).

Piret-1949
J. F. Johnson, J. Axelson, and E. L. Piret, Application of Gas Adsorption Measurements to an Investigation of Crushing of Quartz, Chem. Eng. Prog. 45, 708 (December 1949).

Piret-1950
J. W. Axelson and E. L. Piret, The Crushing of Single Particles of Crystalline Quartz, Ind. Eng. Chem. 42, 665 (April 1950).

Piret-1957
N. F. Schulz, S. R. B. Cooke, and E. L. Piret, Energy --- New Surface Relationship in the Crushing of Solids, Chem. Eng. Prog. 53, 254 (May 1957).

Piret-1961
W. J. Kenny and E. L. Piret, Slow Compression Crushing of Single Particles of Glass, AIChE J. 7, 199 (June 1961).

Piret-1962
R. A. Zeleny and E. L. Piret, Dissipation of Energy in Single Particle Crushing, Ind. Eng. Chem. Process Des. Dev. 1, 37-41 (January 1962).

Potter
R. A. Potter, U.S. Patent 3953355 (1976).

Queeney
R. A. Queeney and R. L. Turner, Fracture Resistance of Metal-Infiltrated Porous Ceramics, in [BRADT], pp. 807-815.

Quist
A. S. Quist, Appl. Spectrosc. 25, 82 (1971).

Relyea
J. F. Relyea, Controlled-Sample Program Results, Waste Isolation Safety Assessment Program, Task 4. Second Contractor Meeting Proceedings, October 2-5, 1978, R. J. Serne, Chairman, PNL-SA-7352 (1979).

Richardson
F. D. Richardson, Physical Chemistry of Melts in Metallurgy, Vol. 1, Academic Press, New York, pp. 38-67 (1974).

Ritter
J. E. Ritter, Effect of Polymeric Coatings on Strength of Soda-Lime Glass, in [BRADT], pp. 735-747.

Roesler
F. C. Roesler, Brittle Fractures Near Equilibrium, Proc. Phys. Soc. (London) 69, 981 B (1956).

Rossman
R. P. Rossman and W. R. Smith, Ind. Eng. Chem. 35, 972 (1943).

Samsonov
G. V. Samsonov, High-Temperature Compounds of Rare Earth Metals with Non-metals, Consultants Bureau, New York (1965).

Schaefer
H. Schaefer, F. E. Wittig, and W. Wilborn, Neue Bildungsweisen, chemisches Verhalten und Bildungspenthalpie von AlOCl, Z. Anorg. Allg. Chem. 297, 78 (1958).

Schellinger
A. K. Schellinger, Calorimetric Method for the Determination of the Surface Energy of A Brittle Crystalline Solid, Science 111, 693-694 (June 23, 1950).

Schroeder
H. J. Schroeder, Trennung Natürlicher Radionuklide mittels Ammonium Molybdatophosphat, Radiochim. Acta 1, 1, 29-31 (1962).

Seitz-1979A
M. G. Seitz, P. Rickert, S. Fried, A. Friedman, and M. J. Steindler, Migratory Properties of Some Nuclear-Waste Elements in Geologic Media, Nucl. Technol. 44, 284-296 (July 1979).

Seitz-1979B
M. G. Seitz, P. G. Rickert, S. M. Fried, A. M. Friedman, and M. J. Steindler, Transport Properties of Nuclear Wastes in Geologic Media, Annual Report for the Waste Isolation Safety Assessment Program, for period October 1, 1977 to September 30, 1978, R. Serne, Chairman, PNL-SA-7352 (1979).

Seitz-1979C
M. Seitz and R. Couture, Trace-Element Transport in Lithic Material by Fluid Flow at High-Temperature, Quarterly Progress Report, Oct. to Dec. 1978, Argonne National Laboratory Report ANL-79-29 (1979).

Seitz-1979D
M. Seitz, P. Rickert, S. Fried, A. Friedman, and M. J. Steindler, Transport Properties of Nuclear Wastes in Geologic Media, Waste Isolation Safety Assessment Program Quarterly Technical Progress Report for October through December, 1978, A. Brandstetter, M. A. Harwell, G. L. Benson, D. J. Bradley, J. R. Raymond, and R. J. Serne, Pacific Northwest Laboratory (1979).

Serne
R. J. Serne, Chairman, Waste Isolation Safety Assessment Program, Task 4, Contractor Information Meeting Proceedings, Sept. 20-23, 1977, PNL-SA-6957 (1978); Second Contractor Meeting Proceeding, Oct. 2-5, 1978, PNL-SA-7352 (1979).

Shaffer
J. H. Shaffer, Preparation and Handling of Salt Mixture for the Molten Salt Reactor Experiment, ORNL-4616 (1971).

Shiao
S. Y. Shiao, P. Rafferty, and R. E. Meyer Ion-Exchange Equilibria between Montmorillonite and Solutions of Moderate - to High Ionic Strength, Radioactive Waste in Geologic Storage, S. Fried, Ed., ACS Symposium Series 100, American Chemical Society, Washington D. C. (1979).

Smith-1942
R. C. Smith Jr. and H. C. Howard, Ind. Eng. Chem. 34, 438 (1942).

Smith-1978
D. H. Smith et al., Molten-Salt Processes Applied to Ceramic Fuels, 2nd PDPM Information Exchange Meeting, Argonne National Laboratory, November 7-8, 1978.

Smith-1979
D. H. Smith and H. F. McDuffie, Molten Salt Processes Applied to Ceramic Fuels, First Annual Report, ORNL/TM-6763, in press.

SPEX
Spex Industries; drawings and blueprints of a prototype high-temperature furnace for Raman spectroscopy supplied through Hollis Davis.

Steindler-1978A
M. J. Steindler et al., Chemical Engineering Division Fuel Cycle Programs Progress Report, January - September 1977, Argonne National Laboratory Report ANL-78-11.

Steindler-1978B
M. J. Steindler et al., Chemical Engineering Division Fuel Cycle Programs Quarterly Progress Report October-December 1977, Argonne National Laboratory Report ANL-78-37.

Steindler-1978C
M. J. Steindler et al., Chemical Engineering Division Fuel Cycle Programs Quarterly Progress Report, January-March 1978 Argonne National Laboratory Report ANL-78-68.

Steindler-1978D
M. J. Steindler et al., Chemical Engineering Division Fuel Cycle Programs Quarterly Progress Report, April-June 1978, Argonne National Laboratory Report ANL-78-76.

Steindler-1979A
M. J. Steindler et al., Chemical Engineering Division Fuel Cycle Section Quarterly Progress Report, July-September 1978, Argonne National Laboratory Report ANL-79-6.

Steindler-1979B
M. J. Steindler et al., Chemical Engineering Division Fuel Cycle Programs, Quarterly Progress Report, October-December 1978, Argonne National Laboratory Report ANL-79-29.

Tagawa
H. Tagawa, Nippon Genshiryoku Gakkaishi 13(5), 267-274 (1971).

Taylor-1947
N. W. Taylor, Mechanism of Fracture of Glass and Similar Brittle Solids, J. Appl. Phys. 18, 943 (November 1947).

Taylor-1961
A. Taylor, N. J. Doyle, and B. J. Kagle, The Constitution Diagram of the Molybdenum-Hafnium Binary System, J. Less Common Met. 3, 265-280 (1961).

Taylor-1964
S. R. Taylor, Abundance of Chemical Elements in the Continental Crust, Geochim. Cosmochim. Acta 20, 1280-1281 (1964).

Thonstead
J. Thonstead and E. Hove, On the Anode's Overvoltage in Aluminum Electrolysis, Can. J. Chem. 42, 1542 (1964).

Traylor
E. D. Traylor, L. Burris, and C. J. Geankoplis, Mass Transport From a Uranium Sphere to Liquid Cadmium in Highly Turbulent Flow, Ind. Eng. Chem. Fundam. 4(2), 120 (May 1965).

Wachter
J. Wachter, Oak Ridge National Laboratory, personal communication (February 1979).

Wahlberg-1962
J. S. Wahlberg and M. J. Fishman, Adsorption of Cesium on Clay Minerals, Geological Survey Bulletin 1140-A (1962).

Wahlberg-1965
J. S. Wahlberg, J. H. Baker, R. W. Vernon and R. S. Dewar, Exchange Adsorption of Strontium on Clay Minerals, Geological Survey Bulletin 1140-C (1965).

Washburn
E. W. Washburn, Ed., The International Critical Tables, Vol. II, McGraw-Hill, New York, p. 463 (1927).

Westsik
J. H. Westsik, Jr., and R. P. Turcotte, Hydrothermal Reactions of Nuclear Waste Solids, a Preliminary Study, Battelle Pacific Northwest Laboratories Report PNL-2759 (September 1978).

White
D. E. White, J. D. Hern, and G. A. Waring, Chemical Composition of Subsurface Waters, Section F, Data of Geochemistry, U.S. Geol. Survey Prof. Paper 440-F.

Winsch-1965
I. O. Winsch, K. R. Tobias, R. D. Pierce, and L. Burris, Jr., Sampling of Liquid Metals, Argonne National Laboratory Report ANL-7088 (September 1965).

Winsch-1967
I. O. Winsch, M. L. Kyle, R. D. Pierce, and L. Burris, Jr., Tungsten Crucibles in Pyrochemical Processing of Nuclear Fuels, Nucl. Appl. 3, 245-251 (1967).

Wriedt
H. A. Wriedt, Thermodynamics of Ferritic Solutions to the Iron-Zinc System at 700°C to 900°C, Trans. Metall. Soc. AIME 239(8), 1120-1128 (1967).

Young
J. P. Young and J. C. White, Anal. Chem. 31, 1892 (1959).

Distribution for ANL-79-45

Internal:

W. E. Massey
M. Ader
J. K. Bates
L. Burris
F. A. Cafasso
T. F. Cannon
R. A. Couture
E. J. Croke
P. R. Fields
K. F. Flynn
S. Fried
A. M. Friedman
B. R. T. Frost
T. J. Gerding
D. R. Hamrin
J. E. Harmon
L. J. Jardine
J. H. Kittel (2)
V. M. Kolba
M. Krumpelt
B. J. Kullen
R. A. Leonard
W. J. Mecham
A. Melton
K. M. Myles
M. V. Nevitt
R. H. Pelto
W. B. Seefeldt
M. G. Seitz
M. Seliga
J. Simmons
M. J. Steindler (10)
L. E. Trevorrow
S. Vogler
D. S. Webster
A. A. Ziegler
A. B. Krisciunas
ANL Contract File
ANL Libraries (4)
TIS Files (6)

External:

DOE-TIC, for distribution per UC-10 and UC-70 (353)
Manager, Chicago Operations and Regional Office, DOE
Chief, Office of Patent Counsel, DOE-CORO
S. A. Mann, DOE-CORO
Argonne Universities Association:
President
C. B. Alcock, U. Toronto
J. T. Banchero, U. Notre Dame
P. W. Gilles, U. Kansas
R. I. Newman, Fripp Island, S. C.
S. W. Ahrends, Oak Ridge Operations Office, USDOE (2)
T. W. Ambrose, Battelle Pacific Northwest Lab.
C. K. Anderson, Combustion Engineering
R. E. Barletta, Brookhaven National Lab.
G. S. Barney, Rockwell Hanford Operations
Battelle-Columbus Labs.
R. C. Baxter, Allied-General Nuclear Services
B. C. Blanke, USDOE-DA, Miamisburg, O.
E. Bondictti, Oak Ridge National Lab.
D. Bowersox, Los Alamos Scientific Lab.
M. G. Britton, Corning Glass Works
C. L. Brown, Battelle Pacific Northwest Lab.
R. Brown, Allied Chemical Corp., Idaho Falls
L. L. Burger, Battelle Pacific Northwest Lab.
D. Camp, Lawrence Livermore Lab.
D. O. Campbell, Oak Ridge National Lab.
W. Carbiener, Battelle-Columbus Labs.
W. T. Cave, Mound Lab.
B. H. Cherry, GPU Services Corp.
E. D. Clayton, Battelle Pacific Northwest Lab.
J. M. Cleveland, U. S. Geological Survey, Lakewood, Colo.
F. E. Coffman, USDOE-MFE
J. J. Cohen, Lawrence Livermore Lab.
C. R. Cooley, Office of Nuclear Waste Management, USDOE

G. R. Corey, Commonwealth Edison, Chicago
J. L. Crandall, Savannah River Lab.
M. C. Cullingford, Nuclear Regulatory Commission
R. Cunningham, USNRC, Nuclear Materials Safety & Safeguards
G. H. Daly, Waste Technology Branch, USDOE (2)
J. C. Dempsey, Office of Nuclear Waste Management, USDOE
B. R. Dickey, Allied Chemical Corp., Idaho Falls
J. E. Dieckhoner, Div. Waste Products, USDOE
J. Dietz, Los Alamos Scientific Lab.
R. L. Dillon, Battelle Pacific Northwest Lab.
R. G. Dosch, Sandia Labs., Albuquerque
G. H. Dyer, Bechtel Corp.
Eastern Environmental Radiation Lab., HEW
G. Eichholz, Georgia Inst. Technology
O. J. Elgert, Richland Operations Office, USDOE (2)
B. Erdal, Los Alamos Scientific Lab.
E. D. Erickson, Rocky Flats Plant
D. Ferguson, Oak Ridge National Lab.
Foster Wheeler Corporation, Library (HQAP)
C. W. Francis, Oak Ridge National Lab.
R. G. Gavin, Savannah River Lab. (3)
R. G. Geier, Rockwell Hanford Operations, Richland
General Electric Co., San Jose (DOE)
A. Giambusso, USDOE-AIA
E. S. Goldberg, Savannah River Operations Office, USDOE (2)
S. Goldsmith, Battelle Pacific Northwest Lab.
J. P. Hamric, Idaho Operations Office, USDOE
S. G. Harbinson, San Francisco Operations Office, USDOE
M. Harwell, Battelle Pacific Northwest Lab.
C. A. Heath, Div. Waste Isolation, USDOE
J. L. Heffter, NOAA, Silver Spring
L. L. Hench, U. Florida
T. B. Hindman, Jr., USDOE-SR
B. F. Judson, General Electric Co., San Jose
S. V. Kaye, Oak Ridge National Lab.
G. R. Keepin, Los Alamos Scientific Lab.
R. G. Kepler, Sandia Labs., Albuquerque
C. J. Kershner, Mound Lab.
F. J. Kiernan, Aerojet Energy Conversion Co., Washington
J. F. Kircher, Battelle-Columbus Labs.
K. Kraus, Oak Ridge, Tenn.
S. J. Lambert, Sandia Labs., Albuquerque
G. Lehmkul, Rocky Flats Plant
S. Levine, USNRC, Div. of Reactor Safety Research
W. H. Lewis, Nuclear Fuel Services, Rockville
R. C. Liikala, Battelle Pacific Northwest Lab.
J. L. Liverman, Deputy Asst. Secy. for Environment, USDOE
Los Alamos Scientific Lab., Director
A. L. Lotts, Oak Ridge National Lab.
R. Y. Lowrey, Albuquerque Operations Office, USDOE (2)
L. Machta, NOAA, Silver Spring
R. Maher, Savannah River Plant
J. C. Mailen, Oak Ridge National Lab.
W. J. Maraman, Los Alamos Scientific Lab.

A. B. Martin, Rockwell International, Canoga Park (2)
M. L. Matthews, Nuclear Power Development, USDOE
D. J. McGoff, Waste Technology Branch, USDOE
D. L. McIntosh, Savannah River Lab.
W. H. McVey, USDOE-NPD
R. E. Meyer, Oak Ridge National Lab.
S. Meyers, Office of Nuclear Waste Mgmt., USDOE
R. B. Minogue, USNRC, Office of Standards Development
J. Mishima, Battelle Pacific Northwest Lab.
NASA, John F. Kennedy Space Center
Ronald D. Nelson, Battelle Pacific Northwest Lab. (3)
I. Neretnieks, Lawrence Berkeley Lab.
Y. Ng, Lawrence Livermore Lab.
G. K. Oertel, Div. Waste Products, USDOE
R. D. Oldenkamp, Atomics International
D. A. Orth, Savannah River Plant
B. Paige, Allied Chemical Corp., Idaho Falls
H. Palmour III, North Carolina State U.
J. H. Pashley, Oak Ridge Gaseous Diffusion Plant
A. M. Platt, Battelle Pacific Northwest Lab. (3)
H. Postma, Oak Ridge National Lab.
C. A. Preskitt, IRT Corp., San Diego
J. J. Reilly, Brookhaven National Lab.
J. F. Relyea, Battelle Pacific Northwest Lab.
L. M. Richards, Atlantic Richfield Co., Los Angeles
G. L. Ritter, Exxon Nuclear Corp., Richland
D. M. Rohrer, Los Alamos Scientific Lab.
R. Romatowski, Office of Nuclear Waste Mgmt., USDOE
H. E. Roser, USDOE, Albuquerque Operations Office
R. Roy, Pennsylvania State U.
K. J. Schneider, Battelle Pacific Northwest Lab.
R. L. Seale, U. Arizona
T. A. Sellers, Sandia Labs.
J. Serne, Battelle Pacific Northwest Lab.
B. Silva, Lawrence Berkeley Lab.
A. Squire, Hanford Engineering Development Lab.
J. A. Stiegler, Sandia Labs.
S. Stoller, The S. M. Stoller Corp.
K. Street, Lawrence Livermore Lab.
G. Stukenbroeker, NL Industries, Wilmington, Del.
J. L. Swanson, Battelle Pacific Northwest Lab.
J. Tewhey, Lawrence Livermore Lab. (3)
USDOE Div. of Nuclear Power Development, Nuclear Fuel Cycle Programs Br.
USDOE Office of Basic Energy Sciences
USDOE Div. of RRT, Engineering
USDOE Div. of RRT, Technology
USDOE Idaho Operations Office
USDOE New Brunswick Laboratory
USDOE San Francisco Operations Office
USDOE Southern California Energy Office
H. H. Van Tuyl, Battelle Pacific Northwest Lab.
V. C. A. Vaughn, Oak Ridge National Lab.
E. E. Voiland, General Electric Co., Morris, Ill.
B. L. Vondra, Oak Ridge National Lab.

R. D. Walton, Jr., Office of Nuclear Waste Mgmt., USDOE
C. D. Watson, Oak Ridge National Lab.
L. L. Wendell, Battelle Pacific Northwest Lab.
J. B. Whitsett, Idaho Operations Office, USDOE
W. J. Wilcox, Oak Ridge Gaseous Diffusion Plant
A. K. Williams, Allied-General Nuclear Services, Barnwell
R. O. Williams, Rocky Flats Plant
D. D. Wodrich, Rockwell Hanford Operations
J. E. Yanoski, Office of Nuclear Energy Programs, USDOE
D. Zeigler, Rocky Flats Plant
Arizona, U. of, Dept. of Nucl. Engineering
A. H. Emmons, U. Missouri
H. S. Isbin, U. Minnesota
W. R. Kimel, U. Missouri
Maine Univ., Prof. in charge of Chem. Engr. Lib.
Marquette U., Dept. of Chemistry
Michigan Technological U., Library
D. W. Moeller, Kresge Ctr. for Environmental Health, Boston
G. Murphy, Iowa State U.
H. Rosson, U. Kansas
L. Schwendiman, Pacific Northwest Lab.
E. R. Stansberry, Purdue U.
B. S. Swanson, Illinois Inst. Technology
B. W. Wilkinson, Michigan State U.
W. E. Wilson, Washington State U.
W. F. Witzig, Pennsylvania State U.

☆U.S. GOVERNMENT PRINTING OFFICE: 1980.– 651-118/23